BLIND ADAPTIVE CYCLIC FILTERING AND BEAMFORMING ALGORITHMS

By

JIE ZHANG, M. Sc., Academia Sinica

A Thesis
Submitted to the School of Graduate Studies
in Partial Fulfilment of the Requirements
for the Degree
Doctor of Philosophy

McMaster University
July 2001

BLIND ADAPTIVE CYCLIC FILTERING AND BEAMFORMING ALGORITHMS

DOCTOR OF PHILOSOPHY (July 2001) MCMASTER UNIVERSITY
(Electrical and Computer Engineering) Hamilton, Ontario

TITLE: **Blind Adaptive Cyclic Filtering and Beamforming Algorithms**

AUTHOR: Jie Zhang
M. Sc., Academia Sinica

SUPERVISOR(S): Dr. Kon Max Wong
Professor,
Department of Electrical and Computer Engineering

NUMBER OF PAGES: xix, 186

Abstract

In a multi-user communication system such as the wireline or wireless communication systems, a commonly encountered problem is the extraction of the desired signal from Co-Channel Interference (CCI) and Adjacent Channel Interference (ACI). To combat the CCI and ACI, the conventional filtering techniques are unable to carry out the job. The optimum FREquency-SHift (FRESH) filtering technique proposed by W. A. Gardner enables us to suppress spectrally overlapped signals by using the cyclostationarity of the signals. However, to design the optimum FRESH filter, we must have the statistical knowledge of the desired signal or a training signal which, in practice, are not often available. This thesis proposes a blind adaptive FRESH filtering algorithm which does not need a training signal to extract the desired signal from spectrally overlapping interference. We call this new technique Blind Adaptive (BA)-FRESH filtering. Comparing the BA-FRESH filter with the FRESH filter with a training signal which is called Trained Adaptive FRESH (TA-FRESH) filter, it has been proved that BA-FRESH and TA-FRESH have same performances when the data length is infinite. When the data length is finite, there are performance differences between BA-FRESH and TA-FRESH. Convergence of the BA-FRESH and TA-FRESH filter coefficients, the finite sample output signal to interference plus noise ratio (SINR), and the finite sample output mean square error (MSE) are analyzed and their convergence rates are obtained. Moreover, the finite sample output probability error of BA-FRESH and TA-FRESH are analyzed. Using the central limit theorem, the analytic formulae of finite sample output probability error of BA-FRESH and TA-FRESH are obtained. Numerical results are presented to examine these results. We found that the analytic results and simulation results agree closely.

On the other hand, various cyclic beamforming techniques such as the spectral Self-COherence REstoral (SCORE), the Cyclic Adaptive Beamforming (CAB), the Constrained Cyclic Adaptive Beamforming (C-CAB) and the Robust Cyclic Adaptive Beamforming (R-CAB) algorithms can be used to combat CCI and ACI efficiently. However, when the desired signal and the interferences are very closely spaced in arrival directions, system performance improvement using these cyclic beamforming alone is limited because the beamformers are just spatial filters. By combining the spatial beamforming with the temporal FRESH filtering, a large system performance improvement may be achieved due to the full utilization of the signal information in both time and space domains. A Blind Adaptive Space-Time (BLAST) algorithm is proposed in this thesis. The BLAST algorithm is a blind adaptive time varying space-time filter. It does not require a training signal and it can generate the reference signal from the corrupted signal. Because the algorithm exploits not only spatial information but also temporal information of the signals, it has the advantages of both spatial and temporal filters. The BLAST algorithm can be viewed as the expansion of the BA-FRESH filtering algorithm to the space-time domain. Comparing the BLAST filter with the space-time filter with a training signal which is called Trained Adaptive Space-Time (TAST) filter, it has been proved that BLAST and TAST have same performances when the data length is infinite. When the data length is finite, there are performance differences between BLAST and TAST. Convergence of the BLAST and TAST filter coefficients, the finite sample output signal to interference plus noise ratio (SINR), and the finite sample output mean square error (MSE) are analyzed. Their convergence rates are obtained. Moreover, the finite sample output probability error of BLAST and TAST are also analyzed. Using the central limit theorem, the analytic formulae of finite sample output probability error of BLAST and TAST are obtained. Numerical results are presented. We found the analytic results and simulation results agree closely. The analytic and simulation results show that the use of the proposed algorithms to extract desired signals from the corrupted signal is promising.

Acknowledgements

I wish to express my sincere thank to my supervisor Dr. K. M. Wong for his constant encouragement, continued assistant, expert guidance throughout the course of this work. I would also like to thank Dr. Z. Q. Luo for being my co-supervisor, and Dr. J. P. Reilly and Dr. P. Yip for being my supervisory committee members. Their tremendous help, constant attention and support are invaluable to my work. Without their guidance and help, this work would not have been possible.

Many thanks go to other friends, especially Dr. T. N. Davidson, Dr. A. Gershman, and Dr. Q. Jin, for their positive suggestions and valuable help. I also want to acknowledge the financial support provided by TRIO (Telecommunication Research Institute of Ontario), CMC (Canadian Marconi Company), and the Department of Electrical and Computer Engineering (McMaster University) during my graduate studies.

Finally, I want to thank my parents, my wife Y. P. Zhang and my daughter for their help and support. They have provided an excellent environment for my studies and my life.

Acronyms

Through this thesis, the following acronyms are used:

ACI	Adjacent-Channel Interference
ADC	American Digital Cellular
AMPS	Advanced Mobile Phone System
AWGN	Additive White Gaussian Noise
BPSK	Binary Phase-Shift Keying
BA-FRESH	Blind Adaptive FREquency SHift
BLAST	BLind Adaptive Spatial-Temporal
BER	Bit-Error Rate
BSS	Blind Signal Separation
CTI	Cross Talk Interference
CCI	Co-Channel Interference
CDMA	Code Division Multiple Access
CMA	Constant Modules Algorithm
CAB	Cyclic Adaptive Beamforming
C-CAB	Constrained Cyclic Adaptive Beamforming
DOA	Direction-Of-Arrival
DSB-AM	Double Side Band-Amplitude Modulation
DSP	Digital Signal Processing
FM	Frequency Modulation
FIR	Finite Impulse Response
FRESH	FREquency SHift

GPS	Global Position System
GSM	Global System for Mobile communications
IS-95	Interim Standard-95
ISI	Inter-Symbol Interference
JDC	Japanese Digital Cellular
LCL	Linear Conjugate Linear
LCMV	Linearly Constrained Minimum Variance
LMS	Least Mean Square
MSE	Mean Square Error
MMSE	Minimum Mean Square Error
PCS	Personal Communications System
PDF	Probability Density Function
QPSK	Qudriphase-Shift Keying
RF	Radio Frequency
dB	decibel
R-CAB	Robust Cyclic Adaptive Beamforming
RLS	Recursive Least Square
SCD	Spectrum Correlation Density
SOI	Signal Of Interest
SCORE	Self-COherence REstoral
SIR	Signal to Interference Ratio
SINR	Signal to Interference plus Noise Ratio
SNR	Signal to Noise Ratio
TA-FRESH	Trained Adaptive FREquency SHift
TAST	Trained Adaptive Spatial-Temporal
TDMA	Time Division Multiple Access
WSS	Wide Sense Stationary

Notations

Through this thesis, the following notations are used:

$\sum_n$	Summation over n
A^*	Conjugate of A
$\langle \cdot \rangle$	Time average over infinite samples
$\langle \cdot \rangle_N$	Time average over N samples
Re$[A]$	Taking the real part of A
Im$[A]$	Taking the imaginary part of A
$tr(A)$	The trace of A
$\|\|A\|\|$	L_2-norm of A
A^T	Transpose of matrix A
$A^\dagger$	Conjugate transpose of matrix A
$O(\cdot)$	Order of
$E[A]$	Expectation of A

Contents

List of Figures

List of Tables

Chapter 1

Introduction

1.1 Background

The field of wireless mobile communications is growing at an explosive rate, covering many technical areas. This growth necessitates more efficient utilization of the electromagnetic spectrum and high quality system performance. However, there are many practical difficulties which must be overcome. These include Co-Channel Interference (CCI), Adjacent Channel Interference (ACI), Inter-Symbol Interference (ISI) and multi-path fading problems, [1–3]. To solve these problems, many research efforts have been made [8, 10, 15, 16]. This thesis focuses on the interference rejection problem which is important for several reasons. Firstly, frequency re-use techniques are employed in various mobile cellular phone systems such as Advanced Mobile Phone System (AMPS), Pan-European Global System for Mobile communications (GSM), American Digital Cellular (ADC), and Japanese Digital Cellular (JDC) systems. The concept of frequency re-use refers to the use of radio channels on the same carrier frequency to cover the different areas. The capacity of these cellular systems is inherently interference limited [4], particularly by CCI and ACI. Although we can split cells and decrease power to combat the CCI and ACI, cell splitting is expensive because we have to increase the number of base stations. So we need efficient interference rejection techniques to improve utilization of spectrum. Secondly, to further increase the utilization

of spectrum, as new technology supersedes old technology, we need to co-utilize old systems with new systems such as the Interim Standard-95 (IS-95) based on CDMA overlay or co-existence with Advanced Mobile Phone System (AMPS) on cellular telephone spectrum [4]. To implement these systems, the key issue is also how to combat mutual interferences which come from the two kinds of systems. Moreover, for other mobile communications systems such Global Position Systems (GPS) and satellite-based mobile Communication Systems, we also often meet interference problems. For example, commercial air-borne GPS system are susceptible being jammed unintentionally [6]. Therefore, we see that developing efficient receivers of mobile communication system which combat CCI and ACI has great commercial values. This lays the main practical background for this thesis.

Spectral-correlation theory in cyclostationary signals is a branch of modern spectral analysis. By developing and exploiting the spectral correlation properties of communication signals, we can greatly improve the performance of conventional signal processors [34]. To combat CCI and ACI which may overlap spectrally with the desired signal, the conventional filtering techniques [7] are unable to carry out the job. The optimum FREquency-SHift (FRESH) filtering technique, called the cyclic Wiener filter proposed by W. A. Gardner [13] enables us to separate spectrally overlapped signals by using the cyclostationarity of the signals. The initial idea of FRESH filtering for cyclostationary signals was proposed by W. A. Gardner in 1972. The general development of the frequency-domain theory of cyclic Wiener filtering was presented in 1985 [20]. Both these pioneering treatments were based on the probabilistic theory of stochastic process where performance is measured in term of ensemble averaged squared error. In 1987, a dual frequency-domain theory based on non-probabilistic theory of time series where performance is measured in terms of time-averaged squared error, was introduced [24]. Cyclic Wiener filtering theory was summarized and design equation of optimum FRESH filter was presented in 1993 [13]. However, to design the cyclic Wiener filter, one must have statistical knowledge of the desired signal or a training signal which, in practice, are often not available. Moreover, the idea of retrieving cyclostationary signals in a multi-user environment has been studied and blind channel identification and equalization methods using induced cyclostationarity have also been proposed [10, 12].

In addition, various Blind Signal Separation (BSS) method have been developed in recent years [69]. The basic form of the BSS problems is to consider a set a of unknown source signal $s_1(t), s_2(t), \cdots s_m(t)$ that are mutually independent of each other. These signals are linearly mixed in an unknown environment to produce the m by 1 observation vector $\boldsymbol{x}(t) = \boldsymbol{A}\boldsymbol{s}(t)$, where $\boldsymbol{s}(t) = [s_1(t)\ s_2(t) \cdots s_m(t)]^T$ and $\boldsymbol{x}(t) = [x_1(t)\ x_2(t) \cdots x_m(t)]^T$. $\boldsymbol{A}$ is an unknown nonsingular mixing matrix of dimensions m-by-m. That is, the number of sensors where $\boldsymbol{x}(t)$ is observed is equal to the number of sources that produce $\boldsymbol{s}(t)$. The BSS method is to find a mixing matrix $\boldsymbol{W}$ defined ideally as $\boldsymbol{y} = \boldsymbol{W}\boldsymbol{x} = \boldsymbol{W}\boldsymbol{A}\boldsymbol{s} \rightarrow \boldsymbol{D}\boldsymbol{P}\boldsymbol{s}$, where $\boldsymbol{y}$ is the output signal vector produced by the demixer, $\boldsymbol{D}$ is a non-singular diagonal matrix, and $\boldsymbol{P}$ is a permutation matrix. However, it is difficult to apply the BSS methods to suppress CCI and ACI in some cases, especially in a mobile wireless system. For example, consider the received signal $y(t) = s_1(t) + s_2(t) + n(t)$, where $s_1(t)$ is desired signal, $s_2(t)$ is the interference, and $n(t)$ is white noise. In this case, $\boldsymbol{A}$ is a vector ($\boldsymbol{A} = [1\ 1\ 1]$) instead of a non-singular matrix. It is difficult to use the BSS methods to extract the desired signal $s_1(t)$. However, one can extract the desired signal $s_1(t)$ provided that the desired signal has different cyclic frequency from that of the interference. This is one of reasons why we exploit signal cyclostionarity instead of the BSS methods to suppress the CCI and ACI.

In this thesis, we firstly propose an blind adaptive FRESH filtering algorithm which doesn't need a training signal to extract the desired signal from spectrally overlapping interference. We call this new technique Blind Adaptive (BA)-FRESH filtering. The structure of this BA-FRESH filter [18] is proposed. The performance of BA-FRESH filter is compared with that of the Trained Adaptive FRESH (TA-FRESH) filter. When the data length is infinite, both filters have same performance. But when the data length is finite, there is a performance difference between the two filters. Hence, the filter coefficients convergence performance, the output signal to interference plus noise ratio (SINR), and the output mean square error (MSE) of BA-FRESH and TA-FRESH are analyzed. The finite sample output probability errors of BA-FRESH and TA-FRESH are examined theoretically and by simulations. The analytic and simulation results show that the use of such a blind adaptive filtering technique to extract desired signals from spectrally overlapping interference is promising.

To combat CCI and ACI, it is well known that applying digital beamforming techniques can suppress interferences present in the communication channel. In the past, a lot of researches has been done to spatially extract the desired signal by either forming a beam towards the single user or by putting nulls in the directions where the interfering signals impinge the antenna [82, 83]. These conventional methods require the knowledge of the direction of arrival (DOA) of the signal of interest (SOI) or require the use of a training signal to train the systems which, in turn, require an extra amount of bandwidth and the need of synchronization. To overcome these shortcomings, several blind cyclic beamforming algorithms have been proposed such as the spectral Self-COherence REstoral (SCORE), the Cyclic Adaptive Beamforming (CAB), the Constrained Cyclic Adaptive Beamforming (C-CAB) and the Robust Cyclic Adaptive Beamforming (R-CAB) algorithms. For these cyclic blind adaptive beamforming algorithms, the weighting coefficients of the beamformer are adjusted blindly by exploiting cyclostationarity to form a main beam toward the desired signal such as the CAB algorithm or form the nulls toward interferences such as the SCORE and the C-CAB algorithms [15, 29], provided that the desired signal and interferences have different cyclic frequencies and they come from different directions. However, in practical wireless communication systems, we often meet cases in which the DOA difference between the desired signal and interference is very small [1, 4]. Moreover, because users are mobile and multi-path propagation effects exist, the received signal may come from multiple directions and it is possible that the desired signal and the interferences are very closely spaced in arrival direction. Under such environments, system performance improvement by using blind beamforming alone is obviously limited because the beamformers are just spatial filters and they just exploit the spatial information of the observed signals. However, by combining both spatial beamforming and temporal FRESH filtering processing, a large system performance improvement may be achieved due to full utilization of the signal information in both temporal and spatial domains. To design a conventional space-time filter [14], one needs to know a training signal or statistical knowledge of the desired signal which, in practice, are not often available. Moreover, a popular optimum criterion in space-time processing is maximum likelihood, but its computation complexity is often prohibitive [53]. To satisfy the practical demands for future mobile personal communication

systems, a new BLind Adaptive Space-Time (BLAST) algorithm is proposed in this thesis. By exploiting the spectral correlation of cyclostationary signals, the space-time filtering method requires no desired signals and generates the training signal from the corrupted signal. The algorithm exploits both spatial and temporal information of the signals. Hence, it has advantages over spatial filter or temporal filter alone. It can be viewed as extension of the BA-FRESH filtering technique into the spatial-time domain. One of the advantages of the BLAST filter over an array beamforming algorithm or a filtering algorithm is that fewer antenna elements or shorter FIR filter are required to achieve a given performance level, because the spectral diversity and the spatial diversity can complement each other. The structure of this BLAST filter is proposed in this thesis. The performance of BLAST filter is compared with that of the Trained Adaptive Space-Time (TAST) filter. When the data length is infinite, both filters have same performance. But when the data length is finite, there exist performance differences between the two filters. Hence, the filter coefficient convergence performance, the output SINR, and the output MSE of BLAST and TAST are analyzed. The finite sample output probability errors of BLAST and TAST are examined theoretically and by simulation. The theoretical and simulation results show that the use of such a blind adaptive space-time filtering technique to extract desired signals from spectrally or spatially overlapping interference is promising.

1.2 Contributions and Organization of Thesis

The motivation of this thesis is that exploiting the cyclostationarity of signals proposes novel blind algorithms which can be used to combat CCI and ACI in mobile communication systems. The major contributions of the thesis is that the two kinds of cyclic DSP algorithms are proposed and their performances are analyzed.

- Using the cyclostationarity of communication signals, a Blind Adaptive FREquency SHift (BA-FRESH) filtering algorithm is proposed. This algorithm has a unique optimum solution which can be recursively implemented. The BA-FRESH filtering algorithm does not require a training signal nor statistical knowledge of the desired signal.

For the infinite sample case, BA-FRESH and TA-FRESH have same performance.

- Convergence performances of BA-FRESH and TA-FRESH are analyzed and compared. For the finite sample case, the solutions of both BA-FRESH and TA-FRESH asymptotically converge in the mean square sense to the same optimum solution with convergence rates $O(\frac{1}{N})$, where N is the data length. When the observed data length is finite, the normalized output signal to interference plus noise ratio (SINR) of BA-FRESH and TA-FRESH asymptotically converge in the mean square sense to the same optimum value with the convergence rate $O(\frac{1}{N})$. When the observed data length is finite, the normalized output Mean Square Errors (MSE) of BA-FRESH and TA-FRESH asymptotically converge in the mean square sense to the same optimum value with the convergence rate $O(\frac{1}{N})$.

- The finite sample output probability errors of BA-FRESH and TA-FRESH are analyzed. Using the central limit theorem, approximate analytic expressions of the finite sample output probability errors of BA-FRESH and TA-FRESH are obtained. Compared the analytic results with simulation results, the theoretical curves and practical curves match well.

- Exploiting the cyclostationarity of communication signals and extending BA-FRESH algorithm into the space-time domain, a BLind Adaptive Space-Time (BLAST) algorithm is proposed. The BLAST algorithm is a space-time filter which exploits not only the spatial information but also the temporal information of the signals. It also does not require training signal nor the statistics knowledge of the desired signal. The algorithm has a unique optimum solution and the solution can be recursively arrived at. For the infinite sample case, BLAST and TAST have same performance.

- Convergence performances of BLAST and TAST are analyzed and compared. For the finite sample case, the solutions of both BLAST and TAST asymptotically converge in the mean square sense to the same optimum solution with convergence rates $O(\frac{1}{N})$, where N is the data length. When the observed data length is finite, the normalized output signal to interference plus noise ratio (SINR) of BLAST and TAST asymptotically converge in the mean square sense to the same optimum value with

the convergence rate $O(\frac{1}{N})$. When the observed data length is finite, the normalized output Mean Square Errors (MSE) of BLAST and TAST asymptotically converge in the mean square sense to the same optimum value with the convergence rate $O(\frac{1}{N})$.

- The finite sample output probability errors of BLAST and TAST are analyzed. Using the central limit theorem, approximate analytic expressions of the finite sample output probability errors of BLAST and TAST are obtained. Numerical examples are presented to examine these results. Compared the analytic results with simulation results, the theoretical curves and practical curves match well.

Organization of the thesis The practical background and thesis contributions are given in Chapter 1. Chapter 2 reviews cyclostationarity of signals. The characterization of cyclostationary process is reviewed and the spectral correlations of some communication signals are analyzed. Some advantages of utilizing spectral correlation of these man-made signals on signal processing are discussed. In Chapter 3, we propose the BA-FRESH filtering algorithm and examine its convergence performance. The existing FRESH filtering algorithm is firstly reviewed. A blind adaptive method called the BA-FRESH filtering technique is proposed and its recursive implementation formula is given. Comparing the BA-FRESH filter with TA-FRESH filter, it is proved that two kinds of filters have the same optimum solution when the observed data length is infinite. For the finite sample case, the convergence performance of BA-FRESH and TA-FRESH are analyzed and compared. Chapter 4 examines the finite sample probability errors of BA-FRESH and TA-FRESH. Theoretical finite sample probability error formulae of BA-FRESH and TA-FRESH are obtained. Based on the BA-FRESH algorithm, we propose the BLAST algorithm and analyzed its convergence performances in Chapter 5. The existing cyclic adaptive beamforming algorithms are firstly reviewed. A blind adaptive space-time filtering technique called the BLAST is proposed and its recursive implementation formula is given. Comparing the BLAST filter with the TAST filter, it is proved that two kinds of space-time filters have the same optimum solution when the observed data length is infinite. For finite sample cases, the convergence performance of BLAST and TAST are analyzed and compared. Chapter 6 examines the finite sample probability errors of BLAST and TAST. Theoretical finite sample probability

error formulae of BLAST and TAST are obtained. Finally, Chapter 7 concludes the thesis with a summary of the unique work performed, and future work which is suggested to promote BA-FRESH and BLAST as practically competitive efficient interference canceling techniques. Appendixes contain the proofs involved in the thesis.

Chapter 2

Cyclostationarity of Communication Signals

In this chapter, we firstly review the concepts of cyclostationarity which is used in the thesis and point out the relationship between them. Some important properties of cyclostationary signals and computation formula which are used in the thesis are given. Using BPSK signal as an typical example, cyclostationarity of some communication signals is examined. Finally, some advantages of utilizing the cyclostationarity of man-made signals on filtering tasks are discussed.

2.1 Characterization of Cyclostationary Process

At present, many conventional statistical signal processing methods treat random signals as if they were statistically stationary. However, for most man-made signals encountered in communication, telemetry, radar, and sonar systems, some statistical parameters do vary periodically with time. Examples include sinusoidal carriers in amplitude, phase and frequency modulation systems. Although in some cases these periodicities can be ignored by signal processors, in many cases there can be much to gain in terms of improvements in the performance of these signal processors by recognizing and exploiting the underlying period-

icity. This typically requires that the random signals be modeled as cyclostationary signals, in which case the statistical parameters vary in time with single or multiple periodicities. The concept of cyclostationarity in signals was popularized by W. A. Gardner [20] [22].

Cyclostationary stochastic process A cyclostationary process is a non-stationary process. A stochastic process, $x(t)$, is said to be *cyclostationary* in the wide sense if its mean and autocorrelation are periodic with a period, T_0, for all t_1 and t_2, that is,

$$E[x(t)] = \mu_x(t) = \mu_x(t + T_0) \tag{2.1.1}$$

$$E[x(t_1)x^*(t_2)] = R_{xx}(t_1, t_2) = R_{xx}(t_1 + T_0, t_2 + T_0) \tag{2.1.2}$$

where E denotes the probabilistic expectation.

We can focus our attention on the autocorrelation function. Since t_1 and t_2 are arbitrary, let $t_1 = t + \tau/2$, $t_2 = t - \tau/2$, then we have

$$R_{xx}(t_1, t_2) = R_{xx}(t + \tau/2, t - \tau/2), \tag{2.1.3}$$

then $R_{xx}(t + \tau/2, t - \tau/2)$ is a function of two independent variables t and τ. It is the *time dependent correlation function.* For each value of τ, it is periodic in t with period T_0,

$$R_{xx}(t + T_0 + \tau/2, t + T_0 - \tau/2) = R_{xx}(t + \tau/2, t - \tau/2). \tag{2.1.4}$$

It is assumed that the Fourier series representation for this periodic function converges, that is, Dirichlet condition is satisfied. $R_{xx}(t + \tau/2, t - \tau/2)$ can be expressed as

$$R_{xx}(t + \tau/2, t - \tau/2) = \sum_{n=-\infty}^{\infty} R_{xx}^{\alpha}(\tau) e^{j2\pi\alpha t} \tag{2.1.5}$$

where $R_{xx}^{\alpha}(\tau)$ denotes the Fourier coefficients. $\alpha = nf_0$. $f_0 = 1/T_0$. α is called a cycle frequency. α ranges over all integer multiples of fundamental frequency $1/T_0$. $R_{xx}^{\alpha}(\tau)$ is

referred to *cyclic autocorrelation function.*

$$R_{xx}^{\alpha}(\tau) = \frac{1}{T_0}\int_{-\frac{T_0}{2}}^{\frac{T_0}{2}} R_{xx}\left(t+\frac{\tau}{2}, t-\frac{\tau}{2}\right)e^{-j2\pi\alpha t}dt. \tag{2.1.6}$$

For communication signals, T_0 is usually the period of the baud or half of the period of the carrier. The set $\{R_{xx}^{\alpha}(\tau)\}$ and the function $R_{xx}(t+\tau/2, t-\tau/2)$ have one-to-one correspondence. The *finite time average cyclic autocorrelation function* is defined as

$$\hat{R}_{xx}^{\alpha}(\tau)_T = \left\langle x\left(t+\frac{\tau}{2}\right)x^*\left(t-\frac{\tau}{2}\right)e^{-j2\pi\alpha t}\right\rangle_T \tag{2.1.7}$$

where $\langle\cdot\rangle_T$ denotes time average over T samples. $*$ denotes complex conjugate.

A wide sense cyclostationary process is to be called *cycloergodic in autocorrelation* if, with probability 1,

$$\hat{R}_{xx}^{\alpha}(\tau)_T \underset{\text{m.s.}}{\longrightarrow} R_{xx}^{\alpha}(\tau), \quad T\to\infty \tag{2.1.8}$$

where $\underset{\text{m.s.}}{\longrightarrow}$ denotes convergence in the mean-square sense. From an engineering view, we assume that the cyclostationary signals we discussed are cycloergodic in autocorrelation. In this thesis, we can directly use the infinite time-average cyclic correlation to substitute for the probabilistic cyclic correlation function. We also drop T from the time average autocorrelation function.

The Fourier transform of autocorrelation $R_{xx}(t+\tau/2, t-\tau/2)$ is called *time-dependent spectral density function* which is denoted as $S_{xx}(t,f)$

$$S_{xx}(t,f) = \int_{-\infty}^{\infty} R_{xx}\left(t+\frac{\tau}{2}, t-\frac{\tau}{2}\right)e^{-j2\pi f\tau}d\tau. \tag{2.1.9}$$

For each value of f, $S_{xx}(t,f)$ is periodic in t with period T_0. If it is assumed that the Fourier series representation for this periodic function converges, so that $S_{xx}(t,f)$ can be expressed as

$$S_{xx}(t,f) = \sum_{n=-\infty}^{\infty} S_{xx}^{\alpha}(f)e^{j2\pi\alpha t} \tag{2.1.10}$$

where $S_{xx}^{\alpha}(f)$ is the Fourier coefficients. $\alpha = nf_0$. $f_0 = 1/T_0$. α is cycle frequency. $S_{xx}^{\alpha}(f)$

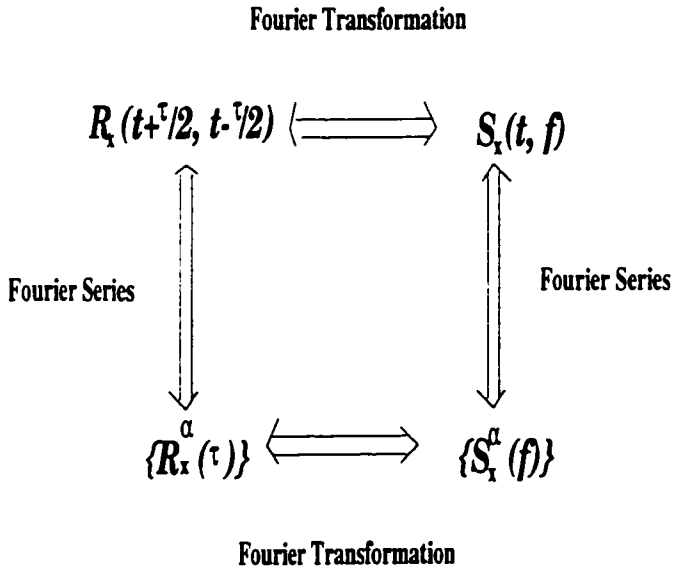

Figure 2.1: Relationship of four functions

is called *cyclic spectral density function*. The set $\{S_{xx}^\alpha(f)\}$ and the function $S_{xx}(t,f)$ are one to one corresponding.

According to the above definitions, we can see that $S_{xx}^\alpha(f)$ is the Fourier transform of cyclic autocorrelation $R_{xx}^\alpha(\tau)$, that is,

$$S_{xx}^\alpha(f) = \int_{-\infty}^{\infty} R_{xx}^\alpha(\tau) e^{-j2\pi\alpha\tau} d\tau. \tag{2.1.11}$$

The relationship of four functions are summarized in Fig. 2.1. Because of this relationship, when we study cyclostationary process, we can just study cyclic correlation functions and cyclic spectral correlation density functions. Given α, they are one dimensional functions. The time dependent correlation functions and time dependent spectral density function are two dimensional functions. So treating the former is easier than treating the latter in mathematics.

Let us analyze an important property of cyclic correlation function. Consider $u(t)$ and $v(t)$ to be the frequency shifted versions of cyclostationary signal $x(t)$, which are defined by

$$u(t) = x(t)e^{-j\pi\alpha t} \quad \text{and} \quad v(t) = x(t)e^{j\pi\alpha t} \tag{2.1.12}$$

where α is cycle frequency of the signal $x(t)$. Consider cross-correlation function between $u(t)$ and $v(t)$

$$\begin{aligned} R_{uv} &= \langle u(t+\tau/2)v^*(t-\tau/2)\rangle \\ &= \left\langle x(t+\tau/2)e^{-j\pi\alpha(t+\tau/2)}x^*(t-\tau/2)e^{-j\pi\alpha(t-\tau/2)}\right\rangle \\ &= \left\langle x(t+\tau/2)x^*(t-\tau/2)e^{-j2\pi\alpha t}\right\rangle = R^{\alpha}_{xx}(\tau). \end{aligned} \tag{2.1.13}$$

Therefore, the cyclic autocorrelation function of signal $x(t)$ is simply the time-averaged cross-correlation between frequency-shifted versions of $x(t)$. This relationship reveals that *a signal $x(t)$ exhibits cyclostationarity if and only if there exist correlation between some frequency shifted version of the signals. The magnitude of correlation is measured by cyclic correlation function $R^{\alpha}_{xx}(\tau)$.*

Computation of cyclic correlation function In practical communication systems, we often meet two kinds of signals; continuous signals and discrete signals. For analog signal $x(t)$, its cyclic autocorrelation function is defined as

$$R^{\alpha}_{xx}(\tau) = \left\langle x\left(t+\frac{\tau}{2}\right)x^*\left(t-\frac{\tau}{2}\right)e^{-j2\pi\alpha t}\right\rangle. \tag{2.1.14}$$

Its cyclic conjugate correlation function is defined as

$$R^{\alpha}_{xx^*}(\tau) = \left\langle x\left(t+\frac{\tau}{2}\right)x\left(t-\frac{\tau}{2}\right)e^{-j2\pi\alpha t}\right\rangle. \tag{2.1.15}$$

For discrete-time cyclostationary signals $x(n)$, its cyclic autocorrelation function is defined as

$$R^{\alpha}_{xx}(k) = \left\langle x(n+k)x^*(n)e^{-j2\pi\alpha n}\right\rangle = \lim_{N\to\infty}\frac{1}{N}\sum_{n=1}^{N}x(n+k)x^*(n)e^{-j2\pi\alpha n}. \tag{2.1.16}$$

Similarly, its cyclic conjugate correlation function is defined as

$$R^{\alpha}_{xx^*}(k) = \left\langle x(n+k)x(n)e^{-j2\pi\alpha n}\right\rangle = \lim_{N\to\infty}\frac{1}{N}\sum_{n=1}^{N}x(n+k)x(n)e^{-j2\pi\alpha n} \tag{2.1.17}$$

where we have normalized the sampling period to one. In practice, the total number of data samples N is finite, therefore an estimate of $\hat{R}^{\alpha}_{xx}(k)$ can be obtained by

$$\hat{R}^{\alpha}_{xx}(k) = \left\langle x(n+k)x^*(n)e^{-j2\pi\alpha n}\right\rangle_N = \frac{1}{N}\sum_{n=1}^{N} x(n+k)x^*(n)e^{-j2\pi\alpha n}. \tag{2.1.18}$$

Similarly, an estimate of $\hat{R}^{\alpha}_{xx^*}(k)$ can be obtained by

$$\hat{R}^{\alpha}_{xx^*}(k) = \left\langle x(n+k)x(n)e^{-j2\pi\alpha n}\right\rangle_N = \frac{1}{N}\sum_{n=1}^{N} x(n+k)x(n)e^{-j2\pi\alpha n}. \tag{2.1.19}$$

A signal $x(n)$ is said to exhibit cyclostationarity if its cyclic autocorrelation or cyclic conjugate autocorrelation are not equal to zero at some frequency shift α. Conventionally, the cyclostationary properties of signals are studied by the locations of spectral line at different frequency shift α. A spectral line is considered as a particular sharp impulse of the cyclic autocorrelation or the cyclic conjugate correlation function. For convenience, a signal that possesses a spectral line at a frequency shift which equals α, is referred to as the signal exhibiting cyclostationarity at cycle frequency α.

These concepts are also easily expanded to signal vectors. For example, let $\boldsymbol{x}(n)$ be a complex signal vector. The finite sample cyclic autocorrelation matrix of $\boldsymbol{x}(n)$ and the finite sample cyclic conjugate correlation matrix of $\boldsymbol{x}(n)$ are defined respectively as

$$\hat{\boldsymbol{R}}^{\alpha}_{xx}(\tau) = \left\langle \boldsymbol{x}(n)\boldsymbol{x}^{\dagger}(n+\tau)e^{-j2\pi\alpha n}\right\rangle_N = \frac{1}{N}\sum_{n=1}^{N} \boldsymbol{x}(n)\boldsymbol{x}^{\dagger}(n+\tau)e^{-j2\pi\alpha n} \tag{2.1.20}$$

and

$$\hat{\boldsymbol{R}}^{\alpha}_{xx^*}(\tau) = \left\langle \boldsymbol{x}(n)\boldsymbol{x}^{T}(n+\tau)e^{-j2\pi\alpha n}\right\rangle_N = \frac{1}{N}\sum_{n=1}^{N} \boldsymbol{x}(n)\boldsymbol{x}^{T}(n+\tau)e^{-j2\pi\alpha n} \tag{2.1.21}$$

respectively, where $\dagger$ denotes the conjugate transpose and T denotes the transpose.

2.2 Cyclostationarity of BPSK Signal

In this section, we examine the cyclostationarity of communication signals by analytic and simulation methods. We choose the BPSK signal as a typical example. Based on the BPSK signal model, we analyze the cyclostationarity of the signal and verify it by simulation methods.

The BPSK signal model: The BPSK (Binary Phase Shift Keying) signal can be modeled as [43]

$$x(t) = \sum_{k=-\infty}^{\infty} d_k g(t - kT_b)\cos(2\pi f_c t) \tag{2.2.1}$$

where T_b is the baud duration, f_c is the carrier frequency. $g(t)$ is the impulse response of the pulse shaping filter. A common pulse shaping function is the Nyquist-shaping pulse which can be modeled in the time domain as

$$g(t) = \mathrm{sinc}(2Bt)\frac{\cos(2\pi\rho Bt)}{1 - 16\rho^2 B^2 t^2} \tag{2.2.2}$$

where $B = \frac{1}{T_b}$ and ρ is the roll-off factor which is equal to 1 for 100% roll-off. d_k is a zero mean white binary sequence. It can be viewed as a sampled sequence of a continuous stationary white process $d(t)$, that is, the cyclic autocorrelation function of $d(t)$ is

$$R_{dd}^{\alpha}(\tau) = \left\langle d(t + \frac{\tau}{2})d^*(t - \frac{\tau}{2})e^{-j2\pi\alpha t}\right\rangle = \begin{cases} \delta(\tau) & \alpha = 0 \\ 0 & \alpha \neq 0 \end{cases} . \tag{2.2.3}$$

The cyclostationarity of BPSK signal: Using Eqs. (2.1.14) and (2.2.1), we obtain the cyclic autocorrelation function of $x(t)$ as

$$R_{xx}^{\alpha}(\tau) = \frac{1}{2}R_{aa}^{\alpha}(\tau)\cos(2\pi f_c\tau) + \frac{1}{4}R_{aa}^{\alpha+2f_c}(\tau) + \frac{1}{4}R_{aa}^{\alpha-2f_c}(\tau) \tag{2.2.4}$$

where $R_{aa}^{\alpha}(\tau)$ is the cyclic autocorrelation function of $a(t)$. $a(t)$ is defined as

$$a(t) = \sum_{k=-\infty}^{\infty} d_k g(t - kT_b) = \sum_{k=-\infty}^{\infty} d_k \int_{-\infty}^{\infty} g(t-\tau)\delta(\tau - kT_b)d\tau \tag{2.2.5}$$

$$= \int_{-\infty}^{\infty} g(t-\tau) \sum_{k=-\infty}^{\infty} d_k \delta(\tau - kT_b) d\tau = g(t) \star q(t)$$

where $q(t) = \sum_{k=-\infty}^{\infty} d_k \delta(\tau - kT_b)$. This equation shows that $a(t)$ is the output of a time invariant filter $g(t)$ when input is $q(t)$. Using the Fourier transform on Eq. (2.2.4), we obtain the cyclic spectral density function of $x(t)$ as

$$S_{xx}^{\alpha}(f) = \frac{1}{4}\left[S_{aa}^{\alpha}(f+f_c) + S_{aa}^{\alpha}(f-f_c) + S_{aa}^{\alpha+2f_c}(f) + S_{aa}^{\alpha-2f_c}(f)\right] \tag{2.2.6}$$

where $S_{aa}^{\alpha}(f)$ is the cyclic spectral density function of $a(t)$.

Using the input output cyclic spectral density relationship for filtering [20] to Eq. (2.2.5), we obtain

$$S_{aa}^{\alpha}(f) = G(f+\alpha/2) S_{qq}^{\alpha}(f) G^*(f-\alpha/2) \tag{2.2.7}$$

where $G(f)$ is the Fourier transformation of $g(t)$. $S_{qq}^{\alpha}(f)$ is the cyclic spectral density function of $q(t)$. Moreover, expanding $\sum_{k=-\infty}^{\infty} \delta(t - kT_b)$ as Fourier series, we have

$$q(t) = \sum_{k=-\infty}^{\infty} d_k \delta(t - kT_b) = d(t) \sum_{k=-\infty}^{\infty} \delta(t - kT_b) = \frac{1}{T_b} d(t) \sum_{k=-\infty}^{\infty} e^{j2\pi kt/T_b}. \tag{2.2.8}$$

Using Eq. (2.1.14), the cyclic autocorrelation function of $q(t)$ is

$$\begin{aligned} R_{qq}^{\alpha}(\tau) &= \left\langle d(t+\tau/2) d^*(t-\tau/2) \sum_{n_1=-\infty}^{\infty} \sum_{n_2=-\infty}^{\infty} \frac{1}{T_b^2} e^{j2\pi n_1 (t+\tau/2)/T_b} e^{-j2\pi n_2 (t-\tau/2)/T_b} e^{-j2\pi\alpha t} \right\rangle \\ &= \frac{1}{T_b^2} \sum_{n_1=-\infty}^{\infty} \sum_{n_2=-\infty}^{\infty} e^{j\pi n_1 \tau/T_b} e^{j\pi n_2 \tau/T_b} R_{dd}^{\alpha+(n_2-n_1)/T_b)}(\tau) \end{aligned} \tag{2.2.9}$$

where $R_{dd}^{\alpha}(\tau)$ is the cyclic autocorrelation function of $d(t)$. Letting $m = n_2 - n_1$, $n = n_1$, we have

$$R_{qq}^{\alpha}(\tau) = \frac{1}{T_b^2} \sum_{n,m} e^{j2\pi n\tau/T_b} e^{j\pi m\tau/T_b} R_{dd}^{\alpha+m/T_b}(\tau). \tag{2.2.10}$$

The Fourier transformation of $R_{qq}^{\alpha}(\tau)$ is

$$S_{qq}^{\alpha}(f) = \frac{1}{T_b^2} \sum_{n,m} S_{dd}^{\alpha-m/T_b}(f - m/2T_b - n/T_b). \tag{2.2.11}$$

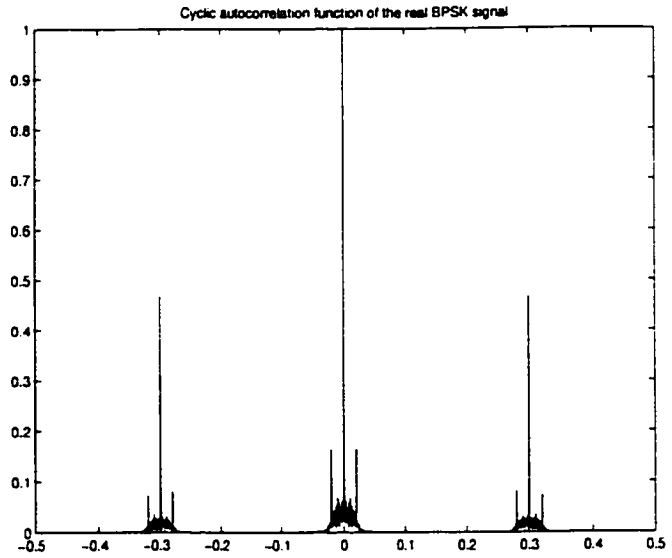

Figure 2.2: Cyclic autocorrelation function of BPSK signal when the Nyquist-shaped filter has a 100% roll-off factor

Because $d(t)$ is a stationary process, we obtain

$$S_{qq}^{\alpha}(f) = \begin{cases} \frac{1}{T_b^2}\sum_{n,m} S_{dd}(f - m/2T_b - n/T_b) & \alpha = m/T_b \\ 0 & \alpha \neq m/T_b \end{cases} = S_{qq}(f)\delta(\alpha - m/T_b) \quad (2.2.12)$$

where $\delta(.)$ denotes Kronecker delta function. $S_{qq}(f) = \frac{1}{T_b^2}\sum_{n,m} S_{dd}(f + m/2T_b + n/T_b)$, $S_{dd}(f)$ is the power spectrum density of $d(t)$. After normalizing $S_{qq}(f)$ to be one and substituting Eq. (2.2.12) into Eq. (2.2.7), we have

$$S_{aa}^{\alpha}(f) = \begin{cases} G(f + \alpha/2)G^*(f - \alpha/2) & \alpha = m/T_b \\ 0 & \alpha \neq m/T_b \end{cases} . \quad (2.2.13)$$

Substituting Eq. (2.2.13) into Eq. (2.2.6), we obtain

$$S_{xx}^{\alpha}(f) = \frac{1}{4}\begin{cases} G(f + f_c + \frac{\alpha}{2})G^*(f + f_c - \frac{\alpha}{2}) & \\ +G(f - f_c + \frac{\alpha}{2})G^*(f - f_c - \frac{\alpha}{2}) & \alpha = m/T_b \\ G(f + \alpha/2)G^*(f - \alpha/2) & \alpha = \pm 2f_c + m/T_b \\ 0 & \text{otherwise} \end{cases} . \quad (2.2.14)$$

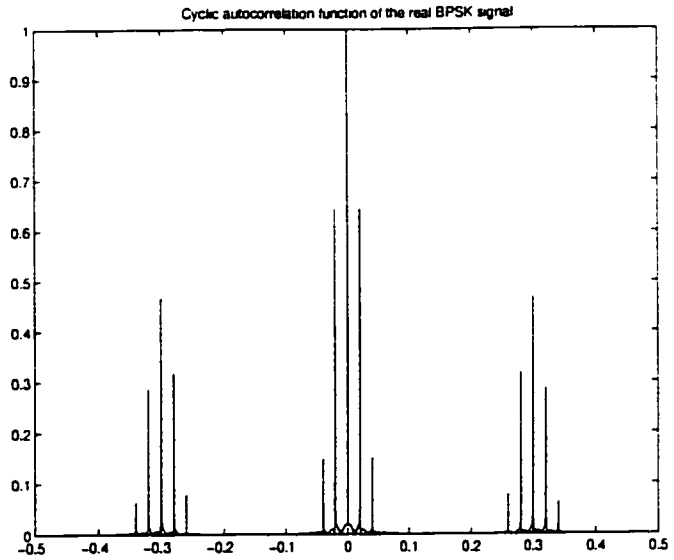

Figure 2.3: Cyclic autocorrelation function of BPSK signal when the Nyquist-shaped filter has a 300% roll-off factor

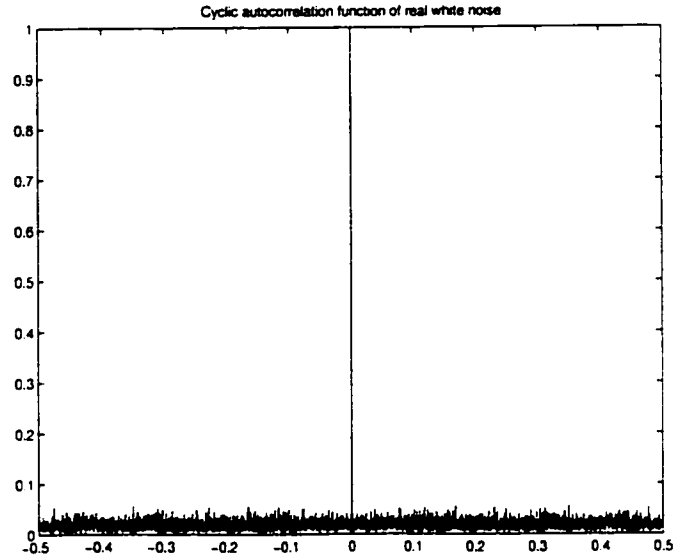

Figure 2.4: Cyclic autocorrelation function of white noise

From Eq. (2.2.14), we see that the cycle frequencies of the BPSK signal appear at $\alpha = \pm 2f_c + m/T_b$ and $\alpha = m/T_b$, where $m \in \{0, \pm 1 \ldots\}$ and T_b is the baud period, f_c is the carrier frequency of the BPSK signal.

Now, we use simulation to verify the result. In our simulation, the message signal is a binary Nyquist-shaped pulse sequence with amplitude at $\{-1, 1\}$. The baud rate and carrier frequency is normalized with the sampling rate. The normalized baud rate is 0.02. The normalized frequency f_c of the BPSK signal is chosen to be 0.15. τ is equal to zero. When the Nyquist-shaped filter has a 100% roll-off factor, the cyclic autocorrelation function of the BPSK signal is plotted against the frequency shift α in Fig. 2.2. We can see that a strong spectral line is locating at $\alpha = \pm 0.3$ and pairs of weaker spectral lines are locating at $\alpha = \pm 0.02, 0.3 \pm 0.02$ and -0.3 ± 0.02 respectively. This result matches the analytic result. For same scenario, when the Nyquist-shaped filter has a 300% roll-off factor, the cyclic autocorrelation function of the BPSK signal is plotted against the frequency shift α in Fig. 2.3. Comparing Fig. 2.2 with Fig. 2.3, we find that the cyclostationarity of the BPSK signal is increased when the roll-off factor is increased. We also plot the cyclic autocorrelation function of white noise in Fig. 2.4. It is shown that there is no spectral line at non-zero frequency shift α.

2.3 Examples of the Cyclostationarity of Other Communication Signals

In this section, we continue to study the cyclostationarity of some communication signals.

The DSB-AM Signal The signal model for a DSB-AM (Double Side Band - Amplitude Modulation) signal is

$$x(t) = m(t)\cos(2\pi f_c t + \theta), \tag{2.3.1}$$

where f_c is the carrier frequency, θ is the initial phase and $m(t)$ is the band limited real message signal. In addition, the sampled message $m(n)$ is assumed to be highly correlated with itself but less correlated with the frequency shifted version of itself. Its autocorrelation

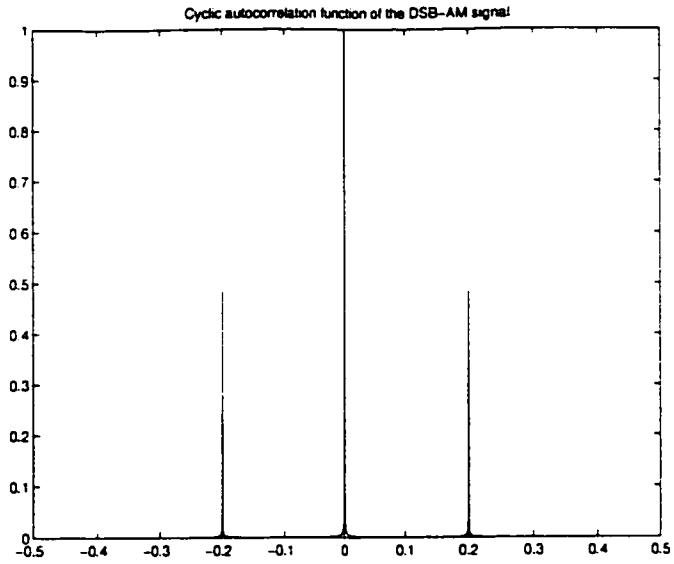

Figure 2.5: The Cyclic autocorrelation function of DSB-AM signal

function $R(t,\tau)$ is

$$R_x(t+\tau/2, t-\tau/2) = \frac{1}{2}R_m(\tau)(\cos(2\pi f_c\tau) + \cos(2\pi 2f_c t + 2\theta)). \tag{2.3.2}$$

Obviously, this is periodic function in t. The period is $1/2f_c$. So the cyclic frequency $\alpha = 2f_c$. we would expect that there are sharp spectral lines located at frequency shift $\alpha = 2f_c$. In our simulation, the normalized carrier frequency f_c is chosen to be 0.1. In Figure 2.5, the cyclic autocorrelation function of the signal $s(t)$ is plotted against the frequency shift α. As expected, we can see that a strong spectral line is located at $\alpha = \pm 0.2$. We further study this signal. By taking the cyclic autocorrelation of the signal $x(t)$, we obtain

$$R_x^\alpha(\tau) = \left\langle x(t+\frac{\tau}{2})x^*(t-\frac{\tau}{2})e^{-j2\pi\alpha t}\right\rangle \tag{2.3.3}$$

$$= \frac{1}{4}e^{j2\pi f_c\tau}\left\langle m(t+\frac{\tau}{2})m^*(t-\frac{\tau}{2})e^{-j2\pi\alpha t}\right\rangle + \frac{1}{4}e^{-j2\pi f_c\tau}\left\langle m(t+\frac{\tau}{2})m^*(t-\frac{\tau}{2})e^{-j2\pi\alpha t}\right\rangle$$

$$+\frac{1}{4}e^{j2\theta}\left\langle m(t+\frac{\tau}{2})m^*(t-\frac{\tau}{2})e^{-j2\pi(\alpha-2f_c)t}\right\rangle + \frac{1}{4}e^{-j2\theta}\left\langle m(t+\frac{\tau}{2})m^*(t-\frac{\tau}{2})e^{-j2\pi(\alpha+2f_c)t}\right\rangle.$$

because $m(t)$ is stationary signal, when $\theta = 0$, we obtain

$$R_x^\alpha(\tau) = \begin{cases} \frac{1}{4}R_m(\tau)(e^{j2\pi f_c\tau} + e^{-j2\pi f_c\tau}) & \alpha = 0 \\ \frac{1}{4}R_m(\tau) & \alpha = \pm 2f_c \\ 0 & \text{otherwise.} \end{cases} \tag{2.3.4}$$

By taking Fourier transform, we get the cyclic spectrum density of $x(t)$ as follow:

$$S_x^\alpha(f) = \begin{cases} \frac{1}{4}S_m(f + f_c) + \frac{1}{4}S_m(f - f_c) & \alpha = 0 \\ \frac{1}{4}S_m(f) & \alpha = \pm 2f_c \\ 0 & \text{otherwise.} \end{cases} \tag{2.3.5}$$

The QPSK Signal The QPSK (Qudriphase-Shift Keying) signal can be modeled as

$$x(t) = m_1(t)\cos(2\pi f_c t) - m_2(t)\sin(2\pi f_c t), \tag{2.3.6}$$

where

$$m_1(t) = \sum_{k=-\infty}^{\infty} u_k p(t - kT_b), \quad m_2(t) = \sum_{k=-\infty}^{\infty} v_k p(t - kT_b). \tag{2.3.7}$$

Here T_b is the baud duration, f_c is the carrier frequency. u_k and v_k are a stationary white binary sequence respectively. They are assumed to be independent. $p(t)$ is the impulse response of a Nyquist-shaped filter with a roll-off factor. By using definition of cyclic correlation function, we obtain

$$\begin{aligned} R_x^\alpha(\tau) &= \frac{1}{2}\left[R_{m_1}^\alpha(\tau) + R_{m_2}^\alpha(\tau)\right]\cos(2\pi f_c\tau) + \frac{1}{2}\left[R_{m_1m_2}^\alpha(\tau) - R_{m_2m_1}^\alpha(\tau)\right]\sin(2\pi f_c\tau) \\ &\quad + \frac{1}{4}\sum_{n=-1,1}\left\{\left[R_{m_1}^{\alpha+2nf_c}(\tau) - R_{m_2}^{\alpha+2nf_c}(\tau)\right] - nj\left[R_{m_2m_1}^{\alpha+2nf_c}(\tau) + R_{m_2m_1}^{\alpha+2nf_c}(\tau)\right]\right\} \end{aligned} \tag{2.3.8}$$

By using the Fourier transform, we obtain

$$S_x^\alpha(f) = \frac{1}{4}\sum_{n=-1,1}\left\{\left[S_{m_1}^\alpha(f + nf_c) + S_{m_2}^\alpha(f + nf_c)\right] - nj\left[S_{m_2m_1}^\alpha(f + nf_c) - S_{m_1m_2}^\alpha(f + nf_c)\right]\right\}$$

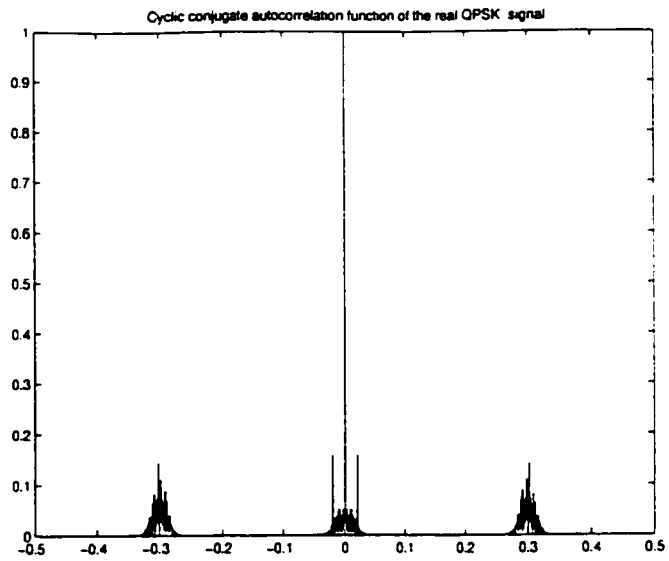

Figure 2.6: Cyclic autocorrelation function of QPSK signal when the Nyquist-shaped filter has a 100% roll-off factor

$$+\frac{1}{4}\sum_{n=-1,1}\left\{\left[S_{m_1}^{\alpha+2nf_c}(f)-S_{m_2}^{\alpha+2nf_c}(f)\right]-nj\left[S_{m_2m_1}^{\alpha+2nf_c}(f)+S_{m_1m_2}^{\alpha+2nf_c}(f)\right]\right\} \tag{2.3.9}$$

For balanced QPSK signal, we have

$$S_{m_1}^{\alpha}(f)=S_{m_2}^{\alpha}(f) \tag{2.3.10}$$

Because $m_1(t)$ and $m_2(t)$ are uncorrelated, we obtain

$$S_x^{\alpha}(f)=\frac{1}{2}\sum_{n=-1,1}S_{m_1}^{\alpha}(f+nf_c)=\frac{1}{2}\left[S_{m_1}^{\alpha}(f+f_c)+S_{m_1}^{\alpha}(f-f_c)\right] \tag{2.3.11}$$

Calculating $S_{m_1}^{\alpha}(f)$, we obtain

$$S_x^{\alpha}(f)=\begin{cases}\frac{1}{2}[P(f+f_c+\alpha/2)P^*(f+f_c-\alpha/2) & \\ \quad +P(f-f_c+\alpha/2)P^*(f-f_c-\alpha/2)] & \alpha=m/T_b \\ 0 & \alpha\neq m/T_b\end{cases} \tag{2.3.12}$$

where $P(f)$ is the Fourier transform of $p(t)$. From Eq. (2.3.12), we see that the cycle frequencies of the balanced QPSK signal appear at $\alpha=m/T_b$, where m is an integer. Now,

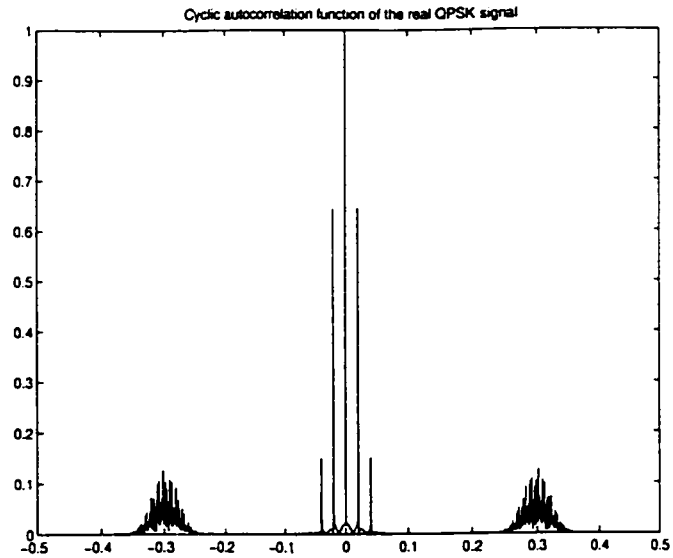

Figure 2.7: Cyclic autocorrelation function of QPSK signal when the Nyquist-shaped filter has a 300% roll-off factor

we use simulation to verify the result. In our simulation, the message signal is a binary Nyquist-shaped pulse sequence with amplitude at $\{-1, 1\}$. The normalized baud rate is 0.02 and the normalized frequency f_c of the QPSK signal is chosen to be 0.15. When the Nyquist-shaped filter has a 100% roll-off factor, the cyclic autocorrelation function of the QPSK signal is plotted against the frequency shift α in Fig. 2.6. We can see that a pair of the spectral line are locating at $\alpha = \pm 0.02$. The balanced QPSK signal has no spectral line at $\pm 2f_c$. This result matches the analytic result. When the Nyquist-shaped filter has a 300% roll-off factor, the cyclic autocorrelation function of the QPSK signal is plotted against the frequency shift α in Fig. 2.7. Comparing Fig. 2.6 with Fig. 2.7, we observed that the cyclostationarity of the QPSP signal is increased when the roll-off factor of the Nyquist-shaped filter is increased.

2.4 Exploitation of Cyclostationarity for Signal Extraction

In a multi-user communication system such as the mobile wireless communication system, a commonly encountered problems is the extraction of the desired signal from co-channel

interference (CCI) and adjacent channel interference (ACI) which may overlap spectrally or spatially with the desired signal. We know that most man-made signals exhibit cyclostationarity. In practice, the cycle frequencies of these co-channel and adjacent channel interfering signal and those of the desired signal are usually distinct and only dependent on their relative baud rate and their unique carrier frequency. This distinctive characteristic of spectral redundancy allows the possibility of signal extraction. As a result, signals can be extracted by using the knowledge of their own cycle frequency α, even when all the signals are occupying the same spectral band. For example, by considering a received signal

$$x(n) = \sum_{l=1}^{L} s_l(n) + \nu(n) \tag{2.4.1}$$

where $s_l(n)$ for $l \in \{1, \cdots L\}$ represent both the desired signal and the interfering signals, all of which are assumed to be statistically independent to each other, and $\nu(n)$ is the additive white noise. The cyclic autocorrelation of the received signal can be expressed as

$$\hat{R}^{\alpha}_{xx}(0) = \sum_{l=1}^{L} \hat{R}^{\alpha}_{ss_l}(0) + \hat{R}^{\alpha}_{\nu\nu}(0). \tag{2.4.2}$$

If there is only the desired signal $s_k(n)$ which exhibit cyclostationarity at α_k, then we have

$$\hat{R}^{\alpha_k}_{xx}(0) = \hat{R}^{\alpha_k}_{ss_k}(0). \tag{2.4.3}$$

Therefore, the cyclic autocorrelation of $s_k(n)$ is selected regardless of the temporal or spatial overlap among the interference and noise. In fact, this property also can be used in other signal processing tasks to improve the performances of those signal processors. In this thesis, we mainly use this property for signal extraction.

It is worthy to point out that the cyclostationarity of a signal (the spectral redundancy of the signal) is usually related to the bandwidth requirement of the signal. Generally speaking, the greater the excess bandwidth of a digital signal (bandwidth is excess of the Nyquist bandwidth of $\frac{1}{2T_b}$, where T_b is the band rate of the signal) is, the more the cyclic frequencies with nonzero cyclic spectrum density (or cyclic conjugate spectrum density) exist [37]. The spectral redundancy inherent in the excess bandwidth can be used effectively

to improve system performance, but the price is that high bandwidth-efficiency is reduced. In practice, we have to make tradeoffs between the spectral redundancy and the spectral efficiency in a system design.

Chapter 3

The BA-FRESH Algorithm and Its Convergence

In a multi-user communication system, a commonly encountered problem is the extraction of the desired signal from co-channel interference which may overlap spectrally with the desired signal. In such cases, conventional filtering techniques [7] are unable to carry out the job. The optimum frequency-shift (FRESH) filtering technique, proposed by W. A. Gardner [13] enables us to separate spectrally overlapped signals by using the cyclostationarity of the signals. To design the cyclic Wiener filter, however, we must have the statistical knowledge of the desired signal or a training signal which, in practice, are not often available. In this Chapter, we propose an alternative blind adaptive FRESH filtering technique using the knowledge of signal cyclostationarity to extract the desired signal from the spectrally overlapping interference. We call this new technique blind adaptive (BA)-FRESH filtering. The structure of this BA-FRESH filter [16] is proposed. We proved that the BA-FRESH algorithm is equivalent to the trained adaptive FRESH (TA-FRESH) algorithm when observed data length is infinite. Recursive implementation formula of the BA-FRESH filter is given. For the BA-FRESH and TA-FRESH algorithms, the convergence of the filter coefficients, the output SINR, and the output MSE are analyzed. Finally, Numerical results are presented to examine these results theoretically and by simulations.

3.1 The FRESH Filtering Algorithm

Consider the situation where the input $x(t)$ of the FRESH filter consists of the desired signal $s(t)$ corrupted by an interfering signal $u(t)$ which may spectrally overlap with $s(t)$ together with white noise $\nu(t)$, i.e.,

$$x(t) = s(t) + u(t) + \nu(t). \tag{3.1.1}$$

Consider a FRESH filter whose input and output are related [13]

$$y(t) = \int_{-\infty}^{\infty} h(t,\tau)x(\tau)d\tau \tag{3.1.2}$$

where $x(t)$ is the filter's input, $y(t)$ is the filter's output, and $h(t,\tau)$ is the impulse response function of the time variant filter. Here we assume that the input signal is a real signal. The impulse response $h(t,\tau)$ is a function of two variable t and τ. where t represents the output time and τ represents the input time. In practice, the filter can be used to do the better job of receiving $s(t)$ from the corrupted signal $x(t)$ than the time invariant filter does. $h(t,\tau)$ is assumed to be a periodic function. $h(t,\tau)$ can be expanded in following series form [37]

$$h(t,\tau) = \sum_{m=1}^{M} h_m(t-\tau)e^{j2\pi\alpha_m\tau} \tag{3.1.3}$$

where α_m $(m = 1, 2, \cdots M)$ is the cycle frequencies of a desired signals. M is the number of branches in the FRESH filter. Obviously, when $M = 1$ and $\alpha_1 = 0$, $h(t,\tau) = h(t-\tau)$. This is the time-invariant case. Substituting Eq. (3.1.3) into Eq. (3.1.2), we obtain the output of the filter as

$$y(t) = \int_{-\infty}^{\infty} \sum_{m=1}^{M} h_m(t-\tau)e^{j2\pi\alpha_m\tau}x(\tau)d\tau = \sum_{m=1}^{M} h_m(t) \star \left[x(t)e^{j2\pi\alpha_m t}\right] \tag{3.1.4}$$

where $\star$ denotes convolution. The Fourier transform of $y(t)$ is

$$Y(f) = \sum_{m=1}^{M} H_m(f)X(f-\alpha_m) \tag{3.1.5}$$

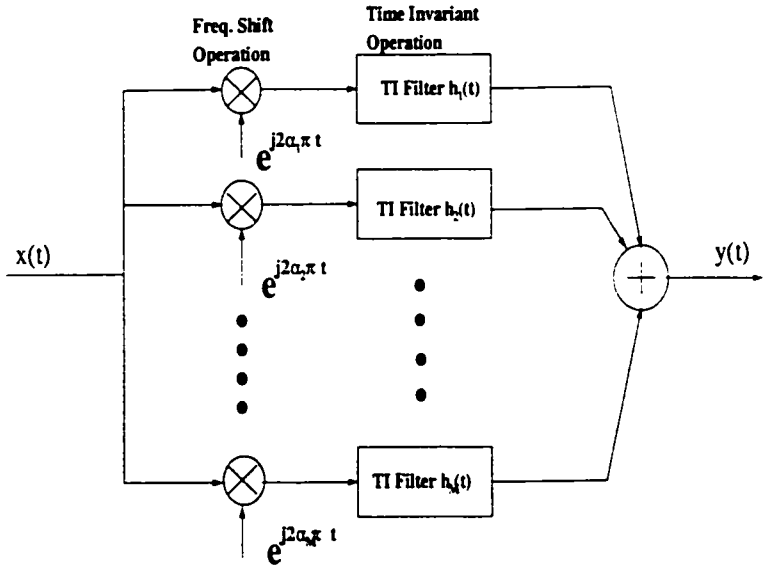

Figure 3.1: Structure of the FRESH filter

where $H_m(f)$ is the Fourier transformation of $h_m(t)$. $h_m(t)$ is the impulse response of the mth FIR filter of the FRESH filter. $X(f)$ is the Fourier transformation of the input $x(t)$. The formula show that the input is subjected to frequency shift operation, then followed by Time-Invariant (TI) filtering operation. So it is called as FREquency SHift (FRESH) filter. The structure of FRESH filter is shown in Fig. 3.1. When we know the cycle frequencies of the desired signal α_m $(m = 1, 2, \cdots M)$, the frequency shift part is determined. Now the problem is how to optimally determine transfer function $H_m(f)$, $m = 1, 2, \cdots M$.

In order to optimally determine the transfer function $H_m(f)$, the time averaged Minimum Mean Square Error (MMSE) criteria is considered

$$\min_{\boldsymbol{h}} J = \min_{\boldsymbol{h}} \left\langle (s(t) - y(t))^2 \right\rangle \tag{3.1.6}$$

where $\langle \cdot \rangle$ denotes the time average. $s(t)$ is the desired signal. $y(t)$ is the output of the FRESH filter. $\boldsymbol{h}(t)$ is the impulse response vector of the time-invariant filters. It can be expressed as

$$\boldsymbol{h}(t) = [h_1(t) \;\; h_2(t) \;\; \cdots \;\; h_M(t)]^T . \tag{3.1.7}$$

From Eq. (3.1.4), we know

$$y(t) = \sum_{m=1}^{M} \int_{-\infty}^{\infty} h_m(\tau) e^{j2\pi\alpha_m(t-\tau)} x(t-\tau) d\tau. \tag{3.1.8}$$

It means that $y(t)$ is linear combination of all variables $x(t-\tau)e^{j2\pi\alpha_m(t-\tau)}$. Let these variables span a subspace Υ. In non-probabilistic theory, an inner product in Υ is defined as

$$(x, y) = \langle xy^* \rangle \tag{3.1.9}$$

where $*$ denotes the conjugate. $(.,.)$ denotes the inner product. $\langle \cdot \rangle$ denotes the time average. Using the projection theorem in Hilbert space, we can obtain the necessary and sufficient orthogonal condition for minimum error in Eq. (3.1.6), that is,

$$\left(s(t) - y(t), x(t-\tau)e^{j2\pi\alpha_m(t-\tau)}\right) = \left\langle (s(t) - y(t)) x^*(t-\tau) e^{-j2\pi\alpha_m(t-\tau)} \right\rangle = 0. \tag{3.1.10}$$

It shows that the error $s(t) - y(t)$ must be orthogonal (zero correlation) to all variables $x(t-\tau)e^{j2\pi\alpha_k(t-\tau)}$. Substituting Eq. (3.1.4) into Eq. (3.1.10), we obtain

$$\left\langle (s(t)x^*(t-\tau)e^{-j2\pi\alpha_k(t-\tau)} - \left[\sum_{m=0}^{M} h_m(t) \star x(t)e^{j2\pi\alpha_m t}\right] x^*(t-\tau)e^{-j2\pi\alpha_k(t-\tau)} \right\rangle = 0. \tag{3.1.11}$$

Let $t = t_1 + \tau/2$ and using the definition of the cyclic cross-correlation function, we can obtain from the first term of Eq (3.1.11),

$$\left\langle (s(t_1 + \tau/2)x^*(t_1 - \tau/2)e^{-j2\pi\alpha_k(t_1 - \tau/2)} \right\rangle = R_{sx}^{\alpha_k}(\tau) e^{j\pi\alpha_k\tau}. \tag{3.1.12}$$

Computing the second term of Eq. (3.2.11), we obtain

$$\left\langle \left[\sum_{m=1}^{M} h_m(t) \star x(t)e^{j2\pi\alpha_m t}\right] x^*(t-\tau)e^{-j2\pi\alpha_k(t-\tau)} \right\rangle = \sum_{m=1}^{M} h_m(\tau) \star R_{xx}^{\alpha_k - \alpha_m}(\tau) e^{j\pi(\alpha_k + \alpha_m)\tau}. \tag{3.1.13}$$

Therefore, we have

$$R_{sx}^{\alpha_k}(\tau)e^{j\pi\alpha_k\tau} - \sum_{m=1}^{M} h_m(\tau) \star R_{xx}^{\alpha_k-\alpha_m}(\tau)e^{j\pi(\alpha_k+\alpha_m)\tau} = 0. \tag{3.1.14}$$

Taking the Fourier transformation of Eq. (3.3.14), we obtain

$$\sum_{m=1}^{M} H_m(f)S_{xx}^{\alpha_k-\alpha_m}(f-(\alpha_k+\alpha_m)/2) = S_{sx}^{\alpha_k}(f-\alpha_k/2) \tag{3.1.15}$$

where $k = 1, 2, \cdots M$. When we define following matrixes

$$\boldsymbol{S}_{xx}^{\alpha}(f) = \begin{pmatrix} S_{xx}^{\alpha_1-\alpha_1}(f-(\alpha_1+\alpha_1)/2) & \cdots S_{xx}^{\alpha_1-\alpha_M}(f-(\alpha_1+\alpha_M)/2) \\ S_{xx}^{\alpha_2-\alpha_1}(f-(\alpha_2+\alpha_1)/2) & \cdots S_{xx}^{\alpha_2-\alpha_M}(f-(\alpha_2+\alpha_M)/2) \\ & \vdots \\ S_{xx}^{\alpha_M-\alpha_1}(f-(\alpha_M+\alpha_1)/2) & \cdots S_{xx}^{\alpha_M-\alpha_M}(f-(\alpha_M+\alpha_M)/2) \end{pmatrix} \tag{3.1.16}$$

$$\boldsymbol{H}(f) = \begin{pmatrix} H_1(f) \\ H_2(f) \\ \vdots \\ H_M(f) \end{pmatrix} \qquad \boldsymbol{S}_{sx}^{\alpha}(f) = \begin{pmatrix} S_{sx}^{\alpha_1}(f-\alpha_1/2) \\ S_{sx}^{\alpha_2}(f-\alpha_2/2) \\ \vdots \\ S_{sx}^{\alpha_M}(f-\alpha_M/2) \end{pmatrix}, \tag{3.1.17}$$

we can write Eq. (3.1.15) into a matrix form

$$\boldsymbol{S}_{xx}^{\alpha}(f)\boldsymbol{H}(f) = \boldsymbol{S}_{sx}^{\alpha}(f) \tag{3.1.18}$$

where $\boldsymbol{S}_{xx}^{\alpha}(f)$ is the auto-spectral density matrix of the input $x(t)$. $\boldsymbol{S}_{sx}^{\alpha}(f)$ is the cross-spectral density vector between the desired signal $s(t)$ and the input $x(t)$. This is the design equation of the optimum FRESH filter. From Eq. (3.1.18), we see that the design of an optimum FRESH filter to extract the desired signal necessitates knowledge of the auto-spectral density matrix of the input as well as the cross-spectral density vector between the input and the desired output. Alternatively, the standard LMS or RLS algorithms [7] can be used to design the optimum FRESH filter, in which case, a training signal is needed. In practice, it is not often available or it costs too much. To solve this problem, we propose a

blind adaptive FRESH filter in next section.

3.2 Proposed BA-FRESH Filtering Algorithm

In this section, we consider the case where there is no training signal and we have no knowledge of the statistics of the desired signal, i.e., we blindly adapt the FRESH filter with prior knowledge of only its modulation type, its carrier frequency, and its baud rate. Moreover, in order to implement our algorithms on computers, we use discrete time model in the following sections.

The real input $x(n)$ to the BA-FRESH filter consists of a desired signal $s(n)$ which is corrupted by an interfering signal $u(n)$ spectrally overlapping with $s(n)$ together with ergodic white noise $\nu(n)$, i.e.,

$$x(n) = s(n) + u(n) + \nu(n). \tag{3.2.1}$$

Our purpose is to extract the desired signal $s(n)$ by adjusting the FRESH filter coefficients so that the output closely approximates $s(n)$. Since there is no reference signal available, a suitable reference is created by adding a secondary branch so that the BA-FRESH filter is, as shown in Fig. 3.2, comprised of a primary branch consisting of a FRESH filter and a secondary branch. The output $r(n)$ of this secondary branch is an α'-shifted version of the input $x(n)$ where α' is a cycle frequency of $s(n)$. The rationale is that if the output $y(n)$ is a close approximation of $s(n)$ and is relatively free from containing $u(n)$ and $\nu(n)$, then it must have high correlation with the α'-shifted version of $s(n)$ and must have low correlation with the α'-shifted versions of $u(n)$ and $\nu(n)$ respectively. Thus, the correlation of the two signals may provide a measure of the suppression of the interference and the closeness of the output to the desired signal. In using this measure, we must ensure that the FRESH filter in the primary branch has no common frequency shift with the secondary branch.

Now, suppose the primary FRESH filter consists of M FIR filters each being of length N_o. Let the coefficients of the mth FIR filter be $h_m(n)$, then the coefficient vector

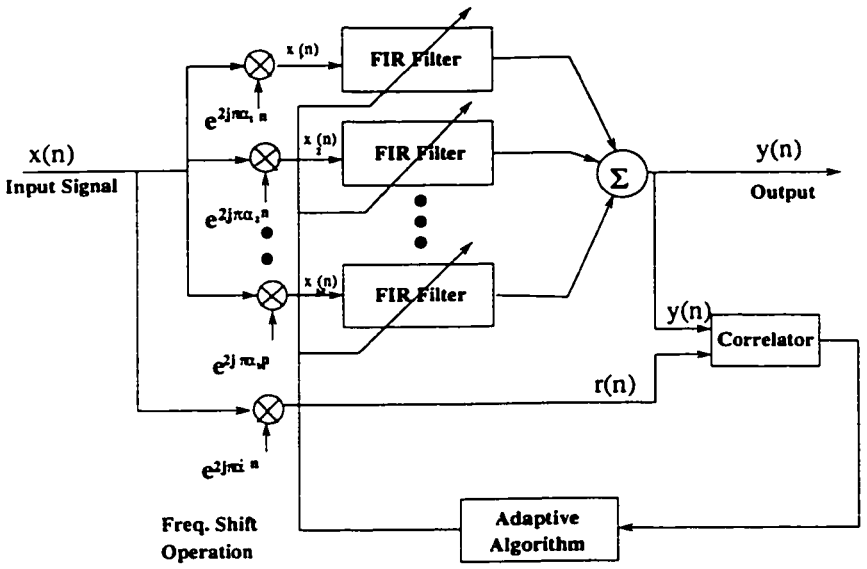

Figure 3.2: Structure of the BA-FRESH filter

of the filter is

$$\boldsymbol{h}_m = [h_m(0)\ \ h_m(1)\ \ \cdots\ \ h_m(N_o-1)]^T, \quad m = 1, 2, \cdots M. \tag{3.2.2}$$

Furthermore, if we denote the modulated input signal vector by $\tilde{\boldsymbol{x}}_m(n)$ such that

$$\tilde{\boldsymbol{x}}_m(n) = \left[x(n)e^{j2\pi\alpha_m n}\ \ \cdots\ \ x(n-N_o+1)e^{j2\pi\alpha_m(n-N_o+1)}\right]^T, \tag{3.2.3}$$

then the output $y(n)$ of the BA-FRESH filter can be written as

$$y(n) = \sum_{m=1}^{M} \boldsymbol{h}_m^{\dagger}\tilde{\boldsymbol{x}}_m(n) = \boldsymbol{h}^{\dagger}\tilde{\boldsymbol{x}}(n) \tag{3.2.4}$$

where $\dagger$ denoting the Hermitian conjugate of a vector or matrix. $\boldsymbol{h}$ and $\tilde{\boldsymbol{x}}(n)$ are defined respectively

$$\boldsymbol{h} = \left[\boldsymbol{h}_1^T\ \ \boldsymbol{h}_2^T\ \ \cdots\ \ \boldsymbol{h}_M^T\right]^T, \quad \text{and} \quad \tilde{\boldsymbol{x}}(n) = \left[\tilde{\boldsymbol{x}}_1^T(n)\ \ \tilde{\boldsymbol{x}}_2^T(n)\ \ \cdots\ \ \tilde{\boldsymbol{x}}_M^T(n)\right]^T. \tag{3.2.5}$$

With $\alpha' \neq \alpha_m$, $m = 1, 2, \cdots M$, the BA-FRESH filter seeks to maximize the normalized correlation between $y(n)$ and $r(n)$ by adjusting the coefficients of $\boldsymbol{h}$ where $r(n) = x(n)e^{j2\pi\alpha' n}$,

i.e.,

$$\max_{\boldsymbol{h}} J(\boldsymbol{h}) = \max_{\boldsymbol{h}} \frac{|R_{yr}|^2}{|R_{yy}|\,|R_{rr}|} \tag{3.2.6}$$

where

$$|R_{yr}|^2 = |\langle y(n)r^*(n)\rangle|^2 = |\boldsymbol{h}^\dagger \boldsymbol{\rho}_{\tilde{x}r}|^2 \tag{3.2.7}$$

$$|R_{yy}| = |\langle y(n)y^*(n)\rangle| = |\boldsymbol{h}^\dagger \boldsymbol{R}_{\tilde{x}\tilde{x}}\boldsymbol{h}| \tag{3.2.8}$$

$$|R_{rr}| = |\langle r(n)r^*(n)\rangle| \tag{3.2.9}$$

and $\boldsymbol{R}_{\tilde{x}\tilde{x}} = \langle \tilde{\boldsymbol{x}}(n)\tilde{\boldsymbol{x}}^\dagger(n)\rangle$, $\boldsymbol{\rho}_{\tilde{x}r} = \langle \tilde{\boldsymbol{x}}(n)r^*(n)\rangle$. We know by Cauchy-Schwarz inequality,

$$J(\boldsymbol{h}) = \frac{|\boldsymbol{h}^\dagger \boldsymbol{R}_{\tilde{x}\tilde{x}}^{1/2}\boldsymbol{R}_{\tilde{x}\tilde{x}}^{-1/2}\boldsymbol{\rho}_{\tilde{x}r}|^2}{|\boldsymbol{h}^\dagger \boldsymbol{R}_{\tilde{x}\tilde{x}}\boldsymbol{h}||R_{rr}|} \leq \frac{|\boldsymbol{h}^\dagger \boldsymbol{R}_{\tilde{x}\tilde{x}}^{1/2}|^2\,|\boldsymbol{R}_{\tilde{x}\tilde{x}}^{-1/2}\boldsymbol{\rho}_{\tilde{x}r}|^2}{|\boldsymbol{h}^\dagger \boldsymbol{R}_{\tilde{x}\tilde{x}}\boldsymbol{h}||R_{rr}|}. \tag{3.2.10}$$

For equality, we have

$$\boldsymbol{h}_{BF} = \boldsymbol{R}_{\tilde{x}\tilde{x}}^{-1}\boldsymbol{\rho}_{\tilde{x}r}. \tag{3.2.11}$$

Since $\boldsymbol{R}_{\tilde{x}\tilde{x}}$ is the correlation matrix of an ergodic process having no linear dependency between samples, then $\boldsymbol{R}_{\tilde{x}\tilde{x}}$ is almost positive definite and therefore non-singular [7]. Eq. (3.2.11) is the Wiener-Hopf equation for the BA-FRESH filter. The solution necessitates the knowledge of $\boldsymbol{R}_{\tilde{x}\tilde{x}}$ and $\boldsymbol{\rho}_{\tilde{x}r}$. If such knowledge is not available, then a recursive method for updating the tap-weights of the FRESH filter in the primary branch can be obtained following the Widrow-Hoff least-mean-square (LMS) algorithm [7] by using the output $r(n)$ of the secondary branch as the reference and choosing an appropriate step-size. Alternatively, we may window the frequency shifted data vectors $\tilde{\boldsymbol{x}}(n)$ to obtain finite-sample time-averaged estimates of the data correlation matrix $\boldsymbol{R}_{\tilde{x}\tilde{x}}$ and the cross-correlation vector $\boldsymbol{\rho}_{\tilde{x}r}$. Denote the N-sample estimated values of $\boldsymbol{R}_{\tilde{x}\tilde{x}}, \boldsymbol{\rho}_{\tilde{x}r}$, and $\boldsymbol{h}_{BF}$ by $\hat{\boldsymbol{R}}_{\tilde{x}\tilde{x}}(N)$, $\hat{\boldsymbol{\rho}}_{\tilde{x}r}(N)$, and $\hat{\boldsymbol{h}}_{BF}(N)$ respectively. Thus, from Eq. (3.2.11), we have

$$\hat{\boldsymbol{h}}_{BF}(N) = \hat{\boldsymbol{R}}_{\tilde{x}\tilde{x}}^{-1}(N)\hat{\boldsymbol{\rho}}_{\tilde{x}r}(N) = \langle \tilde{\boldsymbol{x}}(n)\tilde{\boldsymbol{x}}(n)^\dagger\rangle_N^{-1}\langle \tilde{\boldsymbol{x}}(n)r^*(n)\rangle_N \tag{3.2.12}$$

where

$$\hat{\boldsymbol{R}}_{\tilde{x}\tilde{x}}(n) = \left(1 - \frac{1}{n}\right)\hat{\boldsymbol{R}}_{\tilde{x}\tilde{x}}(n-1) + \frac{1}{n}\tilde{\boldsymbol{x}}(n)\tilde{\boldsymbol{x}}^\dagger(n) \tag{3.2.13}$$

and

$$\hat{\rho}_{\tilde{x}r}(n) = \left(1 - \frac{1}{n}\right)\hat{\rho}_{\tilde{x}r}(n-1) + \frac{1}{n}\tilde{\boldsymbol{x}}(n)r^*(n). \tag{3.2.14}$$

Using the matrix inversion lemma [7], we have

$$\boldsymbol{A}^{-1} = \boldsymbol{B}^{-1} - \frac{\boldsymbol{B}^{-1}\boldsymbol{C}\boldsymbol{C}^\dagger\boldsymbol{B}^{-1}}{1 + \boldsymbol{C}^\dagger\boldsymbol{B}^{-1}\boldsymbol{C}} \tag{3.2.15}$$

if

$$\boldsymbol{A} = \boldsymbol{B} + \boldsymbol{C}\boldsymbol{C}^\dagger \tag{3.2.16}$$

where $\boldsymbol{A}$ and $\boldsymbol{B}$ are non-singular square matrices. Then, we can apply Eq. (3.2.15) to Eq. (3.2.13) and obtain

$$\hat{\boldsymbol{R}}^{-1}_{\tilde{x}\tilde{x}}(n) = \frac{n}{n-1}\hat{\boldsymbol{R}}^{-1}_{\tilde{x}\tilde{x}}(n-1) - \frac{\frac{n}{(n-1)^2}\hat{\boldsymbol{R}}^{-1}_{\tilde{x}\tilde{x}}(n-1)\tilde{\boldsymbol{x}}(n)\tilde{\boldsymbol{x}}^\dagger(n)\hat{\boldsymbol{R}}^{-1}_{\tilde{x}\tilde{x}}(n-1)}{1 + \frac{1}{n-1}\tilde{\boldsymbol{x}}^\dagger(n)\hat{\boldsymbol{R}}^{-1}_{\tilde{x}\tilde{x}}(n-1)\tilde{\boldsymbol{x}}(n)}. \tag{3.2.17}$$

Thus the desired filter response at the Nth step is given by

$$\begin{aligned}\hat{\boldsymbol{h}}_{BF}(N) \;=\; & \left\{\boldsymbol{I} - \frac{\frac{1}{N-1}\hat{\boldsymbol{R}}^{-1}_{\tilde{x}\tilde{x}}(N-1)\tilde{\boldsymbol{x}}(N)\tilde{\boldsymbol{x}}^\dagger(N)}{1 + \frac{1}{N-1}\tilde{\boldsymbol{x}}^\dagger(N)\hat{\boldsymbol{R}}^{-1}_{\tilde{x}\tilde{x}}(N-1)\tilde{\boldsymbol{x}}(N)}\right\} \\ & \left\{\hat{\boldsymbol{h}}_{BF}(N-1) + \frac{1}{N-1}\hat{\boldsymbol{R}}^{-1}_{\tilde{x}\tilde{x}}(N-1)\tilde{\boldsymbol{x}}(N)r^*(N)\right\}.\end{aligned} \tag{3.2.18}$$

The Eq. (3.2.18) provides us with a means to utilize the previously calculated values and up-date the new filter coefficients.

If a copy of the desired signal $s(n)$ is available, we can use it as a reference instead of using $r(n)$. We call the optimum FRESH filter with a training signal as Trained Adaptive (TA)-FRESH filter. The TA-FRESH filter [20] is shown in Fig. 3.3. It can then be designed to minimize the mean-square error of the output. Here, the error is given by

$$e_{TF}(n) = s(n)e^{j2\pi\alpha' n} - y(n) = s(n)e^{j2\pi\alpha' n} - \boldsymbol{h}^\dagger\tilde{\boldsymbol{x}}(n) \tag{3.2.19}$$

and the cost function is $J_{TF} = E\left[e_{TF}(n)e^*_{TF}(n)\right]$. Using the gradient method shown in

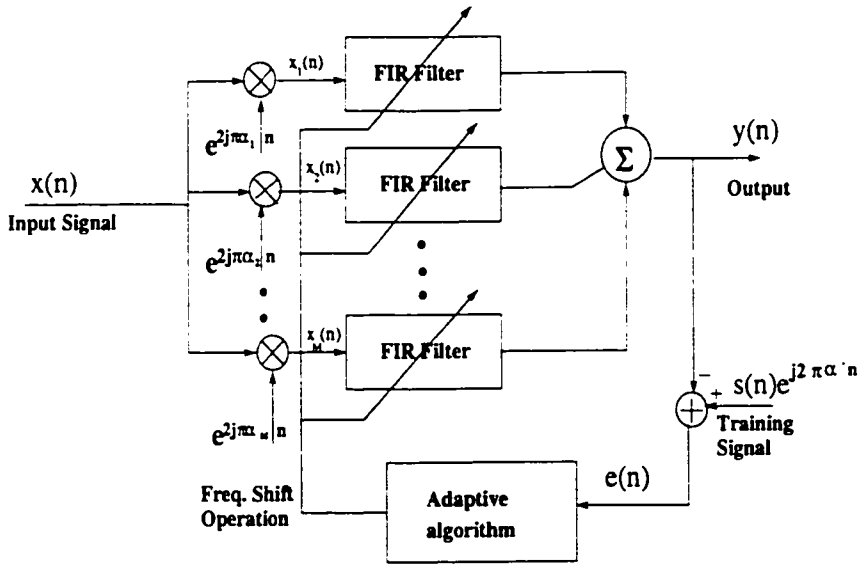

Figure 3.3: Structure of the TA-FRESH filter

Appendix A, we have this optimum solution of the TA-FRESH filter as

$$\boldsymbol{h}_{TF} = \boldsymbol{R}_{\tilde{x}\tilde{x}}^{-1}\boldsymbol{\rho}_{\tilde{x}\tilde{s}'} \tag{3.2.20}$$

where $\boldsymbol{\rho}_{\tilde{x}\tilde{s}'}$ is the cross-correlation vector between $\tilde{\boldsymbol{x}}(n)$ and $\tilde{s}'(n)$ with

$$\tilde{s}'(n) = s(n)e^{j2\pi\alpha' n}. \tag{3.2.21}$$

Denote the N-sample estimated values of $\boldsymbol{R}_{\tilde{x}\tilde{x}}, \boldsymbol{\rho}_{\tilde{x}\tilde{s}'}$, and $\boldsymbol{h}_{TF}$ by $\hat{\boldsymbol{R}}_{\tilde{x}\tilde{x}}(N)$, $\hat{\boldsymbol{\rho}}_{\tilde{x}\tilde{s}'}(N)$, and $\hat{\boldsymbol{h}}_{TF}(N)$ respectively. Thus, from Eq. (3.2.20), we have

$$\hat{\boldsymbol{h}}_{TF}(N) = \hat{\boldsymbol{R}}_{\tilde{x}\tilde{x}}^{-1}(N)\hat{\boldsymbol{\rho}}_{\tilde{x}\tilde{s}'}(N) = \langle\tilde{\boldsymbol{x}}(n)\tilde{\boldsymbol{x}}(n)^{\dagger}\rangle_N^{-1}\langle\tilde{\boldsymbol{x}}(n)\tilde{s}'^{*}(n)\rangle_N. \tag{3.2.22}$$

We note from Eqs. (3.2.11) and (3.2.20) that the difference between $\boldsymbol{h}_{BF}$ and $\boldsymbol{h}_{TF}$ is in the cross-correlation vector. Now, we show that $\boldsymbol{h}_{BF}$ and $\boldsymbol{h}_{TF}$ both have the same value under infinite sample time average realization.

Property 3.1: *Assume that Ψ_s is the set of cycle frequencies of desired signal and Ψ_u is the set of cycle frequency of interference. When the parameter α_m $m = 1, 2 \cdots M$ and α'*

satisfy

$$\alpha_m,\ (\alpha_m - \alpha') \in (\Psi_s - \Psi_u) \quad and \quad \alpha_m \neq \alpha', \quad \forall m, \tag{3.2.23}$$

the BA-FRESH filter and the TA-FRESH filter have same optimal filter coefficients $\boldsymbol{h}_{opt}$ *under infinite sample time average realization where*

$$\boldsymbol{h}_{opt} = \boldsymbol{R}_{\tilde{x}\tilde{x}}^{-1}\boldsymbol{\rho}_{\tilde{s}\tilde{s}'} = \boldsymbol{R}_{\tilde{x}\tilde{x}}^{-1}\left\langle \tilde{\boldsymbol{s}}(n)s^*(n)e^{-j2\pi\alpha' n}\right\rangle \tag{3.2.24}$$

with

$$\tilde{\boldsymbol{s}}(n) = \left[\tilde{\boldsymbol{s}}_1^T(n)\ \ \tilde{\boldsymbol{s}}_2^T(n)\ \ \cdots\ \ \tilde{\boldsymbol{s}}_M^T(n)\right]^T \tag{3.2.25}$$

and

$$\tilde{\boldsymbol{s}}_m(n) = \left[s(n)e^{j2\pi\alpha_m n}\ \ \cdots\ \ s(n-N_o+1)e^{j2\pi\alpha_m(n-N_o+1)}\right]^T, \tag{3.2.26}$$

$\tilde{s}'(n)$ *is defined in Eq. (3.2.21).*

Proof: The input $x(n)$ consists of the desired signal $s(n)$, the interference signal $u(n)$, and the noise $\nu(n)$. Thus,

$$\tilde{\boldsymbol{x}}(n) = \tilde{\boldsymbol{s}}(n) + \tilde{\boldsymbol{u}}(n) + \tilde{\boldsymbol{\nu}}(n) \tag{3.2.27}$$

where $\tilde{\boldsymbol{s}}(n)$ is defined in Eq. (3.2.25), $\tilde{\boldsymbol{u}}(n)$ and $\tilde{\boldsymbol{\nu}}(n)$ are similarly defined. The reference training signal $r(n)$ is,

$$r(n) = (s(n) + u(n) + \nu(n))e^{j2\pi\alpha' n}. \tag{3.2.28}$$

Because $s(n)$, $u(n)$, and $\nu(n)$ are independent, under the infinite sample time average realization, we have

$$\left\langle \tilde{\boldsymbol{s}}(n)u^*(n)e^{-j2\pi\alpha' n}\right\rangle = 0 \qquad \left\langle \tilde{\boldsymbol{s}}(n)\nu^*(n)e^{-j2\pi\alpha' n}\right\rangle = 0 \tag{3.2.29}$$

$$\left\langle \tilde{\boldsymbol{u}}(n)s^*(n)e^{-j2\pi\alpha' n}\right\rangle = 0 \qquad \left\langle \tilde{\boldsymbol{u}}(n)\nu^*(n)e^{-j2\pi\alpha' n}\right\rangle = 0 \tag{3.2.30}$$

$$\left\langle \tilde{\boldsymbol{\nu}}(n)s^*(n)e^{-j2\pi\alpha' n}\right\rangle = 0 \qquad \left\langle \tilde{\boldsymbol{\nu}}(n)u^*(n)e^{-j2\pi\alpha' n}\right\rangle = 0. \tag{3.2.31}$$

So we obtain

$$\boldsymbol{h}_{BF} = \boldsymbol{R}_{\tilde{x}\tilde{x}}^{-1}\left(\left\langle \tilde{\boldsymbol{s}}(n)s^*(n)e^{-j2\pi\alpha' n}\right\rangle + \left\langle \tilde{\boldsymbol{u}}(n)u^*(n)e^{-j2\pi\alpha' n}\right\rangle + \left\langle \tilde{\boldsymbol{\nu}}(n)\nu^*(n)e^{-j2\pi\alpha' n}\right\rangle\right). \tag{3.2.32}$$

We know

$$\left\langle \tilde{\boldsymbol{u}}(n)u^*(n)e^{-j2\pi\alpha' n}\right\rangle = \left\langle \begin{pmatrix} u(n)e^{j2\pi\alpha_1 n} \\ u(n-1)e^{j2\pi\alpha_1(n-1)} \\ \vdots \\ u(n-N_o+1)e^{j2\pi\alpha_1(n-N_o+1)} \\ u(n)e^{j2\pi\alpha_2 n} \\ u(n-1)e^{j2\pi\alpha_2(n-1)} \\ \vdots \\ u(n-N_o+1)e^{j2\pi\alpha_2(n-N_o+1)} \\ \vdots \\ u(n)e^{j2\pi\alpha_M n} \\ u(n-1)e^{j2\pi\alpha_M(n-1)} \\ \vdots \\ u(n-N_o+1)e^{j2\pi\alpha_M(n-N_o+1)} \end{pmatrix} u^*(n)e^{-j2\pi\alpha' n}\right\rangle. \tag{3.2.33}$$

Because we choose the parameters α_m and α' satisfy Eq. (3.2.23), we obtain

$$\left\langle \tilde{\boldsymbol{u}}(n)u^*(n)e^{-j2\pi\alpha' n}\right\rangle = 0. \tag{3.2.34}$$

Similarly, we have

$$\left\langle \tilde{\boldsymbol{\nu}}(n)\nu^*(n)e^{-j2\pi\alpha' n}\right\rangle = 0. \tag{3.2.35}$$

Therefore, we obtain

$$\boldsymbol{h}_{BF} = \boldsymbol{R}_{\tilde{x}\tilde{x}}^{-1}\boldsymbol{\rho}_{\tilde{s}s'} = \boldsymbol{h}_{opt}. \tag{3.2.36}$$

Using Eq. (3.2.20) and noting $s(n)$, $u(n)$, and $\nu(n)$ are independent, we obtain

$$\boldsymbol{h}_{TF} = \boldsymbol{R}_{\tilde{x}\tilde{x}}^{-1}\boldsymbol{\rho}_{\tilde{s}\tilde{s}'} = \boldsymbol{h}_{opt}. \quad \square \tag{3.2.37}$$

Property 3.1 shows that when data collection time is infinite, the optimum solution of the BA-FRESH filter is same as that of the TA-FRESH filter, as if we have the training signal.

It is worthy to point out that separation signal capability of BA-FRESH and TA-FRESH algorithm is related to not only the spectral overlapping percentage but also the excess bandwidth of signals. The excess bandwidth is directly determined by the pulse shaping roll-off coefficient. The greater excess bandwidth of a signal, the more spectrum redundancy, that is say, the increasing excess bandwidth is helpful to increasing the separation signal capability. For example, if QPSK signal are used with 30% excess bandwidth (roff-off factor = 0.3), overlapping of 40% will make them inseparable regardless of what filter coefficients are selected.

3.3 Convergence Rate of the Filter Coefficients

For the optimum filter coefficients of the BA-FRESH and TA-FRESH algorithms, there are differences between the finite sample time realization of the filter coefficients and the infinite sample time realization of the filter coefficients. When the number of sample goes to infinite, the differences will go to zero. In this section, we study the convergence of this difference. We know that the finite sample filter coefficients of the BA-FRESH and TA-FRESH filter are random variables. In this thesis, saying the convergence of random variables, we mean the convergence in mean square [85, 86]. A random sequence X_n is said to converge in mean square if there exists a random variable X such that

$$E\left[\|X_n - X\|^2\right] \to 0 \quad \text{as} \quad n \to \infty. \tag{3.3.1}$$

If Eq. (3.3.1) holds, then the random variable X is called the mean square limit of the sequence X_n. This definition also holds for random vectors. Moreover, we define the time-

averaged autocorrelation matrix and cross-correlation vector over N samples respectively as

$$\hat{\boldsymbol{R}}_{\tilde{x}\tilde{x}}(N) = \left\langle \tilde{\boldsymbol{x}}(n)\tilde{\boldsymbol{x}}^{\dagger}(n) \right\rangle_N \quad \text{and} \quad \hat{\boldsymbol{\rho}}_{\tilde{x}v}(N) = \left\langle \tilde{\boldsymbol{x}}(n)v^{*}(n) \right\rangle_N . \tag{3.3.2}$$

Thus, the finite-sample time-average realizations of $\boldsymbol{h}_{BF}$ and $\boldsymbol{h}_{TF}$ in Eqs. (3.2.11) and (3.2.20) are placed respectively by

$$\hat{\boldsymbol{h}}_{BF}(N) = \hat{\boldsymbol{R}}_{\tilde{x}\tilde{x}}^{-1}(N)\hat{\boldsymbol{\rho}}_{\tilde{x}r}(N) \quad \text{and} \quad \hat{\boldsymbol{h}}_{TF}(N) = \hat{\boldsymbol{R}}_{\tilde{x}\tilde{x}}^{-1}(N)\hat{\boldsymbol{\rho}}_{\tilde{x}\tilde{s}'}(N). \tag{3.3.3}$$

We further define the L_2-norms of a vector $\boldsymbol{v}$ and a matrix $\boldsymbol{A}$ respectively as

$$\|\boldsymbol{v}\| = \left(\boldsymbol{v}^{\dagger}\boldsymbol{v}\right)^{\frac{1}{2}} \quad \text{and} \quad \|\boldsymbol{A}\| = \max_{\|\boldsymbol{v}\|=1} \left(\|\boldsymbol{A}\boldsymbol{v}\|\right). \tag{3.3.4}$$

We now have the following property:

Theorem 3.1: *Let Ψ_s and Ψ_u respectively denote the set of cycle frequencies of the desired signal $s(n)$ and interference $u(n)$. Let α_m, $m = 1, 2 \cdots M$, and α' be respectively the frequency shift parameters in the primary and secondary branches of the BA-FRESH filter such that*

$$\alpha_m, \ (\alpha_m - \alpha') \in (\Psi_s - \Psi_u) \quad \textit{and} \quad \alpha_m \neq \alpha', \quad \forall m, \tag{3.3.5}$$

both $\hat{\boldsymbol{h}}_{BF}(N)$ and $\hat{\boldsymbol{h}}_{TF}(N)$ converge in the mean-square sense to

$$\boldsymbol{h}_{opt} = \boldsymbol{R}_{\tilde{x}\tilde{x}}^{-1}\boldsymbol{\rho}_{\tilde{s}\tilde{s}'} \tag{3.3.6}$$

where $\boldsymbol{h}_{opt}$ is defined in Eq. (3.2.24). Furthermore, the rates of convergence for both $\hat{\boldsymbol{h}}_{BF}(N)$ and $\hat{\boldsymbol{h}}_{TF}(N)$ are at $O(\frac{1}{N})$, where $O(\cdot)$ denotes "order of".

Proof: The input $x(n)$ consists of the desired signal $s(n)$, the interfering signal $u(n)$, and noise $\nu(n)$. Thus,

$$\tilde{\boldsymbol{x}}(n) = \tilde{\boldsymbol{s}}(n) + \tilde{\boldsymbol{u}}(n) + \tilde{\boldsymbol{\nu}}(n) \tag{3.3.7}$$

where $\tilde{\boldsymbol{s}}(n)$ is defined in Eqs. (3.2.25) and $\tilde{\boldsymbol{u}}(n)$ and $\tilde{\boldsymbol{\nu}}(n)$ are similarly defined. For finite

N, we have

$$\begin{aligned} E\left[\left\|\boldsymbol{R}_{\tilde{x}\tilde{x}}^{-1}-\hat{\boldsymbol{R}}_{\tilde{x}\tilde{x}}^{-1}(N)\right\|^2\right] &= E\left[\left\|\boldsymbol{R}_{\tilde{x}\tilde{x}}^{-1}(\hat{\boldsymbol{R}}_{\tilde{x}\tilde{x}}(N)-\boldsymbol{R}_{\tilde{x}\tilde{x}})\hat{\boldsymbol{R}}_{\tilde{x}\tilde{x}}^{-1}(N)\right\|^2\right] \\ &\leq \max\left[\left\|\hat{\boldsymbol{R}}_{\tilde{x}\tilde{x}}^{-1}(N)\right\|^2\right]\left\|\boldsymbol{R}_{\tilde{x}\tilde{x}}^{-1}\right\|^2 E\left[\left\|\hat{\boldsymbol{R}}_{\tilde{x}\tilde{x}}(N)-\boldsymbol{R}_{\tilde{x}\tilde{x}}\right\|^2\right] \end{aligned} \tag{3.3.8}$$

where we have used the Schwarz inequality. Now, from Eq. (3.3.2) and the property of matrix norms [70], we have

$$\begin{aligned} E\left[\left\|\hat{\boldsymbol{R}}_{\tilde{x}\tilde{x}}(N)-\boldsymbol{R}_{\tilde{x}\tilde{x}}\right\|^2\right] &\leq E\,tr\left[\left(\hat{\boldsymbol{R}}_{\tilde{x}\tilde{x}}(N)-\boldsymbol{R}_{\tilde{x}\tilde{x}}\right)\left(\hat{\boldsymbol{R}}_{\tilde{x}\tilde{x}}(N)-\boldsymbol{R}_{\tilde{x}\tilde{x}}\right)^{\dagger}\right] \\ &= trE\left[\frac{1}{N^2}\sum_{n=1}^{N}\left(\tilde{\boldsymbol{x}}(n)\tilde{\boldsymbol{x}}^{\dagger}(n)-\boldsymbol{R}_{\tilde{x}\tilde{x}}\right)\left(\tilde{\boldsymbol{x}}(n)\tilde{\boldsymbol{x}}^{\dagger}(n)-\boldsymbol{R}_{\tilde{x}\tilde{x}}\right)^{\dagger}\right] \\ &\quad +trE\left[\frac{1}{N^2}\sum_{\substack{m\\ m\neq n}}\sum_{n}\left(\tilde{\boldsymbol{x}}(m)\tilde{\boldsymbol{x}}^{\dagger}(m)-\boldsymbol{R}_{\tilde{x}\tilde{x}}\right)\left(\tilde{\boldsymbol{x}}(n)\tilde{\boldsymbol{x}}^{\dagger}(n)-\boldsymbol{R}_{\tilde{x}\tilde{x}}\right)^{\dagger}\right] \\ &= \frac{C_o}{N} \end{aligned} \tag{3.3.9}$$

where C_o is a constant. In the last step, we have used the fact that the desired signal $s(n)$ and the interference $u(n)$ are independent from symbol to symbol and the noise $\nu(n)$ is white. Therefore, we have

$$E\left[\left\|\hat{\boldsymbol{R}}_{\tilde{x}\tilde{x}}(N)-\boldsymbol{R}_{\tilde{x}\tilde{x}}\right\|^2\right]=O\left(\frac{1}{N}\right). \tag{3.3.10}$$

Using the boundedness of $\left\|\boldsymbol{R}_{\tilde{x}\tilde{x}}^{-1}\right\|^2$ and that of $\left\|\hat{\boldsymbol{R}}_{\tilde{x}\tilde{x}}^{-1}(N)\right\|^2$ with probability 1, together with Eq. (3.3.9) in Eq. (3.3.8), we obtain

$$E\left[\left\|\boldsymbol{R}_{\tilde{x}\tilde{x}}^{-1}-\hat{\boldsymbol{R}}_{\tilde{x}\tilde{x}}^{-1}(N)\right\|^2\right]=O\left(\frac{1}{N}\right). \tag{3.3.11}$$

Following similar steps as in Eq. (3.3.9), noting that $\boldsymbol{\rho}_{\tilde{x}r}=\boldsymbol{\rho}_{\tilde{x}\tilde{s}'}=\boldsymbol{\rho}_{\tilde{s}\tilde{s}'}$, we also see that

$$E\left[\left\|\hat{\boldsymbol{\rho}}_{\tilde{x}r}(N)-\boldsymbol{\rho}_{\tilde{s}\tilde{s}'}\right\|^2\right]=O\left(\frac{1}{N}\right) \tag{3.3.12}$$

and

$$E\left[\|\hat{\rho}_{\tilde{x}\tilde{s}'}(N)-\rho_{\tilde{s}\tilde{s}'}\|^2\right]=O\left(\frac{1}{N}\right). \tag{3.3.13}$$

Now, from Eqs. (3.3.3), we have

$$E\left[\left\|\hat{h}_{BF}(N)-h_{opt}\right\|^2\right]=E\left[\left\|R_{\tilde{x}\tilde{x}}^{-1}(\hat{\rho}_{\tilde{x}r}(N)-\rho_{\tilde{s}\tilde{s}'})+(\hat{R}_{\tilde{x}\tilde{x}}^{-1}(N)-R_{\tilde{x}\tilde{x}}^{-1})\hat{\rho}_{\tilde{x}r}(N)\right\|^2\right]$$

$$\leq 2E\left[\left\|R_{\tilde{x}\tilde{x}}^{-1}\right\|^2\left(\|\hat{\rho}_{\tilde{x}r}(N)-\rho_{\tilde{s}\tilde{s}'}\|^2\right)\right]+2E\left[\left(\left\|\hat{R}_{\tilde{x}\tilde{x}}^{-1}(N)-R_{\tilde{x}\tilde{x}}^{-1}\right\|^2\right)\|\hat{\rho}_{\tilde{x}r}(N)\|^2\right] \tag{3.3.14}$$

where we have used the inequality $\|a+b\|^2\leq 2\|a\|^2+2\|b\|^2$ followed by the Schwarz inequality. Similarly, we have

$$\begin{aligned}E\left[\left\|\hat{h}_{TF}(N)-h_{opt}\right\|^2\right] \;\leq\; & 2E\left[\left\|R_{\tilde{x}\tilde{x}}^{-1}\right\|^2\left(\|\hat{\rho}_{\tilde{x}\tilde{s}'}(N)-\rho_{\tilde{s}\tilde{s}'}\|^2\right)\right] \\ & +2E\left[\left(\left\|\hat{R}_{\tilde{x}\tilde{x}}^{-1}(N)-R_{\tilde{x}\tilde{x}}^{-1}\right\|^2\right)\|\hat{\rho}_{\tilde{x}\tilde{s}'}(N)\|^2\right].\end{aligned} \tag{3.3.15}$$

Using the boundedness of $\left\|R_{\tilde{x}\tilde{x}}^{-1}\right\|^2$ together with Eqs. (3.3.11) and (3.3.12) in Eq. (3.3.14) and (3.3.15), we conclude that

$$E\left[\left\|\hat{h}_{BF}(N)-h_{opt}\right\|^2\right]=O\left(\frac{1}{N}\right) \tag{3.3.16}$$

and

$$E\left[\left\|\hat{h}_{TF}(N)-h_{opt}\right\|^2\right]=O\left(\frac{1}{N}\right). \tag{3.3.17}$$

From Eqs. (3.3.16) and (3.3.17), using the triangular inequality, clearly we can see that

$$E\left[\left\|\delta\hat{h}(N)\right\|^2\right]=E\left[\left\|\hat{h}_{BF}(N)-\hat{h}_{TF}(N)\right\|^2\right]=O\left(\frac{1}{N}\right). \tag{3.3.18}$$

Thus, for $N\rightarrow\infty$, both $\hat{h}_{BF}(N)$ and $\hat{h}_{TF}(N)$ converge in the mean-square sense to h_{opt} with the rate of convergence $O\left(\frac{1}{N}\right)$. □

Theorem 3.1 has important implications because it shows that the BA-FRESH filter and the TA-FRESH filter are asymptotically equivalent in the sense that both converge to h_{opt} at the same order. However, the TA-FRESH filter necessitates a copy of the desired

signal.

3.4 The Finite Sample Output SINR Analysis

Based on Theorem 3.1, we can further study the output signal to interference plus noise ratio (SINR) of the BA-FRESH filter and the TA-FRESH filter with finite samples. We denote the output SINR of the BA-FRESH filter with finite samples as $\text{SINR}_{BF}(N)$ and the output SINR of the TA-FRESH filter with finite samples as $\text{SINR}_{TF}(N)$. They are defined respectively as

$$\text{SINR}_{BF}(N) = \frac{\hat{\boldsymbol{h}}_{BF}^{\dagger}(N)\hat{\boldsymbol{R}}_{\tilde{s}\tilde{s}}\hat{\boldsymbol{h}}_{BF}(N)}{\hat{\boldsymbol{h}}_{BF}^{\dagger}(N)\hat{\boldsymbol{R}}_{\tilde{u}+\tilde{v},\tilde{u}+\tilde{v}}\hat{\boldsymbol{h}}_{BF}(N)} \tag{3.4.1}$$

$$\text{SINR}_{TF}(N) = \frac{\hat{\boldsymbol{h}}_{TF}^{\dagger}(N)\hat{\boldsymbol{R}}_{\tilde{s}\tilde{s}}\hat{\boldsymbol{h}}_{TF}(N)}{\hat{\boldsymbol{h}}_{TF}^{\dagger}(N)\hat{\boldsymbol{R}}_{\tilde{u}+\tilde{v},\tilde{u}+\tilde{v}}\hat{\boldsymbol{h}}_{TF}(N)} \tag{3.4.2}$$

where $\hat{\boldsymbol{R}}_{\tilde{s}\tilde{s}} = \langle \tilde{\boldsymbol{s}}(n)\tilde{\boldsymbol{s}}^{\dagger}(n)\rangle_N$, and $\hat{\boldsymbol{R}}_{\tilde{u}+\tilde{v},\tilde{u}+\tilde{v}} = \langle (\tilde{\boldsymbol{u}}(n)+\tilde{\boldsymbol{v}}(n))(\tilde{\boldsymbol{u}}(n)+\tilde{\boldsymbol{v}}(n))^{\dagger}\rangle_N$. $\hat{\boldsymbol{h}}_{BF}(N)$ and $\hat{\boldsymbol{h}}_{TF}(N)$ are defined in Eqs. (3.2.12) and (3.2.22) respectively. For the infinite data length ($N = \infty$), SINR_{opt-F} is defined as

$$\text{SINR}_{opt-F} = \frac{\boldsymbol{h}_{opt}^{\dagger}\boldsymbol{R}_{\tilde{s}\tilde{s}}\boldsymbol{h}_{opt}}{\boldsymbol{h}_{opt}^{\dagger}\boldsymbol{R}_{\tilde{u}+\tilde{v},\tilde{u}+\tilde{v}}\boldsymbol{h}_{opt}}. \tag{3.4.3}$$

We want to evaluate the normalized mean square error between $\text{SINR}_{BF}(N)$, $\text{SINR}_{TF}(N)$ and SINR_{opt-F} respectively, that is,

$$E\left[\frac{\|\text{SINR}_{BF}(N) - \text{SINR}_{opt-F}\|^2}{\|\text{SINR}_{opt-F}\|^2}\right] \text{ and } E\left[\frac{\|\text{SINR}_{TF}(N) - \text{SINR}_{opt-F}\|^2}{\|\text{SINR}_{opt-F}\|^2}\right]. \tag{3.4.4}$$

We have Corollary 3.1 as follows:

Corollary 3.1: *For the same scenario as Theorem 3.1,* $\text{SINR}_{BF}(N)$ and $\text{SINR}_{TF}(N)$ *converges in the mean square sense to* SINR_{opt-F}. *Furthermore the convergence rate for*

$\mathrm{SINR}_{BF}(N)$ and $\mathrm{SINR}_{TF}(N)$ *are* $O(\frac{1}{N})$, *that is*

$$E\left[\frac{\|\mathrm{SINR}_{BF}(N)-\mathrm{SINR}_{opt-F}\|^2}{\|\mathrm{SINR}_{opt-F}\|^2}\right]=O\left(\frac{1}{N}\right) \tag{3.4.5}$$

$$E\left[\frac{\|\mathrm{SINR}_{TF}(N)-\mathrm{SINR}_{opt-F}\|^2}{\|\mathrm{SINR}_{opt-F}\|^2}\right]=O\left(\frac{1}{N}\right). \tag{3.4.6}$$

Proof: Using Eqs. (3.4.1) and (3.4.3), we have

$$\begin{aligned}\mathrm{SINR}_{BF}(N)-\mathrm{SINR}_{opt-F} &= \frac{\hat{\boldsymbol{h}}_{BF}^{\dagger}(N)\hat{\boldsymbol{R}}_{\tilde{s}\tilde{s}}\hat{\boldsymbol{h}}_{BF}(N)}{\hat{\boldsymbol{h}}_{BF}^{\dagger}(N)\hat{\boldsymbol{R}}_{\tilde{u}+\tilde{v},\tilde{u}+\tilde{v}}\hat{\boldsymbol{h}}_{BF}(N)}-\mathrm{SINR}_{opt-F} \\ &= \frac{\hat{\boldsymbol{h}}_{BF}^{\dagger}(N)\left[\hat{\boldsymbol{R}}_{\tilde{s}\tilde{s}}-\mathrm{SINR}_{opt-F}\hat{\boldsymbol{R}}_{\tilde{u}+\tilde{v},\tilde{u}+\tilde{v}}\right]\hat{\boldsymbol{h}}_{BF}(N)}{\hat{\boldsymbol{h}}_{BF}^{\dagger}(N)\hat{\boldsymbol{R}}_{\tilde{u}+\tilde{v},\tilde{u}+\tilde{v}}\hat{\boldsymbol{h}}_{BF}(N)}.\end{aligned} \tag{3.4.7}$$

We define

$$\delta\boldsymbol{h}_{BF}=\hat{\boldsymbol{h}}_{BF}(N)-\boldsymbol{h}_{opt},\quad \delta\hat{\boldsymbol{R}}_{\tilde{s}\tilde{s}}=\hat{\boldsymbol{R}}_{\tilde{s}\tilde{s}}-\boldsymbol{R}_{\tilde{s}\tilde{s}},\quad \text{and}\quad \delta\hat{\boldsymbol{R}}_{\tilde{u}+\tilde{v},\tilde{u}+\tilde{v}}=\hat{\boldsymbol{R}}_{\tilde{u}+\tilde{v},\tilde{u}+\tilde{v}}-\boldsymbol{R}_{\tilde{u}+\tilde{v},\tilde{u}+\tilde{v}}. \tag{3.4.8}$$

For the numerator of Eq. (3.4.7), we have

$$\begin{aligned}\hat{\boldsymbol{h}}_{BF}^{\dagger}(N)\left[\hat{\boldsymbol{R}}_{\tilde{s}\tilde{s}}-\mathrm{SINR}_{opt-F}\hat{\boldsymbol{R}}_{\tilde{u}+\tilde{v},\tilde{u}+\tilde{v}}\right]\hat{\boldsymbol{h}}_{BF}(N) &= \boldsymbol{h}_{opt}^{\dagger}\left[\boldsymbol{R}_{\tilde{s}\tilde{s}}-\mathrm{SINR}_{opt-F}\boldsymbol{R}_{\tilde{u}+\tilde{v},\tilde{u}+\tilde{v}}\right]\boldsymbol{h}_{opt} \\ &\quad +\delta\boldsymbol{h}_{BF}^{\dagger}\left[\boldsymbol{R}_{\tilde{s}\tilde{s}}-\mathrm{SINR}_{opt-F}\boldsymbol{R}_{\tilde{u}+\tilde{v},\tilde{u}+\tilde{v}}\right]\boldsymbol{h}_{opt} \\ &\quad +\boldsymbol{h}_{opt}^{\dagger}\left[\boldsymbol{R}_{\tilde{s}\tilde{s}}-\mathrm{SINR}_{opt-F}\boldsymbol{R}_{\tilde{u}+\tilde{v},\tilde{u}+\tilde{v}}\right]\delta\boldsymbol{h}_{BF} \\ &\quad +\boldsymbol{h}_{opt}^{\dagger}\left[\delta\boldsymbol{R}_{\tilde{s}\tilde{s}}-\mathrm{SINR}_{opt-F}\delta\boldsymbol{R}_{\tilde{u}+\tilde{v},\tilde{u}+\tilde{v}}\right]\boldsymbol{h}_{opt} \\ &\quad +[\text{high order terms}]\end{aligned} \tag{3.4.9}$$

where

$$\begin{aligned}[\text{high order terms}] &= \delta\boldsymbol{h}_{BF}^{\dagger}\left[\boldsymbol{R}_{\tilde{s}\tilde{s}}-\mathrm{SINR}_{opt-F}\boldsymbol{R}_{\tilde{u}+\tilde{v},\tilde{u}+\tilde{v}}\right]\delta\boldsymbol{h}_{BF} \\ &\quad +\delta\boldsymbol{h}_{BF}^{\dagger}\left[\delta\boldsymbol{R}_{\tilde{s}\tilde{s}}-\mathrm{SINR}_{opt-F}\delta\boldsymbol{R}_{\tilde{u}+\tilde{v},\tilde{u}+\tilde{v}}\right]\boldsymbol{h}_{opt} \\ &\quad +\boldsymbol{h}_{opt}^{\dagger}\left[\delta\boldsymbol{R}_{\tilde{s}\tilde{s}}-\mathrm{SINR}_{opt-F}\delta\boldsymbol{R}_{\tilde{u}+\tilde{v},\tilde{u}+\tilde{v}}\right]\delta\boldsymbol{h}_{BF} \\ &\quad +\delta\boldsymbol{h}_{BF}^{\dagger}\left[\delta\boldsymbol{R}_{\tilde{s}\tilde{s}}-\mathrm{SINR}_{opt-F}\delta\boldsymbol{R}_{\tilde{u}+\tilde{v},\tilde{u}+\tilde{v}}\right]\delta\boldsymbol{h}_{BF}.\end{aligned} \tag{3.4.10}$$

For the first term of the right side of Eq. (3.4.9), we obtain by Eq. (3.4.3)

$$\begin{aligned} \boldsymbol{h}_{opt}^{\dagger}\left[\boldsymbol{R}_{\tilde{s}\tilde{s}} - \mathrm{SINR}_{opt-F}\boldsymbol{R}_{\tilde{u}+\tilde{v},\tilde{u}+\tilde{v}}\right]\boldsymbol{h}_{opt} &= \boldsymbol{h}_{opt}^{\dagger}\boldsymbol{R}_{\tilde{s}\tilde{s}}\boldsymbol{h}_{opt} - \mathrm{SINR}_{opt-F}\boldsymbol{h}_{opt}^{\dagger}\boldsymbol{R}_{\tilde{u}+\tilde{v},\tilde{u}+\tilde{v}}\boldsymbol{h}_{opt} \\ &= \boldsymbol{h}_{opt}^{\dagger}\boldsymbol{R}_{\tilde{s}\tilde{s}}\boldsymbol{h}_{opt} - \boldsymbol{h}_{opt}^{\dagger}\boldsymbol{R}_{\tilde{s}\tilde{s}}\boldsymbol{h}_{opt} = 0. \end{aligned} \tag{3.4.11}$$

Using the Schwarz inequality to the second term of the right side of Eq. (3.4.9), We obtain

$$\begin{aligned} &E\left[\left\|\delta\boldsymbol{h}_{BF}^{\dagger}\left[\boldsymbol{R}_{\tilde{s}\tilde{s}} - \mathrm{SINR}_{opt-F}\boldsymbol{R}_{\tilde{u}+\tilde{v},\tilde{u}+\tilde{v}}\right]\boldsymbol{h}_{opt}\right\|^2\right] \\ &\leq E\left[\left\|\delta\boldsymbol{h}_{BF}^{\dagger}\right\|^2\right]\cdot\left\|\left[\boldsymbol{R}_{\tilde{s}\tilde{s}} - \mathrm{SINR}_{opt-F}\boldsymbol{R}_{\tilde{u}+\tilde{v},\tilde{u}+\tilde{v}}\right]\right\|^2\cdot\left\|\boldsymbol{h}_{opt}\right\|^2. \end{aligned} \tag{3.4.12}$$

Noting that the boundednesses of $\left\|\left[\boldsymbol{R}_{\tilde{s}\tilde{s}} - \mathrm{SINR}_{opt-F}\boldsymbol{R}_{\tilde{u}+\tilde{v},\tilde{u}+\tilde{v}}\right]\right\|$ and $\left\|\boldsymbol{h}_{opt}\right\|$ and using Eq. (3.3.18), we obtain

$$E\left[\left\|\delta\boldsymbol{h}_{BF}^{\dagger}\left[\boldsymbol{R}_{\tilde{s}\tilde{s}} - \mathrm{SINR}_{opt-F}\boldsymbol{R}_{\tilde{u}+\tilde{v},\tilde{u}+\tilde{v}}\right]\boldsymbol{h}_{opt}\right\|^2\right] = O\left(\frac{1}{N}\right). \tag{3.4.13}$$

For the third term of the right side of Eq. (3.4.9), we similarly have

$$E\left[\left\|\boldsymbol{h}_{opt}^{\dagger}\left[\boldsymbol{R}_{\tilde{s}\tilde{s}} - \mathrm{SINR}_{opt-F}\boldsymbol{R}_{\tilde{u}+\tilde{v},\tilde{u}+\tilde{v}}\right]\delta\boldsymbol{h}_{BF}\right\|^2\right] = O\left(\frac{1}{N}\right). \tag{3.4.14}$$

We also note that $E\left[\left\|\delta\boldsymbol{R}_{\tilde{s}\tilde{s}}\right\|^2\right] = O\left(\frac{1}{N}\right)$ and $E\left[\left\|\delta\boldsymbol{R}_{\tilde{u}+\tilde{v},\tilde{u}+\tilde{v}}\right\|^2\right] = O\left(\frac{1}{N}\right)$. Using the Schwarz inequality to the fourth term of the right side of Eq. (3.4.9), we obtain

$$E\left[\left\|\boldsymbol{h}_{opt}^{\dagger}\left[\delta\boldsymbol{R}_{\tilde{s}\tilde{s}} - \mathrm{SINR}_{opt-F}\delta\boldsymbol{R}_{\tilde{u}+\tilde{v},\tilde{u}+\tilde{v}}\right]\boldsymbol{h}_{opt}\right\|^2\right] = O\left(\frac{1}{N}\right). \tag{3.4.15}$$

For the fifth term of the right side of Eq. (3.4.9), using the similar steps, we obtain

$$E\left[\left\|\text{high order terms}\right\|^2\right] = O\left(\frac{1}{N^2}\right). \tag{3.4.16}$$

Therefore, we obtain

$$E\left[\left\|\hat{\boldsymbol{h}}_{BF}^{\dagger}(N)\left[\hat{\boldsymbol{R}}_{\tilde{s}\tilde{s}} - \mathrm{SINR}_{opt-F}\hat{\boldsymbol{R}}_{\tilde{u}+\tilde{v},\tilde{u}+\tilde{v}}\right]\hat{\boldsymbol{h}}_{BF}\right\|^2\right] = O\left(\frac{1}{N}\right). \tag{3.4.17}$$

Because $\left[\left\|\hat{\boldsymbol{h}}_{BF}^{\dagger}(N)\hat{\boldsymbol{R}}_{\tilde{u}+\tilde{v},\tilde{u}+\tilde{v}}\hat{\boldsymbol{h}}_{BF}(N)\right\|^2\right]$ is bounded with probability one, that is,

$$\min\left[\left\|\hat{\boldsymbol{h}}_{BF}^{\dagger}(N)\hat{\boldsymbol{R}}_{\tilde{u}+\tilde{v},\tilde{u}+\tilde{v}}\hat{\boldsymbol{h}}_{BF}(N)\right\|^2\right] \geq C_2, \quad N \to \infty \tag{3.4.18}$$

where C_2 is a positive constant, we obtain by using Eqs. (3.4.17) and (3.4.18)

$$E\left[\|\mathrm{SINR}_{BF}(N) - \mathrm{SINR}_{opt-F}\|^2\right] = O\left(\frac{1}{N}\right). \tag{3.4.19}$$

Since $\|\mathrm{SINR}_{opt-F}\|^2$ is a constant, so we conclude that

$$E\left[\frac{\|\mathrm{SINR}_{BF}(N) - \mathrm{SINR}_{opt-F}\|^2}{\|\mathrm{SINR}_{opt-F}\|^2}\right] = O\left(\frac{1}{N}\right). \tag{3.4.20}$$

Using the similar steps, we obtain

$$E\left[\frac{\|\mathrm{SINR}_{TF}(N) - \mathrm{SINR}_{opt-F}\|^2}{\|\mathrm{SINR}_{opt-F}\|^2}\right] = O\left(\frac{1}{N}\right). \quad \square \tag{3.4.21}$$

3.5 The Finite Sample Output MSE Analysis

In this section, we study the finite sample MSE (Mean Square Error) of the BA-FRESH filter and that of the TA-FRESH filter. The finite sample MSE of the BA-FRESH filter is denoted as $J_{BF}(N)$ and the finite sample MSE of the TA-FRESH filter is denoted as $J_{TF}(N)$. They are defined respectively as

$$J_{BF}(N) = \left\langle \left(\hat{\boldsymbol{h}}_{BF}^{\dagger}(N)\tilde{\boldsymbol{x}}(n) - \tilde{s}'(n)\right)\left(\hat{\boldsymbol{h}}_{BF}^{\dagger}(N)\tilde{\boldsymbol{x}}(n) - \tilde{s}'(n)\right)^{*}\right\rangle \tag{3.5.1}$$

$$J_{TF}(N) = \left\langle \left(\hat{\boldsymbol{h}}_{TF}^{\dagger}(N)\tilde{\boldsymbol{x}}(n) - \tilde{s}'(n)\right)\left(\hat{\boldsymbol{h}}_{TF}^{\dagger}(N)\tilde{\boldsymbol{x}}(n) - \tilde{s}'(n)\right)^{*}\right\rangle \tag{3.5.2}$$

where $\hat{\boldsymbol{h}}_{BF}(N)$ and $\hat{\boldsymbol{h}}_{TF}(N)$ are defined in Eqs. (3.2.12) and (3.2.22) respectively. $\tilde{\boldsymbol{x}}(n)$ and $\tilde{s}'(n)$ are defined in Eqs. (3.2.5) and (3.2.21). Let the infinite sample MSE of the BA-FRESH filter which is equal to that of the TA-FRESH filter be denoted by J_{opt-F}. J_{opt-F}

is defined as

$$J_{opt-F} = \left\langle \left(\boldsymbol{h}_{opt}^{\dagger} \tilde{\boldsymbol{x}}(n) - \tilde{s}^{'}(n) \right) \left(\boldsymbol{h}_{opt}^{\dagger} \tilde{\boldsymbol{x}}(n) - \tilde{s}^{'}(n) \right)^{*} \right\rangle \tag{3.5.3}$$

where $\boldsymbol{h}_{opt}$ is defined in Eq. (3.2.24). We like to evaluate the normalized mean square error between $J_{BF}(N)$, $J_{TF}(N)$ and J_{opt-F} respectively, that is,

$$E\left[\frac{\|J_{BF}(N) - J_{opt-F}\|^2}{\|J_{opt-F}\|^2}\right] \quad \text{and} \quad E\left[\frac{\|J_{TF}(N) - J_{opt-F}\|^2}{\|J_{opt-F}\|^2}\right]. \tag{3.5.4}$$

We have Corollary 3.2 as following:

Corollary 3.2: *For the same scenario as Theorem 3.1, $J_{BF}(N)$ and $J_{TF}(N)$ converge in the mean square sense to J_{opt-F}. Furthermore the convergence rates for $J_{BF}(N)$ and $J_{TF}(N)$ are $O\left(\frac{1}{N}\right)$, that is*

$$E\left[\frac{\|J_{BF}(N) - J_{opt-F}\|^2}{\|J_{opt-F}\|^2}\right] = O\left(\frac{1}{N}\right) \tag{3.5.5}$$

$$E\left[\frac{\|J_{TF}(N) - J_{opt-F}\|^2}{\|J_{opt-F}\|^2}\right] = O\left(\frac{1}{N}\right). \tag{3.5.6}$$

Proof: Using Eq. (3.5.1), we have

$$\begin{aligned} J_{BF}(N) &= \left\langle \left(\hat{\boldsymbol{h}}_{BF}^{\dagger}(N) \tilde{\boldsymbol{x}}(n) - \tilde{s}^{'}(n) \right) \left(\hat{\boldsymbol{h}}_{BF}^{\dagger}(N) \tilde{\boldsymbol{x}}(n) - \tilde{s}^{'}(n) \right)^{*} \right\rangle \qquad (3.5.7) \\ &= \langle s(n) s^{*}(n) \rangle - \hat{\boldsymbol{h}}_{BF}^{\dagger}(N) \boldsymbol{\rho}_{\tilde{\boldsymbol{x}}\tilde{s}'} - \left(\hat{\boldsymbol{h}}_{BF}^{\dagger}(N) \boldsymbol{\rho}_{\tilde{\boldsymbol{x}}\tilde{s}'} \right)^{\dagger} - \hat{\boldsymbol{h}}_{BF}^{\dagger}(N) \boldsymbol{R}_{\tilde{\boldsymbol{x}}\tilde{\boldsymbol{x}}} \hat{\boldsymbol{h}}_{BF}(N), \end{aligned}$$

Substituting Eqs. (3.4.8) and (3.5.3) into (3.5.7), we obtain

$$J_{BF}(N) = J_{opt-F} - \delta \boldsymbol{h}_{BF}^{\dagger} \boldsymbol{\rho}_{\tilde{\boldsymbol{x}}\tilde{s}'} - \delta \boldsymbol{h}_{BF}^{T} \boldsymbol{\rho}_{\tilde{\boldsymbol{x}}\tilde{s}'}^{*} + \delta \boldsymbol{h}_{BF}^{\dagger} \boldsymbol{R}_{\tilde{\boldsymbol{x}}\tilde{\boldsymbol{x}}} \boldsymbol{h}_{opt} + \boldsymbol{h}_{opt}^{\dagger} \boldsymbol{R}_{\tilde{\boldsymbol{x}}\tilde{\boldsymbol{x}}} \delta \boldsymbol{h}_{BF} + \delta \boldsymbol{h}_{BF}^{\dagger} \boldsymbol{R}_{\tilde{\boldsymbol{x}}\tilde{\boldsymbol{x}}} \delta \boldsymbol{h}_{BF}. \tag{3.5.8}$$

Using the inequality $\|\boldsymbol{a} + \boldsymbol{b}\|^2 \leq 2\|\boldsymbol{a}\|^2 + 2\|\boldsymbol{b}\|^2$, we obtain

$$\begin{aligned} E\left[\|J_{BF}(N) - J_{opt-F}\|^2\right] \leq\ & 2E\left[\left\| -\delta \boldsymbol{h}_{BF}^{\dagger} \boldsymbol{\rho}_{\tilde{\boldsymbol{x}}\tilde{s}'} - \delta \boldsymbol{h}_{BF}^{T} \boldsymbol{\rho}_{\tilde{\boldsymbol{x}}\tilde{s}'}^{*} + \delta \boldsymbol{h}_{BF}^{\dagger} \boldsymbol{R}_{\tilde{\boldsymbol{x}}\tilde{\boldsymbol{x}}} \boldsymbol{h}_{opt} + \boldsymbol{h}_{opt}^{\dagger} \boldsymbol{R}_{\tilde{\boldsymbol{x}}\tilde{\boldsymbol{x}}} \delta \boldsymbol{h}_{BF} \right\|^2\right] \\ & + 2E\left[\left\| \delta \boldsymbol{h}_{BF}^{\dagger} \boldsymbol{R}_{\tilde{\boldsymbol{x}}\tilde{\boldsymbol{x}}} \delta \boldsymbol{h}_{BF} \right\|^2\right]. \end{aligned} \tag{3.5.9}$$

Using the Schwarz inequality and the inequality $\|\boldsymbol{a}+\boldsymbol{b}\|^2 \leq 2\|\boldsymbol{a}\|^2 + 2\|\boldsymbol{b}\|^2$ to Eq. (3.5.9), we obtain

$$E\left[\|J_{BF}(N) - J_{opt-F}\|^2\right] = O\left(\frac{1}{N}\right). \tag{3.5.10}$$

Because $\|J_{opt-F}\|^2$ is a constant, we conclude that

$$E\left[\frac{\|J_{BF}(N) - J_{opt-F}\|^2}{\|J_{opt-F}\|^2}\right] = O\left(\frac{1}{N}\right). \tag{3.5.11}$$

Using the similar steps, we obtain

$$E\left[\frac{\|J_{TF}(N) - J_{opt-F}\|^2}{\|J_{opt-F}\|^2}\right] = O\left(\frac{1}{N}\right). \quad \square \tag{3.5.12}$$

3.6 Numerical Results

In this section, we present numerical simulation results showing the performances of the BA-FRESH filter in comparison to those of the TA-FRESH filter. In the examples, we consider only one desired signal and one interfering signal and they are both BPSK signals. Thus, the desired signal and the interfering signal are given respectively by

$$s(nT_s) = \sum_{k=-\infty}^{\infty} d(k)g(nT_s - kT_{b_1})\cos(2\pi f_1 nT_s) \tag{3.6.1}$$

$$u(nT_s) = \sum_{k=-\infty}^{\infty} d_u(k)g(nT_s - kT_{b_2})\cos(2\pi f_2 nT_s) \tag{3.6.2}$$

where T_{b_1} and T_{b_2} are the baud periods, f_1 and f_2 are the carrier frequencies offset of $s(nT_s)$ and $u(nT_s)$ respectively and T_s is the sampling period. $\{d(k)\}$ and $\{d_u(k)\}$ are random binary sequences. For both the desired and interfering signals, we assume that $g(nT_s)$ and $g_u(nT_s)$ are the pulse obtained by the square root raised-cosine pulse shaping filter with a 100% roll-off factor [31]. We choose that the length of $g(n)$ which is equal to the length of $g_u(n)$ is equal to 159. The noise is a real stationary white Gaussian noise.

Example 3.1: In this example, we examine the output signal to interference plus noise ratio (SINR) of the BA-FRESH filter and the TA-FRESH filter with finite symbols. We

denote the output SINR of the BA-FRESH filter with finite symbols as $\mathrm{SINR}_{BF}(N)$ and the output SINR of the TA-FRESH filter with finite symbols as $\mathrm{SINR}_{TF}(N)$. They are defined respectively as

$$\mathrm{SINR}_{BF}(N) = \frac{\hat{\boldsymbol{h}}_{BF}^{\dagger}(N)\hat{\boldsymbol{R}}_{\tilde{s}\tilde{s}}\hat{\boldsymbol{h}}_{BF}(N)}{\hat{\boldsymbol{h}}_{BF}^{\dagger}(N)\hat{\boldsymbol{R}}_{\tilde{u}+\tilde{v},\tilde{u}+\tilde{v}}\hat{\boldsymbol{h}}_{BF}(N)} \tag{3.6.3}$$

$$\mathrm{SINR}_{TF}(N) = \frac{\hat{\boldsymbol{h}}_{TF}^{\dagger}(N)\hat{\boldsymbol{R}}_{\tilde{s}\tilde{s}}\hat{\boldsymbol{h}}_{TF}(N)}{\hat{\boldsymbol{h}}_{TF}^{\dagger}(N)\hat{\boldsymbol{R}}_{\tilde{u}+\tilde{v},\tilde{u}+\tilde{v}}\hat{\boldsymbol{h}}_{TF}(N)} \tag{3.6.4}$$

where $\hat{\boldsymbol{R}}_{\tilde{s}\tilde{s}} = \langle \tilde{\boldsymbol{s}}(n)\tilde{\boldsymbol{s}}^{\dagger}(n)\rangle_N$, and $\hat{\boldsymbol{R}}_{\tilde{u}+\tilde{v},\tilde{u}+\tilde{v}} = \langle (\tilde{\boldsymbol{u}}(n)+\tilde{\boldsymbol{v}}(n))(\tilde{\boldsymbol{u}}(n)+\tilde{\boldsymbol{v}}(n))^{\dagger}\rangle_N$. $\hat{\boldsymbol{h}}_{BF}(N)$ and $\hat{\boldsymbol{h}}_{TF}(N)$ are defined in Eqs. (3.2.12) and (3.2.22) respectively. N denotes the number of symbols. The desired and interfering signals are BPSK signals as given by Eqs. (3.6.1) and (3.6.2) respectively. The baud rates of the two signals are equal, being 5kHz for both the desired signal and the interference. The carrier frequency of the desired signal is f_1 = 10kHz. The cycle frequencies used in the BA-FRESH filter and the TA-FRESH filter are set at α_1 = 20kHz, α_2 = −20kHz and the cycle frequency used in the reference path of the BA-FRESH filter is set at α' = 0kHz. Three scenarios are examined. In the first case, we examine the effect of different spectral overlapping between the two signals to $\mathrm{SINR}_{BF}(N)$ and $\mathrm{SINR}_{TF}(N)$. The bandwidths of the signal and interference depend on their baud rates which are fixed at 5kHz making the approximate bandwidth of both 10kHz. We fix the carrier frequency offset for the desired signal at 10kHz while varying that for the interference so that the percentage of spectral overlap are 40%, 30%, 20% and 10%. The percentage of spectral overlap is defined as

$$a = \frac{B_s + B_i - |f_i - f_s|}{2B_s} \times 100\% \tag{3.6.5}$$

where B_s and B_i are the baud rates and f_s and f_i are the carrier frequencies of the signal and interference respectively. We vary the carrier frequency offset of the interference so that the spectral overlapping between the two signals can be varied as 40%, 30%, 20% and 10% respectively. The length of each FIR filter is 10. The input signal to noise ratio (SNR) and the input signal to interference ratio (SIR) are fixed at 10dB and 0dB respectively. The

output SINR of BA-FRESH and TA-FRESH with finite samples are plotted in Fig. 3.4(a) to Fig. 3.4(d) respectively. It can be observed that the output SINR of BA-FRESH and TA-FRESH converge to same value when the number of symbols is larger than 100. For fixed number of branch of BA-FRESH and TA-FRESH, when the frequency overlapping is reduced, the performance of BA-FRESH and TA-FRESH is increased. In the second case, we examine the effect of different input SIR to the output $\text{SINR}_{BF}(N)$ and the output $\text{SINR}_{TF}(N)$. The scenario is similar to the first case except that input SIR is 5dB. The output SINR of BA-FRESH and TA-FRESH with finite symbols are plotted in Fig. 3.5(a) to Fig. 3.5(d) respectively. It can be observed that the output SINR of BA-FRESH and TA-FRESH is increased when we increase the input SIR. In the third case, we examine the effect of different length of the FIR filter to the output $\text{SINR}_{BF}(N)$ and the output $\text{SINR}_{TF}(N)$. The scenario is similar to the first case except that the length of the FIR filter is fixed at 6 and 16 respectively. When the length of the FIR filter is fixed at 6, the output SINR of BA-FRESH and TA-FRESH against different spectral overlapping are plotted in Fig. 3.6(a) to Fig. 3.6(d) respectively. When the length of the FIR filter is fixed at 16, the output SINR of BA-FRESH and TA-FRESH against different spectral overlapping are plotted in Fig. 3.7(a) to Fig. 3.7(d) respectively. Compared with Fig. 3.4 with Fig. 3.6 and 3.7, it can be observed that the output SINR of BA-FRESH and TA-FRESH is increased when we increase the length of the FIR filter. In all the observations, the BA-FRESH and TA-FRESH filters have very similar performances after the number of symbols is larger than 100.

Example 3.2: In this example, we examine the output eye diagram of the BA-FRESH filter and the transfer functions of each FIR filter in the BA-FRESH filter compared with those of the TA-FRESH filter. The scenario is similar to Example 3.1 except that the carrier frequency offset of the interference is 17kHz, that is the spectral overlapping is 30%. The input SNR is 20dB, and the length of FIR filter is 10. The filter coefficients of BA-FRESH and TA-FRESH with number of symbol ($N = 250$) are calculated from Eqs. (3.2.12) and (3.2.22) respectively. The input and output eye diagrams of BA-FRESH is shown in Fig. 3.8(a). It is observed that the input eye diagram is close and the output eye diagram is open. In order to compare, the input and output eye diagrams of TA-FRESH is shown

in Fig. 3.8(b). It is observed the output eye diagram of BA-FRESH is very similar to that of TA-FRESH. Moreover, we also compare the transfer functions of the FIR filter in BA-FRESH with those of the FIR filter in TA-FRESH. The two transfer functions of BA-FRESH and TA-FRESH are shown in Fig. 3.8(c) and 3.8(d) respectively. Again, it is observed that the transfer function differences between BA-FRESH and TA-FRESH are very small when number of symbols is large.

Example 3.3: In this example, we examine the filter coefficient convergence and the finite sample mean square error (MSE) of the BA-FRESH and the TA-FRESH filters under the condition that the spectral overlapping between the desired signal and the interference are fixed at 40%, 30%, 20% and 10% respectively. The scenario is similar to that of Example 3.1, except that the length of FIR filter is 10, input SNR and SIR are fixed at 0dB and 0dB respectively. For the filter coefficients with finite symbols, $\hat{\boldsymbol{h}}_{BF}$ and $\hat{\boldsymbol{h}}_{TF}$ in this example are calculated from Eqs. (3.2.12) and (3.2.22). $\boldsymbol{h}_{opt}$ in this example is calculated from Eq. (3.2.24) using time-averages of 150 symbols. The normalized convergence of $E\left[\left\|\boldsymbol{h}_{opt}-\hat{\boldsymbol{h}}_{BF}(N)\right\|^2\right]/\|\boldsymbol{h}_{opt}\|^2$ and $E\left[\left\|\boldsymbol{h}_{opt}-\hat{\boldsymbol{h}}_{TF}(N)\right\|^2\right]/\|\boldsymbol{h}_{opt}\|^2$, each being averaged over 10 realizations, are plotted in Fig. 3.9(a) to Fig. 3.9(d), in which the spectral overlapping between the desired and interfering signals are fixed at 40%, 30%, 20% and 10% respectively. It is observed that both the BA-FRESH filter coefficients and the TA-FRESH filter coefficients converge to the optimum filter coefficients when the number of symbols is large, with the TA-FRESH filter being the faster in convergence. For the output MSE with finite symbols, $\boldsymbol{J}_{BF}(N)$ and $\boldsymbol{J}_{TF}(N)$ in this example are calculated from Eqs. (3.5.1) and (3.5.2). $\boldsymbol{J}_{opt-ST}$ in this example is calculated from Eq. (3.5.3) using time-averages of 150 symbols. The normalized MSE difference of $E\left[\|\boldsymbol{J}_{opt-ST}-\boldsymbol{J}_{BF}(N)\|^2\right]/\|\boldsymbol{J}_{opt-ST}\|^2$ and $E\left[\|\boldsymbol{J}_{opt-ST}-\boldsymbol{J}_{TF}(N)\|^2\right]/\|\boldsymbol{J}_{opt-ST}\|^2$, each being averaged over 10 realizations, are plotted in Fig. 3.10(a) to Fig. 3.10(d), in which the frequency overlapping between the desired and interfering signals are fixed at 40%, 30%, 20% and 10% respectively. It is observed that both the normalized output MSE of the BA-FRESH filter and that of the TA-FRESH filter converge to zero when the number of symbols is large, with the TA-FRESH filter being the faster in convergence.

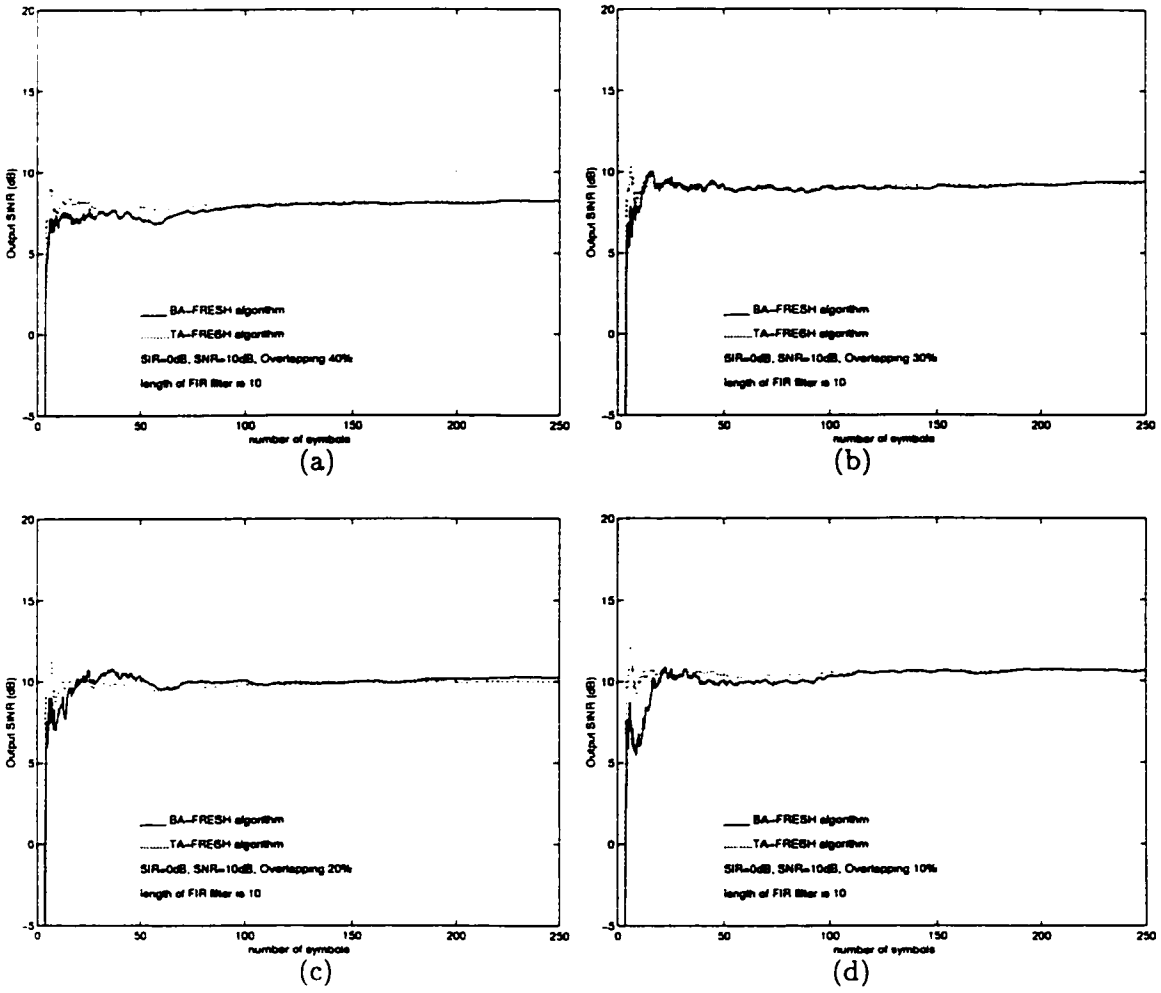

Figure 3.4: Output SINR of BA-FRESH and TA-FRESH against the spectral overlapping 40%, 30%, 20% and 10% when N_o is 10, input SIR is 0dB, and SNR is 10dB

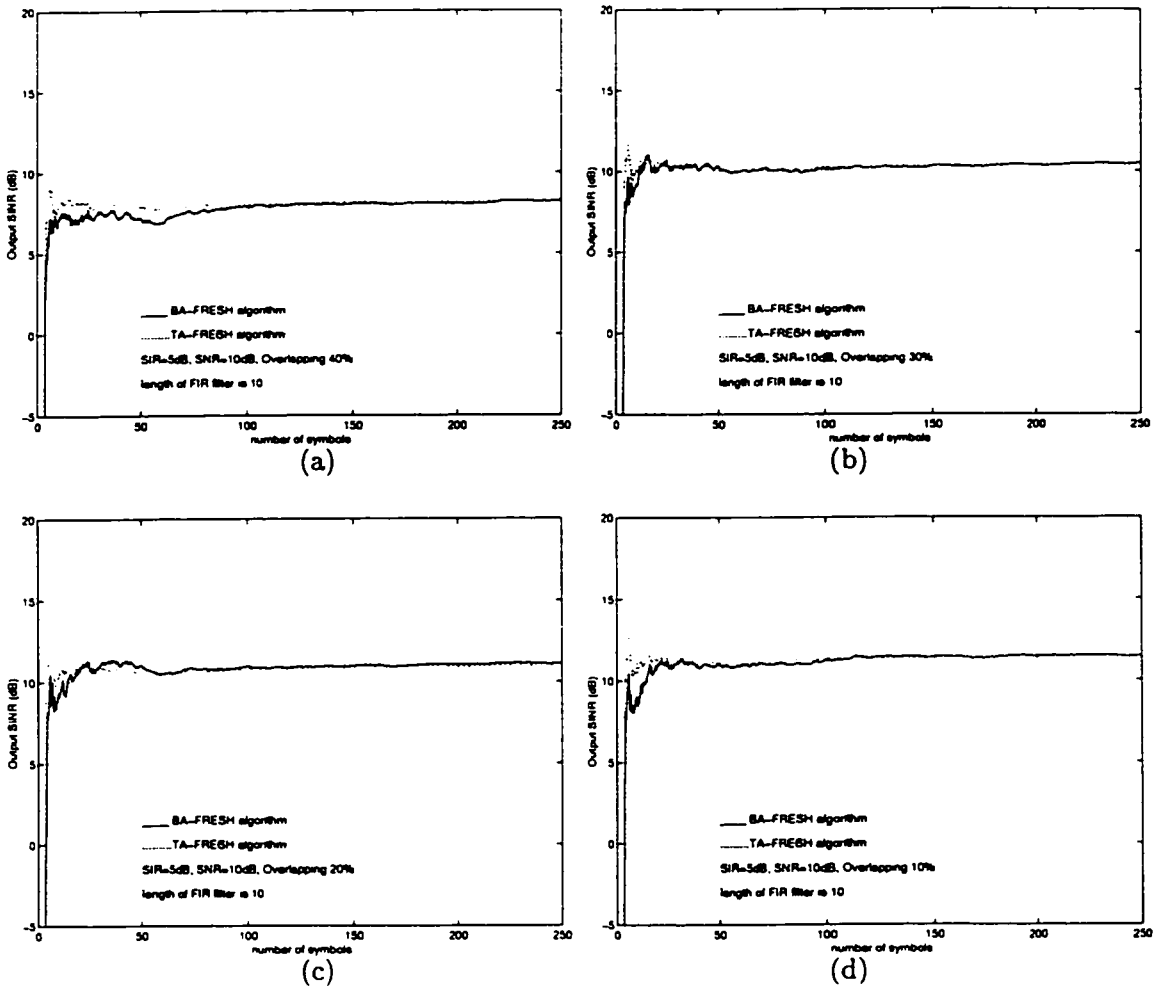

Figure 3.5: Output SINR of BA-FRESH and TA-FRESH against the spectral overlapping 40%, 30%, 20% and 10% when N_o is 10, input SIR is 5dB, and SNR is 10dB

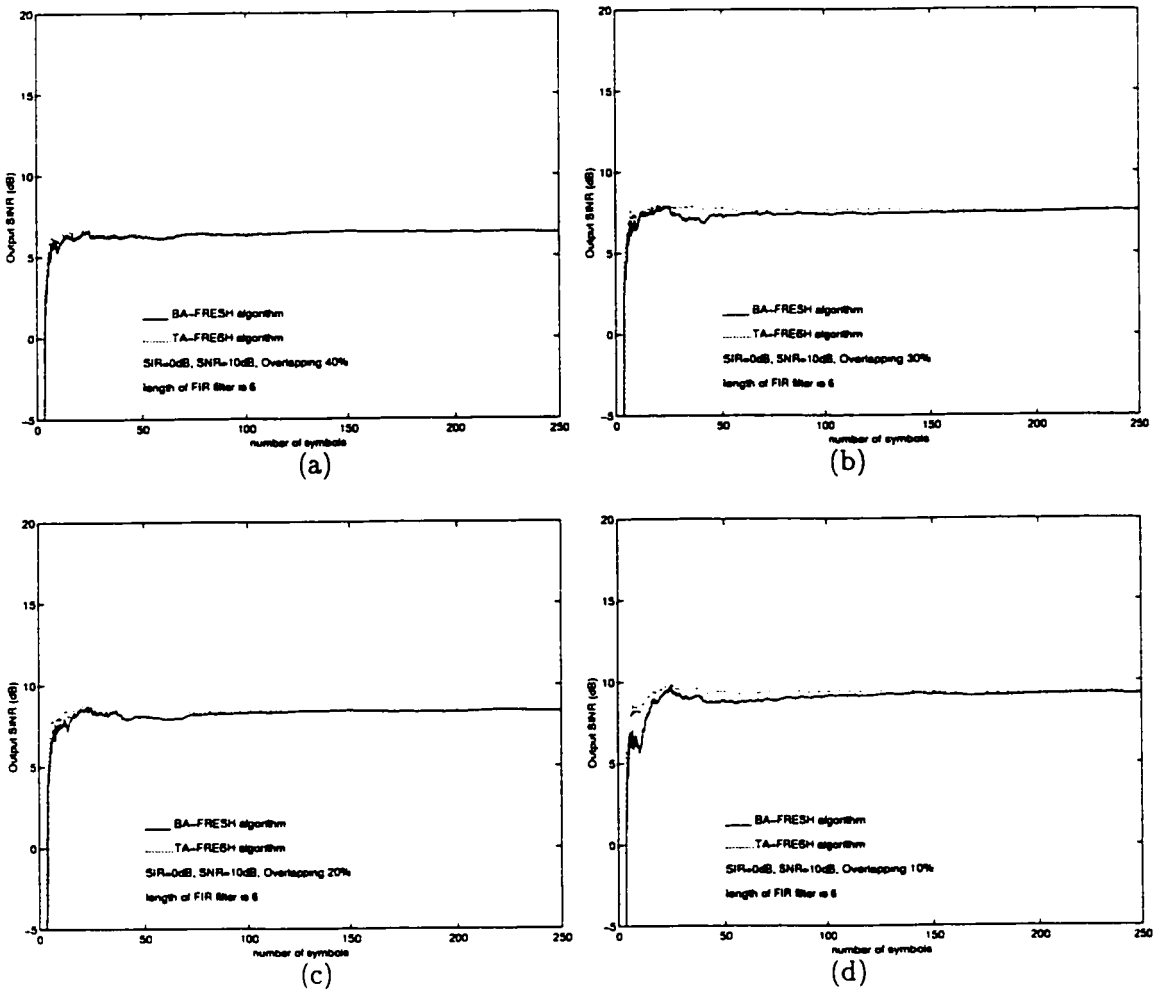

Figure 3.6: Output SINR of BA-FRESH and TA-FRESH against the spectral overlapping 40%, 30%, 20% and 10% when N_o is 6, input SIR is 0dB, and SNR is 10dB

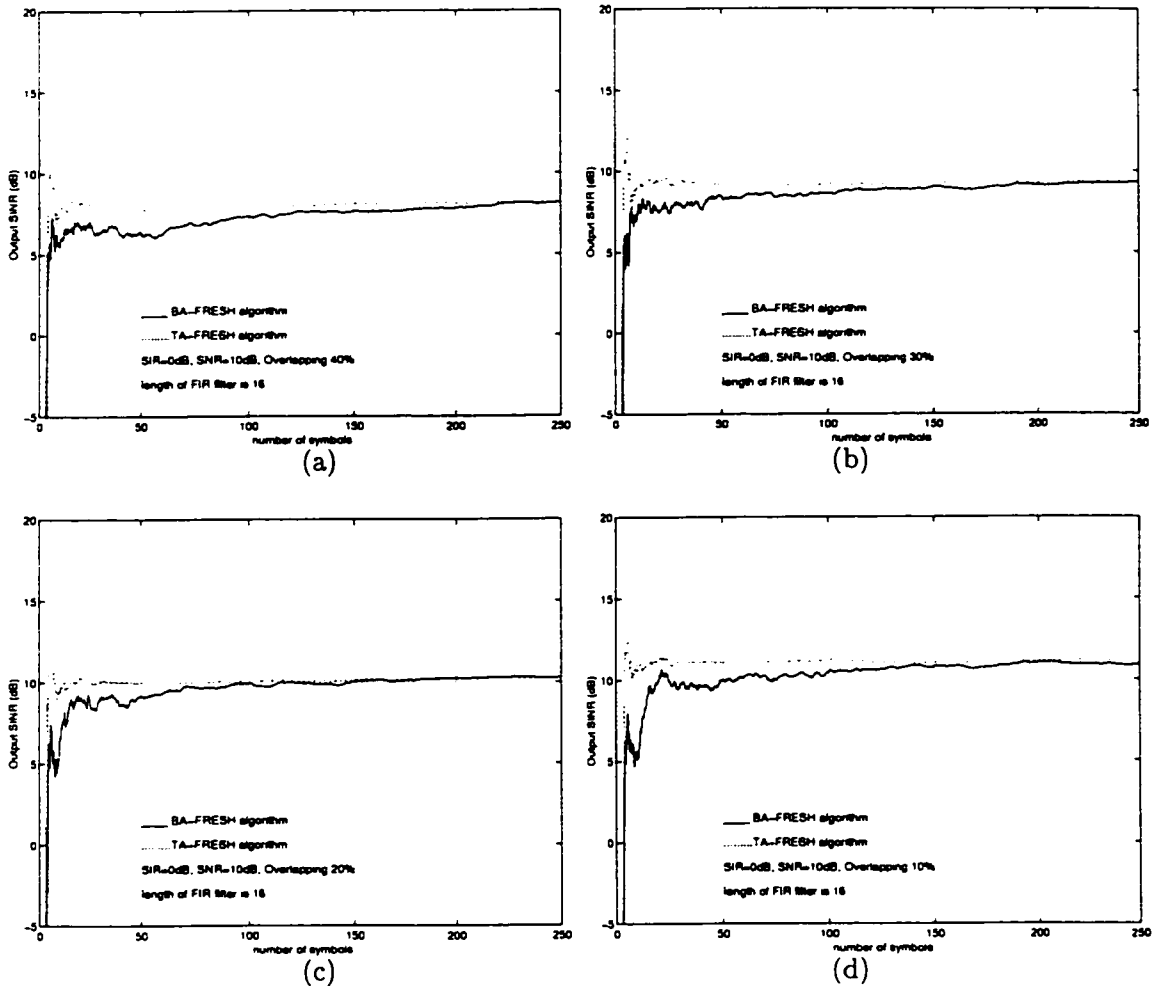

Figure 3.7: Output SINR of BA-FRESH and TA-FRESH against the spectral overlapping 40%, 30%, 20% and 10% when N_o is 16, input SIR is 0dB, and SNR is 10dB

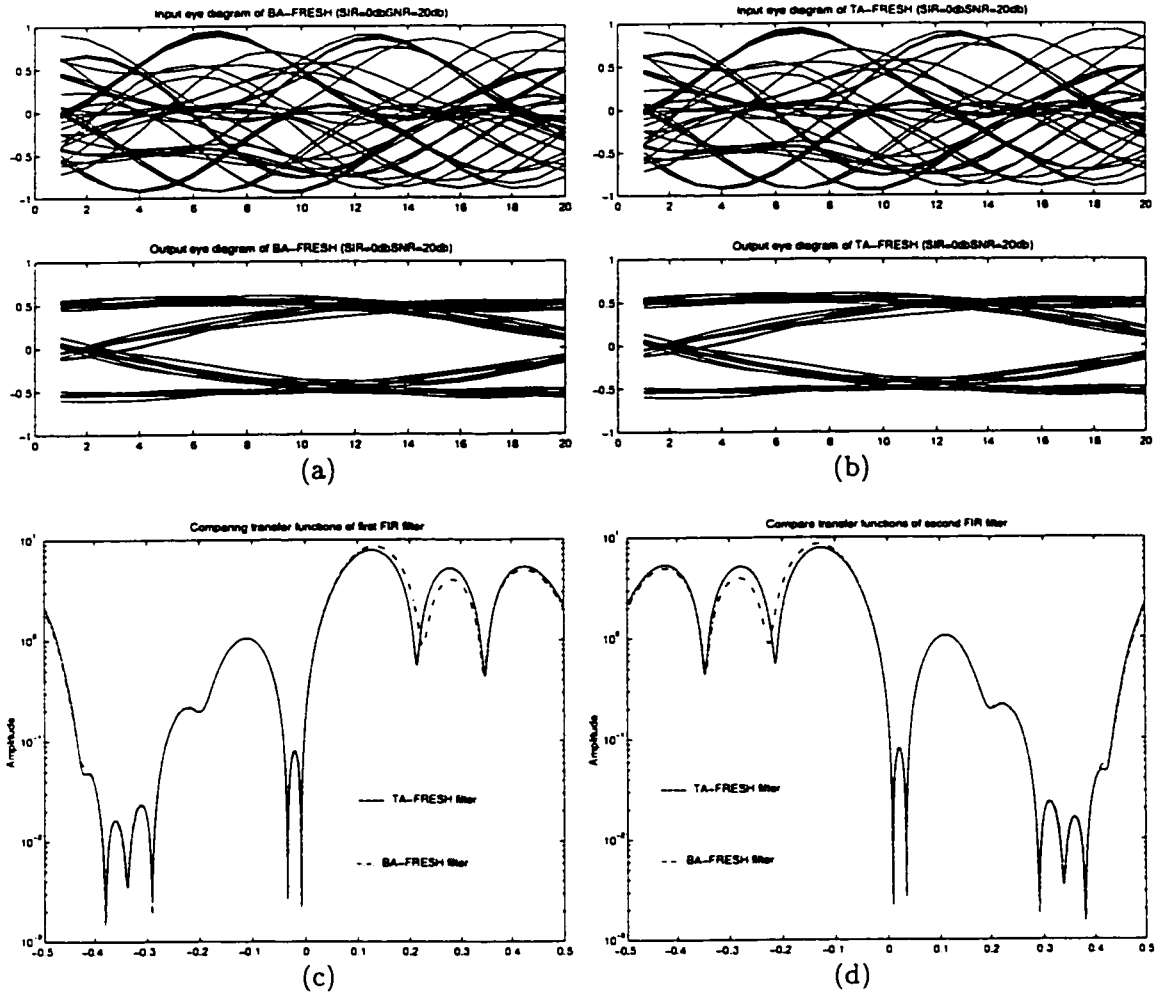

Figure 3.8: Output eye diagrams and the transfer functions of BA-FRESH compared with those of TA-FRESH when input SIR is 0dB, SNR is 20dB, and the spectral overlapping is 30%

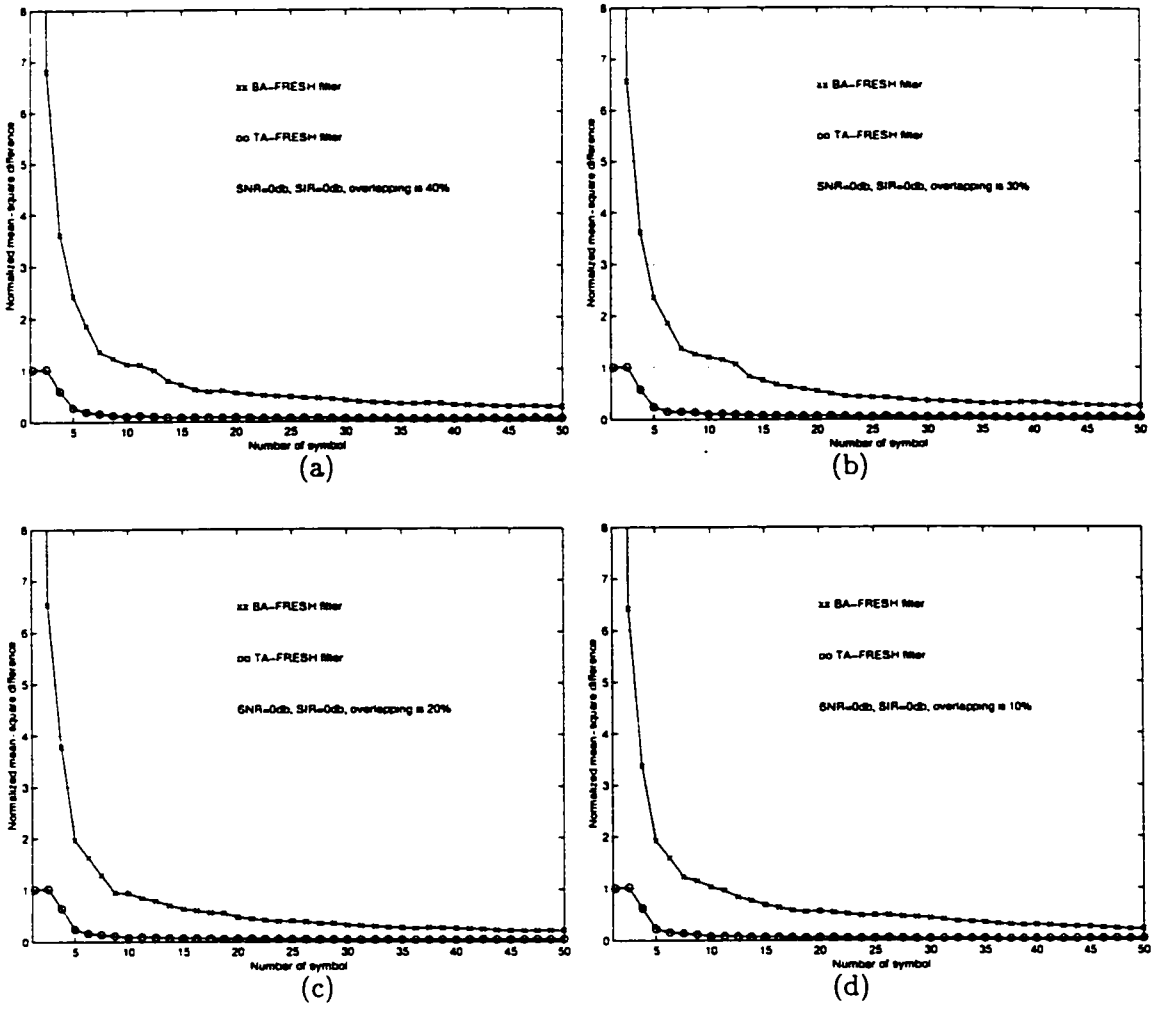

Figure 3.9: Normalized convergence of BA-FRESH and TA-FRESH against different spectral overlapping 40%, 30%, 20% and 10% when input SNR is 0dB and input SIR is 0dB

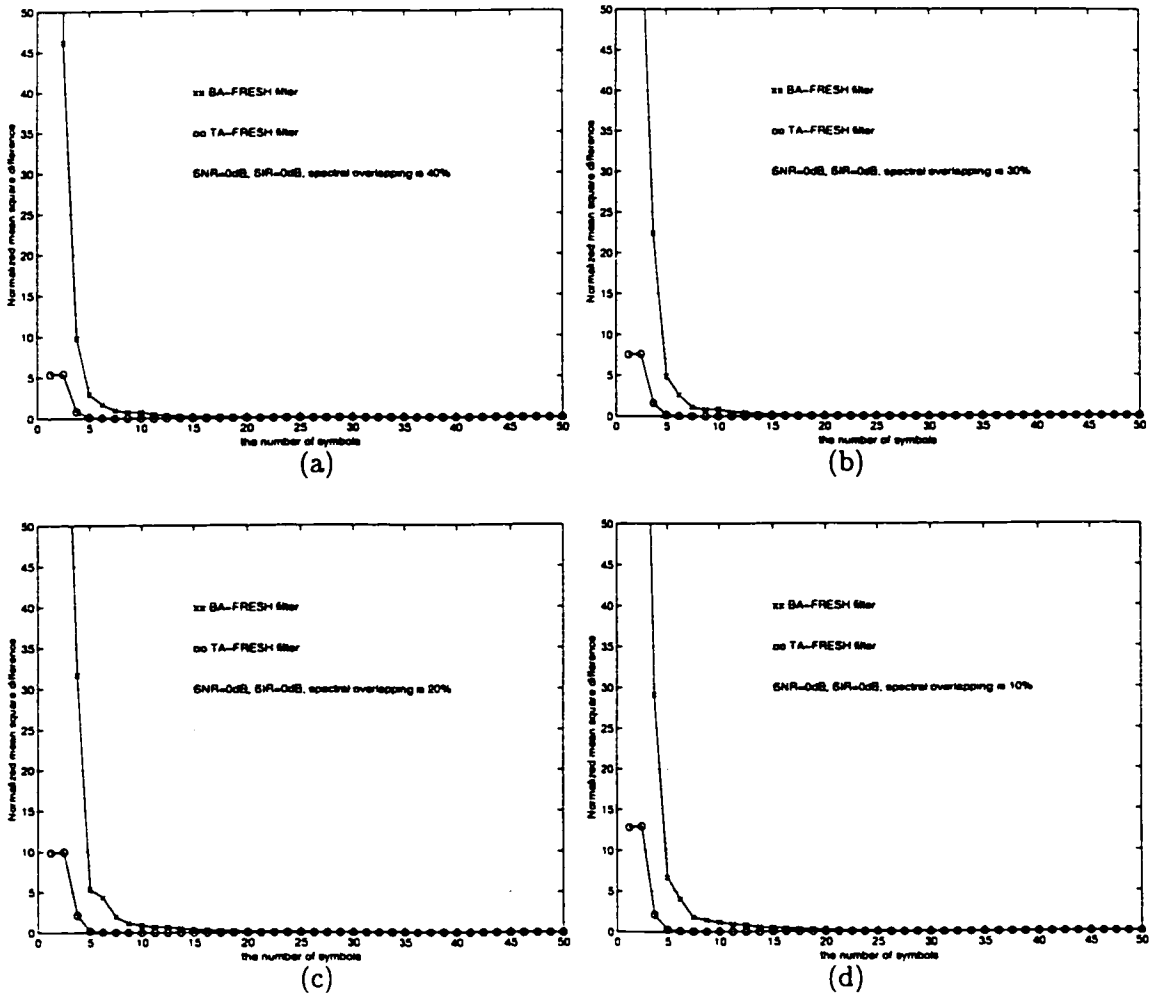

Figure 3.10: Normalized MSE of BA-FRESH and TA-FRESH against different spectral overlapping 40%, 30%, 20% and 10% when input SNR is 0dB and input SIR is 0dB

Chapter 4

Probability Error Analysis of BA-FRESH and TA-FRESH

The finite sample output probability error of the BA-FRESH and TA-FRESH algorithms are studied theoretically and by simulation in this chapter. Let N be the length of input data. $\boldsymbol{h}(N)$ is the finite sample time realization of the BA-FRESH or TA-FRESH filter coefficient vector. $\boldsymbol{h}(N)$ is a function of N and it is also a random vector for given N. We do K experiments to obtain K realizations of $\boldsymbol{h}(N)$ as $\boldsymbol{h}^{(1)}(N)$, $\boldsymbol{h}^{(2)}(N)$, $\cdots$, $\boldsymbol{h}^{(K)}(N)$. For the kth experiment with given $\boldsymbol{h}^{(k)}(N)$, we can obtain the simulation value of the finite sample probability error $P_{e\_s}^{k}$. Defining the P_{e_s} as $P_{e\_s} = \frac{1}{K}\sum_{k=1}^{K} P_{e\_s}^{k}$, P_{e_s} is called the simulation value of the finite sample probability error of $\boldsymbol{h}(N)$. We also hope to obtain theoretical formulae to compute the finite sample probability error of BA-FRESH and TA-FRESH theoretically. Because the analysis procedures to BA-FRESH and TA-FRESH are similar, we use BA-FRESH as an example to do this analysis. Firstly, the input signals and system model are given in this chapter. The input of threshold is analyzed. Statistical analysis of the output noise, statistical analysis of the output component of the desired signal, and statistical analysis of the output interference is given. The output probability error theoretical formulae of BA-FRESH and TA-FRESH are obtained. At last, numerical examples are presented to examine the output probability error of BA-FRESH and TA-

FRESH in different scenarios theoretically and by simulations.

4.1 The System Model of BA-FRESH and TA-FRESH

The system model which we consider is shown in Fig. 4.1. Because the analysis procedures to BA-FRESH and TA-FRESH are very similar, we use BA-FRESH as an example to do this analysis.

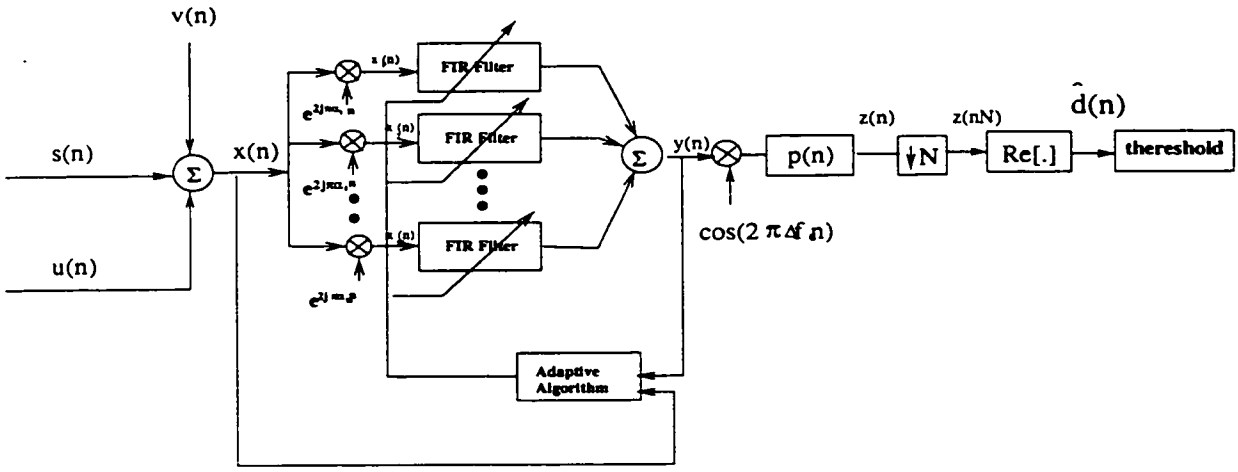

Figure 4.1: System model of BA-FRESH and TA-FRESH

Input Signals: For the input signals, we assume that the desired signal $s(n)$ and the interference $u(n)$ are real BPSK signals which have same baud rate. They are statistically independent of each other. Let the sampling rate of these signal is $1/T_s$. For given the baud rate $1/T_b$, we choose the sampling rate such that

$$T_s = T_b/N_s \tag{4.1.1}$$

where N_s is an integer. In the following analysis, we normalize T_s as one in our expressions.

The desired signal $s(n)$ can be modeled as

$$s(n) = \sum_{k=-\infty}^{\infty} d(k)g(n - kN_s)\cos(2\pi\Delta f_c n) \tag{4.1.2}$$

where Δf_c is the frequency offset of the desired signal. The message signal of the desired signal is $d(n)$ where $d(n) = \pm 1$ is a random signal. The signal $d(n) = +1$ and $d(n) = -1$ occur independently with equal probability and therefore, the variance of $d(n)$ is equal to one. The function $g(n)$ is a square root raised cosine pulse shaping filter with a roll-off factor equal to one [31]. We normalize $g(n)$ such that $\sum_n g(n)g^*(n) = 1$.

The interference $u(n)$ can be modeled as

$$u(n) = A_u \sum_{k=-\infty}^{\infty} d_u(k) g_u(n - kN_s) \cos(2\pi \Delta f_u n) \tag{4.1.3}$$

where A_u is the amplitude of the interference and Δf_u is the frequency offset of the interference. The symbol $d_u(n) = +1$ and $d_u(n) = -1$ occur independently with equal probability and the variance of $d_u(n)$ is one. The function $g_u(n)$ is the normalized square root raised cosine pulse shaping filter with a roll-off factor equal to one.

The input noise $v(n)$ is assumed to be a stationary white zero mean Gaussian noise and have

$$E[v(n)] = 0, \qquad E[v(n_1)v^*(n_2)] = \sigma_v^2 \delta(n_1 - n_2) \tag{4.1.4}$$

where σ_v^2 is the variance of $v(n)$ and $\delta(n)$ is the Kronecker delta function.

The input of the BA-FRESH filter is

$$x(n) = s(n) + u(n) + v(n). \tag{4.1.5}$$

BA-FRESH algorithm: The frequency shift in the BA-FRESH filter $\alpha_m (m = 1, 2 \cdots M)$ can be chosen as $\pm 2\Delta f_c + p/T_b$, where M is the number of branches of FRESH filter. p is an integer. Here, the frequency offset can be viewed as a design parameter and we choose the frequency offset Δf_c to be a multiple of $1/T_b$. Therefore, we have

$$\Delta f_c = N_c/T_b, \qquad \alpha_m = N_m/T_b, \quad m = 1, 2, \cdots M. \tag{4.1.6}$$

where N_c and N_m are integers, $N_m = \pm 2N_c + p$. We choose the low-pass filter $p(n)$ as the

normalized square root raised cosine pulse shaping filter $g(-n)$.

The filter coefficient $h_m(n)$ $(m = 1, 2, \cdots M)$ denotes the impulse response of the mth FIR filter in the BA-FRESH filter or in the TA-FRESH filter, where M is the number of branches of the FRESH filter. These filter coefficients consist of the filter coefficient vector of the BA-FRESH filter $\boldsymbol{h}_{BF}$ which is defined in Eq. (3.2.11) or that of the TA-FRESH filter $\boldsymbol{h}_{TF}$ which is defined in Eq. (3.2.20). In the following analysis, the filter coefficients are assumed to be the filter coefficient vector of the BA-FRESH filter. We will note that the our analysis procedure is also suitable to analyze the output probability error of the TA-FRESH filter. Moreover, for analysis simplicity, we will assume that the filter coefficient vector is uncorrelated with the input white noise $\nu(n)$, the input desired binary signal $d(n)$ and the input interfering binary signals $d_u(n)$. We call this assumption as the uncorrelation assumption. For the infinite sample time average realization, using the property 3.1, we note that the filter coefficients vector of the BA-FRESH filter $\boldsymbol{h}_{BF}$ is equal to the filter coefficients vector of the TA-FRESH filter $\boldsymbol{h}_{TF}$. These filter coefficient vectors are constant vectors $\boldsymbol{h}_{opt}$ which is defined in Eq. (3.2.24). Therefore, the uncorrelation assumption is valid in the infinite sample case. For the finite sample time average realization, the filter coefficient vectors $\hat{\boldsymbol{h}}_{BF}(N)$ and $\hat{\boldsymbol{h}}_{TF}(N)$ are defined in Eqs. (3.2.12) and (3.2.22) respectively. They are random vectors. It is difficult to examine the uncorrelation assumption theoretically in the finite sample case. Here, we use an experimental method to examine the assumption. We generate K random samples of the correlation $\boldsymbol{g}_k(N) = a_k(N)\boldsymbol{h}_k(N)$, where $a_k(N)$ denotes input binary signal or the input white noise. $\boldsymbol{h}_k(N)$ denotes the kth finite sample time average realization of the filter coefficients $\hat{\boldsymbol{h}}_{BF}(N)$ or $\hat{\boldsymbol{h}}_{TF}(N)$, where N is number of samples. We calculate the normalized correlation value $\bar{g} = (\|\frac{1}{K}\sum_k \boldsymbol{g}_k(N)\|^2)/(\frac{1}{K}\sum_k \|\boldsymbol{g}_k(N)\|^2)$. We found these correlation values are very small, that is, $\bar{g} < 10^{-3}$, see Appendix B. Therefore, we say the uncorrelation assumption is valid in the finite sample case. In the section 4.3, comparing the theoretical results in which we use the uncorrelation assumption with the simulation results, we will see that that the theoretical results and the simulation results match well. This fact also shows that the uncorrelation assumption is valid in the finite sample case.

4.2 The Input of Threshold

When the input $x(n)$ passes through the BA-FRESH filter, the output of the BA-FRESH filter is

$$y(n) = \sum_{l=1}^{M} \sum_{k} h_l(n-k) e^{j2\pi\alpha_l k} x(k). \tag{4.2.1}$$

The output of the low-pass filter is

$$\begin{aligned} z(n) &= \sum_{k} p(n-k)\cos(2\pi\Delta f_c k) y(k) \qquad (4.2.2)\\ &= \sum_{k} \frac{1}{2} p(n-k) e^{-j2\pi\Delta f_c(n-k)} e^{j2\pi\Delta f_c n} y(k) + \sum_{k} \frac{1}{2} p(n-k) e^{j2\pi\Delta f_c(n-k)} e^{-j2\pi\Delta f_c n} y(k). \end{aligned}$$

Substituting Eq. (4.2.1) into Eq. (4.2.2), we have

$$\begin{aligned} z(n) &= \sum_{l=1}^{M} \sum_{k_2} \sum_{k_1} \frac{1}{2} p(n-k_1) e^{-j2\pi\Delta f_c(n-k_1)} e^{-j2\pi\alpha_l(n-k_1)} h_l(k_1-k_2) \qquad (4.2.3)\\ &\quad e^{-j2\pi\alpha_l(k_1-k_2)} x(k_2) e^{j2\pi\Delta f_c n} e^{j2\pi\alpha_l n}\\ &+ \sum_{l=1}^{M} \sum_{k_2} \sum_{k_1} \frac{1}{2} p(n-k_1) e^{j2\pi\Delta f_c(n-k_1)} e^{-j2\pi\alpha_l(n-k_1)} h_l(k_1-k_2)\\ &\quad e^{-j2\pi\alpha_l(k_1-k_2)} x(k_2) e^{-j2\pi\Delta f_c n} e^{j2\pi\alpha_l n}. \end{aligned}$$

Using Eq. (4.1.6) and noting that $T_b = N_s$, we have that $e^{j2\pi\Delta f_c n N_s} = 1$ and $e^{j2\pi\alpha_l n N_s} = 1$. Hence, the output of the sampler $z(nN_s)$ is

$$\begin{aligned} z(nN_s) &= \sum_{l=1}^{M} \sum_{k_2} \sum_{k_1} \frac{1}{2} p(nN_s-k_1) e^{-j2\pi\Delta f_c(nN_s-k_1)} e^{-j2\pi\alpha_l(nN_s-k_1)} \qquad (4.2.4)\\ &\quad h_l(k_1-k_2) e^{-j2\pi\alpha_l(k_1-k_2)} x(k_2)\\ &+ \sum_{l=1}^{M} \sum_{k_2} \sum_{k_1} \frac{1}{2} p(nN_s-k_1) e^{j2\pi\Delta f_c(nN_s-k_1)} e^{-j2\pi\alpha_l(nN_s-k_1)} h_l(k_1-k_2) e^{-j2\pi\alpha_l(k_1-k_2)} x(k_2). \end{aligned}$$

Let $nN_s - k_1 = m$, we obtain

$$z(nN_s) = \sum_{l=1}^{M} \sum_{m} \sum_{k_2} h_l(nN_s - m - k_2) e^{-j2\pi\alpha_l(nN_s-m-k_2)} \tag{4.2.5}$$

$$\frac{1}{2}p(m)e^{-j2\pi\Delta f_c m}e^{-j2\pi\alpha_l m}x(k_2)$$
$$+\sum_{l=1}^{M}\sum_{m}\sum_{k_2}h_l(nN_s-m-k_2)e^{-j2\pi\alpha_l(nN_s-m-k_2)}\frac{1}{2}p(m)e^{j2\pi\Delta f_c m}e^{-j2\pi\alpha_l m}x(k_2).$$

Let $nN_s - k_2 = k$, we obtain

$$\begin{aligned} z(nN_s) &= \sum_{l=1}^{M}\sum_{m}\sum_{k}h_l(k-m)e^{-j2\pi\alpha_l(k-m)}\frac{1}{2}p(m)e^{-j2\pi\Delta f_c m}e^{-j2\pi\alpha_l m}x(nN_s-k) \\ &+ \sum_{l=1}^{M}\sum_{m}\sum_{k}h_l(k-m)e^{-j2\pi\alpha_l(k-m)}\frac{1}{2}p(m)e^{j2\pi\Delta f_c m}e^{-j2\pi\alpha_l m}x(nN_s-k) \\ &= \sum_{k}H(k)x(nN_s-k) \end{aligned} \tag{4.2.6}$$

where we define $H(n)$ as

$$H(n) = \sum_{l=1}^{M}\sum_{m=0}^{L_2-1}h_l(n-m)e^{-j2\pi\alpha_l(n-m)}p(m)e^{-j2\pi\alpha_l m}\cos 2\pi\Delta f_c m. \tag{4.2.7}$$

We note that the length of $H(n)$ is $N_o + L_2 - 1$. N_o is the length of the filter $h_l(n)$. Here, we assume $h_l(n)$, $(l = 1, 2, \cdots M)$ has same length. L_2 is the length of the filter $p(n)$, that is, the length of the filter $g(n)$. Substituting Eq. (4.1.5) into Eq. (4.2.6), we may express the output of the sampler as

$$z(nN_s) = \sum_{k=1}^{N_o+L_2-1}H(k)s(nN_s-k) + \sum_{k=1}^{N_o+L_2-1}H(k)u(nN_s-k) + \sum_{k=1}^{N_o+L_2-1}H(k)v(nN_s-k). \tag{4.2.8}$$

We divide $H(n)$ into two parts

$$H(n) = H_R(n) + jH_I(n) \tag{4.2.9}$$

where $H_R(n)$ is the real part of $H(n)$ and $H_I(n)$ is the imaginary part of $H(n)$. Moreover, $H_R(n)$ is

$$H_R(n) = \sum_{l=1}^{M}\sum_{m=0}^{L_2-1}\mathrm{Re}\left[h_l(n-m)e^{-j2\pi\alpha_l(n-m)}p(m)e^{-j2\pi\alpha_l m}\right]\cos 2\pi\Delta f_c m \tag{4.2.10}$$

where Re [·] denotes taking the real part.

The input of the threshold is

$$\hat{d}(n) = \sum_{k=1}^{N_o+L_2-1} H_R(k)s(nN_s-k) + \sum_{k=1}^{N_o+L_2-1} H_R(k)u(nN_s-k) + \sum_{k=1}^{N_o+L_2-1} H_R(k)v(nN_s-k). \tag{4.2.11}$$

Define

$$\gamma_o d(n) + \xi_{ISI}(n) = \sum_{k=1}^{N_o+L_2-1} H_R(k)s(nN_s-k) \tag{4.2.12}$$

$$\xi_{CTI}(n) = \sum_{k=1}^{N_o+L_2-1} H_R(k)u(nN_s-k) \tag{4.2.13}$$

$$\eta(n) = \sum_{k=1}^{N_o+L_2-1} H_R(k)v(nN_s-k). \tag{4.2.14}$$

We have

$$\hat{d}(n) = \gamma_o d(n) + \xi_{ISI}(n) + \xi_{CTI}(n) + \eta(n) \tag{4.2.15}$$

where $\gamma_o d(n)$ denotes the output component of the desired symbol. $\xi_{ISI}(n)$ denotes the output component of the Inter-Symbol Interference (ISI). $\xi_{CTI}(n)$ denotes the output component of the Cross-Talk Interference (CTI). $\eta(n)$ denotes the output component of the noise. Defining

$$\eta_e(n) = \eta(n) + \xi_{ISI}(n) + \xi_{CTI}(n), \tag{4.2.16}$$

we have that the input of the threshold is

$$\hat{d}(n) = \gamma_o d(n) + \eta_e(n) \tag{4.2.17}$$

where γ_o is the coefficient of the desired symbol. η_e is the combination of the output noise component, the output ISI component and the output CTI component.

4.3 Statistical Analysis of $\eta(n)$

The output noise component $\eta(n)$ is

$$\eta(n) = \sum_{k=1}^{N_o+L_2-1} H_R(k)v(nN_s - k). \tag{4.3.1}$$

Because the system is a linear system, the output noise $\eta(n)$ has Gaussian probability density function (PDF) when the input noise has Gaussian PDF. Using the uncorrelation assumption, we note that $H_R(k)$ is uncorrelated with $\nu(nN_s - k)$. Using Eq. (4.3.1), the mean of the output noise $\eta(n)$ is

$$E[\eta(n)] = \sum_{k=1}^{N_o+L_2-1} E[H_R(k)]E[v(nN_s - k)] = 0. \tag{4.3.2}$$

Using Eq. (4.3.1), the variance of the output noise $\eta(n)$ is

$$\begin{aligned} \sigma_\eta^2 &= E[\eta(n)\eta^*(n)] \\ &= \sum_{k_1}\sum_{k_2} E[H_R(k_1)H_R^*(k_2)]E[v(nN_s - k_1)v^*(nN_s - k_2)] \\ &= \sigma_v^2 \sum_{k} E[H_R(k)H_R^*(k)] \end{aligned} \tag{4.3.3}$$

where σ_v^2 is the variance of the input noise $v(n)$. We note that $H_R(k)$ is defined in Eq. (4.2.10) and σ_v^2 is a constant. Substituting Eq. (4.2.10) into Eq. (4.3.3), we obtain

$$\begin{aligned} \sigma_\eta^2 = \sigma_v^2 \sum_{k=1}^{N_o+L_2-1} \sum_{l_1=1}^{M} \sum_{m_1=0}^{L_2-1} \sum_{l_2=1}^{M} \sum_{m_2=0}^{L_2-1} \cos(2\pi\Delta f_c m_1)\cos(2\pi\Delta f_c m_2) \\ E\left[\mathrm{Re}\left[h_{l_1}(k-m_1)e^{-j2\pi\alpha_{l_1}(k-m_1)}p(m_1)e^{-j2\pi\alpha_{l_1}m_1}\right]\right. \\ \left.\mathrm{Re}\left[h_{l_2}(k-m_2)e^{-j2\pi\alpha_{l_2}(k-m_2)}p(m_2)e^{-j2\pi\alpha_{l_2}m_2}\right]\right]. \end{aligned} \tag{4.3.4}$$

4.4 Statistical Analysis of the Output Component of the Desired Signal

When the input desired signal $s(n)$ pass through the system, the input of the threshold is

$$\gamma_o d(n) + \xi_{ISI}(n) = \sum_{k=1}^{N_o+L_2-1} H_R(k) s(nN_s - k) \tag{4.4.1}$$

where $s(n)$ and $H_R(n)$ are defined in Eqs. (4.1.2) and (4.2.10) respectively. Substituting Eq. (4.1.2) into Eq. (4.4.1) and using Eq. (4.1.6), we obtain

$$\gamma_o d(n) + \xi_{ISI}(n) = \sum_{m=-\infty}^{\infty} d(m) \sum_{k=1}^{N_o+L_2-1} g(nN_s - mN_s - k) \cos(2\pi\Delta f_c k) H_R(k). \tag{4.4.2}$$

We define

$$\gamma(n) = \sum_{k=1}^{N_o+L_2-1} g(nN_s - k) \cos(2\pi\Delta f_c k) H_R(k) \tag{4.4.3}$$

where we note that the length of $\gamma(n)$ is K_1,

$$K_1 = \lceil \frac{1}{N_s}(N_o + 2L_2 - 2) \rceil \tag{4.4.4}$$

where $\lceil . \rceil$ denotes taking integer. Substituting Eq. (4.2.10) into Eq. (4.4.3), we obtain

$$\gamma(n) = \sum_{k=1}^{N_o+L_2-1} \sum_{l=1}^{M} \sum_{m=0}^{L_2-1} g(nN_s - k) \operatorname{Re}\left[h_l(k-m) e^{-j2\pi\alpha_l(k-m)} p(m) e^{-j2\pi\alpha_l m}\right] \cos(2\pi\Delta f_c m) \cos(2\pi\Delta f_c k). \tag{4.4.5}$$

Using Eqs. (4.4.2) and (4.4.3), we obtain

$$\begin{aligned} \gamma_o d(n) + \xi_{ISI}(n) &= \sum_{m=-\infty}^{\infty} d(m)\gamma(n-m) = \sum_{m=-\infty}^{\infty} d(n-m)\gamma(m) \\ &= \gamma(0) d(n) + \sum_{m \neq n} d(n-m)\gamma(m). \end{aligned} \tag{4.4.6}$$

Here, we define

$$\gamma_o = \gamma(0), \quad \xi_{ISI}(n) = \sum_{m \neq n} d(n-m)\gamma(m) = \sum_{m} d(n-m)\gamma_1(m) \tag{4.4.7}$$

where $\gamma_o d(n)$ is the desired symbol component. $\xi_{ISI}(n)$ is the ISI component.

$$\begin{aligned} \gamma_o &= \sum_{k=1}^{N_o+L_2-1} \sum_{l=1}^{M} \sum_{m=0}^{L_2-1} g(-k)\mathrm{Re}\left[h_l(k-m)e^{-j2\pi\alpha_l(k-m)}p(m)e^{-j2\pi\alpha_l m}\right] \\ &\quad \cos(2\pi\Delta f_c m)\cos(2\pi\Delta f_c k). \end{aligned} \tag{4.4.8}$$

The mean of γ_o is

$$\begin{aligned} \mu_{\gamma_o} = E[\gamma_o] &= \sum_{k=1}^{N_o+L_2-1} \sum_{l=1}^{M} \sum_{m=0}^{L_2-1} g(-k) \\ &\quad \mathrm{Re}\left[E[h_l(k-m)]e^{-j2\pi\alpha_l(k-m)}p(m)e^{-j2\pi\alpha_l m}\right]\cos(2\pi\Delta f_c m)\cos(2\pi\Delta f_c k). \end{aligned} \tag{4.4.9}$$

The variance of γ_o is

$$\sigma^2_{\gamma_o} = E[(\gamma_o - \mu_{\gamma_o})(\gamma_o - \mu_{\gamma_o})^*]. \tag{4.4.10}$$

For the ISI term,

$$\gamma_1(n) = \begin{cases} \gamma(n) & n \neq 0 \\ 0 & n = 0 \end{cases}$$

$$\begin{cases} \sum_{k=1}^{N_o+L_2-1}\sum_{l=1}^{M}\sum_{m=0}^{L_2-1} g(nN_s-k)\mathrm{Re}\left[h_l(k-m)e^{-j2\pi\alpha_l(k-m)}p(m)e^{-j2\pi\alpha_l m}\right] & \\ \cos(2\pi\Delta f_c m)\cos(2\pi\Delta f_c k) & n \neq 0 \\ 0 & n = 0 \end{cases} \tag{4.4.11}$$

where the length of $\gamma_1(n)$ is K_1. Using the uncorrelation assumption, we note that $\gamma(m)$ is uncorrelated with $d(n-m)$. Using Eq. (4.4.7), we also note that the mean of of $\xi_{ISI}(n)$ is zero. The variance of $\xi_{ISI}(n)$ is

$$\begin{aligned} \zeta_{ISI} &= E[\xi_{ISI}(n)\xi^*_{ISI}(n)] \\ &= \sum_{m_1=1}^{K_1}\sum_{m_2=1}^{K_1} E[d(n-m_1)d(n-m_2)]E[\gamma_1(m_1)\gamma_1^*(m_2)] = \sum_{k=1}^{K_1} E[\gamma_1(k)\gamma_1^*(k)]. \end{aligned} \tag{4.4.12}$$

We also note that ζ_{ISI} is a constant. Substituting Eq. (4.4.11) into (4.4.12), we obtain

$$\begin{aligned}\zeta_{ISI} = & \sum_{k=1}^{K_1}\sum_{k_1=1}^{N_o+L_2-1}\sum_{l_1=1}^{M}\sum_{m_1=0}^{L_2-1}\sum_{k_2=1}^{N_o+L_2-1}\sum_{m_2=0}^{L_2-1}\sum_{l_2=1}^{M} g(kN_s-k_1)g(kN_s-k_2) \quad (4.4.13)\\ & E\left[\mathrm{Re}\left[h_{l_1}(k_1-m_1)p(m_1)e^{-j2\pi\alpha_{l_1}(k_1-m_1)}e^{-j2\pi\alpha_{l_1}m_1}\right]\right.\\ & \left.\mathrm{Re}\left[h_{l_2}(k_2-m_2)p(m_2)e^{-j2\pi\alpha_{l_2}(k_2-m_2)}e^{-j2\pi\alpha_{l_2}m_2}\right]\right]\\ & \cos(2\pi\Delta f_c m_1)\cos(2\pi\Delta f_c m_2)\cos(2\pi\Delta f_c k_1)\cos(2\pi\Delta f_c k_2).\end{aligned}$$

4.5 Statistical Analysis of $\xi_{CTI}(n)$

When the input interference $u(n)$ passes through the system, the input of threshold which is called the cross-talk interference is

$$\xi_{CTI}(n) = \sum_{k=1}^{N_o+L_2-1} H_R(k)u(nN_s-k) \quad (4.5.1)$$

where $u(n)$ and $H_R(n)$ are defined in Eqs. (4.1.3) and (4.2.10) respectively. ξ_{CTI} denotes the CTI component which is defined as

$$\begin{aligned}\xi_{CTI}(n) &= \sum_{k=1}^{N_o+L_2-1} H_R(k)u(nN_s-k) \quad (4.5.2)\\ &= A_u\sum_{m=-\infty}^{\infty} d_u(n-m)\sum_{k=1}^{N_o+L_2-1} g_u(mN_s-k)\cos(2\pi\Delta f_u(nN_s-k))H_R(k).\end{aligned}$$

When we define

$$\beta(m,n) = A_u\sum_{k=1}^{N_o+L_2-1} g_u(mN_s-k)H_R(k)\cos(2\pi\Delta f_u(nN_s-k)), \quad (4.5.3)$$

we have

$$\xi_{CTI}(n) = \sum_{m=-\infty}^{\infty} d_u(n-m)\beta(m,n). \quad (4.5.4)$$

Using the uncorrelation assumption, we note that $d_u(n-m)$ is uncorrelated with $\beta(m,n)$. We note that the mean of $\xi_{CTI}(n)$ is zero and the variance of $\xi_{CTI}(n)$ is

$$\begin{aligned}\zeta_{CTI}(n) &= E[\xi_{CTI}(n)\xi^*_{CTI}(n)] \\ &= \sum_{m_1}\sum_{m_2} E[d_u(n-m_1)d_u(n-m_2)]E[\beta(m_1,n)\beta^*(m_2,n)] \\ &= \sum_{m} E[\beta(m,n)\beta^*(m,n)].\end{aligned} \tag{4.5.5}$$

Here, the length of $\beta(m,n)$ is K_2,

$$K_2 = \lceil \frac{1}{N_s}(N_o + L_2 + L_3 - 2) \rceil, \tag{4.5.6}$$

L_3 is the length of $g_u(n)$. Using Eqs. (4.2.10), (4.5.3) and (4.5.5), we obtain

$$\begin{aligned}\zeta_{CTI}(n) = A_u^2 &\sum_{k=1}^{K_2}\sum_{k_1=1}^{N_o+L_2-1}\sum_{l_1=1}^{M}\sum_{m_1=0}^{L_2-1}\sum_{k_2=1}^{N_o+L_2-1}\sum_{m_2=0}^{L_2-1}\sum_{l_2=1}^{M} \\ &g_u(kN_s-k_1)E\left[\mathrm{Re}\left[h_{l_1}(k_1-m_1)p(m_1)e^{-j2\pi\alpha_{l_1}(k_1-m_1)}e^{-j2\pi\alpha_{l_1}m_1}\right]\right. \\ &\left. g_u(kN_s-k_2)\ \mathrm{Re}\left[h_{l_2}(k_2-m_2)p(m_2)e^{-j2\pi\alpha_{l_2}(k_2-m_2)}e^{-j2\pi\alpha_{l_2}m_2}\right]\right] \\ &\cos(2\pi\Delta f_c m_1)\cos(2\pi\Delta f_c m_2)\cos(2\pi\Delta f_u(nN_s-k_1))\cos(2\pi\Delta f_u(nN_s-k_2)).\end{aligned} \tag{4.5.7}$$

From Eq. (4.5.7), we note that $\zeta_{CTI}(n)$ is a periodic function. The minimum integer value of n which make $\Delta f_u n N_s$ be an integer is the period of the function $\zeta_{CTI}(n)$. Let Q denote the period of $\zeta_{CTI}(n)$. Q may be determined as

$$Q = \min\{n : \Delta f_u n N_s = \text{integer}\} \tag{4.5.8}$$

where N_s is defined in Eq. (4.1.1). For example, when $\Delta f_u = 0.17$, and $N_s = 20$, we have $Q = 5$, because $5k$ can make $\Delta f_u n N_s$ be an integer, where k is an integer. The average value of $\zeta_{CTI}(n)$ is

$$\begin{aligned}\zeta_{CTIave} = \frac{A_u^2}{Q} &\sum_{n=0}^{Q-1}\sum_{k=1}^{K_2}\sum_{k_1=1}^{N_o+L_2-1}\sum_{l_1=1}^{M}\sum_{m_1=0}^{L_2-1}\sum_{k_2=1}^{N_o+L_2-1}\sum_{m_2=0}^{L_2-1}\sum_{l_2=1}^{M} \\ &g_u(kN_s-k_1)E\left[\mathrm{Re}\left[h_{l_1}(k_1-m_1)p(m_1)e^{-j2\pi\alpha_{l_1}(k_1-m_1)}e^{-j2\pi\alpha_{l_1}m_1}\right]\right.\end{aligned} \tag{4.5.9}$$

$$g_u(kN_s - k_2)\ \mathrm{Re}\left[h_{l_2}(k_2 - m_2)p(m_2)e^{-j2\pi\alpha_{l_2}(k_2-m_2)}e^{-j2\pi\alpha_{l_2}m_2}\right]\Big]$$
$$\cos(2\pi\Delta f_c m_1)\cos(2\pi\Delta f_c m_2)\cos(2\pi\Delta f_u(nN_s - k_1))\cos(2\pi\Delta f_u(nN_s - k_2)).$$

4.6 Analysis of the Output Probability Error

Using Eq. (4.2.17), the input of the threshold is

$$\hat{d}(n) = \gamma_o d(n) + \eta_e(n) \tag{4.6.1}$$

where $d(n)$ is the desired symbol, γ_o is the random coefficient of the desired symbol which is defined as in Eq. (4.4.8). $\eta_e(n)$ is the sum of the output noise component, the output ISI interference, and the output CTI interference and it is also a random variable which is defined in Eq. (4.2.16). We know γ_o and η_e are results of a large amount of random variables acting together. γ_o and η_e can be approximated as having Gaussian distributions respectively, that is,

- γ_o is approximated as having Gaussian distribution

$$\gamma_o \sim N(\mu_{\gamma_o}, \sigma^2_{\gamma_o}) \tag{4.6.2}$$

  where μ_{γ_o} and $\sigma^2_{\gamma_o}$ are the mean and variance of γ_o respectively. μ_{γ_o} and $\sigma^2_{\gamma_o}$ are defined in Eqs. (4.4.9) and (4.4.10) respectively. The approximation accuracy is shown in Appendix C.

- η_e is approximated having Gaussian distribution

$$\eta_e \sim N(0, \sigma^2_{\eta_e}) \tag{4.6.3}$$

  where $\sigma^2_{\eta_e}$ is the variance of η_e. Using Eq. (4.2.16), We know

$$E[\eta_e(n)] = E[\eta(n)] + E[\xi_{ISI}(n)] + E[\xi_{CTI}(n)] = 0. \tag{4.6.4}$$

Using the uncorrelation assumption and noting that the input noise, input desired signal, and input interference are uncorrelated, we have that the variance of $\eta_e(n)$ is

$$\sigma_{\eta_e}^2 = E[\eta_e(n)\eta_e^*(n)] = \sigma_\eta^2 + \zeta_{ISI} + \zeta_{CTI} \tag{4.6.5}$$

σ_η^2, ζ_{ISI} and ζ_{CTI} are the variance of η, ξ_{ISI} and ξ_{CTI} respectively. They are defined in Eqs. (4.3.4), (4.4.13) and (4.5.7). Because ξ_{CTI} is periodic function, we take average value to ζ_{CTI}. The average variance is ζ_{CTIave} which is defined in Eq. (4.5.9). Therefore, the variance of η_e should be modified as

$$\sigma_{\eta_e}^2 = \sigma_\eta^2 + \zeta_{ISI} + \zeta_{CTIave}. \tag{4.6.6}$$

The approximation accuracy is shown in Appendix D.

From the uncorrelation assumption, we also note that

$$E[\gamma_o\eta^*] = 0, \quad E[\gamma_o\xi_{ISI}^*] = 0, \quad \text{and} \quad E[\gamma_o\xi_{CTI}^*] = 0. \tag{4.6.7}$$

Therefore, we have

$$E[\gamma_o\eta_e^*] = 0. \tag{4.6.8}$$

Because γ_o and η_e have Gaussian distributions and they are uncorrelated each other, we conclude that γ_o and η_e are independent each other.

Let P_e denote the probability error of $\hat{d}(n)$, then

$$\begin{aligned} P_e &= \text{Prob}\left\{[\hat{d}(n) > 0 \cap d(n) = -1] \cup [\hat{d}(n) < 0 \cap d(n) = 1]\right\} \\ &= \frac{1}{2}\text{Prob}(-\gamma_o + \eta_e > 0) + \frac{1}{2}\text{Prob}(\gamma_o + \eta_e < 0). \end{aligned} \tag{4.6.9}$$

Using the distribution approximations, we obtain

$$P_e = \frac{1}{2}\int_{-\infty}^{\infty} p(\gamma_o)\int_{\gamma_o}^{\infty} \frac{1}{\sqrt{2\pi\sigma_{\eta_e}^2}} \exp^{\frac{-\eta_e^2}{2\sigma_{\eta_e}^2}} d\eta_e d\gamma_o + \frac{1}{2}\int_{-\infty}^{\infty} p(\gamma_o)\int_{-\infty}^{-\gamma_o} \frac{1}{\sqrt{2\pi\sigma_{\eta_e}^2}} \exp^{\frac{-\eta_e^2}{2\sigma_{\eta_e}^2}} d\eta_e d\gamma_o$$

$$= \int_{-\infty}^{\infty} p(\gamma_o) \int_{\gamma_o}^{\infty} \frac{1}{\sqrt{2\pi\sigma_{\eta_e}^2}} \exp^{\frac{-\eta_e^2}{2\sigma_{\eta_e}^2}} d\eta_e d\gamma_o \tag{4.6.10}$$

where $p(\gamma_o)$ is the probability density functions of γ_o.

Let $z = \frac{\eta_e}{\sqrt{2\sigma_{\eta_e}^2}}$, we have

$$P_e = \int_{-\infty}^{\infty} p(\gamma_o) \frac{1}{\sqrt{\pi}} \int_{\frac{\gamma_o}{\sqrt{2\sigma_{\eta_e}^2}}}^{\infty} e^{-z^2} dz d\gamma_o = \frac{1}{2} \int_{-\infty}^{\infty} p(\gamma_o) \text{erfc}\left(\frac{\gamma_o}{\sqrt{2\sigma_{\eta_e}^2}}\right) d\gamma_o, \tag{4.6.11}$$

where $\text{erfc}(x) = \frac{2}{\sqrt{\pi}} \int_x^{\infty} e^{-z^2} dz$. Because γ_o also has Gaussian distribution, we obtain

$$P_e = \frac{1}{2} \int_{-\infty}^{\infty} \frac{1}{\sqrt{2\pi\sigma_{\gamma_o}^2}} \exp^{\frac{-(\gamma_o - \mu_{\gamma_o})^2}{2\sigma_{\gamma_o}^2}} \text{erfc}\left(\frac{\gamma_o}{\sqrt{2\sigma_{\eta_e}^2}}\right) d\gamma_o. \tag{4.6.12}$$

After some computations shown in Appendix E, we obtain

$$P_e = \frac{1}{2}\text{erfc}\left(\sqrt{\frac{(\mu_{\gamma_o})^2}{2\sigma_{\gamma_o}^2 + 2\sigma_{\eta_e}^2}}\right) = \frac{1}{2}\text{erfc}\left(\sqrt{\frac{(\mu_{\gamma_o})^2}{2(\sigma_{\gamma_o}^2 + \sigma_\eta^2 + \zeta_{ISI} + \zeta_{CTIave})}}\right). \tag{4.6.13}$$

Here, μ_{γ_o} and $\sigma_{\gamma_o}^2$ are the mean and the variance of γ_o and they are defined in Eqs. (4.4.9), (4.4.10) respectively. σ_η^2 is the output noise power of the system. ζ_{ISI} is the output ISI interference power of the system. ζ_{CTIave} is the average output cross talk interference power of the system. They are defined in Eqs. (4.3.4), (4.4.13) and (4.5.9) respectively.

In the above analysis, the filter coefficients are assumed to be the filter coefficients of the BA-FRESH filter. We note that the above analytic steps are also suitable for the output probability error analysis of the TA-FRESH filter when the filter coefficients are the filter coefficients of the TA-FRESH filter. For the finite sample case, there is difference between output probability error of BA-FRESH and that of TA-FRESH because there is filter coefficient difference between BA-FRESH and TA-FRESH. When the number of sample is increased, the probability error difference between BA-FRESH and TA-FRESH will be reduced because the filter coefficient difference between BA-FRESH and TA-FRESH is reduced. Moreover, using the property 3.1, we note that the filter coefficients of the BA-

FRESH filter with infinite sample time average realization is equal to the filter coefficients of the TA-FRESH filter with infinite sample time average realization. Therefore, for the infinite sample time average realization of the filter coefficients, the output probability error of the BA-FRESH filter should be same as the output probability error of the TA-FRESH filter.

4.7 Numerical Results

In this section, we present numerical simulation results showing the performances of the BA-FRESH filter in comparison to those of the TA-FRESH filter. In the examples, we use BPSK signals for both the desired and the interfering signals. Thus, the desired signal and the interfering signal are given respectively by

$$s(nT_s) = \sum_{k=-\infty}^{\infty} d(k)g(nT_s - kT_{b_1})\cos(2\pi f_1 nT_s) \tag{4.7.1}$$

$$u(nT_s) = \sum_{k=-\infty}^{\infty} d_u(k)g(nT_s - kT_{b_2})\cos(2\pi f_2 nT_s) \tag{4.7.2}$$

where T_{b_1} and T_{b_2} are the baud periods, f_1 and f_2 are the carrier frequencies of $s(nT_s)$ and $u(nT_s)$ respectively and T_s is the sampling period. $\{d(k)\}$ and $\{d_u(k)\}$ are random binary sequences. For both the desired and interfering signals, we assume that $g(nT_s)$ and $g_u(nT_s)$ are the pulse obtained by the square root raised-cosine pulse shaping filter with a 100% roll-off factor [31]. We choose that the length of $g(n)$ which is equal to the length of $g_u(n)$ is equal to 159. The noise is real stationary white Gaussian noise.

Example 4.1: In this example, we examine the output probability error of the BA-FRESH filter and the TA-FRESH filter against the different number of finite symbols while we fix the input SIR and the spectral overlapping between the desired signal and the interfering signal. The spectral overlapping is defined in Chapter 3. The output probability errors of BA-FRESH and TA-FRESH are evaluated both theoretically and by simulation. The theoretical probability errors of BA-FRESH and TA-FRESH are evaluated by using Eq. (4.6.13). The desired and interfering signals are BPSK signals as given by Eqs. (4.7.1)

and (4.7.2) respectively. The baud rates of the two signals are equal, being 5kHz for both the desired signal and the interference. The carrier frequency offset of the desired signal is f_1 = 10kHz and the carrier frequency offset of the interference is 17kHz. The spectral overlapping between the desired signal and the interference is 3kHz which is equal to 30% spectral overlapping. The cycle frequencies used in the BA-FRESH filter and the TA-FRESH filter are set at α_1 = 20kHz, α_2 = −20kHz and the cycle frequency used in the reference path of the BA-FRESH filter is set at α' = 0kHz. The length of the FIR filter is 10. The input SIR is fixed at 0dB. The number of symbols is chosen as 15, 25, 50, and 150. The output probability error of BA-FRESH and TA-FRESH are shown in Fig. 4.2(a) to 4.2(d). It can be observed that the theoretical results match the simulation results well. When the number of symbols is increased, the output probability errors of BA-FRESH and TA-FRESH are reduced. When the number of symbols is increased from 15 to 50, the output probability error is reduced fast, but when the number of samples is increased from 50 to 150, the output probability error is reduced slowly. For the same finite symbols, the output probability error of the TA-FRESH filter is lower than that of the BA-FRESH filter. Moreover, when the number of symbols is increased, the difference of the probability error between BLAST and TAST is reduced. It can be expected that the probability error difference between BA-FRESH and TA-FRESH converges to zero when the number of symbols goes to infinite.

Example 4.2: In this example, we examine the output probability error of the BA-FRESH filter and the TA-FRESH filter against the different spectral overlapping and the different input SIR while we fix the number of symbols. The output probability errors of BA-FRESH and TA-FRESH are evaluated both theoretically and by simulations. The scenarios are similar to Example 4.1 except the number of symbols, the input SIR, and the spectral overlapping. Two scenarios are examined. In the first case, we examine the output probability error of the BA-FRESH filter and the TA-FRESH filter against the different spectral overlapping. We fix that the number of symbols is 15 and the input SIR is 0dB. The spectral overlapping between the desired signal and the interference is 40%, 30%, 20% and 10% respectively. Theoretical probability errors of BA-FRESH and TA-FRESH are evaluated by using Eq. (4.6.13). The output probability error of BA-FRESH and TA-FRESH against

spectral overlapping 40%, 30%, 20% and 10% are shown in Fig. 4.3(a) to 4.3(d) respectively. It can be observed that the theoretical and simulation results match well. When the spectral overlapping is reduced, the output probability errors of BA-FRESH and TA-FRESH are reduced. The second scenario is same as the first scenario in this example except that we increase the input SIR to 5dB. The output probability error of BA-FRESH and TA-FRESH against spectral overlapping 40%, 30%, 20% and 10% are shown in Fig. 4.4(a) to 4.4(d) respectively. Here, the spectral overlapping 40%, 30%, 20% and 10% are equivalent to the spectral overlapping 4kHz, 3kHz, 2kHz, and 1kHz respectively. Again, it can be observed that the theoretical and simulation results match well. Compared with Fig. 4.3 with Fig. 4.4, it can be observed that when the input SIR is increased, the output probability errors of BA-FRESH and TA-FRESH are reduced.

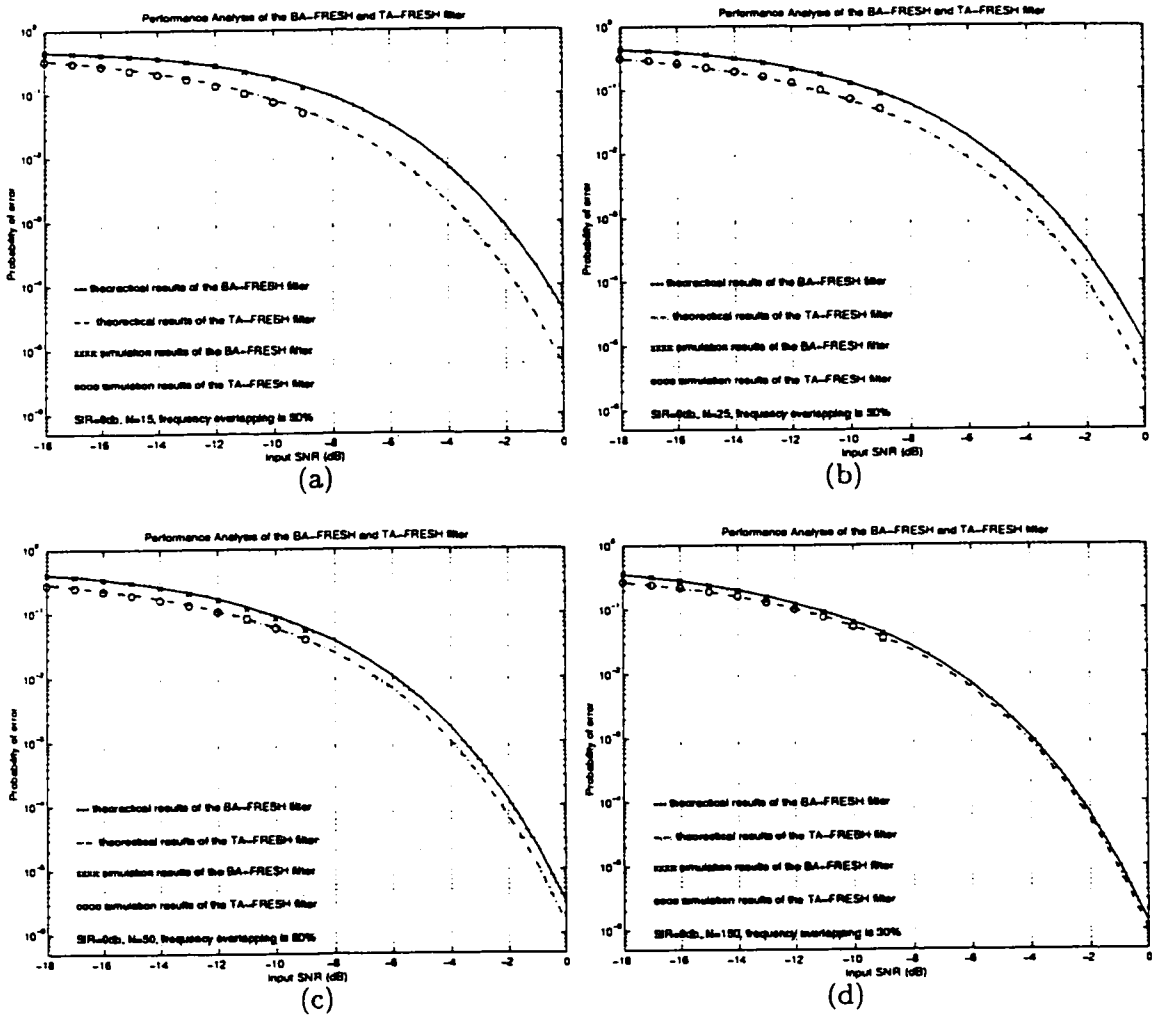

Figure 4.2: Output probability of error of BA-FRESH and TA-FRESH against the number of symbols 15, 25, 50, and 150 when the input SIR is 0dB and the spectral overlapping is 30% (3kHz)

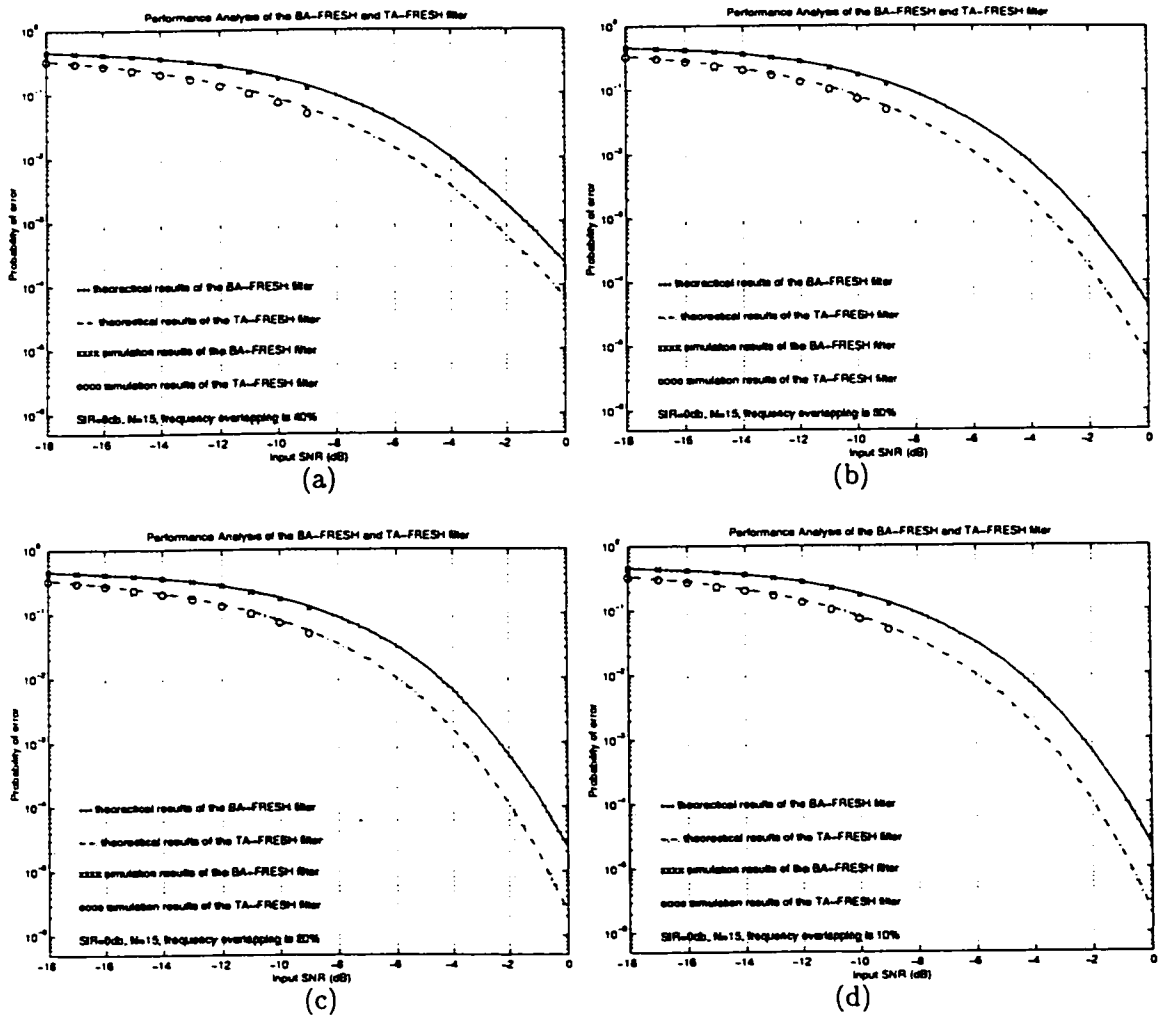

Figure 4.3: Output probability of error of BA-FRESH and TA-FRESH against the spectral overlapping 40%, 30%, 20% and 10% (4kHz, 3kHz, 2kHz, and 1kHz) when the input SIR is 0dB, and the number of symbols is 15

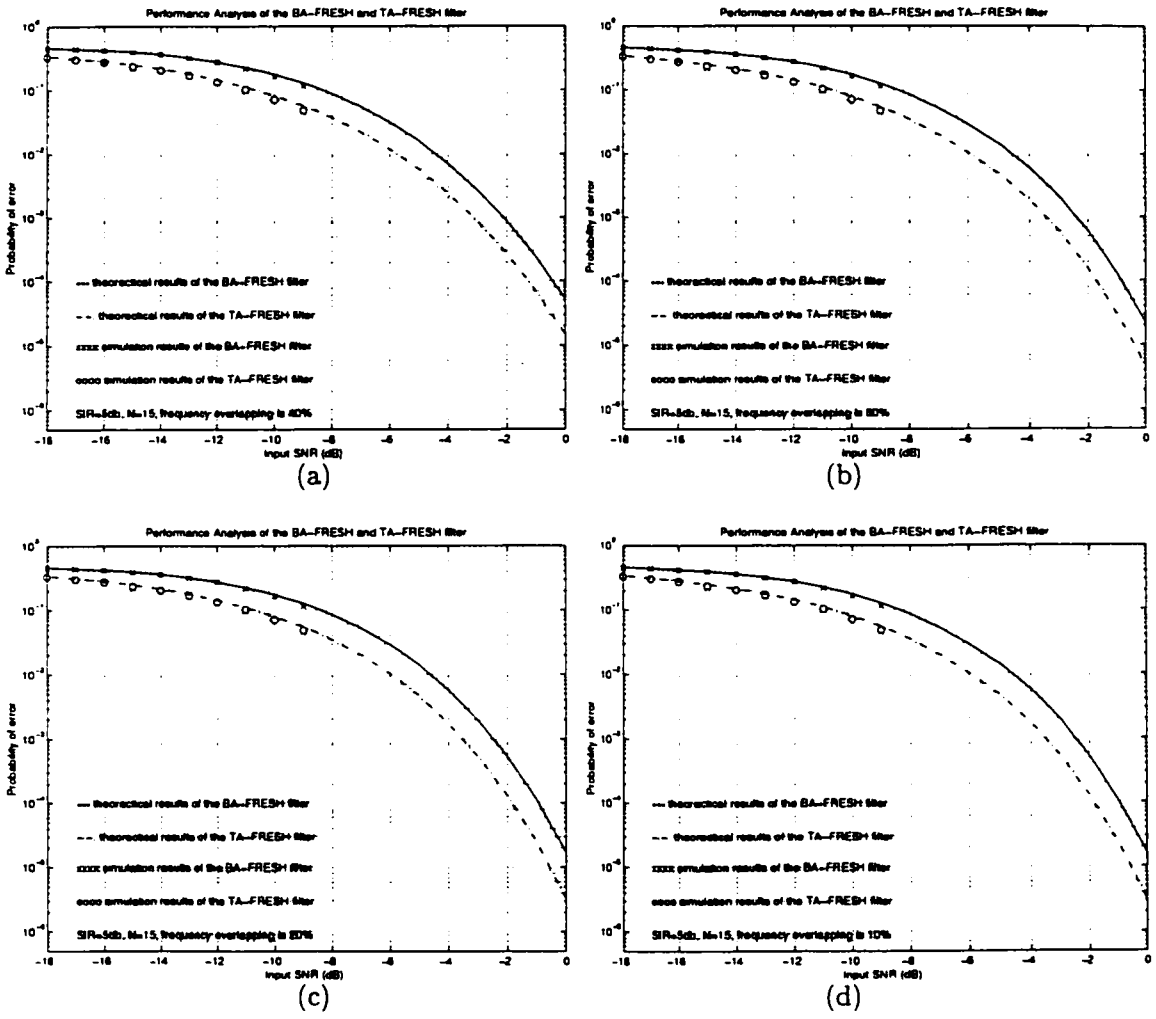

Figure 4.4: Output probability of error of BA-FRESH and TA-FRESH against the spectral overlapping 40%, 30%, 20% and 10% (4kHz, 3kHz, 2kHz, and 1kHz) when the input SIR is 5dB and the number of symbols is 15

Chapter 5

Proposed BLAST Algorithm and Its Convergence

In this chapter, blind adaptive beamforming algorithms are first reviewed. Then to satisfy the practical demands for future mobile personal communication systems, a new kind of blind adaptive space-time (BLAST) algorithm is proposed. By exploiting the spectral correlation of cyclostationary signals, the BLAST algorithm does not require a training signal and it can generate the training signal from the corrupted signal. It has been proved that the BLAST algorithm is equivalent to the trained adaptive space-time (TAST) algorithm when observed data length is infinite. Because the algorithm exploits not only spatial information of signals but also temporal information of the signals, it has the advantages of spatial filters and temporal filters. It can be viewed as the extension of the BA-FRESH filtering algorithm in the spatial domain. Recursive implementation formula of the BLAST filter is given. For the BLAST and TAST algorithms, the convergence of the filter coefficients, the output SINR, and the output MSE are analyzed. At last, Numerical results are presented to examine these results theoretically and by simulation.

5.1 Existing Blind Beamforming Algorithms

In mobile radio system, it is often too expensive to provide an adaptive processor with a unique training signal for each signal received. Also, information about the desired signal and the interferences are usually unknown. Therefore, an economical and effective blind adaptive signal extraction technique is in demand. In order to solve these problems, using the cyclostationarity of communication signals, some blind adaptive beamforming algorithms are proposed such as the SCORE algorithm [29], the CAB algorithm, and the C-CAB algorithm [15, 19]. These adaptation techniques are blind and they don't require any knowledge of the training signal or the DOAs (Directions Of Arrival) of the desired signal and the interferences provided that cycle frequencies of the desired signal is different from those of the interferences.

The Received Signal Model: Consider that multiple narrow band signals being received by an array of L sensors. An $L \times 1$ vector $\boldsymbol{x}(n) = [x_1(n)\ x_2(n)\ \cdots\ x_L(n)]^T$ is used to denote the complex envelopes of the output digitized data. The vector $\boldsymbol{x}(n)$ can then be modeled as

$$\boldsymbol{x}(n) = \boldsymbol{d}(\theta_s)s(n) + \boldsymbol{u}(n) + \boldsymbol{\nu}(n). \tag{5.1.1}$$

$s(n)$ is the desired signal, $\boldsymbol{d}(\theta_s)$ is the steering vector of the desired signal at the direction of arrival θ_s, $\boldsymbol{u}(n)$ is the combination of interference, and $\boldsymbol{\nu}(n)$ is the additive white noise. It is assumed that the spatial direction of the signal of interest and those of the interferences are resolvable by the antenna beam. The goal of a spatial signal extraction algorithm is to find a beam weighting vector $\boldsymbol{w}$ according to certain criteria such that the desired signal can be extracted by

$$y(n) = \boldsymbol{w}^{\dagger}\boldsymbol{x}(n) \tag{5.1.2}$$

where $\dagger$ represents the conjugate transpose.

The SCORE Algorithm: The SCORE algorithm was proposed by [29] for blindly adapting an antenna array for spatial extraction. The idea for the SCORE algorithm is constructed by maximizing the strength of the cross-correlation function between the output

signal $y(n)$ and a reference signal $r(n)$,

$$\Im_{sc}(\boldsymbol{w}, \boldsymbol{c}) = \frac{|\hat{R}_{yr}|^2}{|\hat{R}_{yy}| \cdot |\hat{R}_{rr}|} \tag{5.1.3}$$

where $r(n) = \boldsymbol{c}^\dagger \boldsymbol{x}^*(n) e^{j2\pi\alpha n}$ and $*$ is the conjugate operation. This is equivalent to maximizing the cost function $\Im_{sc}$ of the SCORE with respect to the two $L \times 1$ vectors $\boldsymbol{w}$ and $\boldsymbol{c}$

$$\max_{\boldsymbol{w}, \boldsymbol{c}} \Im_{sc}(\boldsymbol{w}, \boldsymbol{c}) = \max_{\boldsymbol{w}, \boldsymbol{c}} \frac{|\boldsymbol{w}^\dagger \hat{\boldsymbol{R}}_{xt} \boldsymbol{c}|^2}{\boldsymbol{w}^\dagger \hat{\boldsymbol{R}}_{xx} \boldsymbol{w} \boldsymbol{c}^\dagger \hat{\boldsymbol{R}}_{tt} \boldsymbol{c}} \tag{5.1.4}$$

where $\boldsymbol{t}(n)$ is defined as the control signal,

$$\boldsymbol{t}(n) = [\boldsymbol{x}(n) e^{-j2\pi\alpha n}]^*, \quad r(n) = \boldsymbol{c}^\dagger \boldsymbol{t}(n). \tag{5.1.5}$$

α is chosen such that $s(n)$ and $s(n)e^{-j2\pi\alpha n}$ are correlated and the interference are not. Thus, α should be chosen as the cycle frequency α_c of the desired signal. In addition, $\hat{\boldsymbol{R}}_{xt}$ is interpreted as the cyclic conjugate correlation of $\boldsymbol{x}(n)$,

$$\hat{\boldsymbol{R}}_{xt} = \langle \boldsymbol{x}(n) \boldsymbol{t}^\dagger(n) \rangle_N = \langle \boldsymbol{x}(n) \boldsymbol{x}^T(n) e^{-j2\pi\alpha_c n} \rangle_N = \hat{\boldsymbol{R}}_{xx^*}^{\alpha_c}(0). \tag{5.1.6}$$

The criterion can also be interpreted as maximizing the correlation of $\boldsymbol{w}^\dagger \boldsymbol{x}(n)$ and $\boldsymbol{c}^\dagger \boldsymbol{t}(n)$, under the constraint that $\boldsymbol{w}^\dagger \boldsymbol{R}_{xx} \boldsymbol{w} = 1$ and $\boldsymbol{c}^\dagger \boldsymbol{R}_{tt} \boldsymbol{c} = 1$. Since the signal component in $\boldsymbol{x}(n)$ Therefore, selecting $\boldsymbol{w}$ and $\boldsymbol{c}$ by maximizing the correlation

From the Cauchy-Schwarz Inequality, it can be shown that the weighting vector $\boldsymbol{w}$ is given by following eigenequation [15, 19],

$$\lambda_{max} \boldsymbol{w} = \hat{\boldsymbol{R}}_{xx}^{-1} \hat{\boldsymbol{R}}_{xt} \hat{\boldsymbol{R}}_{tt}^{-1} \hat{\boldsymbol{R}}_{xt}^\dagger \boldsymbol{w}. \tag{5.1.7}$$

Similarly, the control vector is optimized by setting $\boldsymbol{c}$ to be

$$\lambda_{max} \boldsymbol{c} = \hat{\boldsymbol{R}}_{tt}^{-1} \hat{\boldsymbol{R}}_{xt}^\dagger \hat{\boldsymbol{R}}_{xx}^{-1} \hat{\boldsymbol{R}}_{xt} \boldsymbol{c}. \tag{5.1.8}$$

The geometrical meaning of the SCORE algorithm is that the SCORE algorithm puts

nulls at the directions of the interferences instead of forming a beam towards the desired signal [71].

The CAB Algorithm: The CAB algorithm is another blind adaptive beamforming technique which utilizes the cyclostationarity of man-made signals. The CAB algorithm simply forms a beam towards the direction of the desired signal, which is different from the SCORE algorithm.

For a given finite data length N, the beam weighting vector $\boldsymbol{w}$ in CAB is determined by choosing $\boldsymbol{w}$ and $\boldsymbol{c}$ so as to maximize the $\boldsymbol{c}^\dagger \boldsymbol{t}(n)$, that is maximizing the cost function of CAB ($\Im_{cab}$) with respected to $\boldsymbol{w}$ and $\boldsymbol{c}$

$$\max_{\boldsymbol{w},\boldsymbol{c}} \Im_{cab}(\boldsymbol{w},\boldsymbol{c}) = \max_{\boldsymbol{w},\boldsymbol{c}} |\langle \boldsymbol{w}^\dagger \boldsymbol{x}(n)\boldsymbol{t}^\dagger(n)\boldsymbol{c}\rangle_N|^2 \tag{5.1.9}$$

with the constraint that $\boldsymbol{w}^\dagger \boldsymbol{w} = 1$ and

$$\max_{\boldsymbol{w},\boldsymbol{c}} |\boldsymbol{w}^\dagger \hat{\boldsymbol{R}}_{xt}\boldsymbol{c}|^2 = \max_{\boldsymbol{w},\boldsymbol{c}} \boldsymbol{w}^\dagger \hat{\boldsymbol{R}}_{xt}\boldsymbol{c} \tag{5.1.10}$$

The solution of $\boldsymbol{w}$ and $\boldsymbol{c}$ can be easily shown by using the Lagrange multiplier method as

$$\xi_{max}\boldsymbol{w} = \hat{\boldsymbol{R}}_{xt}\hat{\boldsymbol{R}}_{xt}^\dagger \boldsymbol{w} \tag{5.1.11}$$

and

$$\xi_{max}\boldsymbol{c} = \hat{\boldsymbol{R}}_{xt}^\dagger \hat{\boldsymbol{R}}_{xt}\boldsymbol{c}. \tag{5.1.12}$$

We notice the $\boldsymbol{w}_{CAB}$ is a consistent estimate of the steering vector $\boldsymbol{d}(\theta_s)$ for the single desired signal case.

The C-CAB Algorithm: The C-CAB algorithm is a constraint blind adaptive beamforming technique which utilizes the cyclostationarity of man-made signals. The C-CAB algorithm is derived from the approximated Linearly Constrained Minimum Variance (LCMV) beamforming. The beam weighting vector for LCMV [82] can be derived as the following,

$$\min_{\boldsymbol{w}} \{\boldsymbol{w}^\dagger \hat{\boldsymbol{R}}_{xx}\boldsymbol{w}\} \tag{5.1.13}$$

such that

$$\boldsymbol{C}^{\dagger}\boldsymbol{w} = \boldsymbol{f} \tag{5.1.14}$$

where $\boldsymbol{C}$ is the constraint matrix and $\boldsymbol{f}$ (which is defined as the response vector) is the characteristics of which are to be determined for particular applications. By linearly constraining satisfy the response vector $\boldsymbol{f}$, we can make sure that the desired signal is passed with the characteristic of response $\boldsymbol{f}$ [19]. As a result, minimizing $\boldsymbol{w}^{\dagger}\hat{\boldsymbol{R}}_{xx}\boldsymbol{w}$ is equivalent to minimizing the expected value of output power, $E(|y|^2) = \boldsymbol{w}^{\dagger}\hat{\boldsymbol{R}}_{xx}\boldsymbol{w}$, contributed by the interference, subject to the constraint that only the desired signal can pass through with response $\boldsymbol{f}$. Replacing the constraint matrix $\boldsymbol{C}$ by the steering vector $\boldsymbol{d}(\theta_s)$ of the desired signal and the response vector $\boldsymbol{f}$ by a scalar response g, $\boldsymbol{d}^{\dagger}(\theta_s)\boldsymbol{w} = g$ represents the square root of the beam pattern power towards the impinging angle of the desired signal. Using Lagrange multiplier method, we can obtain

$$\boldsymbol{w} = \frac{g\hat{\boldsymbol{R}}_{xx}^{-1}\boldsymbol{d}(\theta_s)}{\boldsymbol{d}^{\dagger}(\theta_s)\hat{\boldsymbol{R}}_{xx}^{-1}\boldsymbol{d}(\theta_s)}. \tag{5.1.15}$$

By recognizing both g and $\boldsymbol{d}^{\dagger}(\theta_s)\hat{\boldsymbol{R}}_{xx}^{-1}\boldsymbol{d}(\theta_s)$ are constant values, the solution of LCMV beamformer is

$$\boldsymbol{w}_{LCMV} \propto \hat{\boldsymbol{R}}_{xx}^{-1}\boldsymbol{d}(\theta_s). \tag{5.1.16}$$

In the blind adaptive beamforming with a non-calibrated antenna, the steering vector $\boldsymbol{d}(\theta_s)$ of the signal of interest is unknown to the base station. However, since we note that $\boldsymbol{w}_{CAB}$ is a consistent estimate of $\boldsymbol{d}(\theta_s)$ for the single desired signal case, we may use $\boldsymbol{w}_{CAB}$ to replace the unknown $\boldsymbol{d}(\theta_s)$. For the single desired signal case, the constrain of the C-CAB algorithm and the beam weighting vector $\boldsymbol{w}_{CCAB}$ can be approximated by

$$\min_{\boldsymbol{w}} \langle \boldsymbol{w}^{\dagger}\boldsymbol{x}(n)\boldsymbol{x}^{\dagger}(n)\boldsymbol{w}\rangle_N = \min_{\boldsymbol{w}} \boldsymbol{w}^{\dagger}\hat{\boldsymbol{R}}_{xx}\boldsymbol{w} \tag{5.1.17}$$

subject to $\boldsymbol{w}_{CAB}^{\dagger}\boldsymbol{w} = 1$ and

$$\boldsymbol{w}_{CCAB} = \hat{\boldsymbol{R}}_{xx}^{-1}\boldsymbol{w}_{CAB} \tag{5.1.18}$$

respectively.

The main advantages of the existing cyclic adaptive beamforming algorithms are that they do not require training signals nor the knowledge of the DOAs of the desired signal and the interference. The antenna array calibration is not necessary either. However, the performances of the existing cyclic adaptive beamforming algorithms will deteriorate if the desired signal and the interference are spatially too close to each other. The reason is that those beamforming algorithms are essentially spatial filters and they only exploit the spatial information (DOA difference between the desired signal and interference). In the next section, we propose to combine the BA-FRESH filtering and the cyclic beamforming techniques to separate signals which are spectrally and/or spatially overlapped.

5.2 Structure of Proposed Blind Adaptive Space-Time Filter

The structure of a blind adaptive space-time (BLAST) filter proposed in this chapter is shown in Fig. 5.1. The structure of ith FRESH filter is shown in Fig. 5.2. The input signal is considered as a complex signal which is a complex envelop of a real band pass signal in this chapter. For the BLAST filter, its input antennas consist of an array of L sensors. The output of the sensor array $\boldsymbol{x}(n)$ at nth sample is

$$\boldsymbol{x}(n) = \boldsymbol{d}(\theta_s)s(n) + \sum_{k=1}^{K_o} \boldsymbol{d}(\theta_{u_k})u_k(n) + \boldsymbol{v}(n) \tag{5.2.1}$$

where $s(n)$ is the desired signal and $u_k(n)$ is the kth interfering signal. Here, K_o is the number of the interfering signals, $\boldsymbol{d}(\theta_s)$ is the directional vector of the desired signal, $\boldsymbol{d}(\theta_{u_k})$ is the directional vector of the interference $u_k(n)$, and $\boldsymbol{v}(n)$ is a complex noise. We also assumed that the desired signal and the interferences are independent each other and they have different cycle frequencies. Moreover, $\boldsymbol{x}(n)$ can also be expressed as

$$\boldsymbol{x}(n) = [x_1(n) \quad x_2(n) \quad \cdots \quad x_L(n)]^T \tag{5.2.2}$$

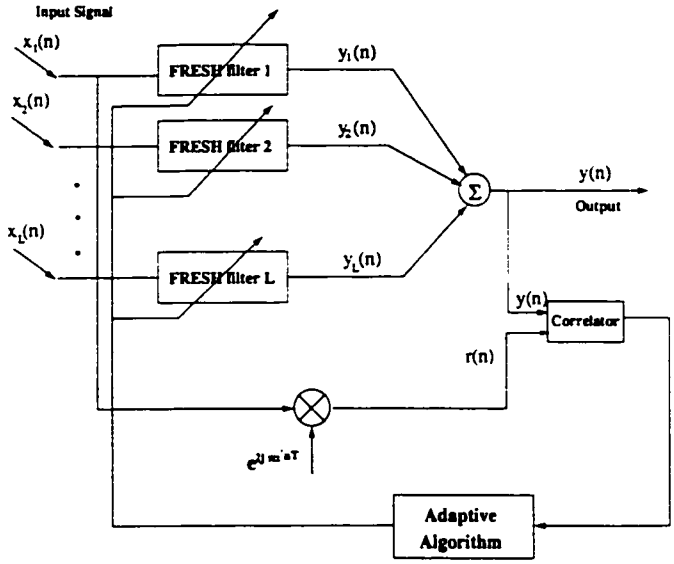

Figure 5.1: Structure of the BLAST filter

where L is the number of sensors, $x_j(n)$, $(j = 1, 2, \cdots L)$ is the received signal on the jth sensor.

For each sensor of the array, it connects to a FRESH filter. The jth FRESH filter $(j = 1, 2, \cdots L)$ consists of M branches shown in Fig. 5.2. Because the input of the FRESH filter is considered as to be a complex signal which is the complex envelop of a real band pass signal, we consider the FRESH filter to have linear conjugate and linear parts shown in Fig. 5.2. The reason why the FRESH filter should have linear conjugate and linear parts when the input signal is a complex signal is explained in [24]. We know that linear time-invariant filtering of a real signal is equivalent to linear time-invariant filtering of its analytic signal which in turn is equivalent to linear time-invariant filtering of its complex envelope. But this is not true for time-variant filtering. In general, linear time-variant filtering of a real signal is equivalent to distinct linear time-variant filtering of each of the analytic signal (or complex envelope) and its complex conjugate, this is proved in [24]. Consequently, if complex signals are to be used, then the problem of optimum and adaptive time-variant polyperiodic filtering must be approached as bivariate filtering problems, where a signal and its conjugate are jointly filtered and then added together [13]. This is called as linear-conjugate-linear (LCL) filtering. For specified the branch number of the FRESH filter and

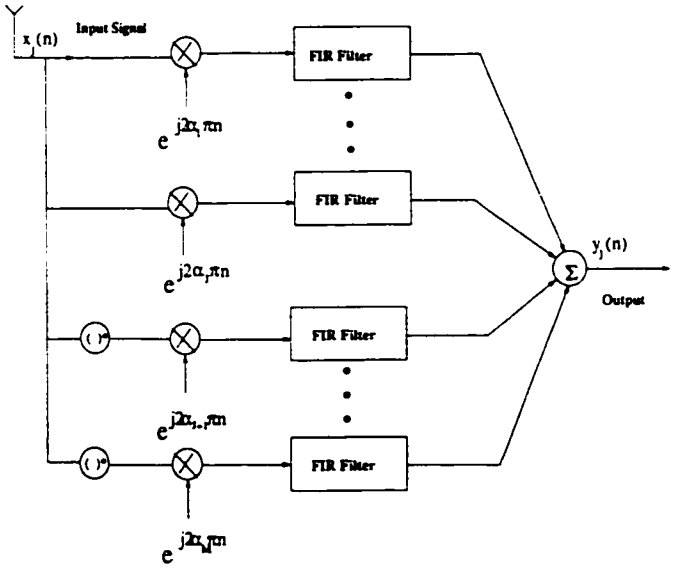

Figure 5.2: Structure of the ith FRESH filter

the frequency shift parameters, the optimum LCL-FRESH filter problem is equivalent to the multi-variate Wiener filtering problem. Moreover, a training signal is needed to design the optimum solution of the LCL-FRESH filter [13].

For the upper J branches of a LCL-FRESH filter, each branch consists a frequency shift operation ($\alpha_i, i = 1, 2, \cdots J$) followed by a FIR filter being of length N_o, here we choose all FIR filters have the same length N_o and $J = M/2$. We denote the LN_o-dimensional frequency-shifted stacked snapshot vector as

$$\tilde{\boldsymbol{x}}_i(n) = \left[\boldsymbol{x}^T(n)e^{j2\pi\alpha_i n} \quad \boldsymbol{x}^T(n-1)e^{j2\pi\alpha_i(n-1)} \quad \cdots \quad \boldsymbol{x}^T(n-N_o+1)e^{j2\pi\alpha_i(n-N_o+1)}\right]^T \tag{5.2.3}$$

where $i = 1.2, \cdots J$. For the lower $M - J$ branches, each branch consists a conjugate frequency shift operation ($\alpha_i, i = J+1, J+2, \cdots M$) followed by a FIR filter being of length N_o. Here, we choose $\alpha_{J+k} = \alpha_k, k = 1, 2, \cdots M/2$. We denote the LN_o-dimensional frequency-shifted stacked snapshot vector as

$$\tilde{\boldsymbol{x}}_i(n) = \left[\boldsymbol{x}^\dagger(n)e^{j2\pi\alpha_i n} \quad \boldsymbol{x}^\dagger(n-1)e^{j2\pi\alpha_i(n-1)} \quad \cdots \quad \boldsymbol{x}^\dagger(n-N_o+1)e^{j2\pi\alpha_i(n-N_o+1)}\right]^T \tag{5.2.4}$$

where $i = J+1, J+2, \cdots M$ and $\dagger$ denotes conjugate transpose. Here, a LN_oM-dimensional frequency-shifted stacked snapshot vector is defined as

$$\tilde{\boldsymbol{x}}(n) = \left[\tilde{\boldsymbol{x}}_1^T(n) \;\; \tilde{\boldsymbol{x}}_2^T(n) \;\; \cdots \;\; \tilde{\boldsymbol{x}}_M^T(n)\right]^T. \tag{5.2.5}$$

Because the received signal $\boldsymbol{x}(n)$ at the sensor array contains the desired signal components $\boldsymbol{s}(n) = \boldsymbol{d}(\theta_s)s(n)$, the interference components $\boldsymbol{u}(n) = \sum_{k=1}^{K_o} \boldsymbol{d}(\theta_{u_k})u_k(n)$ and noise components $\boldsymbol{v}(n)$ respectively, the frequency-shifted stacked snapshot vector $\tilde{\boldsymbol{x}}(n)$ at the nth instant can be written as

$$\tilde{\boldsymbol{x}}(n) = \tilde{\boldsymbol{s}}(n) + \tilde{\boldsymbol{u}}(n) + \tilde{\boldsymbol{v}}(n) \tag{5.2.6}$$

where $\tilde{\boldsymbol{s}}(n)$ is the frequency-shifted stacked desired signal vector at the nth instant. $\tilde{\boldsymbol{u}}(n)$ is the frequency-shifted stacked interference vector at the nth instant, and $\tilde{\boldsymbol{v}}(n)$ is the frequency-shifted stacked noise vector at the nth instant. Here, the frequency-shifted stacked desired signal vector $\tilde{\boldsymbol{s}}(n)$ is defined as

$$\tilde{\boldsymbol{s}}(n) = \begin{pmatrix} \tilde{\boldsymbol{s}}_R(n) \otimes \boldsymbol{d}(\theta_s) \\ \tilde{\boldsymbol{s}}_C(n) \otimes \boldsymbol{d}^*(\theta_s) \end{pmatrix} \tag{5.2.7}$$

where $\otimes$ denotes the Kronecker product. Let $\boldsymbol{a} = [a_1 \; a_2 \; \cdots \; a_K]^T$ and $\boldsymbol{b} = [b_1 \; b_2 \; \cdots \; b_M]^T$. The Kronecker product $\boldsymbol{a} \otimes \boldsymbol{b}$ is defined as $\boldsymbol{a} \otimes \boldsymbol{b} = [a_1\boldsymbol{b}^T \; a_2\boldsymbol{b}^T \; \cdots \; a_M\boldsymbol{b}^T]^T$. $\tilde{\boldsymbol{s}}_R(n)$ and $\tilde{\boldsymbol{s}}_C(n)$ are defined as

$$\tilde{\boldsymbol{s}}_R(n) = \left[\tilde{\boldsymbol{s}}_1^T(n) \;\; \tilde{\boldsymbol{s}}_2^T(n) \;\; \cdots \;\; \tilde{\boldsymbol{s}}_J^T(n)\right]^T, \tag{5.2.8}$$

$$\tilde{\boldsymbol{s}}_i(n) = \left[s(n)e^{j2\pi\alpha_i n}, \;\; s(n-1)e^{j2\pi\alpha_i(n-1)} \cdots s(n-N_o+1)e^{j2\pi\alpha_i(n-N_o+1)}\right]^T \tag{5.2.9}$$

where $i = 1, 2, \cdots J$.

$$\tilde{\boldsymbol{s}}_C(n) = \left[\tilde{\boldsymbol{s}}_{J+1}^T(n) \;\; \tilde{\boldsymbol{s}}_{J+2}^T(n) \;\; \cdots \;\; \tilde{\boldsymbol{s}}_M^T(n)\right]^T, \tag{5.2.10}$$

$$\tilde{\boldsymbol{s}}_i(n) = \left[s^*(n)e^{j2\pi\alpha_i n}, \;\; s^*(n-1)e^{j2\pi\alpha_i(n-1)} \cdots s^*(n-N_o+1)e^{j2\pi\alpha_i(n-N_o+1)}\right]^T \tag{5.2.11}$$

where $i = J+1, J+2, \cdots M$.

The frequency-shifted stacked interfering signal vector $\tilde{\boldsymbol{u}}(n)$ is defined as

$$\tilde{\boldsymbol{u}}(n) = \sum_{k=1}^{K_o} \begin{pmatrix} \tilde{\boldsymbol{u}}_{Rk}(n) \otimes \boldsymbol{d}(\theta_{u_k}) \\ \tilde{\boldsymbol{u}}_{Ck}(n) \otimes \boldsymbol{d}^*(\theta_{u_k}) \end{pmatrix} \tag{5.2.12}$$

where $\otimes$ denotes the Kronecker product. $\tilde{\boldsymbol{u}}_{Rk}(n)$ and $\tilde{\boldsymbol{u}}_{Ck}(n)$ are defined as

$$\tilde{\boldsymbol{u}}_{Rk}(n) = \left[\tilde{\boldsymbol{u}}_{k1}^T(n) \;\; \tilde{\boldsymbol{u}}_{k2}^T(n) \;\; \cdots \;\; \tilde{\boldsymbol{u}}_{kJ}^T(n)\right]^T, \tag{5.2.13}$$

$$\tilde{\boldsymbol{u}}_{ki}(n) = \left[u_k(n)e^{j2\pi\alpha_i n}, \;\; u_k(n-1)e^{j2\pi\alpha_i(n-1)} \cdots u_k(n-N_o+1)e^{j2\pi\alpha_i(n-N_o+1)}\right]^T \tag{5.2.14}$$

where $i = 1, 2, \cdots J$ and $k = 1, 2, \cdots K_o$.

$$\tilde{\boldsymbol{u}}_{Ck}(n) = \left[\tilde{\boldsymbol{u}}_{kJ+1}^T(n) \;\; \tilde{\boldsymbol{u}}_{kJ+2}^T(n) \;\; \cdots \;\; \tilde{\boldsymbol{u}}_{kM}^T(n)\right]^T, \tag{5.2.15}$$

$$\tilde{\boldsymbol{u}}_{ki}(n) = \left[u_k^*(n)e^{j2\pi\alpha_i n}, \;\; u_k^*(n-1)e^{j2\pi\alpha_i(n-1)} \cdots u_k^*(n-N_o+1)e^{j2\pi\alpha_i(n-N_o+1)}\right]^T \tag{5.2.16}$$

where $i = J+1, J+2, \cdots M$ and $k = 1, 2, \cdots K_o$.

The frequency-shifted stacked noise vector $\tilde{\boldsymbol{v}}(n)$ is defined as

$$\tilde{\boldsymbol{v}}(n) = \begin{pmatrix} \tilde{\boldsymbol{v}}_R(n) \\ \tilde{\boldsymbol{v}}_C(n) \end{pmatrix} \tag{5.2.17}$$

$\tilde{\boldsymbol{v}}_R(n)$ and $\tilde{\boldsymbol{v}}_C(n)$ are defined as

$$\tilde{\boldsymbol{v}}_R(n) = \left[\tilde{\boldsymbol{v}}_1^T(n) \;\; \tilde{\boldsymbol{v}}_2^T(n) \;\; \cdots \;\; \tilde{\boldsymbol{v}}_J^T(n)\right]^T. \tag{5.2.18}$$

$$\tilde{\boldsymbol{v}}_i(n) = \left[e^{j2\pi\alpha_i n}, \;\; e^{j2\pi\alpha_i(n-1)} \cdots e^{j2\pi\alpha_i(n-N_o+1)}\right]^T \otimes \boldsymbol{v} \tag{5.2.19}$$

where $i = 1, 2, \cdots J$.

$$\tilde{\boldsymbol{v}}_C(n) = \left[\tilde{\boldsymbol{v}}_{J+1}^T(n) \;\; \tilde{\boldsymbol{v}}_{J+2}^T(n) \;\; \cdots \;\; \tilde{\boldsymbol{v}}_M^T(n)\right]^T, \tag{5.2.20}$$

$$\tilde{\boldsymbol{v}}_i(n) = \left[e^{j2\pi\alpha_i n},\ e^{j2\pi\alpha_i(n-1)} \cdots e^{j2\pi\alpha_i(n-N_o+1)}\right]^T \otimes \boldsymbol{v} \tag{5.2.21}$$

where $i = J+1, J+2, \cdots M$.

Let $\boldsymbol{q}$ be a complex valued LMN_o-dimensional coefficient vector of the BLAST filter. The output $y(n)$ of the BLAST filter at nth sample is

$$y(n) = \boldsymbol{q}^\dagger \tilde{\boldsymbol{x}}(n). \tag{5.2.22}$$

where $\boldsymbol{q} = [q_1\ q_2\ \cdots\ q_{LMN_o}]^T$. The reference signal $r(n)$ of the BLAST filter at nth sample is

$$r(n) = x(n)e^{j2\pi\alpha' n} = \tilde{s}'(n) + \sum_{k=1}^{K_o} \tilde{u}_k'(n) + \tilde{\nu}'(n) \tag{5.2.23}$$

where $x(n)$ is the received signal at the first sensor and α' is the frequency shift parameter in the reference path in the BLAST filter. Here, $\tilde{s}'(n), \tilde{u}_k'(n)$, and $\tilde{\nu}'(n)$ are defined as

$$\tilde{s}'(n) = s(n)e^{j2\pi\alpha' n}, \quad \tilde{u}_k'(n) = u_k(n)e^{j2\pi\alpha' n}, \quad \tilde{\nu}'(n) = \nu(n)e^{j2\pi\alpha' n} \tag{5.2.24}$$

where $s(n)$, $u_k(n)$ and $\nu(n)$ are the desired signal component, the kth interfering signal component, and the noise component which are received at the first sensor respectively.

When we know the coefficient vector $\boldsymbol{q}$ of the BLAST filter, we can obtain these impulse responses of the FIR filters in the FRESH filters. Denoting the impulse responses of the jth FIR filter of the ith FRESH filter as

$$\boldsymbol{h}_{ij} = [h_{ij}(0)\ \ h_{ij}(1) \cdots h_{ij}(N_o-1)]^T, \qquad i = 1,2,\cdots L, \quad j = 1,2,\cdots M. \tag{5.2.25}$$

Using $\boldsymbol{q}$, we can get $\boldsymbol{h}_{ij}$ as

$$\boldsymbol{h}_{ij} = [q_{(j-1)LN_o+i}\ \ q_{(j-1)LN_o+L+i}\ \ \cdots\ \ q_{(j-1)LN_o+(N_o-1)L+i}]^T. \tag{5.2.26}$$

where $i = 1,2,\cdots L, \quad j = 1,2,\cdots M$. If we define $\boldsymbol{h}$ as

$$\boldsymbol{h} = [\boldsymbol{h}_{11}\ \ \boldsymbol{h}_{21} \cdots \boldsymbol{h}_{LM}]^T, \tag{5.2.27}$$

$\boldsymbol{h}$ is a linear transformation of $\boldsymbol{q}$.

5.3 Proposed Blind Adaptive Space-Time (BLAST) Algorithm

With $\alpha' \neq \alpha_m, \quad m = 1, 2, \cdots M$, the BLAST filter seeks to maximize the normalized correlation between $y(n)$ and $r(n)$ by adjusting the coefficients of $\boldsymbol{q}$, i.e.,

$$\max_{\boldsymbol{q}} \Im_{BST}(\boldsymbol{q}) = \max_{\boldsymbol{q}} \frac{|R_{yr}|^2}{|R_{yy}|\,|R_{rr}|} \tag{5.3.1}$$

where $R_{uv} = E[u(n)v^*(n)]$. The rationale behind this algorithm is that if the output $y(n)$ is a close approximation to be the desired signal $s(n)$ and is relatively free from containing the interferences $u_k(n)$ $(k = 1, 2, \cdots K_o)$ and noise $\nu(n)$, then it must have high correlation with the α'-shifted version of $s(n)$ and must have low correlation with the α'-shifted versions of $u_k(n)$ and $\nu(n)$ respectively. Thus, the correlation of the two signals may provide a measure of the suppression of the interference and the closeness of the output to the desired signal. In using this measure, we must ensure that the BLAST filter in the primary branch has no common frequency shift with the reference branch. The optimum filter coefficients which is denoted as $\boldsymbol{q}_{BST}$ can be obtained by substituting Eqs. (5.2.22) and (5.2.23) into (5.3.1) and applying the Schwarz inequality

$$J(\boldsymbol{q}) = \frac{|\boldsymbol{q}^\dagger \boldsymbol{R}_{\tilde{x}\tilde{x}}^{1/2} \boldsymbol{R}_{\tilde{x}\tilde{x}}^{-1/2} \boldsymbol{\rho}_{\tilde{x}r}|^2}{|\boldsymbol{q}^\dagger \boldsymbol{R}_{\tilde{x}\tilde{x}} \boldsymbol{q}||R_{rr}|} \leq \frac{|\boldsymbol{q}^\dagger \boldsymbol{R}_{\tilde{x}\tilde{x}}^{1/2}|^2\,|\boldsymbol{R}_{\tilde{x}\tilde{x}}^{-1/2} \boldsymbol{\rho}_{\tilde{x}r}|^2}{|\boldsymbol{q}^\dagger \boldsymbol{R}_{\tilde{x}\tilde{x}} \boldsymbol{q}||R_{rr}|}. \tag{5.3.2}$$

For equality, we have

$$\boldsymbol{q}_{BST} = \boldsymbol{R}_{\tilde{x}\tilde{x}}^{-1} \boldsymbol{\rho}_{\tilde{x}r} \tag{5.3.3}$$

where $\boldsymbol{R}_{\tilde{x}\tilde{x}} = E\left[\tilde{\boldsymbol{x}}(n)\tilde{\boldsymbol{x}}^\dagger(n)\right]$ and $\boldsymbol{\rho}_{\tilde{x}r} = E[\tilde{\boldsymbol{x}}(n)r^*(n)]$. We note that $\boldsymbol{R}_{\tilde{x}\tilde{x}}$ is a correlation matrix and is almost always positive definite. Thus, it is non-singular [7]. Eq. (5.3.3) is the Wiener-Hoff equation for the BLAST filter the solution of which necessitates the knowledge of $\boldsymbol{R}_{\tilde{x}\tilde{x}}$ and $\boldsymbol{\rho}_{\tilde{x}r}$. If such knowledge is not available, then a recursive method for updating the tap-weights of the BLAST filter in the primary branch can be obtained following the

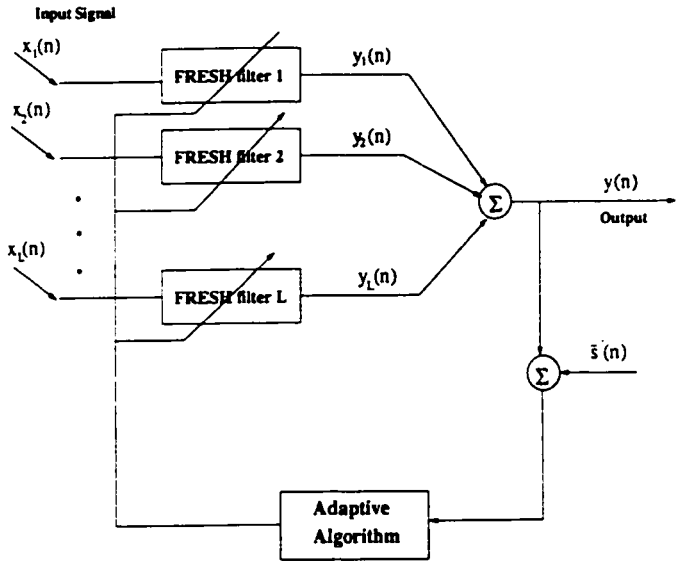

Figure 5.3: Structure of the TAST filter

Widrow-Hoff least-mean-square (LMS) algorithm by using the signal $r(n)$ as the reference signal and choosing an appropriate step-size. Alternatively, we may window the frequency shifted data vectors $\tilde{\boldsymbol{x}}(n)$ to obtain a time-averaged estimates of the data correlation matrix $\boldsymbol{R}_{\tilde{x}\tilde{x}}$ and the cross-correlation vector $\boldsymbol{\rho}_{\tilde{x}r}$. Denote the N-sample estimated values of $\boldsymbol{R}_{\tilde{x}\tilde{x}}$, $\boldsymbol{\rho}_{\tilde{x}r}$, and $\boldsymbol{q}_{BST}$ by $\hat{\boldsymbol{R}}_{\tilde{x}\tilde{x}}(N)$, $\hat{\boldsymbol{\rho}}_{\tilde{x}r}(N)$, and $\hat{\boldsymbol{q}}_{BST}(N)$ respectively. Thus, from Eq. (5.3.3), we have

$$\hat{\boldsymbol{q}}_{BST}(N) = \hat{\boldsymbol{R}}^{-1}_{\tilde{x}\tilde{x}}(N)\hat{\boldsymbol{\rho}}_{\tilde{x}r}(N) = \langle \tilde{\boldsymbol{x}}(n)\tilde{\boldsymbol{x}}(n)^{\dagger}\rangle_N^{-1}\langle \tilde{\boldsymbol{x}}(n)r^{*}(n)\rangle_N. \tag{5.3.4}$$

Applying the standard Recursive Least-Squares (RLS) algorithm [7], we arrive at the recursive formula of the up-dated desired filter response:

$$\begin{aligned}\hat{\boldsymbol{q}}_{BST}(N) &= \left\{\boldsymbol{I} - \frac{\frac{1}{N-1}\hat{\boldsymbol{R}}^{-1}_{\tilde{x}\tilde{x}}(N-1)\tilde{\boldsymbol{x}}(N)\tilde{\boldsymbol{x}}^{\dagger}(N)}{1+\frac{1}{N-1}\tilde{\boldsymbol{x}}^{\dagger}(N)\hat{\boldsymbol{R}}^{-1}_{\tilde{x}\tilde{x}}(N-1)\tilde{\boldsymbol{x}}(N)}\right\} \\ &\quad \left\{\hat{\boldsymbol{q}}_{BST}(N-1) + \frac{1}{N-1}\hat{\boldsymbol{R}}^{-1}_{\tilde{x}\tilde{x}}(N-1)\tilde{\boldsymbol{x}}(N)r^{*}(N)\right\}.\end{aligned} \tag{5.3.5}$$

If a copy of the desired signal $\tilde{s}'(n)$ is available, we can use it as a reference instead of using $r(n)$. We call the space-time filter with a training signal as Trained Adaptive Space-Time (TAST) filter shown in Fig. 5.3. The optimum TAST filter whose weighting coefficient is

denoted as $\boldsymbol{q}_{TST}$ can then be designed to minimize the mean-square error of the output. Here, the error is given by

$$e_{TST}(n) = s(n)e^{j2\pi\alpha' n} - y(n) = s(n)e^{j2\pi\alpha' n} - \boldsymbol{q}_{TST}^{\dagger}\tilde{\boldsymbol{x}}(n) \tag{5.3.6}$$

and the mean square error is

$$J_{TST} = E\left[e_{TST}(n)e_{TST}^{*}(n)\right]. \tag{5.3.7}$$

Using the gradient method, this optimum space-time filter with the training signal is given by

$$\boldsymbol{q}_{TST} = \boldsymbol{R}_{\tilde{x}\tilde{x}}^{-1}\boldsymbol{\rho}_{\tilde{x}\tilde{s}'} \tag{5.3.8}$$

where $\boldsymbol{\rho}_{\tilde{x}\tilde{s}'}$ is the cross-correlation vector between $\tilde{\boldsymbol{x}}(n)$ and $\tilde{s}'(n)$. The proof is shown in Appendix *A*. Denote the N-sample estimated values of $\boldsymbol{R}_{\tilde{x}\tilde{x}}, \boldsymbol{\rho}_{\tilde{x}\tilde{s}'}$, and $\boldsymbol{q}_{TST}$ by $\hat{\boldsymbol{R}}_{\tilde{x}\tilde{x}}(N)$, $\hat{\boldsymbol{\rho}}_{\tilde{x}\tilde{s}'}(N)$, and $\hat{\boldsymbol{q}}_{TST}(N)$ respectively. Thus, from Eq. (5.3.8), we have

$$\hat{\boldsymbol{q}}_{TST}(N) = \hat{\boldsymbol{R}}_{\tilde{x}\tilde{x}}^{-1}(N)\hat{\boldsymbol{\rho}}_{\tilde{x}\tilde{s}'}(N) = \langle\tilde{\boldsymbol{x}}(n)\tilde{\boldsymbol{x}}(n)^{\dagger}\rangle_N^{-1}\langle\tilde{\boldsymbol{x}}(n)\tilde{s}'^{*}(n)\rangle_N. \tag{5.3.9}$$

We note from Eqs. (5.3.3) and (5.3.8) that the difference between $\boldsymbol{q}_{BST}$ and $\boldsymbol{q}_{TST}$ is in the cross-correlation vector. Now, we show that $\boldsymbol{q}_{BST}$ and $\boldsymbol{q}_{TST}$ both have the same value under infinite sample time average realization.

Property 5.1: *Assume that Ψ_s is the set of cycle frequencies of the desired signal and Ψ_u is the set of cycle frequencies of the interferences. Let α_m, $(m = 1, 2, \cdots, M)$ be the frequency shift parameters in the primary branches of the BLAST and the TAST filter. Let α' be the frequency shift parameter in the secondary branches of the BLAST filter such that*

$$\alpha_m - \alpha' \neq 0, \quad \textit{and} \quad \alpha_m, \quad (\alpha_m - \alpha') \in (\Psi_s - \Psi_u), \quad \forall m, \tag{5.3.10}$$

the BLAST filter and the TAST filter have same optimal filter coefficients $\boldsymbol{q}_{opt}$ under infinite

sample time average realization, where

$$\boldsymbol{q}_{opt} = \boldsymbol{R}_{\tilde{x}\tilde{x}}^{-1}\boldsymbol{\rho}_{\tilde{x}\tilde{s}'} = \boldsymbol{R}_{\tilde{x}\tilde{x}}^{-1}\left\langle \tilde{\boldsymbol{s}}(n)s^*(n)e^{-j2\pi\alpha' n}\right\rangle \tag{5.3.11}$$

where $\tilde{\boldsymbol{s}}(n)$ is defined in Eq. (5.2.7).

The proof of the property 5.1 is shown in Appendix A. This property demonstrates that under large sample time-average realization, $\boldsymbol{q}_{BST}$ not only satisfies the criterion Eq. (5.3.1), but also minimizes the output mean-squared error (MSE). The mean-squared error is defined as

$$J_{TST} = \left\langle \left(y(n) - \tilde{s}'(n)\right)\left(y(n) - \tilde{s}'(n)\right)^*\right\rangle \tag{5.3.12}$$

where $y(n)$ and $\tilde{s}'(n)$ are defined in the Eqs. (5.2.22) and (5.2.24) respectively. The property 5.1 is in fact the expansion of the property 3.1 to the space-time domain.

We note that the performances of the BLAST algorithm may be affected in the channel distortion environment. However, the change of the performance of the BLAST algorithm will be small provided that the cycle frequencies of the desired signal almost keep unchanged. This is because the BLAST algorithm mainly exploits the cycle frequencies of the desired signal to extract the desired signal. Moreover, we can combine the BLAST algorithm with equalization technique to eliminate the channel distortion affection.

5.4 Convergence Analysis of the BLAST Algorithm

For the optimum filter coefficients of the BLAST and TAST algorithms, we know that there are the differences between the finite sample time realization of the filter coefficients and the infinite sample time realization of the filter coefficients. In this section, we study the convergence rate of this difference. To this end, we define the time-averaged correlation matrix and cross-correlation vector over N samples respectively as

$$\hat{\boldsymbol{R}}_{\tilde{x}\tilde{x}}(N) = \left\langle \tilde{\boldsymbol{x}}(n)\tilde{\boldsymbol{x}}^\dagger(n)\right\rangle_N \quad \text{and} \quad \hat{\boldsymbol{\rho}}_{\tilde{x}v}(N) = \langle \tilde{\boldsymbol{x}}(n)v^*(n)\rangle_N \tag{5.4.1}$$

Thus, the finite-sample time-average realizations of $\boldsymbol{q}_{BST}$ and $\boldsymbol{q}_{TST}$ in Eqs. (5.3.3) and (5.3.8) are placed respectively by

$$\hat{\boldsymbol{q}}_{BST}(N) = \hat{\boldsymbol{R}}_{\tilde{x}\tilde{x}}^{-1}(N)\hat{\boldsymbol{\rho}}_{\tilde{x}r}(N) \tag{5.4.2}$$

$$\hat{\boldsymbol{q}}_{TST}(N) = \hat{\boldsymbol{R}}_{\tilde{x}\tilde{x}}^{-1}(N)\hat{\boldsymbol{\rho}}_{\tilde{x}\tilde{s}'}(N) \tag{5.4.3}$$

We further define the L_2-norms of a vector $\boldsymbol{v}$ and a matrix $\boldsymbol{A}$ respectively as

$$\|\boldsymbol{v}\| = \left(\boldsymbol{v}^{\dagger}\boldsymbol{v}\right)^{\frac{1}{2}} \quad \text{and} \quad \|\boldsymbol{A}\| = \max_{\|\boldsymbol{v}\|=1}\left(\|\boldsymbol{A}\boldsymbol{v}\|\right). \tag{5.4.4}$$

We now have the following property:

Theorem 5.1: *Let Ψ_s and Ψ_u respectively denote the set of cycle frequencies of the desired signal and interferences. Let α_m, $(m = 1, 2, \cdots M)$ be the frequency shift parametcrs in the primary branches of the BLAST and the TAST filter. Let α' be the frequency shift parameter in the secondary branches of the BLAST filter such that*

$$\alpha_m \neq \alpha', \quad \textit{and} \quad \alpha_m,\ (\alpha_m - \alpha') \in (\Psi_s - \Psi_u) \quad \forall m, \tag{5.4.5}$$

both $\hat{\boldsymbol{q}}_{BST}(N)$ and $\hat{\boldsymbol{q}}_{TST}(N)$ converge in the mean-square sense to

$$\boldsymbol{q}_{opt} = \boldsymbol{R}_{\tilde{x}\tilde{x}}^{-1}\boldsymbol{\rho}_{\tilde{x}\tilde{s}'} \tag{5.4.6}$$

where $\boldsymbol{q}_{opt}$ is defined in Eqs. (5.3.11). Furthermore, the rates of convergence for both $\hat{\boldsymbol{q}}_{BST}(N)$ and $\hat{\boldsymbol{q}}_{TST}(N)$ are at $O(\frac{1}{N})$.

Proof: At the λth sensor of the sensor array, the input $x_\lambda(n)$ consists of the desired signal component, the interference component, and noise component. Thus,

$$\tilde{\boldsymbol{x}}(n) = \tilde{\boldsymbol{s}}(n) + \tilde{\boldsymbol{i}}(n) + \tilde{\boldsymbol{\nu}}(n) \tag{5.4.7}$$

where $\tilde{\boldsymbol{s}}(n)$, $\tilde{\boldsymbol{u}}(n)$, and $\tilde{\boldsymbol{\nu}}(n)$ are defined in Eqs. (5.2.7), (5.2.12), and (5.2.17) respectively.

Now, for finite N, we have

$$\begin{aligned} E\left[\left\|\boldsymbol{R}_{\tilde{x}\tilde{x}}^{-1}-\hat{\boldsymbol{R}}_{\tilde{x}\tilde{x}}^{-1}(N)\right\|^2\right] &= E\left[\left\|\boldsymbol{R}_{\tilde{x}\tilde{x}}^{-1}(\hat{\boldsymbol{R}}_{\tilde{x}\tilde{x}}(N)-\boldsymbol{R}_{\tilde{x}\tilde{x}})\hat{\boldsymbol{R}}_{\tilde{x}\tilde{x}}^{-1}(N)\right\|^2\right] \\ &\leq \left[\left\|\boldsymbol{R}_{\tilde{x}\tilde{x}}^{-1}\right\|^2\right]\max\left[\left\|\hat{\boldsymbol{R}}_{\tilde{x}\tilde{x}}^{-1}(N)\right\|^2\right]E\left[\left\|\hat{\boldsymbol{R}}_{\tilde{x}\tilde{x}}(N)-\boldsymbol{R}_{\tilde{x}\tilde{x}}\right\|^2\right] \end{aligned} \tag{5.4.8}$$

where we have used the Schwarz inequality. From Eq. (5.4.1) and the property of matrix norms [70], we have

$$\begin{aligned} E\left[\left\|\hat{\boldsymbol{R}}_{\tilde{x}\tilde{x}}(N)-\boldsymbol{R}_{\tilde{x}\tilde{x}}\right\|^2\right] &\leq E\,tr\left[\left(\hat{\boldsymbol{R}}_{\tilde{x}\tilde{x}}(N)-\boldsymbol{R}_{\tilde{x}\tilde{x}}\right)\left(\hat{\boldsymbol{R}}_{\tilde{x}\tilde{x}}(N)-\boldsymbol{R}_{\tilde{x}\tilde{x}}\right)^{\dagger}\right] \\ &= trE\left[\frac{1}{N^2}\sum_{n=1}^{N}\left(\tilde{\boldsymbol{x}}(n)\tilde{\boldsymbol{x}}^{\dagger}(n)-\boldsymbol{R}_{\tilde{x}\tilde{x}}\right)\left(\tilde{\boldsymbol{x}}(n)\tilde{\boldsymbol{x}}^{\dagger}(n)-\boldsymbol{R}_{\tilde{x}\tilde{x}}\right)^{\dagger}\right] \\ &\quad +trE\left[\frac{1}{N^2}\sum_{\substack{m\\ m\neq n}}\sum_{n}\left(\tilde{\boldsymbol{x}}(m)\tilde{\boldsymbol{x}}^{\dagger}(m)-\boldsymbol{R}_{\tilde{x}\tilde{x}}\right)\left(\tilde{\boldsymbol{x}}(n)\tilde{\boldsymbol{x}}^{\dagger}(n)-\boldsymbol{R}_{\tilde{x}\tilde{x}}\right)^{\dagger}\right] \\ &= \frac{C_1}{N} \end{aligned} \tag{5.4.9}$$

where C_1 is a constant. In the last step, we have used the fact that the desired signal and the interferences are independent from symbol to symbol and the noise is white. Therefore, we have

$$E\left[\left\|\hat{\boldsymbol{R}}_{\tilde{x}\tilde{x}}(N)-\boldsymbol{R}_{\tilde{x}\tilde{x}}\right\|^2\right]=O\left(\frac{1}{N}\right) \tag{5.4.10}$$

where $O(.)$ denotes "order of". Using the boundedness of $\left\|\boldsymbol{R}_{\tilde{x}\tilde{x}}^{-1}\right\|^2$ and that of $\left\|\hat{\boldsymbol{R}}_{\tilde{x}\tilde{x}}^{-1}(N)\right\|^2$ with probability 1, together with Eq. (5.4.10) in Eq. (5.4.8), we obtain

$$E\left[\left\|\boldsymbol{R}_{\tilde{x}\tilde{x}}^{-1}-\hat{\boldsymbol{R}}_{\tilde{x}\tilde{x}}^{-1}(N)\right\|^2\right]=O\left(\frac{1}{N}\right). \tag{5.4.11}$$

Following similar steps as in Eq. (5.4.9) and noting that $\boldsymbol{\rho}_{\tilde{x}r}=\boldsymbol{\rho}_{\tilde{x}\tilde{s}'}=\boldsymbol{\rho}_{\tilde{s}\tilde{s}'}$, we also see that

$$E\left[\left\|\hat{\boldsymbol{\rho}}_{\tilde{x}r}(N)-\boldsymbol{\rho}_{\tilde{s}\tilde{s}'}\right\|^2\right]=O\left(\frac{1}{N}\right) \tag{5.4.12}$$

and

$$E\left[\left\|\hat{\boldsymbol{\rho}}_{\tilde{x}\tilde{s}'}(N)-\boldsymbol{\rho}_{\tilde{s}\tilde{s}'}\right\|^2\right]=O\left(\frac{1}{N}\right). \tag{5.4.13}$$

Now, from Eqs. (5.4.2) and (5.4.6), we have

$$\begin{aligned} E\left[\left\|\hat{\boldsymbol{q}}_{BST}(N)-\boldsymbol{q}_{opt}\right\|^2\right] &= E\left[\left\|\hat{\boldsymbol{R}}_{\tilde{x}\tilde{x}}^{-1}(N)\hat{\boldsymbol{\rho}}_{\tilde{x}r}(N)-\boldsymbol{R}_{\tilde{x}\tilde{x}}^{-1}\boldsymbol{\rho}_{\tilde{s}\tilde{s}'}\right\|^2\right] \\ &= E\left[\left\|\boldsymbol{R}_{\tilde{x}\tilde{x}}^{-1}(\hat{\boldsymbol{\rho}}_{\tilde{x}r}(N)-\boldsymbol{\rho}_{\tilde{s}\tilde{s}'})+(\hat{\boldsymbol{R}}_{\tilde{x}\tilde{x}}^{-1}(N)-\boldsymbol{R}_{\tilde{x}\tilde{x}}^{-1})\hat{\boldsymbol{\rho}}_{\tilde{x}r}(N)\right\|^2\right] \\ &\leq 2E\left[\left\|\boldsymbol{R}_{\tilde{x}\tilde{x}}^{-1}\right\|^2\left(\|\hat{\boldsymbol{\rho}}_{\tilde{x}r}(N)-\boldsymbol{\rho}_{\tilde{s}\tilde{s}'}\|^2\right)\right] \\ &\quad +2E\left[\left(\left\|\hat{\boldsymbol{R}}_{\tilde{x}\tilde{x}}^{-1}(N)-\boldsymbol{R}_{\tilde{x}\tilde{x}}^{-1}\right\|^2\right)\|\hat{\boldsymbol{\rho}}_{\tilde{x}r}(N)\|^2\right] \end{aligned} \tag{5.4.14}$$

where we have used the inequality $\|\boldsymbol{a}+\boldsymbol{b}\|^2 \leq 2\|\boldsymbol{a}\|^2+2\|\boldsymbol{b}\|^2$ followed by the Schwarz inequality. Similarly, we have

$$\begin{aligned} E\left[\left\|\hat{\boldsymbol{q}}_{TST}(N)-\boldsymbol{q}_{opt}\right\|^2\right] &\leq 2E\left[\left\|\boldsymbol{R}_{\tilde{x}\tilde{x}}^{-1}\right\|^2\left(\|\hat{\boldsymbol{\rho}}_{\tilde{x}\tilde{s}'}(N)-\boldsymbol{\rho}_{\tilde{s}\tilde{s}'}\|^2\right)\right] \\ &\quad +2E\left[\left(\left\|\hat{\boldsymbol{R}}_{\tilde{x}\tilde{x}}^{-1}(N)-\boldsymbol{R}_{\tilde{x}\tilde{x}}^{-1}\right\|^2\right)\|\hat{\boldsymbol{\rho}}_{\tilde{x}\tilde{s}'}(N)\|^2\right]. \end{aligned} \tag{5.4.15}$$

Using the boundedness of $\left\|\boldsymbol{R}_{\tilde{x}\tilde{x}}^{-1}\right\|^2$ together with Eqs. (5.4.11), (5.4.12), and (5.4.13) in Eqs. (5.4.14) and (5.4.15), we conclude that

$$E\left[\left\|\hat{\boldsymbol{q}}_{BST}(N)-\boldsymbol{q}_{opt}\right\|^2\right]=O\left(\frac{1}{N}\right) \tag{5.4.16}$$

and

$$E\left[\left\|\hat{\boldsymbol{q}}_{TST}(N)-\boldsymbol{q}_{opt}\right\|^2\right]=O\left(\frac{1}{N}\right). \tag{5.4.17}$$

From Eqs. (5.4.16) and (5.4.17), using the triangular inequality, clearly we can see that

$$E\left[\|\delta\hat{\boldsymbol{q}}(N)\|^2\right]=E\left[\|\hat{\boldsymbol{q}}_{BST}(N)-\hat{\boldsymbol{q}}_{TST}(N)\|^2\right]=O\left(\frac{1}{N}\right). \tag{5.4.18}$$

Thus, for $N\to\infty$, both $\hat{\boldsymbol{q}}_{BST}(N)$ and $\hat{\boldsymbol{q}}_{TST}(N)$ converge in the mean-square sense to $\boldsymbol{q}_{opt}$ with the rate of convergence $O\left(\frac{1}{N}\right)$. □

Theorem 5.1 has important implications because it shows that the BLAST filter and the TAST filter are asymptotically equivalent in the sense that both converge to $\boldsymbol{q}_{opt}$ at the same order. However, the TAST filter necessitates a copy of the desired signal.

5.5 The Finite Sample Output SINR Analysis

Based on Theorem 5.1, we can further study the output signal to interference plus noise ratio (SINR) of the BLAST filter and the TAST filter with finite samples. We denote the output SINR of the BLAST filter with finite samples as $\mathrm{SINR}_{BST}(N)$ and the output SINR of the TAST filter with finite samples as $\mathrm{SINR}_{TST}(N)$. They are defined respectively as

$$\mathrm{SINR}_{BST}(N) = \frac{\hat{\boldsymbol{q}}_{BST}^{\dagger}(N)\hat{\boldsymbol{R}}_{\tilde{s}\tilde{s}}\hat{\boldsymbol{q}}_{BST}(N)}{\hat{\boldsymbol{q}}_{BST}^{\dagger}(N)\hat{\boldsymbol{R}}_{\tilde{u}+\tilde{v},\tilde{u}+\tilde{v}}\hat{\boldsymbol{q}}_{BST}(N)} \tag{5.5.1}$$

$$\mathrm{SINR}_{TST}(N) = \frac{\hat{\boldsymbol{q}}_{TST}^{\dagger}(N)\hat{\boldsymbol{R}}_{\tilde{s}\tilde{s}}\hat{\boldsymbol{q}}_{TST}(N)}{\hat{\boldsymbol{q}}_{TST}^{\dagger}(N)\hat{\boldsymbol{R}}_{\tilde{u}+\tilde{v},\tilde{u}+\tilde{v}}\hat{\boldsymbol{q}}_{TST}(N)} \tag{5.5.2}$$

where $\hat{\boldsymbol{R}}_{\tilde{s}\tilde{s}} = \langle \tilde{\boldsymbol{s}}(n)\tilde{\boldsymbol{s}}^{\dagger}(n)\rangle_N$, and $\hat{\boldsymbol{R}}_{\tilde{u}+\tilde{v},\tilde{u}+\tilde{v}} = \langle (\tilde{\boldsymbol{u}}(n)+\tilde{\boldsymbol{v}}(n))(\tilde{\boldsymbol{u}}(n)+\tilde{\boldsymbol{v}}(n))^{\dagger}\rangle_N$. For infinite data length ($N=\infty$), SINR_{opt-ST} is defined as

$$\mathrm{SINR}_{opt-ST} = \frac{\boldsymbol{q}_{opt}^{\dagger}\boldsymbol{R}_{\tilde{s}\tilde{s}}\boldsymbol{q}_{opt}}{\boldsymbol{q}_{opt}^{\dagger}\boldsymbol{R}_{\tilde{u}+\tilde{v},\tilde{u}+\tilde{v}}\boldsymbol{q}_{opt}}. \tag{5.5.3}$$

We like to evaluate the mean square error between $\mathrm{SINR}_{BST}(N)$, $\mathrm{SINR}_{TST}(N)$ and SINR_{opt-ST} respectively, that is,

$$E\left[\frac{\|\mathrm{SINR}_{BST}(N)-\mathrm{SINR}_{opt-ST}\|^2}{\|\mathrm{SINR}_{opt-ST}\|^2}\right] \quad \text{and} \quad E\left[\frac{\|\mathrm{SINR}_{TST}(N)-\mathrm{SINR}_{opt-ST}\|^2}{\|\mathrm{SINR}_{opt-ST}\|^2}\right]. \tag{5.5.4}$$

We have Corollary 5.1 as following:

Corollary 5.1: *For the same scenario as in Theorem 5.1,* $\mathrm{SINR}_{BST}(N)$ and $\mathrm{SINR}_{TST}(N)$ *converge in the mean square sense to* SINR_{opt-ST}. *Furthermore the convergence rate for* $\mathrm{SINR}_{BST}(N)$ and $\mathrm{SINR}_{TST}(N)$ *are* $O(\frac{1}{N})$, *that is,*

$$E\left[\frac{\|\mathrm{SINR}_{BST}(N)-\mathrm{SINR}_{opt-ST}\|^2}{\|\mathrm{SINR}_{opt-ST}\|^2}\right] = O\left(\frac{1}{N}\right) \tag{5.5.5}$$

$$E\left[\frac{\|\mathrm{SINR}_{TST}(N)-\mathrm{SINR}_{opt-ST}\|^2}{\|\mathrm{SINR}_{opt-ST}\|^2}\right] = O\left(\frac{1}{N}\right). \tag{5.5.6}$$

Proof: Using Eqs. (5.5.1) and (5.5.3), we have

$$\begin{aligned}\mathrm{SINR}_{BST}(N) - \mathrm{SINR}_{opt-ST} &= \frac{\hat{\boldsymbol{q}}^{\dagger}_{BST}(N)\hat{\boldsymbol{R}}_{\tilde{s}\tilde{s}}\hat{\boldsymbol{q}}_{BST}(N)}{\hat{\boldsymbol{q}}^{\dagger}_{BST}(N)\hat{\boldsymbol{R}}_{\tilde{u}+\tilde{v},\tilde{u}+\tilde{v}}\hat{\boldsymbol{q}}_{BST}(N)} - \mathrm{SINR}_{opt-ST} \\ &= \frac{\hat{\boldsymbol{q}}^{\dagger}_{BST}(N)\left[\hat{\boldsymbol{R}}_{\tilde{s}\tilde{s}} - \mathrm{SINR}_{opt-ST}\hat{\boldsymbol{R}}_{\tilde{u}+\tilde{v},\tilde{u}+\tilde{v}}\right]\hat{\boldsymbol{q}}_{BST}(N)}{\hat{\boldsymbol{q}}^{\dagger}_{BST}(N)\hat{\boldsymbol{R}}_{\tilde{u}+\tilde{v},\tilde{u}+\tilde{v}}\hat{\boldsymbol{q}}_{BST}(N)}.\end{aligned} \tag{5.5.7}$$

We define

$$\delta\boldsymbol{q}_{BST} = \hat{\boldsymbol{q}}_{BST}(N) - \boldsymbol{q}_{opt} \tag{5.5.8}$$

$$\delta\hat{\boldsymbol{R}}_{\tilde{s}\tilde{s}} = \hat{\boldsymbol{R}}_{\tilde{s}\tilde{s}} - \boldsymbol{R}_{\tilde{s}\tilde{s}} \tag{5.5.9}$$

$$\delta\hat{\boldsymbol{R}}_{\tilde{u}+\tilde{v},\tilde{u}+\tilde{v}} = \hat{\boldsymbol{R}}_{\tilde{u}+\tilde{v},\tilde{u}+\tilde{v}} - \boldsymbol{R}_{\tilde{u}+\tilde{v},\tilde{u}+\tilde{v}}. \tag{5.5.10}$$

Considering the numerator of Eq. (5.5.7), we have

$$\begin{aligned}\hat{\boldsymbol{q}}^{\dagger}_{BST}(N)\left[\hat{\boldsymbol{R}}_{\tilde{s}\tilde{s}} - \mathrm{SINR}_{opt-ST}\hat{\boldsymbol{R}}_{\tilde{u}+\tilde{v},\tilde{u}+\tilde{v}}\right]\hat{\boldsymbol{q}}_{BST}(N) &= \boldsymbol{q}^{\dagger}_{opt}\left[\boldsymbol{R}_{\tilde{s}\tilde{s}} - \mathrm{SINR}_{opt-ST}\boldsymbol{R}_{\tilde{u}+\tilde{v},\tilde{u}+\tilde{v}}\right]\boldsymbol{q}_{opt} \\ &+\delta\boldsymbol{q}^{\dagger}_{BST}\left[\boldsymbol{R}_{\tilde{s}\tilde{s}} - \mathrm{SINR}_{opt-ST}\boldsymbol{R}_{\tilde{u}+\tilde{v},\tilde{u}+\tilde{v}}\right]\boldsymbol{q}_{opt} + \boldsymbol{q}^{\dagger}_{opt}\left[\boldsymbol{R}_{\tilde{s}\tilde{s}} - \mathrm{SINR}_{opt-ST}\boldsymbol{R}_{\tilde{u}+\tilde{v},\tilde{u}+\tilde{v}}\right]\delta\boldsymbol{q}_{BST} \\ &+\boldsymbol{q}^{\dagger}_{opt}\left[\delta\boldsymbol{R}_{\tilde{s}\tilde{s}} - \mathrm{SINR}_{opt-ST}\delta\boldsymbol{R}_{\tilde{u}+\tilde{v},\tilde{u}+\tilde{v}}\right]\boldsymbol{q}_{opt} + [\text{high order terms}],\end{aligned} \tag{5.5.11}$$

where

$$\begin{aligned}[\text{high order terms}] &= \delta\boldsymbol{q}^{\dagger}_{BST}\left[\boldsymbol{R}_{\tilde{s}\tilde{s}} - \mathrm{SINR}_{opt-ST}\boldsymbol{R}_{\tilde{u}+\tilde{v},\tilde{u}+\tilde{v}}\right]\delta\boldsymbol{q}_{BST} \\ &+\delta\boldsymbol{q}^{\dagger}_{BST}\left[\delta\boldsymbol{R}_{\tilde{s}\tilde{s}} - \mathrm{SINR}_{opt-ST}\delta\boldsymbol{R}_{\tilde{u}+\tilde{v},\tilde{u}+\tilde{v}}\right]\boldsymbol{q}_{opt} \\ &+\boldsymbol{q}^{\dagger}_{opt}\left[\delta\boldsymbol{R}_{\tilde{s}\tilde{s}} - \mathrm{SINR}_{opt-ST}\delta\boldsymbol{R}_{\tilde{u}+\tilde{v},\tilde{u}+\tilde{v}}\right]\delta\boldsymbol{q}_{BST} \\ &+\delta\boldsymbol{q}^{\dagger}_{BST}\left[\delta\boldsymbol{R}_{\tilde{s}\tilde{s}} - \mathrm{SINR}_{opt-ST}\delta\boldsymbol{R}_{\tilde{u}+\tilde{v},\tilde{u}+\tilde{v}}\right]\delta\boldsymbol{q}_{BST}.\end{aligned} \tag{5.5.12}$$

For the first term of the right side in Eq. (5.5.11), we have

$$\boldsymbol{q}^{\dagger}_{opt}\left[\boldsymbol{R}_{\tilde{s}\tilde{s}} - \mathrm{SINR}_{opt-ST}\boldsymbol{R}_{\tilde{u}+\tilde{v},\tilde{u}+\tilde{v}}\right]\boldsymbol{q}_{opt} = \boldsymbol{q}^{\dagger}_{opt}\boldsymbol{R}_{\tilde{s}\tilde{s}}\boldsymbol{q}_{opt} - \boldsymbol{q}^{\dagger}_{opt}\boldsymbol{R}_{\tilde{s}\tilde{s}}\boldsymbol{q}_{opt} = 0. \tag{5.5.13}$$

Using the Schwarz inequality to the second term of the right side in Eq. (5.5.11), We obtain

$$E\left[\left\|\delta \boldsymbol{q}_{BST}^{\dagger}\left[\boldsymbol{R}_{\tilde{s}\tilde{s}}-\mathrm{SINR}_{opt-ST}\boldsymbol{R}_{\tilde{u}+\tilde{v},\tilde{u}+\tilde{v}}\right]\boldsymbol{q}_{opt}\right\|^{2}\right] \tag{5.5.14}$$
$$\leq E\left[\left\|\delta \boldsymbol{q}_{BST}^{\dagger}\right\|^{2}\right]\cdot\left[\left\|\left[\boldsymbol{R}_{\tilde{s}\tilde{s}}-\mathrm{SINR}_{opt-ST}\boldsymbol{R}_{\tilde{u}+\tilde{v},\tilde{u}+\tilde{v}}\right]\right\|^{2}\right]\cdot\left[\left\|\boldsymbol{q}_{opt}\right\|^{2}\right].$$

Noting that the boundednesses of $\left\|\left[\boldsymbol{R}_{\tilde{s}\tilde{s}}-\mathrm{SINR}_{opt-ST}\boldsymbol{R}_{\tilde{u}+\tilde{v},\tilde{u}+\tilde{v}}\right]\right\|$ and that of $\left\|\boldsymbol{q}_{opt}\right\|$ and using Eq. (5.4.16), we obtain

$$E\left[\left\|\delta \boldsymbol{q}_{BST}^{\dagger}\left[\boldsymbol{R}_{\tilde{s}\tilde{s}}-\mathrm{SINR}_{opt-ST}\boldsymbol{R}_{\tilde{u}+\tilde{v},\tilde{u}+\tilde{v}}\right]\boldsymbol{q}_{opt}\right\|^{2}\right]=O\left(\frac{1}{N}\right). \tag{5.5.15}$$

For the third term of the right side in Eq. (5.5.11), we similarly have

$$E\left[\left\|\boldsymbol{q}_{opt}^{\dagger}\left[\boldsymbol{R}_{\tilde{s}\tilde{s}}-\mathrm{SINR}_{opt-ST}\boldsymbol{R}_{\tilde{u}+\tilde{v},\tilde{u}+\tilde{v}}\right]\delta \boldsymbol{q}_{BST}\right\|^{2}\right]=O\left(\frac{1}{N}\right). \tag{5.5.16}$$

We also note that $E\left[\left\|\delta \boldsymbol{R}_{\tilde{s}\tilde{s}}\right\|^{2}\right]=O\left(\frac{1}{N}\right)$ and $E\left[\left\|\delta \boldsymbol{R}_{\tilde{u}+\tilde{v},\tilde{u}+\tilde{v}}\right\|^{2}\right]=O\left(\frac{1}{N}\right)$. Using the Schwarz inequality to the fourth term of the right side in Eq. (5.5.11), we obtain

$$E\left[\left\|\boldsymbol{q}_{opt}^{\dagger}\left[\delta \boldsymbol{R}_{\tilde{s}\tilde{s}}-\mathrm{SINR}_{opt-ST}\delta \boldsymbol{R}_{\tilde{u}+\tilde{v},\tilde{u}+\tilde{v}}\right]\boldsymbol{q}_{opt}\right\|^{2}\right]=O\left(\frac{1}{N}\right). \tag{5.5.17}$$

For the high order term of the right side in Eq. (5.5.11), using the similar steps, we obtain

$$E\left[\|\text{high order terms}\|^{2}\right]=O\left(\frac{1}{N^{2}}\right). \tag{5.5.18}$$

Therefore, we obtain

$$E\left[\left\|\hat{\boldsymbol{q}}_{BST}^{\dagger}(N)\left[\hat{\boldsymbol{R}}_{\tilde{s}\tilde{s}}-\mathrm{SINR}_{opt-ST}\hat{\boldsymbol{R}}_{\tilde{u}+\tilde{v},\tilde{u}+\tilde{v}}\right]\hat{\boldsymbol{q}}_{BST}\right\|^{2}\right]=O\left(\frac{1}{N}\right). \tag{5.5.19}$$

Because $\left[\left\|\hat{\boldsymbol{q}}_{BST}^{\dagger}(N)\hat{\boldsymbol{R}}_{\tilde{u}+\tilde{v},\tilde{u}+\tilde{v}}\hat{\boldsymbol{q}}_{BST}(N)\right\|^{2}\right]$ is bounded with probability one, that is

$$\min\left[\left\|\hat{\boldsymbol{q}}_{BST}^{\dagger}(N)\hat{\boldsymbol{R}}_{\tilde{u}+\tilde{v},\tilde{u}+\tilde{v}}\hat{\boldsymbol{q}}_{BST}(N)\right\|^{2}\right]\geq C_{1},\quad N\rightarrow\infty \tag{5.5.20}$$

where C_1 is a positive constant. Using Eqs. (5.5.19) and (5.5.20) in Eq. (5.5.7), we obtain

$$E\left[\|\mathrm{SINR}_{BST}(N) - \mathrm{SINR}_{opt-ST}\|^2\right] = O\left(\frac{1}{N}\right). \tag{5.5.21}$$

We know $\|\mathrm{SINR}_{opt-ST}\|^2$ is a constant which is not equal to zero, so we conclude that

$$E\left[\frac{\|\mathrm{SINR}_{BST}(N) - \mathrm{SINR}_{opt-ST}\|^2}{\|\mathrm{SINR}_{opt-ST}\|^2}\right] = O\left(\frac{1}{N}\right). \tag{5.5.22}$$

Using the similar steps, we obtain

$$E\left[\frac{\|\mathrm{SINR}_{TST}(N) - \mathrm{SINR}_{opt-ST}\|^2}{\|\mathrm{SINR}_{opt-ST}\|^2}\right] = O\left(\frac{1}{N}\right). \quad \square \tag{5.5.23}$$

5.6 The Finite Sample Output MSE Analysis

In this section, we study the finite sample MSE (Mean Square Error) of the BLAST filter and that of the TAST filter. The finite sample MSE of the BLAST filter is denoted as $J_{BST}(N)$ and the finite sample MSE of the TAST filter is denoted as $J_{TST}(N)$. They are defined respectively as

$$J_{BST}(N) = \left\langle \left(\hat{\boldsymbol{q}}_{BST}^{\dagger}(N)\tilde{\boldsymbol{x}}(n) - \tilde{s}'(n)\right)\left(\hat{\boldsymbol{q}}_{BST}^{\dagger}(N)\tilde{\boldsymbol{x}}(n) - \tilde{s}'(n)\right)^{*}\right\rangle \tag{5.6.1}$$

$$J_{TST}(N) = \left\langle \left(\hat{\boldsymbol{q}}_{TST}^{\dagger}(N)\tilde{\boldsymbol{x}}(n) - \tilde{s}'(n)\right)\left(\hat{\boldsymbol{q}}_{TST}^{\dagger}(N)\tilde{\boldsymbol{x}}(n) - \tilde{s}'(n)\right)^{*}\right\rangle \tag{5.6.2}$$

where $\hat{\boldsymbol{q}}_{BST}(N)$ and $\hat{\boldsymbol{q}}_{TST}(N)$ are defined in Eqs. (5.4.2) and (5.4.3) respectively. $\tilde{\boldsymbol{x}}(n)$ and $\tilde{s}'(n)$ are defined in Eqs. (5.2.5) and (5.2.24) respectively. Let the infinite sample MSE of the BLAST filter which is equal to that of the TAST filter is denoted as J_{opt-ST}. J_{opt-ST} is defined as

$$J_{opt-ST} = \left\langle \left(\boldsymbol{q}_{opt}^{\dagger}\tilde{\boldsymbol{x}}(n) - \tilde{s}'(n)\right)\left(\boldsymbol{q}_{opt}^{\dagger}\tilde{\boldsymbol{x}}(n) - \tilde{s}'(n)\right)^{*}\right\rangle \tag{5.6.3}$$

where $\boldsymbol{q}_{opt}$ is defined in Eq. (5.3.11). We evaluate the mean square error between $J_{BST}(N)$ and J_{opt-ST} and the mean square error between $J_{TST}(N)$ and J_{opt-ST} respectively, that is,

$$E\left[\frac{\|J_{BST}(N)-J_{opt-ST}\|^2}{\|J_{opt-ST}\|^2}\right] \quad \text{and} \quad E\left[\frac{\|J_{TST}(N)-J_{opt-ST}\|^2}{\|J_{opt-ST}\|^2}\right]. \tag{5.6.4}$$

We have Corollary 5.2 as follows:

Corollary 5.2: *For the same scenario as in Theorem 5.1, $J_{BST}(N)$ and $J_{TST}(N)$ converge in the mean square sense to J_{opt-ST}. Furthermore the convergence rate for $J_{BST}(N)$ and $J_{TST}(N)$ are $O(\frac{1}{N})$, that is,*

$$E\left[\frac{\|J_{BST}(N)-J_{opt-ST}\|^2}{\|J_{opt-ST}\|^2}\right] = O\left(\frac{1}{N}\right) \tag{5.6.5}$$

$$E\left[\frac{\|J_{TST}(N)-J_{opt-ST}\|^2}{\|J_{opt-ST}\|^2}\right] = O\left(\frac{1}{N}\right). \tag{5.6.6}$$

Proof: Using Eqs. (5.6.1) and (5.6.3), we have

$$J_{BST}(N) = \langle s(n)s^*(n)\rangle - \hat{\boldsymbol{q}}_{BST}^{\dagger}(N)\boldsymbol{\rho}_{\tilde{\boldsymbol{x}}\tilde{s}'} - \left(\hat{\boldsymbol{q}}_{BST}^{\dagger}(N)\boldsymbol{\rho}_{\tilde{\boldsymbol{x}}\tilde{s}'}\right)^{\dagger} - \hat{\boldsymbol{q}}_{BST}^{\dagger}(N)\boldsymbol{R}_{\tilde{\boldsymbol{x}}\tilde{\boldsymbol{x}}}\hat{\boldsymbol{q}}_{BST}(N) \tag{5.6.7}$$

$$J_{opt-ST} = \langle s(n)s^*(n)\rangle - \boldsymbol{q}_{opt}^{\dagger}\boldsymbol{\rho}_{\tilde{\boldsymbol{x}}\tilde{s}'} - \left(\boldsymbol{q}_{opt}^{\dagger}\boldsymbol{\rho}_{\tilde{\boldsymbol{x}}\tilde{s}'}\right)^{\dagger} - \boldsymbol{q}_{opt}^{\dagger}\boldsymbol{R}_{\tilde{\boldsymbol{x}}\tilde{\boldsymbol{x}}}\boldsymbol{q}_{opt}. \tag{5.6.8}$$

Subtracting Eq. (5.6.7) by Eq. (5.6.8), we have

$$\begin{aligned}\|J_{BST}(N)-J_{opt-ST}\|^2 \;=\; & \left\|\delta\boldsymbol{q}_{BST}^{\dagger}\boldsymbol{\rho}_{\tilde{\boldsymbol{x}}\tilde{s}'} + (\delta\boldsymbol{q}_{BST}^{\dagger}\boldsymbol{\rho}_{\tilde{\boldsymbol{x}}\tilde{s}'})^{\dagger} + \delta\boldsymbol{q}_{BST}^{\dagger}\boldsymbol{R}_{\tilde{\boldsymbol{x}}\tilde{\boldsymbol{x}}}\boldsymbol{q}_{opt}\right. \\ & \left. + \boldsymbol{q}_{opt}^{\dagger}\boldsymbol{R}_{\tilde{\boldsymbol{x}}\tilde{\boldsymbol{x}}}\delta\boldsymbol{q}_{BST} + \delta\boldsymbol{q}_{BST}^{\dagger}\boldsymbol{R}_{\tilde{\boldsymbol{x}}\tilde{\boldsymbol{x}}}\delta\boldsymbol{q}_{BST}\right\|^2.\end{aligned} \tag{5.6.9}$$

Using the inequality $\|\boldsymbol{a}+\boldsymbol{b}\|^2 \le 2\|\boldsymbol{a}\|^2 + 2\|\boldsymbol{b}\|^2$, we obtain

$$\begin{aligned}E\left[\|J_{BST}(N)-J_{opt-ST}\|^2\right] \;\le\; & 2E\left[\left\|\delta\boldsymbol{q}_{BST}^{T}\boldsymbol{\rho}_{\tilde{\boldsymbol{x}}\tilde{s}'}\right\|^2\right] + 4E\left[\left\|(\delta\boldsymbol{q}_{BST}^{\dagger}\boldsymbol{\rho}_{\tilde{\boldsymbol{x}}\tilde{s}'})^{\dagger}\right\|^2\right] \\ & + 8E\left[\left\|\delta\boldsymbol{q}_{BST}^{\dagger}\boldsymbol{R}_{\tilde{\boldsymbol{x}}\tilde{\boldsymbol{x}}}\boldsymbol{q}_{opt}\right\|^2\right] + 16E\left[\left\|\boldsymbol{q}_{opt}^{\dagger}\boldsymbol{R}_{\tilde{\boldsymbol{x}}\tilde{\boldsymbol{x}}}\delta\boldsymbol{q}_{BST}\right\|^2\right] \\ & + 32E\left[\left\|\delta\boldsymbol{q}_{BST}^{\dagger}\boldsymbol{R}_{\tilde{\boldsymbol{x}}\tilde{\boldsymbol{x}}}\delta\boldsymbol{q}_{BST}\right\|^2\right].\end{aligned} \tag{5.6.10}$$

Using Eq. (5.4.16) and the Schwarz inequality in Eqs. (5.6.10), we obtain

$$E\left[\|J_{BST}(N) - J_{opt-ST}\|^2\right] = O\left(\frac{1}{N}\right). \tag{5.6.11}$$

Because $\|J_{opt-ST}\|^2$ is a constant, we conclude that

$$E\left[\frac{\|J_{BST}(N) - J_{opt-ST}\|^2}{\|J_{opt-ST}\|^2}\right] = O\left(\frac{1}{N}\right). \tag{5.6.12}$$

Using the similar steps, we obtain

$$E\left[\frac{\|J_{TST}(N) - J_{opt-ST}\|^2}{\|J_{opt-ST}\|^2}\right] = O\left(\frac{1}{N}\right). \quad \square \tag{5.6.13}$$

5.7 Numerical Results

In this section, we present some simulation results showing the finite sample performance of the BLAST filter in comparison to the TAST filter. We use BPSK signals for both the desired and the interfering signals. Thus, the desired signal and the interfering signal are given respectively by

$$s(nT_s) = \sum_{k=-\infty}^{\infty} d(k)g(nT_s - kT_{b_1})\cos(2\pi f_1 nT_s) \tag{5.7.1}$$

$$u(nT_s) = \sum_{k=-\infty}^{\infty} d_u(k)g_u(nT_s - kT_{b_2})\cos(2\pi f_2 nT_s) \tag{5.7.2}$$

where T_{b_1} and T_{b_2} are the baud periods, f_1 and f_2 are the carrier frequency offsets of $s(nT_s)$ and $u(nT_s)$ respectively and T_s is the sampling period. $\{d(k)\}$ and $\{d_u(k)\}$ are stationary random binary sequences. For both the desired and interfering signals, we assume that $g(nT_s)$ and $g_u(nT_s)$ are the pulse obtained by the square root raised-cosine pulse shaping filter with a 100% roll-off factor [31]. The length of $g(n)$ which is equal to the length of $g_u(n)$ is equal to 159.

Example 5.1: In this example, we examine the output SINR of the BLAST and the TAST

filtering algorithms compared with the output SINR of the SCORE and the C-CAB beamforming algorithms against different DOA difference $0°, 2°, 5°$, and $10°$. We denote the output SINR of BLAST and TAST with finite symbols as $\text{SINR}_{BST}(N)$ and $\text{SINR}_{TST}(N)$ respectively. The output SINR of SCORE and C-CAB with finite samples are defined in [15]. $\text{SINR}_{BST}(N)$ is defined as

$$\text{SINR}_{BST}(N) = \frac{\hat{\boldsymbol{q}}_{BST}^{\dagger}(N)\hat{\boldsymbol{R}}_{\bar{s}\bar{s}}\hat{\boldsymbol{q}}_{BST}(N)}{\hat{\boldsymbol{q}}_{BST}^{\dagger}(N)\hat{\boldsymbol{R}}_{\bar{u}+\bar{v},\bar{u}+\bar{v}}\hat{\boldsymbol{q}}_{BST}(N)}, \tag{5.7.3}$$

$\text{SINR}_{TST}(N)$ is defined similarly. The desired and interfering signal are BPSK signals as given by Eqs. (5.7.1) and (5.7.2) respectively. The baud rates of the desired signal and the interference are equal which are 5kHz. The carrier frequency offset of the desired signal is fixed at $f_1 = 10$kHz and the interference is fixed at $f_2 = 17$kHz, so that the spectral overlapping between the two signals is 30%. The definition of the spectral overlapping is shown in Chapter 3. The sampling rate $f = 100$kHz. For the parameters of BLAST and TAST, the number of sensors is chosen to be $L = 3$, the order of FIR filters in each FRESH filter is chosen at $N_o = 6$, the number of the branches of FRESH filter is chosen to be $M = 2$. The frequency shift in the two branches are set at $\alpha_1 = 20$kHz, $\alpha_2 = -20$kHz respectively. The frequency shift used in the reference path of the BLAST filter is set at $\alpha' = 0$kHz. For SCORE and C-CAB, the number of sensors is also chosen to be $L = 3$. The DOA of the desired signal is fixed at 0 degree whereas we vary the DOA of the interference so that the DOA difference between the two signals can be varied. Two scenarios are examined. In the first case, the signal to noise ratio (SNR) and the signal to interference ratio (SIR) at the input are fixed at 10dB and 0dB respectively. The output SINR of BLAST, TAST, C-CAB, and SCORE against the different DOA difference $0°, 2°, 5°$, and $10°$ between the desired signal and the interference are plotted in Fig. 5.4(a) to Fig. 5.4(d). In the second case, the signal to noise ratio (SNR) and the signal to interference ratio (SIR) at the input are fixed at 10dB and 5dB respectively. The output SINR of BLAST, TAST, C-CAB, and SCORE against the different DOA difference $0°, 2°, 5°$, and $10°$ between the desired signal and the interference are plotted in Fig. 5.5(a) to Fig. 5.5(d). It can be observed that the output SINR of BLAST and TAST are always better than those of the C-CAB and

SCORE algorithms in two cases. As the DOA difference between the desire signal and the interfering signal decreases, the performance of SCORE and C-CAB degrades. When the DOA difference becomes zero, SCORE and C-CAB fail. However, the performance of BLAST and TAST are different. Although the performance of BLAST and TAST degrade as the DOA difference decreases, it can be observed that when the DOA difference becomes zero, the output SINR of BLAST and TAST is still 7dB in the first case and 9dB in the second case which are much higher than the output SINR of C-CAB and SCORE when the DOA difference is 0°. The main reason for the performance difference is that BLAST and TAST exploit not only the spatial information (DOA difference between the desired signal and interference) but also temporal information (spectral redundancy information), whereas SCORE and C-CAB only exploit the spatial information. When the DOA difference is reduced, the spatial information is reduced but the temporal information still exist there. So the performance of BLAST and TAST is much better than C-CAB and SCORE. It also can be observed that there is the difference between the output SINR of BLAST and that of TAST. The difference becomes negligible when the number of symbols goes to infinity. Moreover, when the DOA difference and/or the input SIR are increased, the output SINR of these algorithms are increased.

Example 5.2: In this example, we examine the output eye diagram of the BLAST filter against different DOA difference between the desired signal and the interfering signal. The scenario is similar to that of Example 5.1, except that the SNR and the SIR at the input are fixed at 20dB and 0dB respectively. The DOA of the desired signal is fixed at 0°, whereas we vary the DOA (degrees) of the interference so that the DOA difference of the two signals can be varied. The output eye diagrams of the BLAST algorithm against different DOA difference $0°, 2°, 5°$, and $10°$ for numbers of symbols being 250 are plotted in Fig. 5.6. In order to compare, we also plot the output eye diagrams of C-CAB and SCORE in Fig. 5.7 when the DOA difference is zero. For C-CAB and SCORE, the number of sensors is still chosen as 3. It can be observed that the output eye diagrams of BLAST against different DOA differences $0°, 2°, 5°$, and $10°$ are open and the output eye diagrams of C-CAB and SCORE are closed when the DOA difference are zero.

Example 5.3: In this example, we examine the filter coefficient convergence and the finite sample mean square error (MSE) of the BLAST and the TAST filters under the condition that the DOA difference between the desired signal and the interference are fixed at $0°, 2°, 5°$, and $10°$ respectively. The scenario is similar to that of Example 5.1, except that the signal to noise ratio (SNR) and the signal to interference ratio (SIR) at the input are fixed at 10dB and 0dB respectively. The DOA of the desired signal is fixed at $0°$ whereas we vary the DOA (degrees) of the interference so that the DOA difference of the two signals can be varied. For the filter coefficients with finite symbols, $\hat{q}_{BST}$ and $\hat{q}_{TST}$ in this example are calculated from Eqs. (5.4.2) and (5.4.3). q_{opt} in this example is calculated from Eq. (5.3.11) using time-averages of 500 symbols. The normalized convergence of $E\left[\left\|q_{opt} - \hat{q}_{BST}(N)\right\|^2\right] / \|q_{opt}\|^2$ and $E\left[\left\|q_{opt} - \hat{q}_{TST}(N)\right\|^2\right] / \|q_{opt}\|^2$, each being averaged over 20 realizations, are plotted in Fig. 5.8(a) to Fig. 5.8(d), in which the DOA difference between the desired and interfering signals are fixed at $0°, 2°, 5°$, and $10°$ respectively. It is observed that both the BLAST filter coefficients and the TAST filter coefficients converge to the optimum filter coefficients when the number of symboles is large, with the TAST filter being the faster in convergence. For the output MSE with finite symbols, $J_{BST}(N)$ and $J_{TST}(N)$ in this example are calculated from Eqs. (5.6.1) and (5.6.2). J_{opt-ST} in this example is calculated from Eq. (5.6.3) using time-averages of 500 symbols. The normalized MSE difference of $E\left[\|J_{opt-ST} - J_{BST}(N)\|^2\right] / \|J_{opt-ST}\|^2$ and $E\left[\|J_{opt-ST} - J_{TST}(N)\|^2\right] / \|J_{opt-ST}\|^2$, each being averaged over 20 realizations, are plotted in Fig. 5.9(a) to Fig. 5.9(d), in which the DOA difference between the desired and interfering signals are fixed at $0°, 2°, 5°$, and $10°$ respectively. It is observed that both the normalized output MSE of the BLAST filter and that of the TAST filter converge to zero when the number of symbols is large, with the TAST filter being the faster in convergence. It is also observed that both the normalized output MSE of the BLAST filter and that of the TAST filter converge slower when the DOA difference is increased. The reason is that both algorithms need more time to adjust their filter coefficients when new spatial information (DOA difference) is added.

Example 5.4: In this example, we examine the output SINR of the BLAST and the TAST filtering algorithms compared with the output SINR of the SCORE and the C-CAB beam-

forming algorithms against different spectral overlapping between the signal and the interference. The scenario is similar to Example 5.1 except that the DOA differences and the spectral overlap between the desired signal and the interference is varied. The signal to noise ratio (SNR) and the signal to interference ratio (SIR) at the input are fixed at 10dB and 0dB respectively. The spectral overlapping is 40%, 30%, 20% and 10% respectively. Two scenarios are examined. In the first case, the DOA difference are fixed at 2°. The output SINR of BLAST, TAST, C-CAB, and SCORE against the different spectral overlapping between the desired signal and the interference are plotted in Fig. 5.10(a) to Fig. 5.10(d). In the second case, the DOA difference are fixed at 10°. The output SINR of BLAST, TAST, C-CAB, and SCORE against the different frequency overlapping between the desired signal and the interference are plotted in Fig. 5.11(a) to Fig. 5.11(d). It can be observed that the output SINR of BLAST and TAST are always better than those of the C-CAB and SCORE algorithms in two cases. When the DOA difference is 2°, the output SINR for SCORE and C-CAB are unacceptably low, and the performance of SCORE and C-CAB do not vary with the change of the spectral overlapping. However, the performance of BLAST and TAST are different. Although the performance of BLAST and TAST is reduced as the spectral overlapping is increased, it can be observed that the output SINR of BLAST and TAST is greater than the that of SCORE and C-CAB. The main reason for the performance difference is that BLAST and TAST exploit not only the spatial information (DOA difference between the desired signal and interference) but also temporal information (spectral redundancy information), whereas SCORE and C-CAB only exploit the spatial information. When the DOA difference is 10°, It can be observed that the output SINR of BLAST and TAST are still better than those of the C-CAB and SCORE algorithms. Although the performances of BLAST and TAST vary with the different frequency overlapping, the performance change in the second scenario is smaller than that in the first scenario.

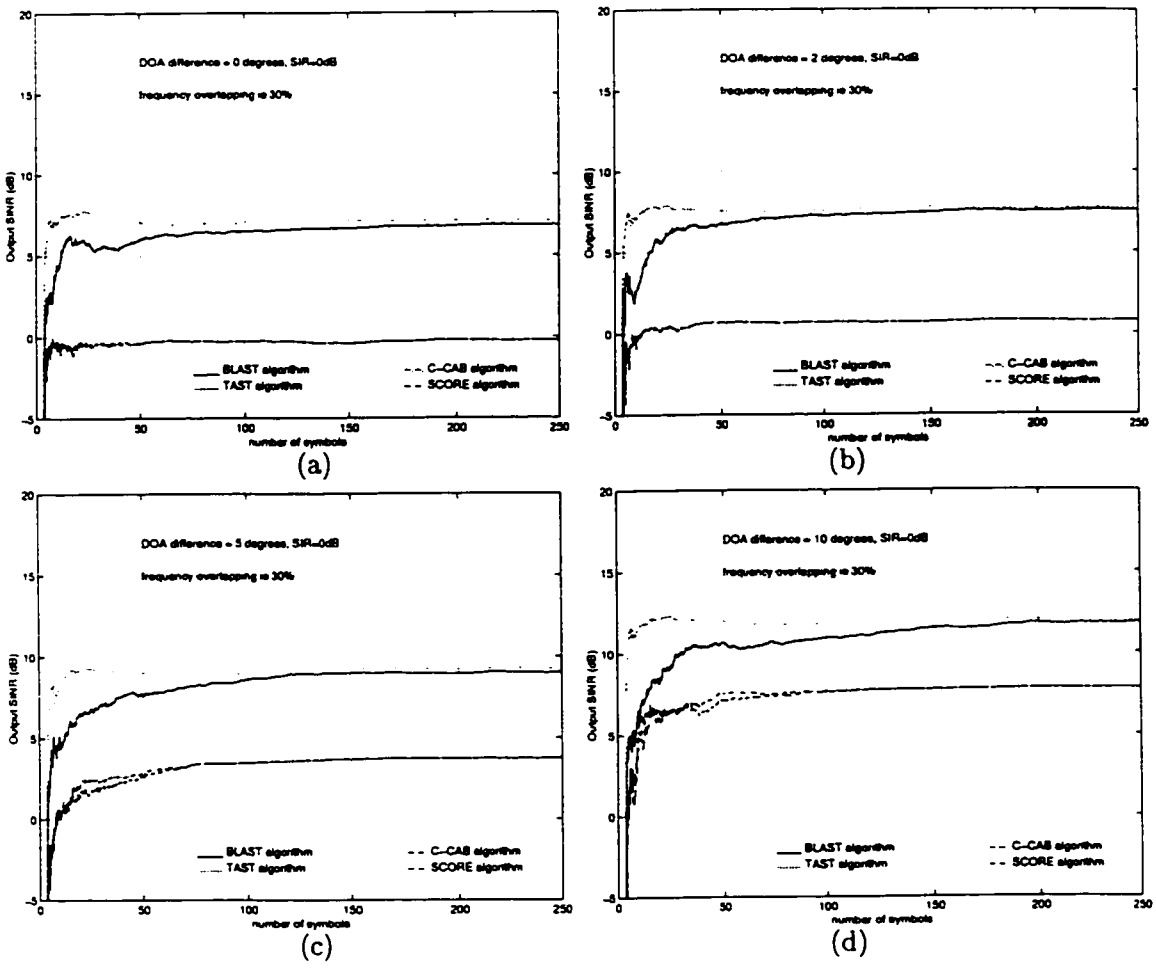

Figure 5.4: Output SINR of BLAST, TAST, C-CAB, and SCORE against DOA difference $0°, 2°, 5°$, and $10°$ when spectral overlapping is 30%, input SIR is 0dB and SNR is 10dB

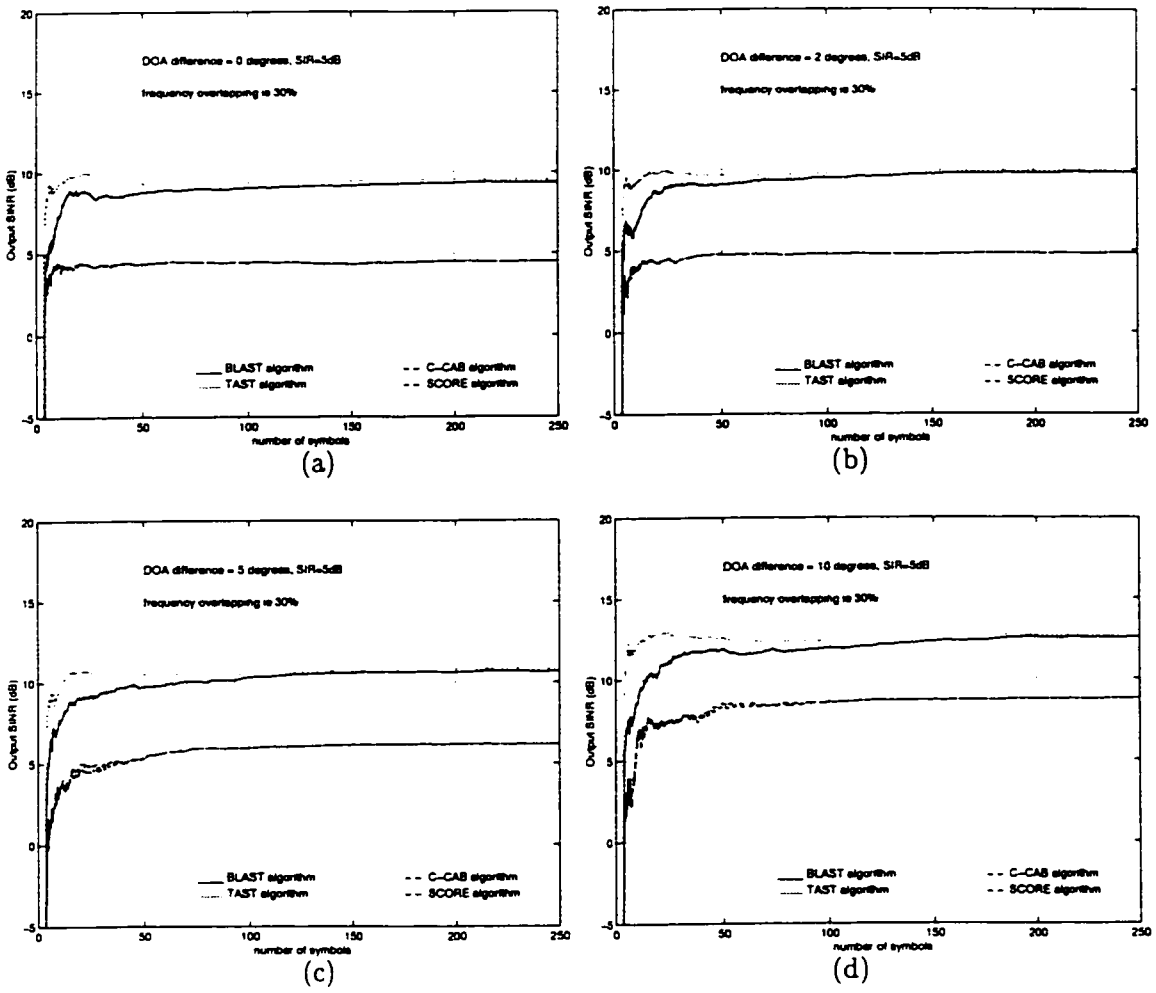

Figure 5.5: Output SINR of BLAST, TAST, C-CAB, and SCORE against DOA difference $0°, 2°, 5°$, and $10°$ when spectral overlapping is 30%, input SIR is 5dB and SNR is 10dB

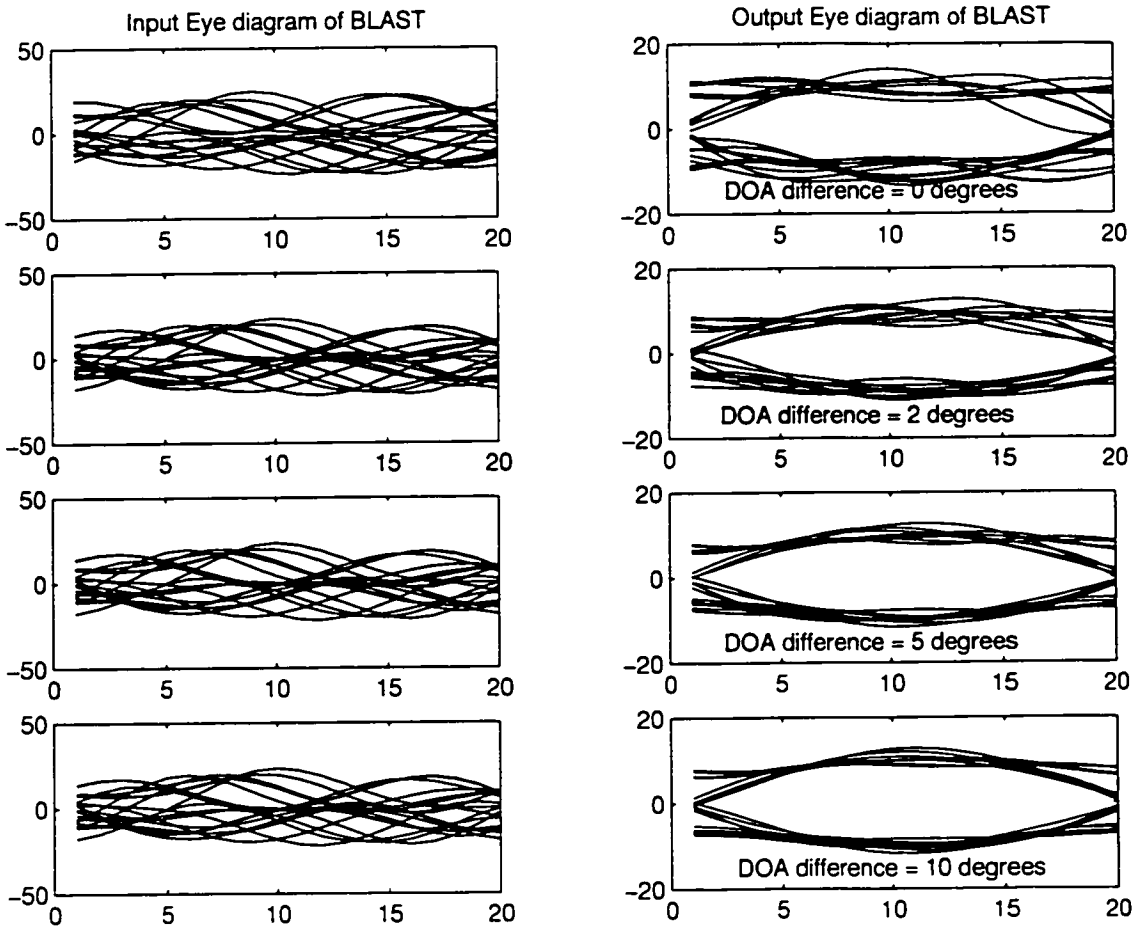

Figure 5.6: Output eye diagrams of BLAST when DOA differences are $0°, 2°, 5°$, and $10°$, input SIR is 0dB, and input SNR is 20dB

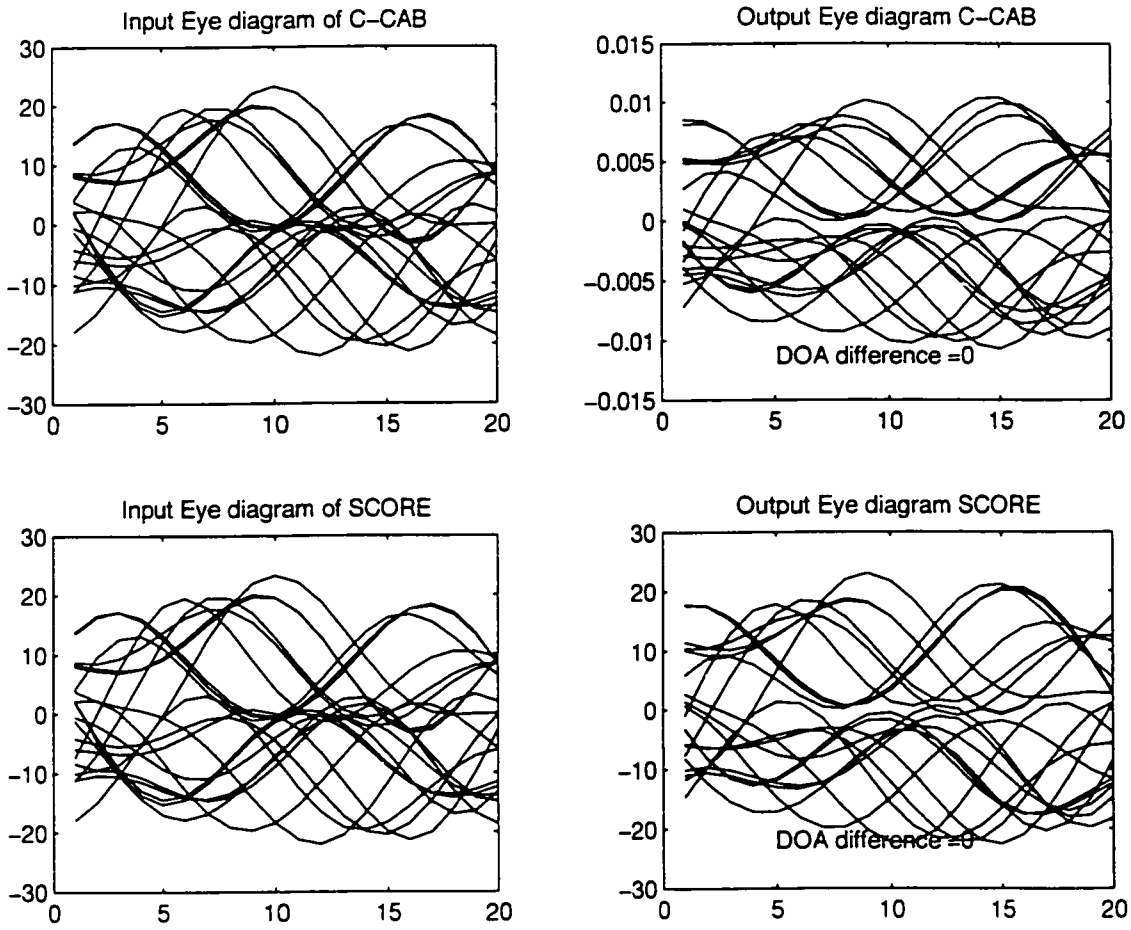

Figure 5.7: Output eye diagrams of C-CAB and SCORE when DOA difference is 0°, input SIR is 0dB, and input SNR is 20dB

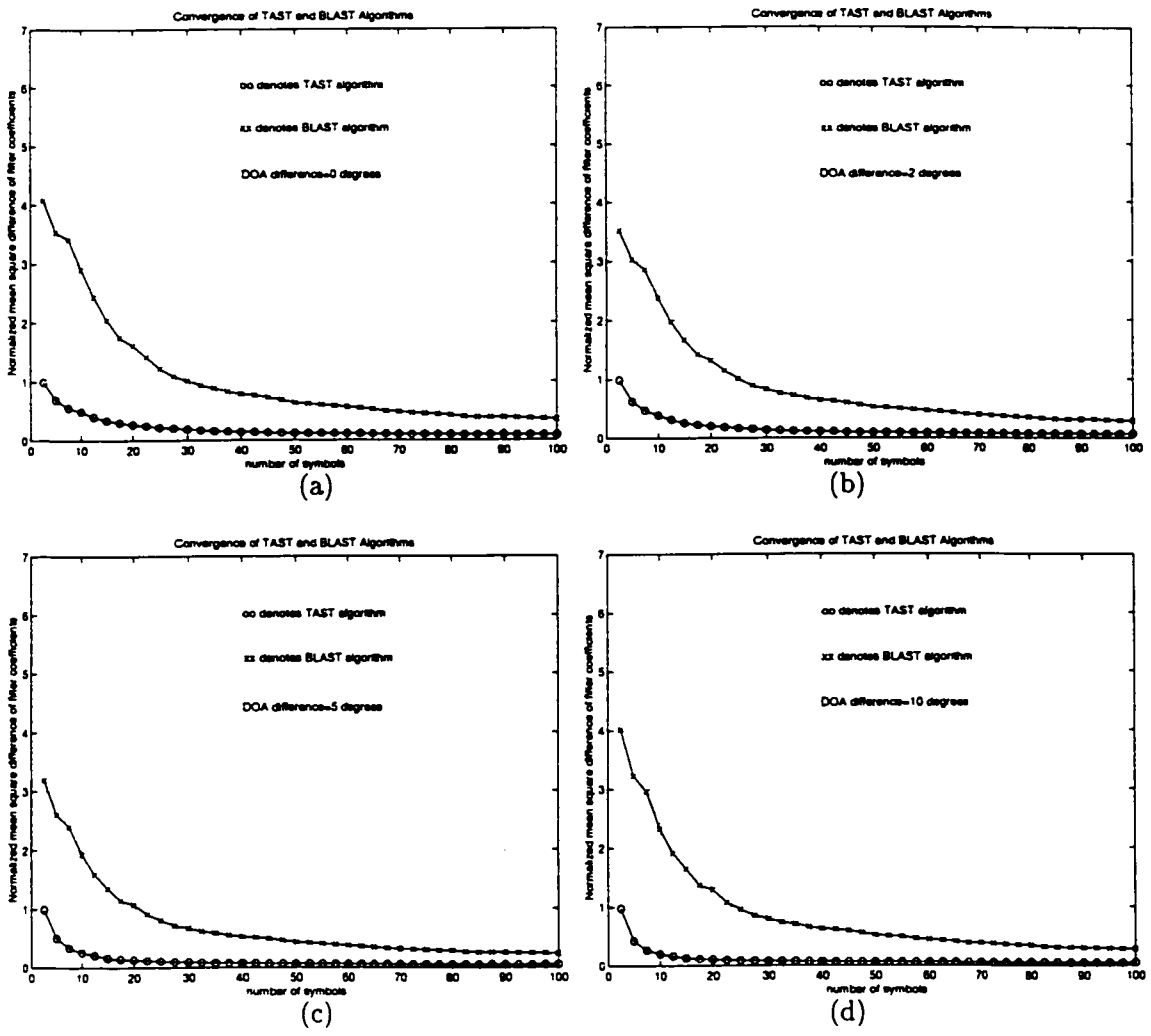

Figure 5.8: Normalized filter coefficient convergence of BLAST and TAST against DOA difference $0°, 2°, 5°$, and $10°$ when input SIR is 0dB, and input SNR is 10dB

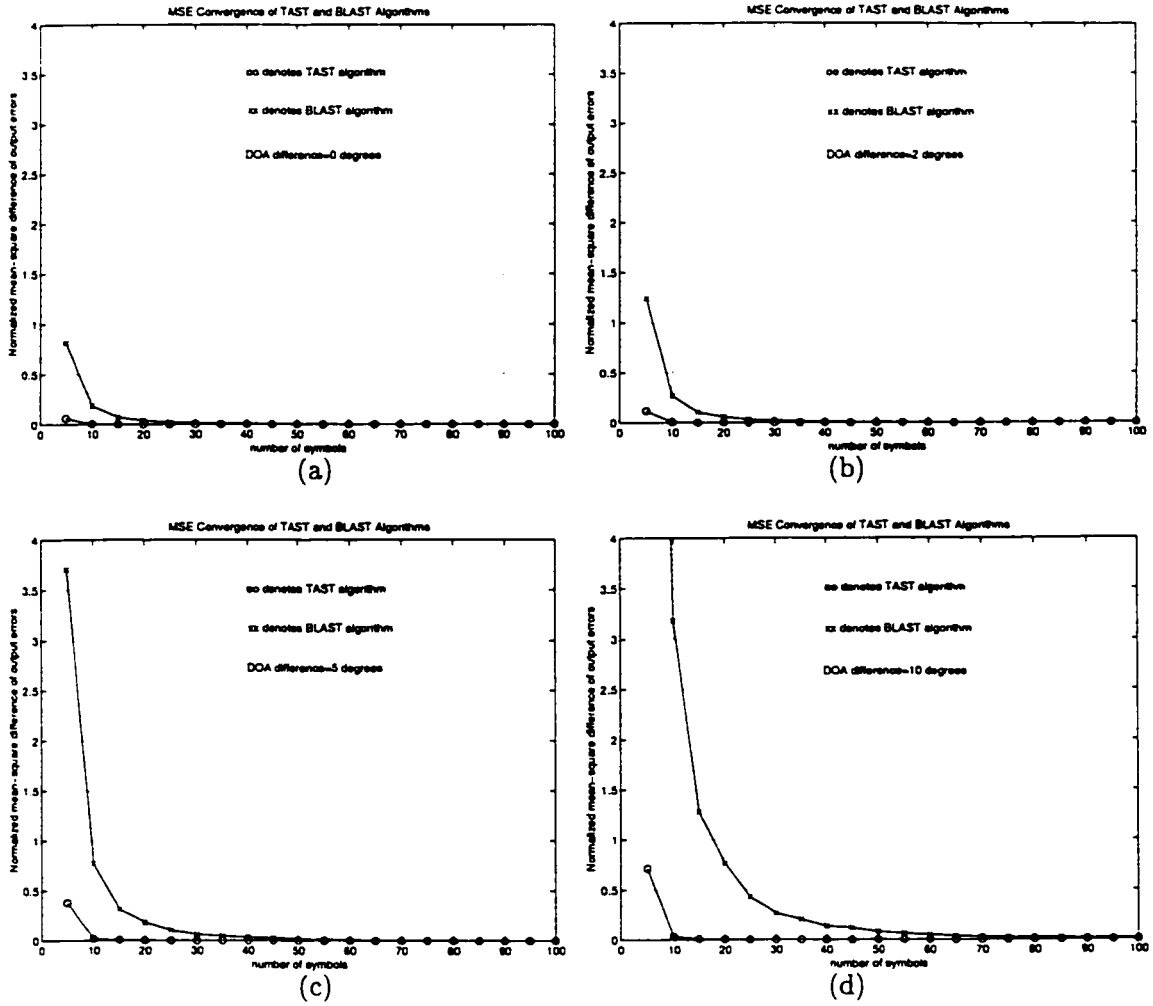

Figure 5.9: Normalized output MSE of BLAST and TAST against DOA difference 0°, 2°, 5°, and 10° when input SIR is 0dB and input SNR is 10dB

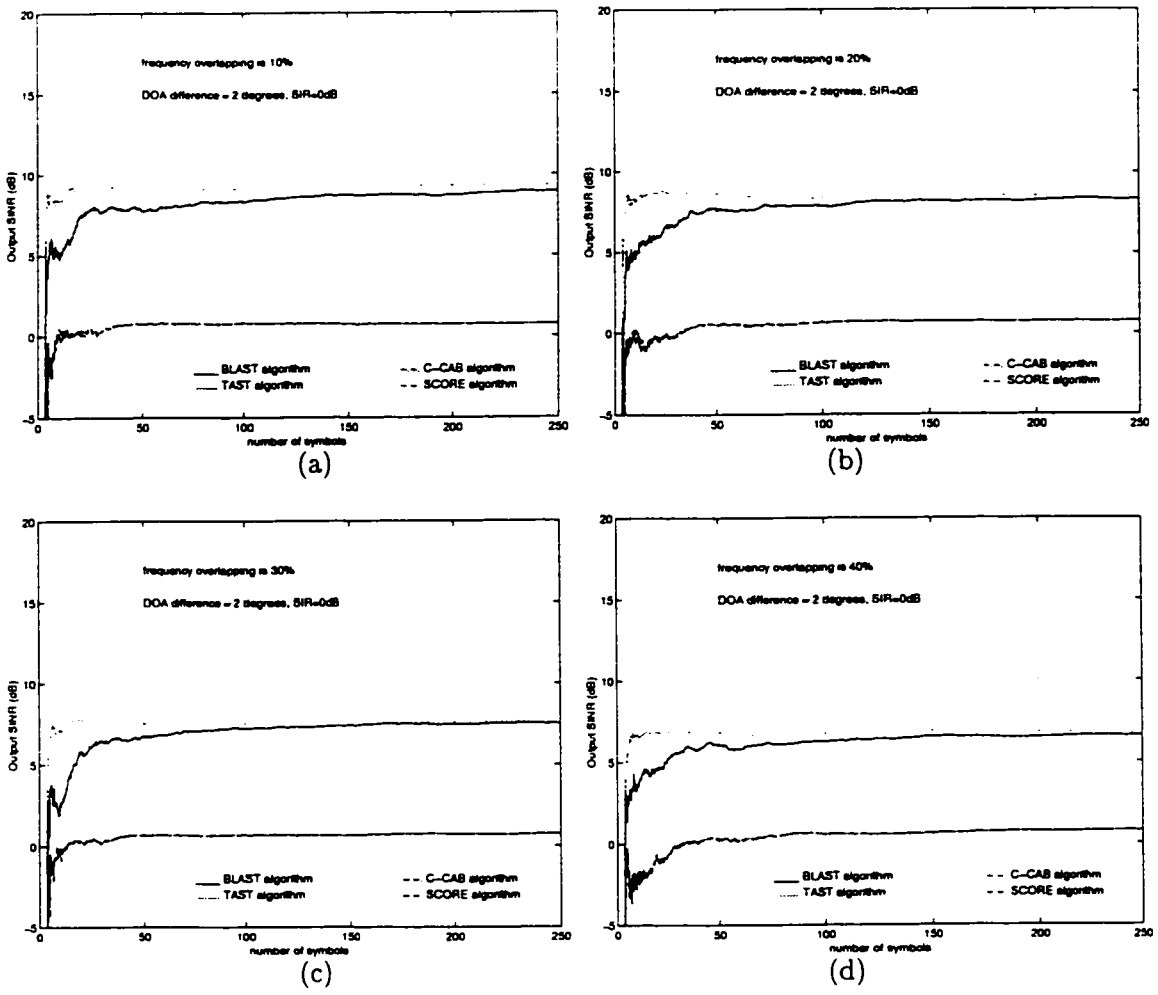

Figure 5.10: Output SINR of BLAST, TAST, C-CAB, and SCORE against different spectral overlapping 40%, 30%, 20%, 10% when input SIR is 0dB, SNR is 10dB, and DOA difference is 2°

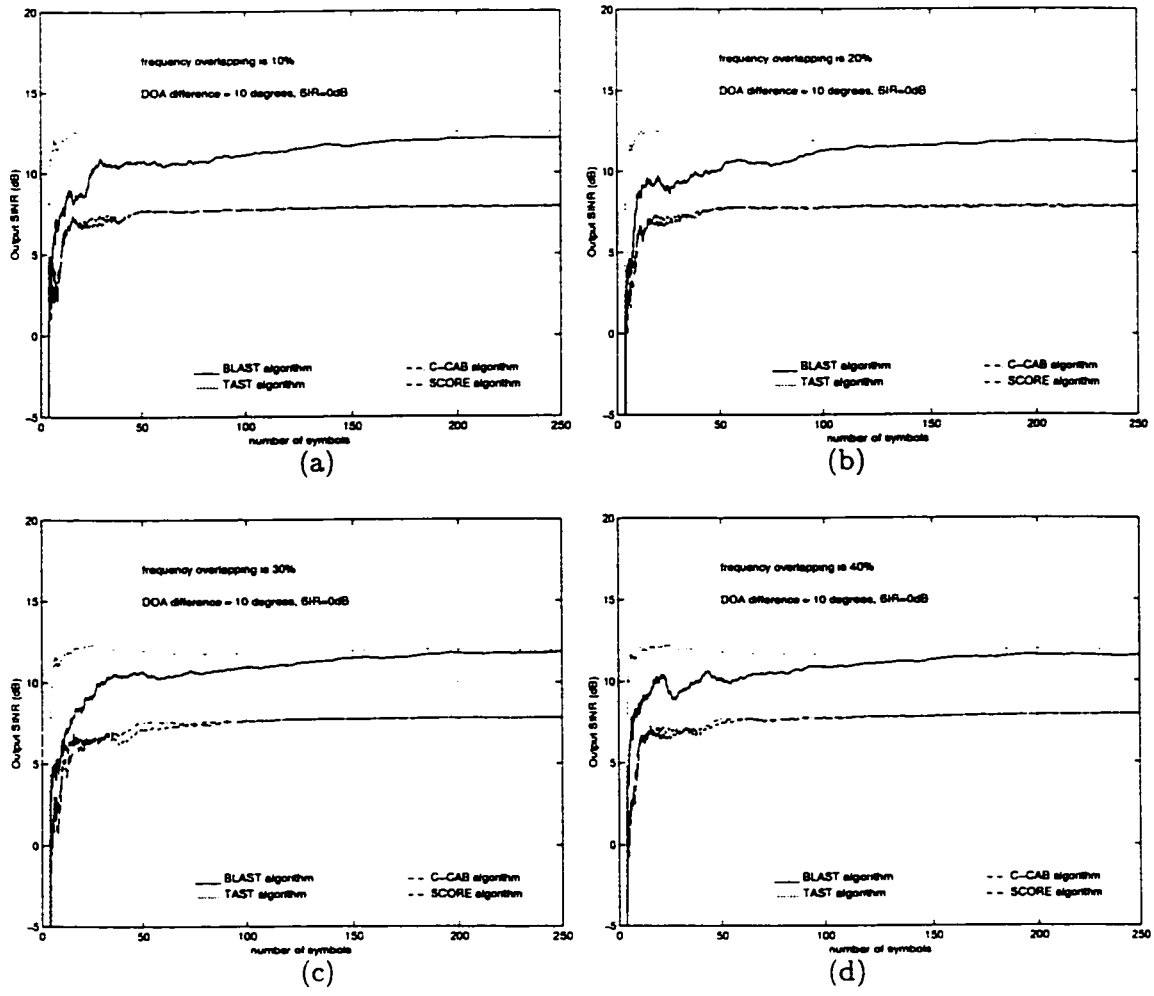

Figure 5.11: Output SINR of BLAST, TAST, C-CAB, and SCORE against different frequency overlapping 40%, 30%, 20%, 10% when input SIR is 0dB, SNR is 10dB, and DOA difference is 10°

Chapter 6

Probability Error Analysis of BLAST and TAST

In Chapter 5, we proposed the BLAST algorithm and analyzed its convergence performance. In this chapter, we continue to analyze the performance of the BLAST algorithm. It is well known that a fundamental performance of a digital system is the output probability error. In this chapter, we'll examine the finite sample output probability error of the BLAST and TAST algorithms theoretically and by simulation. Let N be the length of input data. $\boldsymbol{q}(N)$ is the finite sample time realization of the BLAST or TAST filter coefficient vector. $\boldsymbol{q}(N)$ is a function of N and it is also a random vector for given N. We do K experiments to obtain K realizations of $\boldsymbol{q}(N)$ as $\boldsymbol{q}^{(1)}(N)$, $\boldsymbol{q}^{(2)}(N)$, $\cdots$, $\boldsymbol{q}^{(K)}(N)$. For the kth experiment with given $\boldsymbol{q}^{(k)}(N)$, we can obtain the simulation value of the finite sample probability error $P_{e\_s}^k$. Defining P_{e_s} as $P_{e\_s} = \frac{1}{K}\sum_{k=1}^{K} P_{e\_s}^k$, P_{e_s} is called the simulation value of the finite sample probability error of $\boldsymbol{q}(N)$. We like to obtain theoretical formulae to compute the finite sample probability error of BLAST and TAST. Because the analysis procedures to BLAST and TAST are similar, we use BLAST as an example to do this analysis. Firstly, the input signals and system model are given in this chapter. The input of threshold is analyzed. Statistical analysis of the output noise, statistical analysis of the output component of the desired signal, and statistical analysis of the output interference

are given. The output probability error theoretical formulae of BLAST and TAST are obtained. At last, numerical examples are presented to examine the output probability error of BLAST and TAST in different scenarios theoretically and by simulation.

6.1 The System Model of BLAST and TAST

The system model we considered is shown in Fig. 6.1. Because the analysis procedures to BLAST and TAST are very similar, we use BLAST as an example to do this analysis.

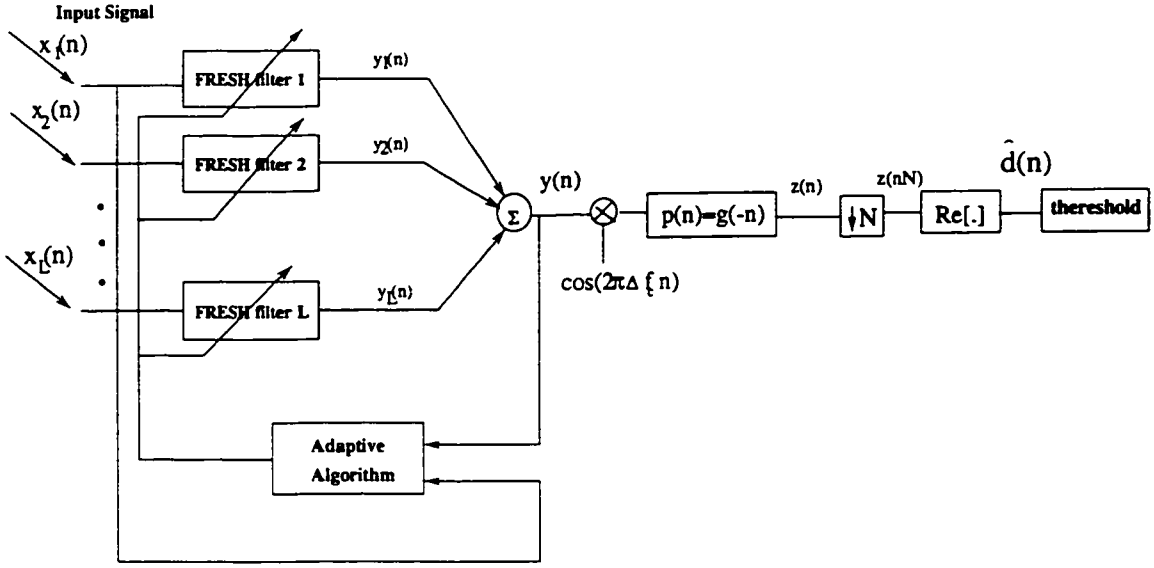

Figure 6.1: System model of BLAST and TAST

Input Signals: For the input signals, we assume that the desired signal source $s(n)$ and interference source $u(n)$ are BPSK signals which have same baud rate. They are statistically independent. Let the sampling rate of these signal is $1/T_s$. For a given baud rate $1/T_b$, we choose the sampling rate such that

$$T_s = T_b/N_s \tag{6.1.1}$$

where N_s is an integer. In the following analysis, we normalize T_s as one in our expressions.

The desired signal $s(n)$ can be modeled as

$$s(n) = \sum_{k=-\infty}^{\infty} d(k)g(n - kN_s)\cos(2\pi\Delta f_c n) \tag{6.1.2}$$

where Δf_c is the frequency offset of the desired signal. The message signal of the desired signal is $d(n)$ where $d(n) = \pm 1$ is a random signal. The signal $d(n) = +1$ and $d(n) = -1$ occur independently with equal probability and therefore, the variance of $d(n)$ is equal to one. The function $g(n)$ is a square root raised cosine pulse shaping filter with a roll-off factor equal to one. We normalize $g(n)$ such that

$$\sum_n g(n)g^*(n) = 1 \tag{6.1.3}$$

where $*$ denotes the conjugate. We use a uniform linear array of sensors for the antenna and define the directional vector of the desired signal as

$$\boldsymbol{d}(\theta_s) = [1 \quad e^{-j2\pi\theta_s} \quad \cdots \quad e^{-j2\pi(L-1)\theta_s}]^T \tag{6.1.4}$$

where L is the number of sensors. θ_s is an angle which is related with incidence angle of the desired signal, ^{T} denotes the transpose. For the received desired signal vector $\boldsymbol{s}(n)$ at the sensor array,

$$\boldsymbol{s}(n) = [s(n) \quad s(n)e^{-j2\pi\theta_s} \quad \cdots \quad s(n)e^{-j2\pi(L-1)\theta_s}]^T = s(n)\boldsymbol{d}(\theta_s). \tag{6.1.5}$$

The desired signal component on the λth sensor is

$$s_\lambda(n) = s(n)e^{-j2\pi(\lambda-1)\theta_s}, \qquad \lambda = 1, 2, \cdots L. \tag{6.1.6}$$

The interference $u(n)$ can be modeled as

$$u(n) = A_u \sum_{k=-\infty}^{\infty} d_u(k)g_u(n - kN_s)\cos(2\pi\Delta f_u n) \tag{6.1.7}$$

where A_u is the amplitude of the interference and Δf_u is the frequency offset of the interfer-

ence. The symbol $d_u(n) = +1$ and $d_u(n) = -1$ occur independently with equal probability and the variance of $d_u(n)$ is one. The function $g_u(n)$ is a normalized square root raised cosine pulse shaping filter with a roll-off factor equal to one. We define the directional vector of the interference as

$$\boldsymbol{d}(\theta_u) = [1 \quad e^{-j2\pi\theta_u} \quad \cdots \quad e^{-j2\pi(L-1)\theta_u}]^T \tag{6.1.8}$$

where θ_u is an angle which is related with incidence angle of the interference. For the received interference vector $\boldsymbol{u}(n)$ at the sensor array,

$$\boldsymbol{u}(n) = [u(n) \quad u(n)e^{-j2\pi\theta_u} \quad \cdots \quad u(n)e^{-j2\pi(L-1)\theta_u}]^T = u(n)\boldsymbol{d}(\theta_u). \tag{6.1.9}$$

The interference component on the λth sensor is

$$u_\lambda(n) = u(n)e^{-j2\pi(\lambda-1)\theta_u}, \qquad \lambda = 1, 2, \cdots L. \tag{6.1.10}$$

The input noise vector $\boldsymbol{v}(n)$ on the sensor array is assumed to be a complex stationary jointly temporally and spatially white zero mean Gaussian noise, it can be written as

$$\boldsymbol{v}(n) = [v_1(n) \quad v_2(n) \quad \cdots \quad v_L(n)]^T \tag{6.1.11}$$

and we have

$$E[v_k(n)] = 0, \qquad k = 1, 2, \cdots L \tag{6.1.12}$$

and

$$E[v_k(n_1)v_m^*(n_2)] = \sigma_v^2\delta(n_1 - n_2)\delta(k - m), \qquad k = 1, 2, \cdots L, \quad m = 1, 2, \cdots L \tag{6.1.13}$$

where σ_v^2 is the variance which is $E[v_k(n)v_k^*(n)]$, $\delta(n)$ is the Kronecker delta function, and $v_k(n)$ is the complex noise on the kth sensor. The real part of $v_k(n)$ and the imaginary part of $v_k(n)$ are also assumed to be uncorrelated. From system design view, we note that noise is white in some systems and the noise is colored in other systems. For colored noise, our

following performance analysis method is still feasible, but the expression will become more tedious. For simply our analysis, we approximate noise being white. Comparing theoretical results with simulation results, theoretical results are very close to the simulation results. Therefore, we say this assumption is feasible.

The input of the BLAST filter is

$$\boldsymbol{x}(n) = \boldsymbol{s}(n) + \boldsymbol{u}(n) + \boldsymbol{v}(n) \tag{6.1.14}$$

where $\boldsymbol{s}(n), \boldsymbol{u}(n)$, and $\boldsymbol{v}(n)$ are defined in Eqs. (6.1.5), (6.1.9), and (6.1.11) respectively.

BLAST algorithm For the BLAST filter, we choose same frequency shifts in each FRESH filter. Because the input signal are BPSK signals, the frequency shift in the FRESH filter $\alpha_i (i = 1, 2, \cdots M)$ can be chosen as $\pm 2\Delta f_c + k/T_b$, where Δf_c is the frequency offset of the desired signal. $1/T_b$ is the baud rate of the desired signal. k is an integer. Here, the frequency offset can be viewed as a design parameter and we choose the frequency offset Δf_c be the multiples of $1/T_b$. Therefore, we have

$$\Delta f_c = N_c/T_b, \qquad \alpha_i = N_l/T_b, \quad i = 1, 2, \cdots M \tag{6.1.15}$$

where N_c and N_l are integers, $N_l = \pm 2N_c + k$. Moreover, we choose the low pass filter $p(n)$ as the normalized square root raised cosine pulse shaping filter $g(-n)$.

The filter coefficient $h_{\lambda,m}(n)$ $(\lambda = 1, 2, \cdots L, m = 1, 2, \cdots M)$ denotes the impulse response of the mth FIR filter in the lth FRESH filter, where M and L are the number of the branch of the FRESH filter and the number of sensors respectively. These filter coefficients consist of the filter coefficient vector of the BLAST filter $\boldsymbol{q}_{BST}$ which is defined in Eq. (5.3.3). For the infinite sample time average realization of $\boldsymbol{q}_{BST}$, $\boldsymbol{q}_{BST}$ is the constant vector $\boldsymbol{q}_{opt}$ which is defined in Eq. (5.3.11). For the finite sample time average realization of $\boldsymbol{q}_{BST}$, $\boldsymbol{q}_{BST}$ is the random vector $\hat{\boldsymbol{q}}_{BST}(N)$ which is defined in Eq. (5.4.2). $\hat{\boldsymbol{q}}_{BST}(N)$ is the function of N, where N is the data length. We don't know the joint probability density function of $\hat{\boldsymbol{q}}_{BST}(N)$. In order to simplify our analysis, we will assume that the filter coefficient vector $\boldsymbol{q}_{BST}$ is uncorrelated with the input white noise $\nu(n)$, the input desired

binary signal $d(n)$ and the input interfering binary signals $d_u(n)$. We call this assumption as the uncorrelation assumption. For the infinite sample time average realization, using the property 5.1, we note that the filter coefficient vector of the BLAST filter $\boldsymbol{q}_{BST}$ is a constant vector $\boldsymbol{q}_{opt}$. Therefore, the uncorrelation assumption is valid in the infinite sample case. For the finite sample time average realization, the filter coefficient vector $\hat{\boldsymbol{q}}_{BST}(N)$ is a random vector. Because we do not know the joint probability density function of $\hat{\boldsymbol{q}}_{BST}(N)$, it is difficult to examine the uncorrelation assumption theoretically in the finite sample case. Here, we use an experimental method to examine the assumption. We generate K random samples of the correlation $\boldsymbol{g}_k(N) = a_k(N)\boldsymbol{q}_k(N)$, where $a_k(N)$ denotes kth experiment input binary signal or the input white noise. $\boldsymbol{q}_k(N)$ denotes the kth experiment finite sample time average realization of the filter coefficient vector $\hat{\boldsymbol{q}}_{BST}(N)$. We calculate the normalized correlation value $\bar{g} = \|\frac{1}{K}\sum_k \boldsymbol{g}_k(N)\|^2 / \frac{1}{K}\sum_k \|\boldsymbol{g}_k(N)\|^2$. We found these correlation values are very small, see Appendix B. Therefore, we say the uncorrelation assumption is valid in the finite sample case.

6.2 The Input of Threshold

When the input signal $\boldsymbol{x}(n)$ passes through the BLAST filter, the output of the λth FRESH filter is

$$y_\lambda(n) = \sum_{l=1}^{J}\sum_k h_{\lambda,l}(k)e^{j2\pi\alpha_l(n-k)}x_\lambda(n-k) + \sum_{l=J+1}^{M}\sum_k h_{\lambda,l}(k)e^{j2\pi\alpha_l(n-k)}x_\lambda^*(n-k) \quad (6.2.1)$$

where $\lambda = 1, 2, \cdots L$. $h_{\lambda,l}(n)$ is the impulse response of the lth FIR filter of the λth FRESH filters. α_l is the frequency shift of the lth branch of the λth FRESH filter. Each FRESH filter is divided into two parts: the FRESH filtering part and the conjugate FRESH filtering part. J is the number of FIR filters in the FRESH filtering part. $M - J$ is the number of FIR filters in conjugate FRESH filtering part. $x_\lambda(n)$ is the received signal on the λth

sensor. The output of the BLAST filter is

$$y(n) = \sum_{\lambda=1}^{L}\sum_{l=1}^{J}\sum_{k} h_{\lambda l}(k)e^{j2\pi\alpha_l(n-k)}x_\lambda(n-k) + \sum_{\lambda=1}^{L}\sum_{l=J+1}^{M}\sum_{k} h_{\lambda l}(k)e^{j2\pi\alpha_l(n-k)}x_\lambda^*(n-k). \tag{6.2.2}$$

The output of the low pass filter is

$$\begin{aligned} z(n) &= \sum_k p(k)\cos(2\pi\Delta f_c(n-k))y(n-k) \qquad (6.2.3)\\ &= \sum_{\lambda=1}^{L}\sum_{l=1}^{J}\sum_{k_1}\sum_{k_2} p(k_1)\cos(2\pi\Delta f_c(n-k_1))h_{\lambda l}(k_2)e^{j2\pi\alpha_l(n-k_1-k_2)}x_\lambda(n-k_1-k_2)\\ &+ \sum_{\lambda=1}^{L}\sum_{l=J+1}^{M}\sum_{k_1}\sum_{k_2} p(k_1)\cos(2\pi\Delta f_c(n-k_1))h_{\lambda l}(k_2)e^{j2\pi\alpha_l(n-k_1-k_2)}x_\lambda^*(n-k_1-k_2). \end{aligned}$$

Using Eq. (6.1.15), we note that $e^{j2\pi\Delta f_c nN_s} = 1$ and $e^{j2\pi\alpha_l nN_s} = 1$. The output of the sampler $z(nN_s)$ is

$$\begin{aligned} z(nN_s) &= \sum_{\lambda=1}^{L}\sum_{l=1}^{J}\sum_{k_1}\sum_{k_2} p(k_1) \qquad (6.2.4)\\ &\quad \cos(2\pi\Delta f_c k_1)h_{\lambda l}(k_2)e^{-j2\pi\alpha_l(k_1+k_2)}x_\lambda(nN_s-k_1-k_2)\\ &\quad + \sum_{\lambda=1}^{L}\sum_{l=J+1}^{M}\sum_{k_1}\sum_{k_2} p(k_1)\cos(2\pi\Delta f_c k_1)h_{\lambda l}(k_2)e^{-j2\pi\alpha_l(k_1+k_2)}x_\lambda^*(nN_s-k_1-k_2). \end{aligned}$$

Let $k_1 + k_2 = k$ and $k_1 = m$, we obtain

$$\begin{aligned} z(nN_s) &= \sum_{\lambda=1}^{L}\sum_{l=1}^{J}\sum_{m}\sum_{k} p(m)\cos(2\pi\Delta f_c m)h_{\lambda l}(k-m)e^{-j2\pi\alpha_l k}x_\lambda(nN_s-k) \qquad (6.2.5)\\ &+ \sum_{\lambda=1}^{L}\sum_{l=J+1}^{M}\sum_{m}\sum_{\lambda} p(m)\cos(2\pi\Delta f_c m)h_{\lambda l}(k-m)e^{-j2\pi\alpha_l k}x_\lambda^*(nN_s-k)\\ &= \sum_{\lambda}\sum_{k} H_\lambda(k)x_\lambda(nN_s-k) + \sum_{\lambda}\sum_{k} G_\lambda(k)x_\lambda^*(nN_s-k) \end{aligned}$$

where we define $H_\lambda(n)$ and $G_\lambda(n)$ as

$$H_\lambda(n) = \sum_{l=1}^{J}\sum_{m=0}^{L_2-1} h_{\lambda l}(n-m)e^{-j2\pi\alpha_l(n-m)}p(m)e^{-j2\pi\alpha_l m}\cos 2\pi\Delta f_c m \tag{6.2.6}$$

$$G_\lambda(n) = \sum_{l=J+1}^{M} \sum_{m=0}^{L_2-1} h_{\lambda l}(n-m) e^{-j2\pi\alpha_l(n-m)} p(m) e^{-j2\pi\alpha_l m} \cos 2\pi\Delta f_c m \quad (6.2.7)$$

where $\lambda = 1, 2, \cdots L$. We note that the length of $H_\lambda(n)$ is equal to the length of $G_\lambda(n)$. The length is $N_o + L_2 - 1$. N_o is the length of the filter $h_{\lambda l}(n)$. Here, we assume $h_{\lambda l}(n)$, $(\lambda = 1, 2, \cdots L, \quad l = 1, 2, \cdots M)$ has same length. L_2 is the length of the filter $p(n)$, which is equal to the length of the filter $g(n)$.

Substituting Eq. (6.1.14) into Eq. (6.2.5), we may express the output of the sampler as

$$\begin{aligned} z(nN_s) = & \sum_{\lambda=1}^{L} \sum_{k=1}^{N_o+L_2-1} [H_\lambda(k) s_\lambda(nN_s - k) + G_\lambda(k) s_\lambda^*(nN_s - k)] \\ & + \sum_{\lambda=1}^{L} \sum_{k=1}^{N_o+L_2-1} [H_\lambda(k) u_\lambda(nN_s - k) + G_\lambda(k) u_\lambda^*(nN_s - k)] \\ & + \sum_{\lambda=1}^{L} \sum_{k=1}^{N_o+L_2-1} [H_\lambda(k) v_\lambda(nN_s - k) + G_\lambda(k) v_\lambda^*(nN_s - k)] . \end{aligned} \quad (6.2.8)$$

We divide $H_\lambda(n)$ and $G_\lambda(n)$ into real part and imaginary parts

$$H_\lambda(n) = H_{R_\lambda}(n) + jH_{I_\lambda}(n) \quad (6.2.9)$$

$$G_\lambda(n) = G_{R_\lambda}(n) + jG_{I_\lambda}(n) \quad (6.2.10)$$

where $H_{R_\lambda}(n)$ and $G_{R_\lambda}(n)$ are the real part of $H_\lambda(n)$ and $G_\lambda(n)$ respectively. $H_{I_\lambda}(n)$ and $G_{I_\lambda}(n)$ are the imaginary part of $H_\lambda(n)$ and $G_\lambda(n)$ respectively. Moreover, $H_{R_\lambda}(n)$ is

$$H_{R_\lambda}(n) = \sum_{l=1}^{J} \sum_{m=0}^{L_2-1} \text{Re}\left[h_{\lambda l}(n-m) e^{-j2\pi\alpha_l(n-m)} p(m) e^{-j2\pi\alpha_l m}\right] \cos 2\pi\Delta f_c m \quad (6.2.11)$$

where Re [.] denotes taking the real part. $H_{I_\lambda}(n)$ is

$$H_{I_\lambda}(n) = \sum_{l=1}^{J} \sum_{m=0}^{L_2-1} \text{Im}\left[h_{\lambda l}(n-m) e^{-j2\pi\alpha_l(n-m)} p(m) e^{-j2\pi\alpha_l m}\right] \cos 2\pi\Delta f_c m \quad (6.2.12)$$

where Im [.] denotes taking the imaginary part. $G_{R_\lambda}(n)$ is

$$G_{R_\lambda}(n) = \sum_{l=J+1}^{M} \sum_{m=0}^{L_2-1} \operatorname{Re}\left[h_{\lambda l}(n-m)e^{-j2\pi\alpha_l(n-m)}p(m)e^{-j2\pi\alpha_l m}\right]\cos 2\pi\Delta f_c m \tag{6.2.13}$$

$G_{I_\lambda}(n)$ is

$$G_{I_\lambda}(n) = \sum_{l=J+1}^{M} \sum_{m=0}^{L_2-1} \operatorname{Im}\left[h_{\lambda l}(n-m)e^{-j2\pi\alpha_l(n-m)}p(m)e^{-j2\pi\alpha_l m}\right]\cos 2\pi\Delta f_c m. \tag{6.2.14}$$

The input to the threshold is

$$\begin{aligned}\hat{d}(n) = {} & \operatorname{Re}\left[\sum_{\lambda=1}^{L}\sum_{k=1}^{N_o+L_2-1}[H_\lambda(k)s_\lambda(nN_s-k)+G_\lambda(k)s_\lambda^*(nN_s-k)]\right] \\ & +\operatorname{Re}\left[\sum_{\lambda=1}^{L}\sum_{k=1}^{N_o+L_2-1}[H_\lambda(k)u_\lambda(nN_s-k)+G_\lambda(k)u_\lambda^*(nN_s-k)]\right] \\ & +\operatorname{Re}\left[\sum_{\lambda=1}^{L}\sum_{k=1}^{N_o+L_2-1}[H_\lambda(k)v_\lambda(nN_s-k)+G_\lambda(k)v_\lambda^*(nN_s-k)]\right].\end{aligned} \tag{6.2.15}$$

Defining

$$\gamma_o d(n)+\xi_{ISI}(n) = \operatorname{Re}\left[\sum_{\lambda=1}^{L}\sum_{k=1}^{N_o+L_2-1}[H_\lambda(k)s_\lambda(nN_s-k)+G_\lambda(k)s_\lambda^*(nN_s-k)]\right] \tag{6.2.16}$$

$$\xi_{CTI}(n) = \operatorname{Re}\left[\sum_{\lambda=1}^{L}\sum_{k=1}^{N_o+L_2-1}[H_\lambda(k)u_\lambda(nN_s-k)+G_\lambda(k)u_\lambda^*(nN_s-k)]\right] \tag{6.2.17}$$

$$\eta(n) = \operatorname{Re}\left[\sum_{\lambda=1}^{L}\sum_{k=1}^{N_o+L_2-1}[H_\lambda(k)v_\lambda(nN_s-k)+G_\lambda(k)v_\lambda^*(nN_s-k)]\right], \tag{6.2.18}$$

we have

$$\hat{d}(n) = \gamma_o d(n)+\xi_{ISI}(n)+\xi_{CTI}(n)+\eta(n) \tag{6.2.19}$$

where $\gamma_o d(n)$ denotes the output component of the desired symbol. $\xi_{ISI}(n)$ denotes the

output Inter-Symbol Interference (ISI) component. $\xi_{CTI}(n)$ denotes the output Cross-Talk Interference (CTI) component. $\eta(n)$ denotes the output component of the noise. Defining

$$\eta_e(n) = \eta(n) + \xi_{ISI}(n) + \xi_{CTI}(n), \tag{6.2.20}$$

we have that the input to the threshold is

$$\hat{d}(n) = \gamma_o d(n) + \eta_e(n) \tag{6.2.21}$$

where γ_o is the coefficient of the desired symbol. η_e is sum of the output noise component, the output ISI component and the output CTI component.

6.3 Statistical Analysis of $\eta(n)$

The output noise component $\eta(n)$ is

$$\begin{aligned}\eta(n) &= \mathrm{Re}\left[\sum_{\lambda=1}^{L}\sum_{k=1}^{N_o+L_2-1}[H_\lambda(k)v_\lambda(nN_s-k)+G_\lambda(k)v_\lambda^*(nN_s-k)]\right] \\ &= \sum_{\lambda=1}^{L}\sum_{k=1}^{N_o+L_2-1}[H_{R_\lambda}(k)v_{R_\lambda}(nN_s-k)-H_{I_\lambda}(k)v_{I_\lambda}(nN_s-k)] \\ &\quad +\sum_{\lambda=1}^{L}\sum_{k=1}^{N_o+L_2-1}[G_{R_\lambda}(k)v_{R_\lambda}(nN_s-k)+G_{I_\lambda}(k)v_{I_\lambda}(nN_s-k)]\end{aligned} \tag{6.3.1}$$

where $v_\lambda(n)$ is the noise on the λth sensor. $v_{R_\lambda}(n)$ and $v_{I_\lambda}(n)$ are the real and the imaginary part of $v_\lambda(n)$ respectively.

Using the uncorrelation assumption and noting that the input noise has zero mean, the mean of the output noise $\eta(n)$ is

$$E[\eta(n)] = \mathrm{Re}\left[\sum_{\lambda=1}^{L}\sum_{k=1}^{N_o+L_2-1}[E[H_\lambda(k)]E[v_\lambda(nN_s-k)]+E[G_\lambda(k)]E[v_\lambda^*(nN_s-k)]]\right] = 0. \tag{6.3.2}$$

Using Eq. (6.1.13) and noting $v_{R_\lambda}(n)$ and $v_{I_\lambda}(n)$ are uncorrelated, the variance of the

output noise $\eta(n)$ is

$$\begin{aligned}\sigma_\eta^2 &= E[\eta(n)\eta^*(n)] \qquad (6.3.3)\\ &= \sum_\lambda \sum_k E\left[H_{R_\lambda}(k)H_{R_\lambda}(k) + H_{R_\lambda}(k)G_{R_\lambda}(k) + G_{R_\lambda}(k)H_{R_\lambda}(k) + G_{R_\lambda}(k)G_{R_\lambda}(k)\right]\sigma_{Rv}^2\\ &\quad + \sum_\lambda \sum_k E\left[H_{I_\lambda}(k)H_{I_\lambda}(k) - H_{I_\lambda}(k)G_{I_\lambda}(k) - G_{I_\lambda}(k)H_{I_\lambda}(k) + G_{I_\lambda}(k)G_{I_\lambda}(k)\right]\sigma_{Iv}^2\end{aligned}$$

where σ_{Rv}^2 is the variance of the input noise $v_{R_\lambda}(n)$ and σ_{Iv}^2 is the variance of the input noise $v_{I_\lambda}(n)$. We note that $H_{R_\lambda}(k)$, $H_{I_\lambda}(k)$, $G_{R_\lambda}(k)$ and $G_{I_\lambda}(k)$ are defined in Eqs. (6.2.11) to (6.2.14), respectively. σ_{Rv}^2 and σ_{Iv}^2 are constants. Substituting Eqs. (6.2.11) to (6.2.14) into Eq. (6.3.3), we obtain

$$\begin{aligned}\sigma_\eta^2 &= \sigma_{Rv}^2 \sum_{\lambda=1}^{L}\sum_{k=1}^{N_o+L_2-1}\sum_{l_1=1}^{J}\sum_{m_1=0}^{L_2-1}\sum_{l_2=1}^{J}\sum_{m_2=0}^{L_2-1} \qquad (6.3.4)\\ &\quad E\left[\mathrm{Re}\left[h_{\lambda l_1}(k-m_1)e^{-j2\pi\alpha_{l_1}(k-m_1)}p(m_1)e^{-j2\pi\alpha_{l_1}m_1}\right]\right.\\ &\quad \left.\mathrm{Re}\left[h_{\lambda l_2}(k-m_2)e^{-j2\pi\alpha_{l_2}(k-m_2)}p(m_2)e^{-j2\pi\alpha_{l_2}m_2}\right]\cos(2\pi\Delta f_c m_1)\cos(2\pi\Delta f_c m_2)\right]\\ &\quad +\sigma_{Rv}^2 \sum_{\lambda=1}^{L}\sum_{k=1}^{N_o+L_2-1}\sum_{l_1=1}^{J}\sum_{m_1=0}^{L_2-1}\sum_{l_2=J+1}^{M}\sum_{m_2=0}^{L_2-1}\\ &\quad E\left[\mathrm{Re}\left[h_{\lambda l_1}(k-m_1)e^{-j2\pi\alpha_{l_1}(k-m_1)}p(m_1)e^{-j2\pi\alpha_{l_1}m_1}\right]\right.\\ &\quad \left.\mathrm{Re}\left[h_{\lambda l_2}(k-m_2)e^{-j2\pi\alpha_{l_2}(k-m_2)}p(m_2)e^{-j2\pi\alpha_{l_2}m_2}\right]\cos(2\pi\Delta f_c m_1)\cos(2\pi\Delta f_c m_2)\right]\\ &\quad +\sigma_{Rv}^2 \sum_{\lambda=1}^{L}\sum_{k=1}^{N_o+L_2-1}\sum_{l_1=J+1}^{M}\sum_{m_1=0}^{L_2-1}\sum_{l_2=1}^{J}\sum_{m_2=0}^{L_2-1}\\ &\quad E\left[\mathrm{Re}\left[h_{\lambda l_1}(k-m_1)e^{-j2\pi\alpha_{l_1}(k-m_1)}p(m_1)e^{-j2\pi\alpha_{l_1}m_1}\right]\right.\\ &\quad \left.\mathrm{Re}\left[h_{\lambda l_2}(k-m_2)e^{-j2\pi\alpha_{l_2}(k-m_2)}p(m_2)e^{-j2\pi\alpha_{l_2}m_2}\right]\cos(2\pi\Delta f_c m_1)\cos(2\pi\Delta f_c m_2)\right]\\ &\quad +\sigma_{Rv}^2 \sum_{\lambda=1}^{L}\sum_{k=1}^{N_o+L_2-1}\sum_{l_1=J+1}^{M}\sum_{m_1=0}^{L_2-1}\sum_{l_2=J+1}^{M}\sum_{m_2=0}^{L_2-1}\\ &\quad E\left[\mathrm{Re}\left[h_{\lambda l_1}(k-m_1)e^{-j2\pi\alpha_{l_1}(k-m_1)}p(m_1)e^{-j2\pi\alpha_{l_1}m_1}\right]\right.\\ &\quad \left.\mathrm{Re}\left[h_{\lambda l_2}(k-m_2)e^{-j2\pi\alpha_{l_2}(k-m_2)}p(m_2)e^{-j2\pi\alpha_{l_2}m_2}\right]\cos(2\pi\Delta f_c m_1)\cos(2\pi\Delta f_c m_2)\right]\\ &\quad +\sigma_{Iv}^2 \sum_{\lambda=1}^{L}\sum_{k=1}^{N_o+L_2-1}\sum_{l_1=1}^{J}\sum_{m_1=0}^{L_2-1}\sum_{l_2=1}^{J}\sum_{m_2=0}^{L_2-1}\\ &\quad E\left[\mathrm{Im}\left[h_{\lambda l_1}(k-m_1)e^{-j2\pi\alpha_{l_1}(k-m_1)}p(m_1)e^{-j2\pi\alpha_{l_1}m_1}\right]\right.\end{aligned}$$

$$\mathrm{Im}\left[h_{\lambda l_2}(k-m_2)e^{-j2\pi\alpha_{l_2}(k-m_2)}p(m_2)e^{-j2\pi\alpha_{l_2}m_2}\right]\cos(2\pi\Delta f_c m_1)\cos(2\pi\Delta f_c m_2)\Big]$$
$$-\sigma_{Iv}^2\sum_{\lambda=1}^{L}\sum_{k=1}^{N_o+L_2-1}\sum_{l_1=1}^{J}\sum_{m_1=0}^{L_2-1}\sum_{l_2=J+1}^{M}\sum_{m_2=0}^{L_2-1}$$
$$E\left[\mathrm{Im}\left[h_{\lambda l_1}(k-m_1)e^{-j2\pi\alpha_{l_1}(k-m_1)}p(m_1)e^{-j2\pi\alpha_{l_1}m_1}\right]\right.$$
$$\mathrm{Im}\left[h_{\lambda l_2}(k-m_2)e^{-j2\pi\alpha_{l_2}(k-m_2)}p(m_2)e^{-j2\pi\alpha_{l_2}m_2}\right]\cos(2\pi\Delta f_c m_1)\cos(2\pi\Delta f_c m_2)\Big]$$
$$-\sigma_{Iv}^2\sum_{\lambda=1}^{L}\sum_{k=1}^{N_o+L_2-1}\sum_{l_1=J+1}^{M}\sum_{m_1=0}^{L_2-1}\sum_{l_2=1}^{J}\sum_{m_2=0}^{L_2-1}$$
$$E\left[\mathrm{Im}\left[h_{\lambda l_1}(k-m_1)e^{-j2\pi\alpha_{l_1}(k-m_1)}p(m_1)e^{-j2\pi\alpha_{l_1}m_1}\right]\right.$$
$$\mathrm{Im}\left[h_{\lambda l_2}(k-m_2)e^{-j2\pi\alpha_{l_2}(k-m_2)}p(m_2)e^{-j2\pi\alpha_{l_2}m_2}\right]\cos(2\pi\Delta f_c m_1)\cos(2\pi\Delta f_c m_2)\Big]$$
$$+\sigma_{Iv}^2\sum_{\lambda=1}^{L}\sum_{k=1}^{N_o+L_2-1}\sum_{l_1=J+1}^{M}\sum_{m_1=0}^{L_2-1}\sum_{l_2=J+1}^{M}\sum_{m_2=0}^{L_2-1}$$
$$E\left[\mathrm{Im}\left[h_{\lambda l_1}(k-m_1)e^{-j2\pi\alpha_{l_1}(k-m_1)}p(m_1)e^{-j2\pi\alpha_{l_1}m_1}\right]\right.$$
$$\mathrm{Im}\left[h_{\lambda l_2}(k-m_2)e^{-j2\pi\alpha_{l_2}(k-m_2)}p(m_2)e^{-j2\pi\alpha_{l_2}m_2}\right]\cos(2\pi\Delta f_c m_1)\cos(2\pi\Delta f_c m_2)\Big].$$

6.4 Statistical Analysis of the Output Component of the Desired Signal

When the input desired signal $s(n)$ pass through the system, the input of the threshold is

$$\gamma_o d(n)+\xi_{ISI}(n) \;=\; \mathrm{Re}\left[\sum_{\lambda=1}^{L}\sum_{k}\left[H_\lambda(k)s_\lambda(nN_s-k)+G_\lambda(k)s_\lambda^*(nN_s-k)\right]\right] \quad (6.4.1)$$

where $s_\lambda(n)$, $H_\lambda(n)$, and $G_\lambda(n)$ are defined in Eqs. (6.1.6), (6.2.6), and (6.2.7), respectively. Substituting Eqs. (6.1.2) and (6.1.6) into Eq. (6.4.1), we obtain

$$\gamma_o d(n)+\xi_{ISI}(n) \;=\; \sum_{\lambda=1}^{L}\sum_{m}d(m)\sum_{k=1}^{N_o+L_2-1}g(nN_s-mN_s-k) \quad (6.4.2)$$
$$\cos(2\pi\Delta f_c k)\mathrm{Re}\left[H_\lambda(k)e^{-j2\pi(\lambda-1)\theta_s}+G_\lambda(k)e^{j2\pi(\lambda-1)\theta_s}\right].$$

We define

$$\gamma(n) = \sum_{\lambda=1}^{L} \sum_{k=1}^{N_o+L_2-1} g(nN_s - k)\cos(2\pi\Delta f_c k)\mathrm{Re}\left[H_\lambda(k)e^{-j2\pi(\lambda-1)\theta_s} + G_\lambda(k)e^{j2\pi(\lambda-1)\theta_s}\right] \tag{6.4.3}$$

where we note that the lengths of $\gamma(n)$ is K_1,

$$K_1 = \lceil \frac{1}{N_s}(N_o + 2L_2 - 2) \rceil \tag{6.4.4}$$

where $\lceil . \rceil$ denotes rounding to nearest integers less than or equal to the number. Substituting Eqs. (6.2.6) and (6.2.7) into Eq. (6.4.3), we obtain

$$\begin{aligned}\gamma(n) &= \sum_{\lambda=1}^{L} \sum_{k=1}^{N_o+L_2-1} \sum_{l=1}^{J} \sum_{m=0}^{L_2-1} g(nN_s - k) \\ &\mathrm{Re}\left[h_{\lambda l}(k-m)e^{-j2\pi\alpha_l(k-m)}p(m)e^{-j2\pi\alpha_l m}e^{-j2\pi(\lambda-1)\theta_s}\right]\cos(2\pi\Delta f_c m)\cos(2\pi\Delta f_c k) \\ &+ \sum_{\lambda=1}^{L} \sum_{k=1}^{N_o+L_2-1} \sum_{l=J+1}^{M} \sum_{m=0}^{L_2-1} g(nN_s - k) \\ &\mathrm{Re}\left[h_{\lambda l}(k-m)e^{-j2\pi\alpha_l(k-m)}p(m)e^{-j2\pi\alpha_l m}e^{j2\pi(\lambda-1)\theta_s}\right]\cos(2\pi\Delta f_c m)\cos(2\pi\Delta f_c k).\end{aligned} \tag{6.4.5}$$

Substituting Eq. (6.4.3) into Eq. (6.4.2), we obtain

$$\gamma_o d(n) + \xi_{ISI}(n) = \sum_m d(m)\gamma(n-m) = \gamma(0)d(n) + \sum_{m\neq n} d(m)\gamma(n-m). \tag{6.4.6}$$

Here, we define

$$\gamma_o = \gamma(0), \quad \xi_{ISI}(n) = \sum_{m\neq n} d(m)\gamma(n-m) \tag{6.4.7}$$

where $\gamma_o d(n)$ is the desired symbol component. $\xi_{ISI}(n)$ is the inter-symbol interference (ISI) component. We note that γ_o is a random variable.

$$\begin{aligned}\gamma_o &= \sum_{\lambda=1}^{L} \sum_{k=1}^{N_o+L_2-1} \sum_{l=1}^{J} \sum_{m=0}^{L_2-1} g(-k) \\ &\mathrm{Re}\left[h_{\lambda l}(k-m)e^{-j2\pi\alpha_l(k-m)}p(m)e^{-j2\pi\alpha_l m}e^{-j2\pi(\lambda-1)\theta_s}\right]\cos(2\pi\Delta f_c m)\cos(2\pi\Delta f_c k) \\ &+ \sum_{\lambda=1}^{L} \sum_{k=1}^{N_o+L_2-1} \sum_{l=J+1}^{M} \sum_{m=0}^{L_2-1} g(-k)\end{aligned} \tag{6.4.8}$$

$$\mathrm{Re}\left[h_{\lambda l}(k-m)e^{-j2\pi\alpha_l(k-m)}p(m)e^{-j2\pi\alpha_l m}e^{j2\pi(\lambda-1)\theta_s}\right]\cos(2\pi\Delta f_c m)\cos(2\pi\Delta f_c k).$$

The mean of γ_o is

$$\begin{aligned}\mu_{\gamma_o} &= \sum_{\lambda=1}^{L}\sum_{k=1}^{N_o+L_2-1}\sum_{l=1}^{J}\sum_{m=0}^{L_2-1} g(-k)\cos(2\pi\Delta f_c m)\cos(2\pi\Delta f_c k) \\ &\quad \mathrm{Re}\left[E[h_{\lambda l}(k-m)]e^{-j2\pi\alpha_l(k-m)}p(m)e^{-j2\pi\alpha_l m}e^{-j2\pi(\lambda-1)\theta_s}\right] \\ &\quad +\sum_{\lambda=1}^{L}\sum_{k=1}^{N_o+L_2-1}\sum_{l=J+1}^{M}\sum_{m=0}^{L_2-1} g(-k)\cos(2\pi\Delta f_c m)\cos(2\pi\Delta f_c k) \\ &\quad \mathrm{Re}\left[E[h_{\lambda l}(k-m)]e^{-j2\pi\alpha_l(k-m)}p(m)e^{-j2\pi\alpha_l m}e^{j2\pi(\lambda-1)\theta_s}\right].\end{aligned} \tag{6.4.9}$$

The variance of γ_o is

$$\begin{aligned}\sigma^2_{\gamma_o} &= E[\gamma_o^2]-\mu^2_{\gamma_o} \\ &= \sum_{\lambda_1=1}^{L}\sum_{\lambda_2=1}^{L}\sum_{k_1=1}^{N_o+L_2-1}\sum_{l_1=1}^{J}\sum_{m_1=0}^{L_2-1}\sum_{k_2=1}^{N_o+L_2-1}\sum_{m_2=0}^{L_2-1}\sum_{l_2=1}^{J} \\ &\quad E\left[g(-k_1)\mathrm{Re}\left[h_{\lambda_1 l_1}(k_1-m_1)p(m_1)e^{-j2\pi\alpha_{l_1}(k_1-m_1)}e^{-j2\pi\alpha_{l_1}m_1}e^{-j2\pi(\lambda_1-1)\theta_s}\right]\right. \\ &\quad g(-k_2)\mathrm{Re}\left[h_{\lambda_2 l_2}(k_2-m_2)p(m_2)e^{-j2\pi\alpha_{l_2}(k_2-m_2)}e^{-j2\pi\alpha_{l_2}m_2}e^{-j2\pi(\lambda_2-1)\theta_s}\right] \\ &\quad \left.\cos(2\pi\Delta f_c m_1)\cos(2\pi\Delta f_c m_2)\cos(2\pi\Delta f_c k_1)\cos(2\pi\Delta f_c k_2)\right] \\ &\quad +\sum_{\lambda_1=1}^{L}\sum_{\lambda_2=1}^{L}\sum_{k_1=1}^{N_o+L_2-1}\sum_{l_1=1}^{J}\sum_{m_1=0}^{L_2-1}\sum_{k_2=1}^{N_o+L_2-1}\sum_{m_2=0}^{L_2-1}\sum_{l_2=J+1}^{M} \\ &\quad E\left[g(-k_1)\mathrm{Re}\left[h_{\lambda_1 l_1}(k_1-m_1)p(m_1)e^{-j2\pi\alpha_{l_1}(k_1-m_1)}e^{-j2\pi\alpha_{l_1}m_1}e^{-j2\pi(\lambda_1-1)\theta_s}\right]\right. \\ &\quad g(-k_2)\mathrm{Re}\left[h_{\lambda_2 l_2}(k_2-m_2)p(m_2)e^{-j2\pi\alpha_{l_2}(k_2-m_2)}e^{-j2\pi\alpha_{l_2}m_2}e^{j2\pi(\lambda_2-1)\theta_s}\right] \\ &\quad \left.\cos(2\pi\Delta f_c m_1)\cos(2\pi\Delta f_c m_2)\cos(2\pi\Delta f_c k_1)\cos(2\pi\Delta f_c k_2)\right] \\ &\quad +\sum_{\lambda_1=1}^{L}\sum_{\lambda_2=1}^{L}\sum_{k_1=1}^{N_o+L_2-1}\sum_{l_1=J+1}^{M}\sum_{m_1=0}^{L_2-1}\sum_{k_2=1}^{N_o+L_2-1}\sum_{m_2=0}^{L_2-1}\sum_{l_2=1}^{J} \\ &\quad E\left[g(-k_1)\mathrm{Re}\left[h_{\lambda_1 l_1}(k_1-m_1)p(m_1)e^{-j2\pi\alpha_{l_1}(k_1-m_1)}e^{-j2\pi\alpha_{l_1}m_1}e^{j2\pi(\lambda_1-1)\theta_s}\right]\right. \\ &\quad g(-k_2)\mathrm{Re}\left[h_{\lambda_2 l_2}(k_2-m_2)p(m_2)e^{-j2\pi\alpha_{l_2}(k_2-m_2)}e^{-j2\pi\alpha_{l_2}m_2}e^{-j2\pi(\lambda_2-1)\theta_s}\right] \\ &\quad \left.\cos(2\pi\Delta f_c m_1)\cos(2\pi\Delta f_c m_2)\cos(2\pi\Delta f_c k_1)\cos(2\pi\Delta f_c k_2)\right] \\ &\quad +\sum_{\lambda_1=1}^{L}\sum_{\lambda_2=1}^{L}\sum_{k_1=1}^{N_o+L_2-1}\sum_{l_1=J+1}^{M}\sum_{m_1=0}^{L_2-1}\sum_{k_2=1}^{N_o+L_2-1}\sum_{m_2=0}^{L_2-1}\sum_{l_2=J+1}^{M}\end{aligned} \tag{6.4.10}$$

$$
\begin{aligned}
&E\left[g(-k_1)\mathrm{Re}\left[h_{\lambda_1 l_1}(k_1-m_1)p(m_1)e^{-j2\pi\alpha_{l_1}(k_1-m_1)}e^{-j2\pi\alpha_{l_1}m_1}e^{j2\pi(\lambda_1-1)\theta_s}\right]\right.\\
&\left.g(-k_2)\mathrm{Re}\left[h_{\lambda_2 l_2}(k_2-m_2)p(m_2)e^{-j2\pi\alpha_{l_2}(k_2-m_2)}e^{-j2\pi\alpha_{l_2}m_2}e^{j2\pi(\lambda_2-1)\theta_s}\right]\right.\\
&\left.\cos(2\pi\Delta f_c m_1)\cos(2\pi\Delta f_c m_2)\cos(2\pi\Delta f_c k_1)\cos(2\pi\Delta f_c k_2)\right]\\
&-\sum_{\lambda_1=1}^{L}\sum_{\lambda_2=1}^{L}\sum_{k_1=1}^{N_o+L_2-1}\sum_{l_1=1}^{J}\sum_{m_1=0}^{L_2-1}\sum_{k_2=1}^{N_o+L_2-1}\sum_{m_2=0}^{L_2-1}\sum_{l_2=1}^{J}\\
&g(-k_1)\mathrm{Re}\left[E[h_{\lambda_1 l_1}(k_1-m_1)]p(m_1)e^{-j2\pi\alpha_{l_1}(k_1-m_1)}e^{-j2\pi\alpha_{l_1}m_1}e^{-j2\pi(\lambda_1-1)\theta_s}\right]\\
&g(-k_2)\mathrm{Re}\left[E[h_{\lambda_2 l_2}(k_2-m_2)]p(m_2)e^{-j2\pi\alpha_{l_2}(k_2-m_2)}e^{-j2\pi\alpha_{l_2}m_2}e^{-j2\pi(\lambda_2-1)\theta_s}\right]\\
&\cos(2\pi\Delta f_c m_1)\cos(2\pi\Delta f_c m_2)\cos(2\pi\Delta f_c k_1)\cos(2\pi\Delta f_c k_2)\\
&+\sum_{\lambda_1=1}^{L}\sum_{\lambda_2=1}^{L}\sum_{k_1=1}^{N_o+L_2-1}\sum_{l_1=1}^{J}\sum_{m_1=0}^{L_2-1}\sum_{k_2=1}^{N_o+L_2-1}\sum_{m_2=0}^{L_2-1}\sum_{l_2=J+1}^{M}\\
&g(-k_1)\mathrm{Re}\left[E[h_{\lambda_1 l_1}(k_1-m_1)]p(m_1)e^{-j2\pi\alpha_{l_1}(k_1-m_1)}e^{-j2\pi\alpha_{l_1}m_1}e^{-j2\pi(\lambda_1-1)\theta_s}\right]\\
&g(-k_2)\mathrm{Re}\left[E[h_{\lambda_2 l_2}(k_2-m_2)]p(m_2)e^{-j2\pi\alpha_{l_2}(k_2-m_2)}e^{-j2\pi\alpha_{l_2}m_2}e^{j2\pi(\lambda_2-1)\theta_s}\right]\\
&\cos(2\pi\Delta f_c m_1)\cos(2\pi\Delta f_c m_2)\cos(2\pi\Delta f_c k_1)\cos(2\pi\Delta f_c k_2)\\
&+\sum_{\lambda_1=1}^{L}\sum_{\lambda_2=1}^{L}\sum_{k_1=1}^{N_o+L_2-1}\sum_{l_1=J+1}^{M}\sum_{m_1=0}^{L_2-1}\sum_{k_2=1}^{N_o+L_2-1}\sum_{m_2=0}^{L_2-1}\sum_{l_2=1}^{J}\\
&g(-k_1)\mathrm{Re}\left[E[h_{\lambda_1 l_1}(k_1-m_1)]p(m_1)e^{-j2\pi\alpha_{l_1}(k_1-m_1)}e^{-j2\pi\alpha_{l_1}m_1}e^{j2\pi(\lambda_1-1)\theta_s}\right]\\
&g(-k_2)\mathrm{Re}\left[E[h_{\lambda_2 l_2}(k_2-m_2)]p(m_2)e^{-j2\pi\alpha_{l_2}(k_2-m_2)}e^{-j2\pi\alpha_{l_2}m_2}e^{-j2\pi(\lambda_2-1)\theta_s}\right]\\
&\cos(2\pi\Delta f_c m_1)\cos(2\pi\Delta f_c m_2)\cos(2\pi\Delta f_c k_1)\cos(2\pi\Delta f_c k_2)\\
&+\sum_{\lambda_1=1}^{L}\sum_{\lambda_2=1}^{L}\sum_{k_1=1}^{N_o+L_2-1}\sum_{l_1=J+1}^{M}\sum_{m_1=0}^{L_2-1}\sum_{k_2=1}^{N_o+L_2-1}\sum_{m_2=0}^{L_2-1}\sum_{l_2=J+1}^{M}\\
&g(kN_s-k_1)\mathrm{Re}\left[E[h_{\lambda_1 l_1}(k_1-m_1)]p(m_1)e^{-j2\pi\alpha_{l_1}(k_1-m_1)}e^{-j2\pi\alpha_{l_1}m_1}e^{j2\pi(\lambda_1-1)\theta_s}\right]\\
&g(-k_2)\mathrm{Re}\left[E[h_{\lambda_2 l_2}(k_2-m_2)]p(m_2)e^{-j2\pi\alpha_{l_2}(k_2-m_2)}e^{-j2\pi\alpha_{l_2}m_2}e^{j2\pi(\lambda_2-1)\theta_s}\right]\\
&\cos(2\pi\Delta f_c m_1)\cos(2\pi\Delta f_c m_2)\cos(2\pi\Delta f_c k_1)\cos(2\pi\Delta f_c k_2).
\end{aligned}
$$

The mean of $\xi_{ISI}(n)$ is

$$E[\xi_{ISI}] = \sum_{m\neq n} E[d(m)]E[\gamma(n-m)] = 0. \tag{6.4.11}$$

The variance of $\xi_{ISI}(n)$ is

$$\zeta_{ISI} = E[\xi_{ISI}(n)\xi^*_{ISI}(n)] = \sum_{k=1}^{K_1-1} E[\gamma(k)\gamma^*(k)] \tag{6.4.12}$$

$$\begin{aligned}
&= \sum_{k=1}^{K_1}\sum_{\lambda_1=1}^{L}\sum_{\lambda_2=1}^{L}\sum_{k_1=1}^{N_o+L_2-1}\sum_{l_1=1}^{J}\sum_{m_1=0}^{L_2-1}\sum_{k_2=1}^{N_o+L_2-1}\sum_{m_2=0}^{L_2-1}\sum_{l_2=1}^{J} \\
&\quad E\left[g(kN_s-k_1)\mathrm{Re}\left[h_{\lambda_1 l_1}(k_1-m_1)p(m_1)e^{-j2\pi\alpha_{l_1}(k_1-m_1)}e^{-j2\pi\alpha_{l_1}m_1}e^{-j2\pi(\lambda_1-1)\theta_s}\right]\right. \\
&\quad \left. g(kN_s-k_2)\mathrm{Re}\left[h_{\lambda_2 l_2}(k_2-m_2)p(m_2)e^{-j2\pi\alpha_{l_2}(k_2-m_2)}e^{-j2\pi\alpha_{l_2}m_2}e^{-j2\pi(\lambda_2-1)\theta_s}\right]\right. \\
&\quad \left.\cos(2\pi\Delta f_c m_1)\cos(2\pi\Delta f_c m_2)\cos(2\pi\Delta f_c k_1)\cos(2\pi\Delta f_c k_2)\right] \\
&\quad +\sum_{k=1}^{K_1}\sum_{\lambda_1=1}^{L}\sum_{\lambda_2=1}^{L}\sum_{k_1=1}^{N_o+L_2-1}\sum_{l_1=1}^{J}\sum_{m_1=0}^{L_2-1}\sum_{k_2=1}^{N_o+L_2-1}\sum_{m_2=0}^{L_2-1}\sum_{l_2=J+1}^{M} \\
&\quad E\left[g(kN_s-k_1)\mathrm{Re}\left[h_{\lambda_1 l_1}(k_1-m_1)p(m_1)e^{-j2\pi\alpha_{l_1}(k_1-m_1)}e^{-j2\pi\alpha_{l_1}m_1}e^{-j2\pi(\lambda_1-1)\theta_s}\right]\right. \\
&\quad \left. g(kN_s-k_2)\mathrm{Re}\left[h_{\lambda_2 l_2}(k_2-m_2)p(m_2)e^{-j2\pi\alpha_{l_2}(k_2-m_2)}e^{-j2\pi\alpha_{l_2}m_2}e^{j2\pi(\lambda_2-1)\theta_s}\right]\right. \\
&\quad \left.\cos(2\pi\Delta f_c m_1)\cos(2\pi\Delta f_c m_2)\cos(2\pi\Delta f_c k_1)\cos(2\pi\Delta f_c k_2)\right] \\
&\quad +\sum_{k=1}^{K_1}\sum_{\lambda_1=1}^{L}\sum_{\lambda_2=1}^{L}\sum_{k_1=1}^{N_o+L_2-1}\sum_{l_1=J+1}^{M}\sum_{m_1=0}^{L_2-1}\sum_{k_2=1}^{N_o+L_2-1}\sum_{m_2=0}^{L_2-1}\sum_{l_2=1}^{J} \\
&\quad E\left[g(kN_s-k_1)\mathrm{Re}\left[h_{\lambda_1 l_1}(k_1-m_1)p(m_1)e^{-j2\pi\alpha_{l_1}(k_1-m_1)}e^{-j2\pi\alpha_{l_1}m_1}e^{j2\pi(\lambda_1-1)\theta_s}\right]\right. \\
&\quad \left. g(kN_s-k_2)\mathrm{Re}\left[h_{\lambda_2 l_2}(k_2-m_2)p(m_2)e^{-j2\pi\alpha_{l_2}(k_2-m_2)}e^{-j2\pi\alpha_{l_2}m_2}e^{-j2\pi(\lambda_2-1)\theta_s}\right]\right. \\
&\quad \left.\cos(2\pi\Delta f_c m_1)\cos(2\pi\Delta f_c m_2)\cos(2\pi\Delta f_c k_1)\cos(2\pi\Delta f_c k_2)\right] \\
&\quad +\sum_{k=1}^{K_1}\sum_{\lambda_1=1}^{L}\sum_{\lambda_2=1}^{L}\sum_{k_1=1}^{N_o+L_2-1}\sum_{l_1=J+1}^{M}\sum_{m_1=0}^{L_2-1}\sum_{k_2=1}^{N_o+L_2-1}\sum_{m_2=0}^{L_2-1}\sum_{l_2=J+1}^{M} \\
&\quad E\left[g(kN_s-k_1)\mathrm{Re}\left[h_{\lambda_1 l_1}(k_1-m_1)p(m_1)e^{-j2\pi\alpha_{l_1}(k_1-m_1)}e^{-j2\pi\alpha_{l_1}m_1}e^{j2\pi(\lambda_1-1)\theta_s}\right]\right. \\
&\quad \left. g(kN_s-k_2)\mathrm{Re}\left[h_{\lambda_2 l_2}(k_2-m_2)p(m_2)e^{-j2\pi\alpha_{l_2}(k_2-m_2)}e^{-j2\pi\alpha_{l_2}m_2}e^{j2\pi(\lambda_2-1)\theta_s}\right]\right. \\
&\quad \left.\cos(2\pi\Delta f_c m_1)\cos(2\pi\Delta f_c m_2)\cos(2\pi\Delta f_c k_1)\cos(2\pi\Delta f_c k_2)\right].
\end{aligned}$$

6.5 Statistical Analysis of $\xi_{CTI}(n)$

When the input interference $u(n)$ passes through the system, the input of threshold is

$$\xi_{CTI}(n) = \mathrm{Re}\left[\sum_{\lambda}\sum_{k=1}^{N_o+L_2-1}\left[H_\lambda(k)u_\lambda(nN_s-k)+G_\lambda(k)u^*_\lambda(nN_s-k)\right]\right] \tag{6.5.1}$$

where $u_\lambda(n)$, $H_\lambda(n)$, and $G_\lambda(n)$ are defined in Eqs. (6.1.10), (6.2.6), and (6.2.7) respectively. Substituting Eqs. (6.1.7) and (6.1.10) into Eq. (6.5.1), we obtain

$$\begin{aligned}\xi_{CTI}(n) &= A_u \sum_{m=-\infty}^{\infty} d_u(m) \sum_{\lambda} \sum_{k=1}^{N_o+L_2-1} g_u(nN_s - mN_s - k) \\ &\quad \mathrm{Re}\left[H_\lambda(k) e^{-j2\pi(\lambda-1)\theta_u} + G_\lambda(k) e^{j2\pi(\lambda-1)\theta_u}\right] \cos(2\pi\Delta f_u(nN_s - k)).\end{aligned} \tag{6.5.2}$$

When we define

$$\begin{aligned}\beta_1(n) &= A_u \sum_{\lambda} \sum_{k=1}^{N_o+L_2-1} g_u(nN_s - k) \\ &\quad \mathrm{Re}\left[H_\lambda(k) \cos(2\pi\Delta f_u k) e^{-j2\pi(\lambda-1)\theta_u} + G_\lambda(k) \cos(2\pi\Delta f_u k) e^{j2\pi(\lambda-1)\theta_u}\right]\end{aligned} \tag{6.5.3}$$

$$\begin{aligned}\beta_2(n) &= A_u \sum_{\lambda} \sum_{k=1}^{N_o+L_2-1} g_u(nN_s - k) \\ &\quad \mathrm{Re}\left[H_\lambda(k) \sin(2\pi\Delta f_u k) e^{-j2\pi(\lambda-1)\theta_u} + G_\lambda(k) \sin(2\pi\Delta f_u k) e^{j2\pi(\lambda-1)\theta_u}\right],\end{aligned} \tag{6.5.4}$$

we obtain

$$\begin{aligned}\xi_{CTI}(n) &= \sum_m d_u(m) \left[\beta_1(n-m) \cos(2\pi\Delta f_u n N_s) + \beta_2(n-m) \sin(2\pi\Delta f_u n N_s)\right] \\ &= \sum_m d_u(n-m) \left[\beta_1(m) \cos(2\pi\Delta f_u n N_s) + \beta_2(m) \sin(2\pi\Delta f_u n N_s)\right] \\ &= \sum_m d_u(n-m) \beta(m,n)\end{aligned} \tag{6.5.5}$$

where we define

$$\begin{aligned}\beta(m,n) &= \beta_1(m) \cos(2\pi\Delta f_u n N_s) + \beta_2(m) \sin(2\pi\Delta f_u n N_s) \\ &= A_u \sum_{\lambda} \sum_{k=1}^{N_o+L_2-1} g_u(mN_s - k) \cos(2\pi\Delta f_u(nN_s - k)) \\ &\quad \mathrm{Re}\left[H_\lambda(k) e^{-j2\pi(\lambda-1)\theta_u} + G_\lambda(k) e^{j2\pi(\lambda-1)\theta_u}\right].\end{aligned} \tag{6.5.6}$$

Using Eq. (6.5.5), we note that the mean of $\xi_{CTI}(n)$ is zero and the variance of $\xi_{CTI}(n)$ is

$$\begin{aligned}\zeta_{CTI}(n) &= E[\xi_{CTI}(n)\xi^*_{CTI}(n)] \\ &= \sum_{k_1}\sum_{k_2} E\left[d_u(n-k_1)d_u^*(n-k_2)\beta(k_1,n)\beta^*(k_2,n)\right] \\ &= \sum_{k} E[\beta(k,n)\beta^*(k,n)].\end{aligned} \tag{6.5.7}$$

Here, $\beta(k,n)$ is a periodic function in n and its length is K_2,

$$K_2 = \lceil \frac{1}{N_s}(N_o + L_2 + L_3 - 2) \rceil, \tag{6.5.8}$$

L_3 is the length of $g_u(n)$. Substituting Eqs. (6.2.6), (6.2.7), and (6.5.6) into Eq. (6.5.7), we obtain

$$\begin{aligned}\zeta_{CTI}(n) &= A_u^2 \sum_{\lambda_1=1}^{L}\sum_{\lambda_2=1}^{L}\sum_{k=1}^{K_2}\sum_{k_1=1}^{N_o+L_2-1}\sum_{l_1=1}^{J}\sum_{m_1=0}^{L_2-1}\sum_{k_2=1}^{N_o+L_2-1}\sum_{m_2=0}^{L_2-1}\sum_{l_2=1}^{J} \\ &\quad E\Big[g_u(kN_s-k_1)\mathrm{Re}\Big[h_{\lambda_1 l_1}(k_1-m_1)p(m_1)e^{-j2\pi\alpha_{l_1}(k_1-m_1)}e^{-j2\pi\alpha_{l_1}m_1}e^{-j2\pi(\lambda_1-1)\theta_u}\Big] \\ &\quad g_u(kN_s-k_2)\mathrm{Re}\Big[h_{\lambda_2 l_2}(k_2-m_2)p(m_2)e^{-j2\pi\alpha_{l_2}(k_2-m_2)}e^{-j2\pi\alpha_{l_2}m_2}e^{-j2\pi(\lambda_2-1)\theta_u}\Big]\Big] \\ &\quad \cos(2\pi\Delta f_c m_1)\cos(2\pi\Delta f_c m_2)\cos(2\pi\Delta f_u(nN_s-k_1))\cos(2\pi\Delta f_u(nN_s-k_2)) \\ &\quad + A_u^2 \sum_{\lambda_1=1}^{L}\sum_{\lambda_2=1}^{L}\sum_{k=1}^{K_2}\sum_{k_1=1}^{N_o+L_2-1}\sum_{l_1=1}^{J}\sum_{m_1=0}^{L_2-1}\sum_{k_2=1}^{N_o+L_2-1}\sum_{m_2=0}^{L_2-1}\sum_{l_2=J+1}^{M} \\ &\quad E\Big[g_u(kN_s-k_1)\mathrm{Re}\Big[h_{\lambda_1 l_1}(k_1-m_1)p(m_1)e^{-j2\pi\alpha_{l_1}(k_1-m_1)}e^{-j2\pi\alpha_{l_1}m_1}e^{-j2\pi(\lambda_1-1)\theta_u}\Big] \\ &\quad g_u(kN_s-k_2)\mathrm{Re}\Big[h_{\lambda_2 l_2}(k_2-m_2)p(m_2)e^{-j2\pi\alpha_{l_2}(k_2-m_2)}e^{j2\pi(\lambda_2-1)\theta_u}\Big]\Big] \\ &\quad \cos(2\pi\Delta f_c m_1)\cos(2\pi\Delta f_c m_2)\cos(2\pi\Delta f_u(nN_s-k_1))\cos(2\pi\Delta f_u(nN_s-k_2)) \\ &\quad + A_u^2 \sum_{\lambda_1=1}^{L}\sum_{\lambda_2=1}^{L}\sum_{k=1}^{K_2}\sum_{k_1=1}^{N_o+L_2-1}\sum_{l_1=J+1}^{M}\sum_{m_1=0}^{L_2-1}\sum_{k_2=1}^{N_o+L_2-1}\sum_{m_2=0}^{L_2-1}\sum_{l_2=1}^{J} \\ &\quad E\Big[g_u(kN_s-k_1)\mathrm{Re}\Big[h_{\lambda_1 l_1}(k_1-m_1)p(m_1)e^{-j2\pi\alpha_{l_1}(k_1-m_1)}e^{-j2\pi\alpha_{l_1}m_1}e^{j2\pi(\lambda_1-1)\theta_u}\Big] \\ &\quad g_u(kN_s-k_2)\mathrm{Re}\Big[h_{\lambda_2 l_2}(k_2-m_2)p(m_2)e^{-j2\pi\alpha_{l_2}(k_2-m_2)}e^{-j2\pi\alpha_{l_2}m_2}e^{-j2\pi(\lambda_2-1)\theta_u}\Big]\Big] \\ &\quad \cos(2\pi\Delta f_c m_1)\cos(2\pi\Delta f_c m_2)\cos(2\pi\Delta f_u(nN_s-k_1))\cos(2\pi\Delta f_u(nN_s-k_2)) \\ &\quad + A_u^2 \sum_{\lambda_1=1}^{L}\sum_{\lambda_2=1}^{L}\sum_{k=1}^{K_2}\sum_{k_1=1}^{N_o+L_2-1}\sum_{l_1=J+1}^{M}\sum_{m_1=0}^{L_2-1}\sum_{k_2=1}^{N_o+L_2-1}\sum_{m_2=0}^{L_2-1}\sum_{l_2=J+1}^{M} \\ &\quad E\Big[g_u(kN_s-k_1)\mathrm{Re}\Big[h_{\lambda_1 l_1}(k_1-m_1)p(m_1)e^{-j2\pi\alpha_{l_1}(k_1-m_1)}e^{-j2\pi\alpha_{l_1}m_1}e^{j2\pi(\lambda_1-1)\theta_u}\Big]\end{aligned} \tag{6.5.9}$$

$$g_u(kN_s-k_2)\mathrm{Re}\left[h_{\lambda_2 l_2}(k_2-m_2)p(m_2)e^{-j2\pi\alpha_{l_2}(k_2-m_2)}e^{-j2\pi\alpha_{l_2}m_2}e^{j2\pi(\lambda_2-1)\theta_u}\right]\Big]$$
$$\cos(2\pi\Delta f_c m_1)\cos(2\pi\Delta f_c m_2)\cos(2\pi\Delta f_u(nN_s-k_1))\cos(2\pi\Delta f_u(nN_s-k_2)).$$

Here, we note that $\zeta_{CTI}(n)$ is a periodic function in n. The minimum integer value of n which make $\Delta f_u n N_s$ be an integer is the period of the function $\zeta_{CTI}(n)$. Let Q denote the period of $\zeta_{CTI}(n)$. Q may be determined as

$$Q=\min\{n:\Delta f_u n N_s=\text{integer}\} \tag{6.5.10}$$

where N_s is defined in Eq. (6.1.1). For example, when $\Delta f_u=0.17$, and $N_s=20$, we have $Q=5$. The average value of $\zeta_{CTI}(n)$ is

$$\begin{aligned}
\zeta_{CTIave} &= \frac{1}{Q}\sum_{n=0}^{Q-1}\zeta_{CTI}(n) \qquad (6.5.11)\\
&= \frac{A_u^2}{Q}\sum_{n=0}^{Q-1}\sum_{\lambda_1=1}^{L}\sum_{\lambda_2=1}^{L}\sum_{k=1}^{K_2}\sum_{k_1=1}^{N_o+L_2-1}\sum_{l_1=1}^{J}\sum_{m_1=0}^{L_2-1}\sum_{k_2=1}^{N_o+L_2-1}\sum_{m_2=0}^{L_2-1}\sum_{l_2=1}^{J}\\
&\quad g_u(kN_s-k_1)g_u(kN_s-k_2)\\
&\quad E\left[\mathrm{Re}\left[h_{\lambda_1 l_1}(k_1-m_1)p(m_1)e^{-j2\pi\alpha_{l_1}(k_1-m_1)}e^{-j2\pi\alpha_{l_1}m_1}e^{-j2\pi(\lambda_1-1)\theta_u}\right]\right.\\
&\quad \left.\mathrm{Re}\left[h_{\lambda_2 l_2}(k_2-m_2)p(m_2)e^{-j2\pi\alpha_{l_2}(k_2-m_2)}e^{-j2\pi\alpha_{l_2}m_2}e^{-j2\pi(\lambda_2-1)\theta_u}\right]\right]\\
&\quad \cos(2\pi\Delta f_c m_1)\cos(2\pi\Delta f_c m_2)\cos(2\pi\Delta f_u(nN_s-k_1))\cos(2\pi\Delta f_u(nN_s-k_2))\\
&+\frac{A_u^2}{Q}\sum_{n=0}^{Q-1}\sum_{\lambda_1=1}^{L}\sum_{\lambda_2=1}^{L}\sum_{k=1}^{K_2}\sum_{k_1=1}^{N_o+L_2-1}\sum_{l_1=1}^{J}\sum_{m_1=0}^{L_2-1}\sum_{k_2=1}^{N_o+L_2-1}\sum_{m_2=0}^{L_2-1}\sum_{l_2=J+1}^{M}\\
&\quad g_u(kN_s-k_1)g_u(kN_s-k_2)\\
&\quad E\left[\mathrm{Re}\left[h_{\lambda_1 l_1}(k_1-m_1)p(m_1)e^{-j2\pi\alpha_{l_1}(k_1-m_1)}e^{-j2\pi\alpha_{l_1}m_1}e^{-j2\pi(\lambda_1-1)\theta_u}\right]\right.\\
&\quad \left.\mathrm{Re}\left[h_{\lambda_2 l_2}(k_2-m_2)p(m_2)e^{-j2\pi\alpha_{l_2}(k_2-m_2)}e^{-j2\pi\alpha_{l_2}m_2}e^{j2\pi(\lambda_2-1)\theta_u}\right]\right]\\
&\quad \cos(2\pi\Delta f_c m_1)\cos(2\pi\Delta f_c m_2)\cos(2\pi\Delta f_u(nN_s-k_1))\cos(2\pi\Delta f_u(nN_s-k_2))\\
&+\frac{A_u^2}{Q}\sum_{n=0}^{Q-1}\sum_{\lambda_1=1}^{L}\sum_{\lambda_2=1}^{L}\sum_{k=1}^{K_2}\sum_{k_1=1}^{N_o+L_2-1}\sum_{l_1=J+1}^{M}\sum_{m_1=0}^{L_2-1}\sum_{k_2=1}^{N_o+L_2-1}\sum_{m_2=0}^{L_2-1}\sum_{l_2=1}^{J}\\
&\quad g_u(kN_s-k_1)g_u(kN_s-k_2)\\
&\quad E\left[\mathrm{Re}\left[h_{\lambda_1 l_1}(k_1-m_1)p(m_1)e^{-j2\pi\alpha_{l_1}(k_1-m_1)}e^{-j2\pi\alpha_{l_1}m_1}e^{j2\pi(\lambda_1-1)\theta_u}\right]\right.\\
&\quad \left.\mathrm{Re}\left[h_{\lambda_2 l_2}(k_2-m_2)p(m_2)e^{-j2\pi\alpha_{l_2}(k_2-m_2)}e^{-j2\pi\alpha_{l_2}m_2}e^{-j2\pi(\lambda_2-1)\theta_u}\right]\right]
\end{aligned}$$

$$\cos(2\pi\Delta f_c m_1)\cos(2\pi\Delta f_c m_2)\cos(2\pi\Delta f_u(nN_s-k_1))\cos(2\pi\Delta f_u(nN_s-k_2))$$
$$+\frac{A_u^2}{Q}\sum_{n=0}^{Q-1}\sum_{\lambda_1=1}^{L}\sum_{\lambda_2=1}^{L}\sum_{k=1}^{K_2}\sum_{k_1=1}^{N_o+L_2-1}\sum_{l_1=J+1}^{M}\sum_{m_1=0}^{L_2-1}\sum_{k_2=1}^{N_o+L_2-1}\sum_{m_2=0}^{L_2-1}\sum_{l_2=J+1}^{M}$$
$$g_u(kN_s-k_1)g_u(kN_s-k_2)$$
$$E\left[\mathrm{Re}\left[h_{\lambda_1 l_1}(k_1-m_1)p(m_1)e^{-j2\pi\alpha_{l_1}(k_1-m_1)}e^{-j2\pi\alpha_{l_1}m_1}e^{j2\pi(\lambda_1-1)\theta_u}\right]\right.$$
$$\left.\mathrm{Re}\left[h_{\lambda_2 l_2}(k_2-m_2)p(m_2)e^{-j2\pi\alpha_{l_2}(k_2-m_2)}e^{-j2\pi\alpha_{l_2}m_2}e^{j2\pi(\lambda_2-1)\theta_u}\right]\right]$$
$$\cos(2\pi\Delta f_c m_1)\cos(2\pi\Delta f_c m_2)\cos(2\pi\Delta f_u(nN_s-k_1))\cos(2\pi\Delta f_u(nN_s-k_2)).$$

6.6 Analysis of the Output Probability Error

Using Eq. (6.2.21), the input to the threshold is

$$\hat{d}(n)=\gamma_o d(n)+\eta_e(n) \tag{6.6.1}$$

where $d(n)$ is the desired symbol, γ_o is the random coefficient of the desired symbol which is defined as in Eq. (6.4.8). $\eta_e(n)$ is the sum of the output noise component, the output ISI interference, and the output CTI interference and it is also a random variable which is defined in Eq. (6.2.20). We know γ_o and η_e are results of a large amount of random variables acting together. γ_o and η_e can be approximated as having Gaussian distributions respectively, that is,

- γ_o is approximated as having Gaussian distribution

$$\gamma_o \sim N(\mu_{\gamma_o},\sigma^2_{\gamma_o}) \tag{6.6.2}$$

  where μ_{γ_o} and $\sigma^2_{\gamma_o}$ are the mean and variance of γ_o respectively. μ_{γ_o} and $\sigma^2_{\gamma_o}$ are defined in Eqs. (6.4.9) and (6.4.10) respectively. The approximation accuracy is shown in Appendix C.

- η_e is approximated as having zero mean Gaussian distribution

$$\eta_e \sim N(0,\sigma^2_{\eta_e}) \tag{6.6.3}$$

where $\sigma^2_{\eta_e}$ is the variance of η_e. Using Eq. (6.2.20), We know

$$E[\eta_e(n)] = E[\eta(n)] + E[\xi_{ISI}(n)] + E[\xi_{CTI}(n)]. \tag{6.6.4}$$

Using Eqs. (6.3.2), (6.4.11), and (6.5.5), we know

$$E[\eta_e(n)] = 0. \tag{6.6.5}$$

Using the uncorrelation assumption and noting that the input noise, input desired signal, and input interference are uncorrelated, we have that the variance of $\eta_e(n)$ is

$$\sigma^2_{\eta_e} = E[\eta_e(n)\eta_e^*(n)] = \sigma^2_\eta + \zeta_{ISI} + \zeta_{CTI} \tag{6.6.6}$$

σ^2_η, ζ_{ISI} and ζ_{CTI} are the variance of η, ξ_{ISI} and ξ_{CTI} respectively. They are defined in Eqs. (6.3.4), (6.4.12) and (6.5.9). Because ζ_{CTI} is a periodic function, we take average value of ζ_{CTI}. The average value ζ_{CTIave} is defined in Eq. (6.5.11). Therefore, the variance of η_e should be modified as

$$\sigma^2_{\eta_e} = \sigma^2_\eta + \zeta_{ISI} + \zeta_{CTIave}. \tag{6.6.7}$$

The approximation accuracy is shown in Appendix D.

From the uncorrelation assumption, we also note that

$$E[\gamma_o\eta^*] = 0, \quad E[\gamma_o\xi^*_{ISI}] = 0, \quad \text{and} \quad E[\gamma_o\xi^*_{CTI}] = 0. \tag{6.6.8}$$

Therefore, we have

$$E[\gamma_o\eta_e^*] = 0. \tag{6.6.9}$$

Because γ_o and η_e have Gaussian distributions and they are uncorrelated each other, we conclude that γ_o and η_e are independent each other.

Let P_e denote the probability error of $\hat{d}(n)$, then

$$\begin{aligned} P_e &= \text{Prob}\left\{[\hat{d}(n) > 0 \cap d(n) = -1] \cup [\hat{d}(n) < 0 \cap d(n) = 1]\right\} \\ &= \frac{1}{2}\text{Prob}(-\gamma_o + \eta_e > 0) + \frac{1}{2}\text{Prob}(\gamma_o + \eta_e < 0). \end{aligned} \tag{6.6.10}$$

Using the Gaussian distribution approximations, we obtain

$$\begin{aligned} P_e &= \frac{1}{2}\int_{-\infty}^{\infty} p(\gamma_o)\int_{\gamma_o}^{\infty} \frac{1}{\sqrt{2\pi\sigma_{\eta_e}^2}} \exp^{\frac{-\eta_e^2}{2\sigma_{\eta_e}^2}} d\eta_e d\gamma_o + \frac{1}{2}\int_{-\infty}^{\infty} p(\gamma_o)\int_{-\infty}^{-\gamma_o} \frac{1}{\sqrt{2\pi\sigma_{\eta_e}^2}} \exp^{\frac{-\eta_e^2}{2\sigma_{\eta_e}^2}} d\eta_e d\gamma_o \\ &= \int_{-\infty}^{\infty} p(\gamma_o)\int_{\gamma_o}^{\infty} \frac{1}{\sqrt{2\pi\sigma_{\eta_e}^2}} \exp^{\frac{-\eta_e^2}{2\sigma_{\eta_e}^2}} d\eta_e d\gamma_o \end{aligned} \tag{6.6.11}$$

where $p(\gamma_o)$ is the probability density functions of γ_o.

Let $z = \frac{\eta_e}{\sqrt{2\sigma_{\eta_e}^2}}$, we have

$$P_e = \int_{-\infty}^{\infty} p(\gamma_o)\frac{1}{\sqrt{\pi}}\int_{\frac{\gamma_o}{\sqrt{2\sigma_{\eta_e}^2}}}^{\infty} e^{-z^2} dz d\gamma_o = \frac{1}{2}\int_{-\infty}^{\infty} p(\gamma_o)\text{erfc}\left(\frac{\gamma_o}{\sqrt{2\sigma_{\eta_e}^2}}\right) d\gamma_o \tag{6.6.12}$$

where $\text{erfc}(x) = \frac{2}{\sqrt{\pi}}\int_x^{\infty} e^{-z^2} dz$. Because γ_o also has Gaussian distribution, we obtain

$$P_e = \frac{1}{2}\int_{-\infty}^{\infty} \frac{1}{\sqrt{2\pi\sigma_{\gamma_o}^2}} \exp^{\frac{-(\gamma_o - \mu_{\gamma_o})^2}{2\sigma_{\gamma_o}^2}} \text{erfc}\left(\frac{\gamma_o}{\sqrt{2\sigma_{\eta_e}^2}}\right) d\gamma_o. \tag{6.6.13}$$

After some computations shown in Appendix E, we obtain

$$P_e = \frac{1}{2}\text{erfc}\left(\sqrt{\frac{(\mu_{\gamma_o})^2}{2\sigma_{\gamma_o}^2 + 2\sigma_{\eta_e}^2}}\right) = \frac{1}{2}\text{erfc}\left(\sqrt{\frac{(\mu_{\gamma_o})^2}{2(\sigma_{\gamma_o}^2 + \sigma_\eta^2 + \zeta_{ISI} + \zeta_{CTIave})}}\right). \tag{6.6.14}$$

Here, μ_{γ_o} and $\sigma_{\gamma_o}^2$ are the mean and the variance of γ_o and they are defined in Eqs. (6.4.9), (6.4.10) respectively. σ_η^2 is the output noise power of the system. ζ_{ISI} is the output ISI interference power of the system. ζ_{CTIave} is the average output cross talk interference power of the system. They are defined in Eqs. (6.3.4), (6.4.12) and (6.5.11) respectively.

In the above analysis, the filter coefficients are assumed to be the filter coefficients of the BLAST filter. We note that the above analytic steps are also suitable for the output probability error analysis of the TAST filter when the filter coefficients are the filter coefficients of the TAST filter. For the finite sample case, there is difference between output probability error of BLAST and that of TAST because there is filter coefficient difference between BLAST and TAST. When the number of sample is increased, the probability error difference between BLAST and TAST will be reduced because the filter coefficient difference between BLAST and TAST is reduced. Moreover, using the property 5.1, we note that the filter coefficients of the BLAST filter with infinite sample time average realization is equal to the filter coefficients of the TAST filter with infinite sample time average realization. Therefore, for the infinite sample time average realization of the filter coefficients, the output probability error of the BLAST filter should be same as the output probability error of the TAST filter.

6.7 Numerical Results

We now present computer numerical examples showing the output probability errors of the BLAST and TAST algorithms. The desired signal and the interfering signal are given respectively by

$$s(nT_s) = \sum_{k=-\infty}^{\infty} d(k)g(nT_s - kT_{b_1})\cos(2\pi f_1 nT_s) \tag{6.7.1}$$

$$u(nT_s) = \sum_{k=-\infty}^{\infty} d_u(k)g(nT_s - kT_{b_2})\cos(2\pi f_2 nT_s) \tag{6.7.2}$$

where T_{b_1} and T_{b_2} are the baud periods, f_1 and f_2 are the carrier frequency offsets of $s(nT_s)$ and $u(nT_s)$ respectively and T_s is the sampling period. $\{d(k)\}$ and $\{d_u(k)\}$ are stationary random binary sequences. For both the desired and interfering signals, we assume that $g(nT_s)$ and $g_u(nT_s)$ are the pulse obtained by the square root raised-cosine pulse shaping filter with a 100% roll-off factor [31]. In the following examples, we'll examine the output probability errors of the BLAST filter and the TAST filter against the different number of finite symbols, the different DOA difference or different spectral overlapping between the

desired signal and the interfering signal. Here the DOA difference between the desired signal and the interference is defined as the difference between the DOA of the desired signal and the DOA of the interference. In the following examples, we fix the DOA of the desired signal at 0° while we vary the DOA of the interference so that the DOA difference between the desired signal and the interference can be changed. The spectral overlapping between the desired signal and the interference is defined in Chapter 3. In the following examples, we choose that the baud rate of the desired signal is equal to the baud rate of the interference, i.e, the bandwidth of desired signal is equal to that of the interference. When we fix the carrier offset of the desired signal, we vary the carrier offset of the interference so that the spectral overlapping between the desired signal and the interference can be changed. Moreover, all frequencies we mentioned are normalized as the relative frequencies, relative the sampling rate.

Example 6.1: In this example, we examine the output probability errors of the BLAST filter and the TAST filter against the different number of finite symbols while we fix the DOA difference and the spectral overlapping between the desired signal and the interfering signal. The output probability errors of the BLAST filter and the TAST filter are evaluated both theoretically and by simulations. The theoretical probability errors of BLAST and TAST are evaluated by using Eq. (6.6.14). The desired and interfering signal are BPSK signals as given by Eqs. (6.7.1) and (6.7.2) respectively. The baud rates of the desired signal and the interference are equal which are 0.05, relative the sampling rate. The carrier frequency offset of the desired signal is fixed at $f_1 = 0.1$ and that of the interference is fixed at $f_2 = 0.17$, so that the two signals overlap on 30%. For the parameters of the BLAST filter and the TAST filter, the number of sensors is chosen at $L = 3$, the length of FIR filters in each FRESH filter is chosen at $N_o = 6$, the number of the branches of FRESH filter is chosen at $M = 2$. The frequency shift in the two branches are set at $\alpha_1 = 0.2$, $\alpha_2 = -0.2$ respectively. The shift frequency used in the reference path of the BLAST filter is set at $\alpha' = 0$. The DOA difference between the desired signal and the interference is fixed at 2°. The signal-to-interference ratio (SIR) at the input is fixed at 0dB whereas we vary the input signal-to-noise ratio (SNR). The filter coefficients of the BLAST and TAST filters in this example are calculated using 15, 25, 50, and 150 symbols respectively. The simulation

results and theoretical results of the BLAST and TAST filters against the different number of samples are shown Fig. 6.2(a) to Fig. 6.2(d). It can be observed that the theoretical results match the simulation results well. When the number of samples is increased, the output probability errors of BLAST and TAST are reduced. When the number of symbols is increased from 15 to 50, the output probability error is reduced fast, but when the number of symbols is increased from 50 to 150, the output probability error is reduced relatively slow. For the same finite symbols, the output probability error of the TAST filter is lower than that of the BLAST filter. The probability error difference between BLAST and TAST converges to zero when the number of symbols goes to infinite.

Example 6.2: In this example, we examine the finite sample output probability errors of the BLAST filter and the TAST filter against the different DOA differences between the desired signal and the interfering signal while we fix the number of finite symbols and the spectral overlapping between the desired signal and the interfering signal. The scenarios is similar to the example 6.1 except the DOA difference between the desired signal and the interfering signal and the number of finite symbols. The output probability errors of BLAST and TAST are evaluated both theoretically and by simulation. The finite sample probability errors of BLAST and TAST using number of symbols $N = 15$ against the different DOA difference 0°, 2°, 5°, and 10° are shown Fig. 6.3(a) to 6.3(d). It can be observed that the theoretical results match the simulation results well. When the DOA difference is increased, the output probability errors of BLAST and TAST are reduced. The reason is that the spatial information exploited by BLAST and TAST is increased when the DOA difference is increased. For the same finite symbol and the same DOA difference, the output probability error of the TAST filter is lower than that of the BLAST filter.

Example 6.3: In this example, we examine the finite symbol output probability errors of the BLAST and the TAST filters against the different spectral overlapping between the desired signal and the interfering signal while we fix the number of finite symbols and the DOA difference between the desired signal and the interfering signal. The scenarios is similar to the example 6.1 except the number of finite symbols, the DOA difference, and the spectral

overlapping between the desired signal and the interfering signal. The output probability errors of BLAST and TAST are evaluated both theoretically and by simulations. The number of symbols is 15. The spectral overlapping is 40%, 30%, 20% and 10% respectively. The DOA difference between the desired signal and the interference is fixed at 2° and 10° degrees respectively. When the DOA difference is 2° and number of symbols is 15, the finite symbol probability errors of BLAST and TAST against the spectral overlapping 40%, 30%, 20%, 10% are shown in Fig. 6.4(a) to 6.4(d). When the DOA difference is 10° and number of symbols is 15, the finite symbol probability errors of BLAST and TAST against the spectral overlapping 40%, 30%, 20%, 10% are shown in Fig. 6.5(a) to 6.5(d). It can be observed that the theoretical results match the simulation results well. For the same finite symbols, the same spectral overlapping, and the same DOA difference, the output probability error of the TAST filter is lower than that of the BLAST filter. When the spectral overlapping is reduced, the output probability errors of the BLAST and TAST filter are reduced. The reason is that the temporal information (spectral overlapping) exploited by BLAST and TAST is increased when the spectral overlapping is reduced. Comparing Fig. 6.4 with 6.5, we also can observed that when the spatial information (DOA difference) is increased, the output probability errors of the BLAST filter and that of the TAST filter are reduced.

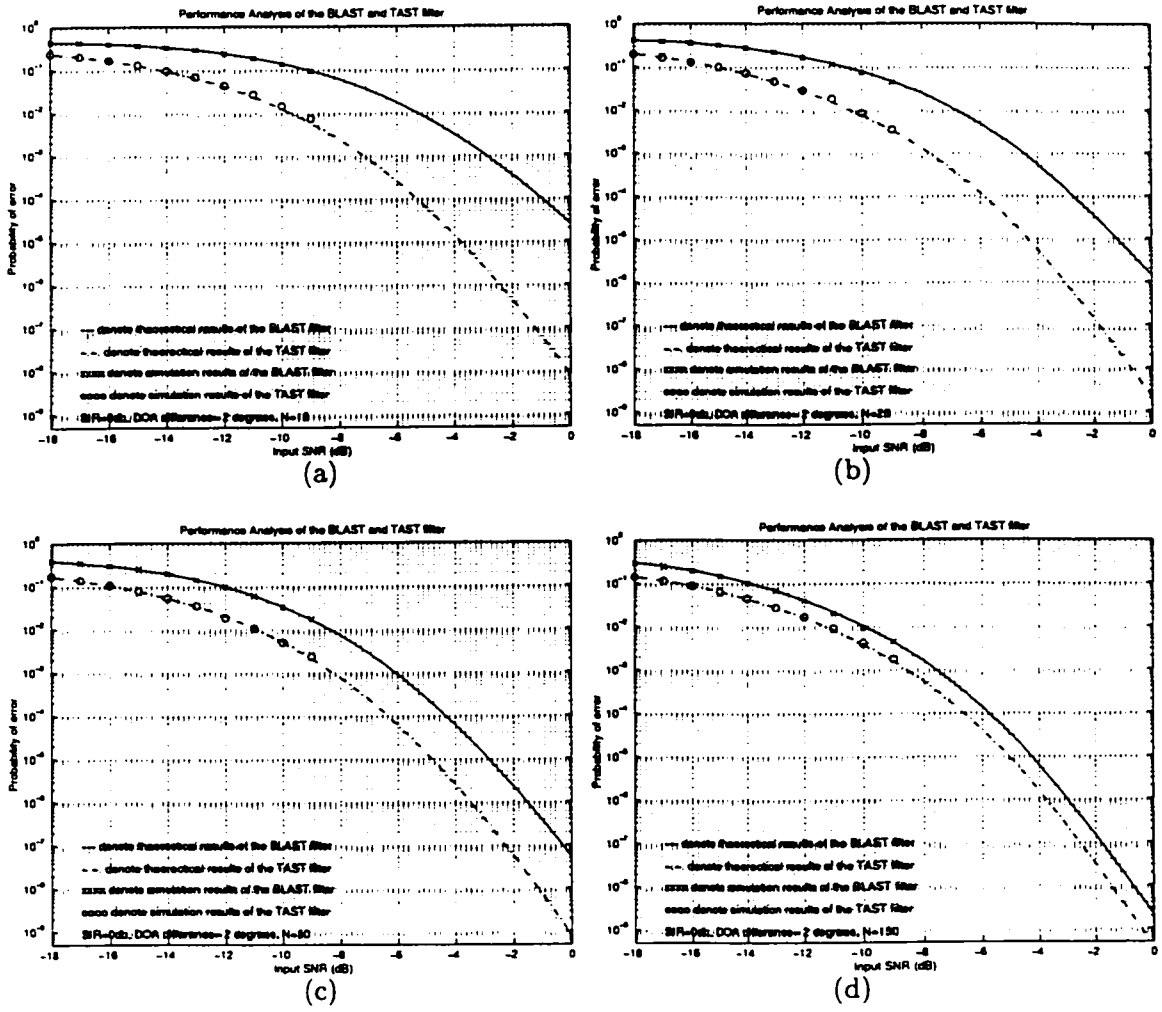

Figure 6.2: Output probability error of BLAST and TAST against different number of symbols N=15, 25, 50, and 150 when DOA difference is 2° and input SIR is 0dB

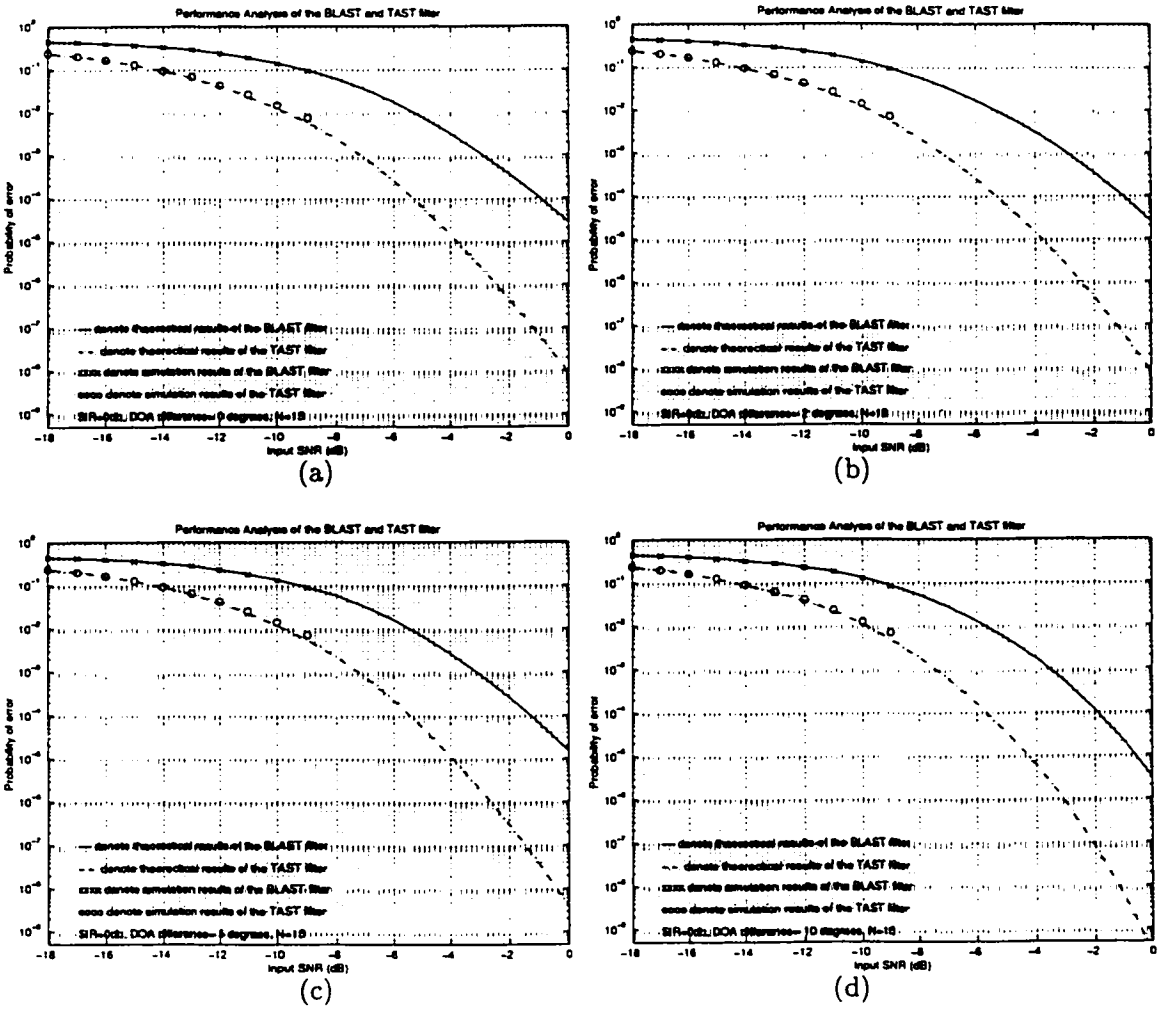

Figure 6.3: Output probability error of BLAST and TAST against different DOA difference 0°, 2°, 5°, and 10° when number of symbols is 15 and input SIR is 0dB

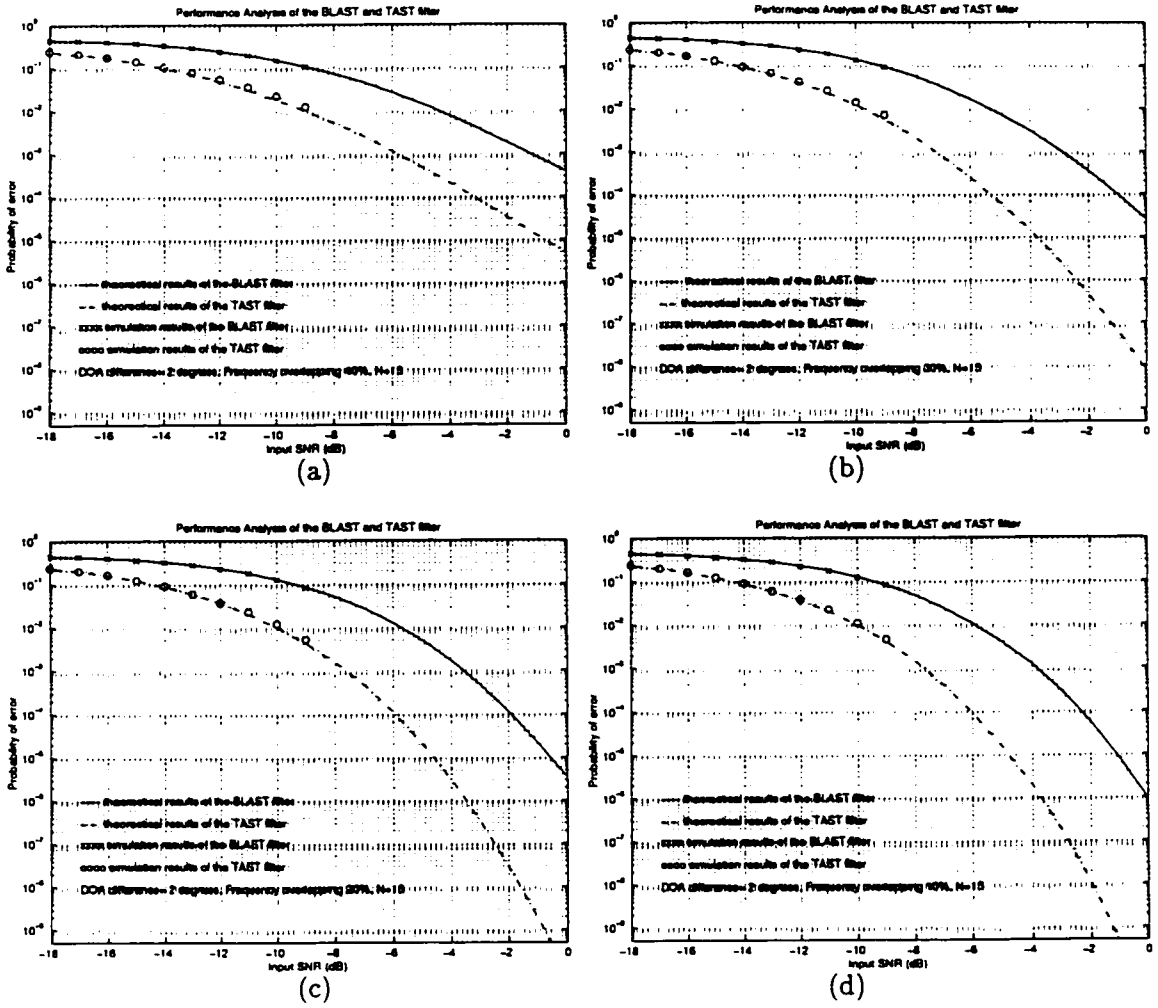

Figure 6.4: Output probability error of BLAST and TAST against different frequency overlapping 40%, 30%, 20%, and 10% when number of symbols is 15, DOA difference is 2°, and input SIR is 0dB

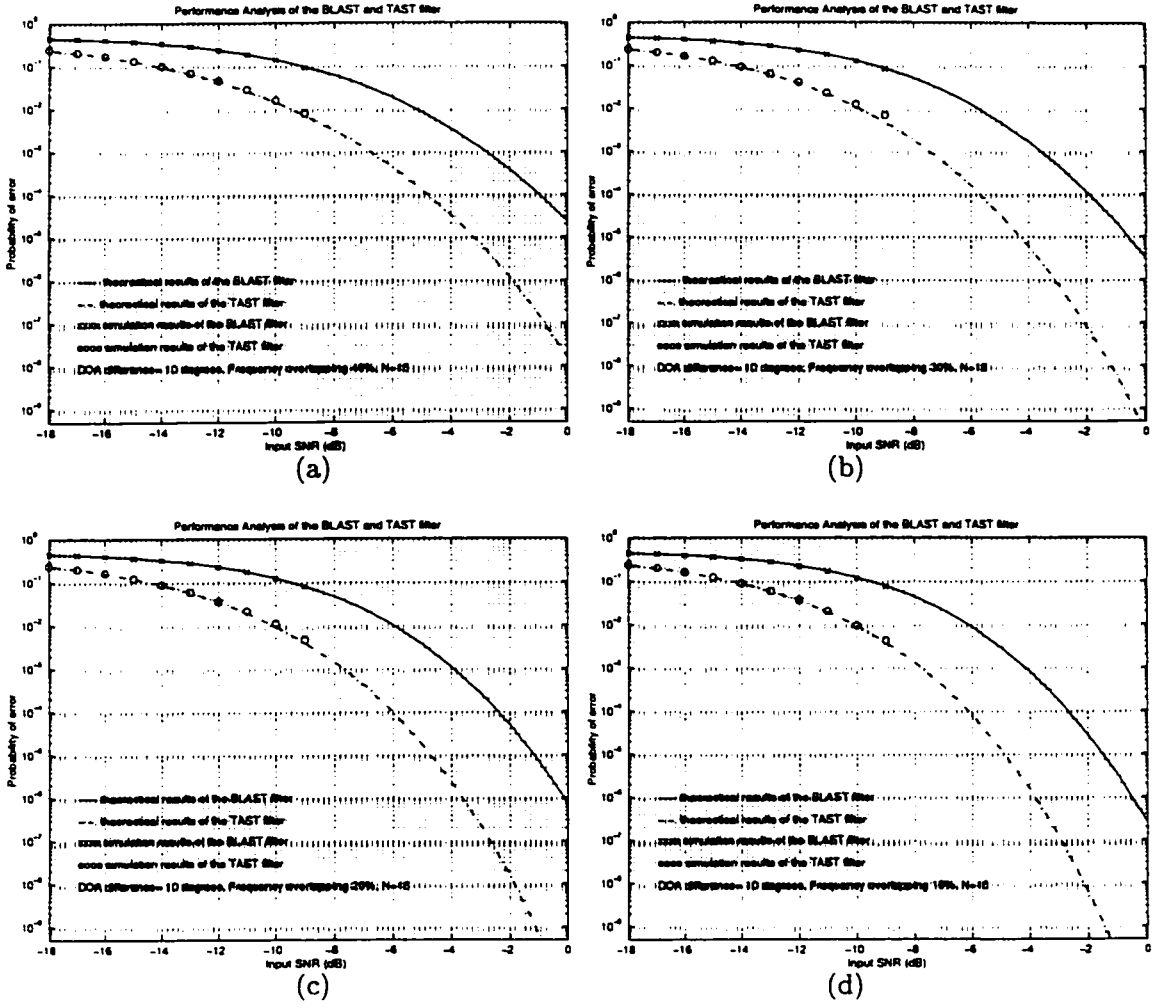

Figure 6.5: Output probability error of BLAST and TAST against different frequency overlapping 40%, 30%, 20%, and 10% when number of symbols is 15, DOA difference is 10° and input SIR is 0dB

Chapter 7

Conclusions

7.1 Thesis Summary

The thesis research background is the multi-user communication systems such as mobile wireless communication systems. Exploiting the cyclostationarity of the signals, two kinds of novel blind adaptive periodically time varying filtering algorithms are proposed to combat the CCI and ACI in multi-user communication systems. One algorithm is the BA-FRESH filtering algorithm and the other is the BLAST filtering algorithm.

For the proposed BA-FRESH filtering algorithm, the structure of the BA-FRESH filter is given. The criteria of the BA-FRESH algorithm is to maximize the normalized cross correlation between the output of the BA-FRESH filter and the frequency shift version of the input corrupted signal. Using the Schwarz inequality, we obtain its unique optimum solution. Using the Recursive Least Square (RLS) algorithm, the recursive implementation formula of the BA-FRESH filter is given. The BA-FRESH filtering algorithm does not require a training signal or the statistical knowledge of the desired signal. Comparing the BA-FRESH filter with the TA-FRESH filter, it is proved that two kinds of filters have same optimum solution when the observed data length is infinite, that is, both the BA-

FRESH filter and the TA-FRESH filter have same performances when the observed data length is infinite. However, when the observed data length is finite, there are differences between the optimum solution of the BA-FRESH filter and that of the TA-FRESH filter. The convergence rates of BA-FRESH and TA-FRESH to infinite sample optimum solution are determined. When the observed data length is finite, the filter coefficients of both the BA-FRESH filter and the TA-FRESH filter asymptotically converge in the mean square sense to the same optimum solution with convergence rates $O(\frac{1}{N})$, where N is the observed data length. Moreover, when the observed data length is finite, we also examine the finite sample output MSE and the finite sample output SINR of BA-FRESH and TA-FRESH. When the observed data length is finite, the finite sample output MSE of both BA-FRESH and TA-FRESH asymptotically converge in the mean square sense to the same optimum MSE respectively with convergence rates $O(\frac{1}{N})$. Similarly, when the observed data length is finite, the finite sample output SINR of both BA-FRESH and TA-FRESH asymptotically converge in the mean square sense to the same optimum SINR respectively with convergence rates $O(\frac{1}{N})$. We know the output probability error is a fundamental performance in a digital communication system. Therefore, the output probability error of the BA-FRESH and the TA-FRESH algorithms are analyzed for infinite sample case and finite sample case. Using the central limit theorem, approximate analytic expressions of the output probability error of BA-FRESH and TA-FRESH are obtained. Numerical results are presented to examine these results. Comparing the theoretical results with the simulation results, we found that the theoretical results and simulation results match well.

In order to exploit both spatial and temporal information of the signals, we proposed the BLAST algorithm. For the BLAST algorithm, it has advantages of both spatial and temporal filter because it exploits not only the spatial information but also the temporal information of the signals. By exploiting the cyclostationarity of the signals, the BLAST algorithm requires no desired signals and it can generate the training signal from the input corrupted signal. It can be viewed as an expansion of the BA-FRESH algorithm in the space-time domain. Moreover, when the length of FIR filter in each FRESH filters reduced as one, the BLAST algorithm is reduced as a blind adaptive cyclostationary beamforming algorithm. The structure of this BLAST filter is given in the thesis. For the BLAST

filter, its input antennas consist of L sensor array. For each sensors of the array, it follows a FRESH filter. By maximizing the cross correlation between the output of the BLAST filter and the frequency shift version of the received signal from the first sensor and using the Schwarz inequality, we obtain the optimum weighing coefficient vector of the BLAST filter. Comparing the optimum solution of the BLAST filter with that of the TAST filter, it is proved that both BLAST and TAST have same optimum solution when the observed data length is infinite, that is, both BLAST and TAST have same performance when the observed data length is infinite. However, when the observed data length is finite, there are differences between the optimum solution of the BLAST filter and that of the TAST filter. The convergence rates of BLAST and TAST to the infinite sample optimum solution are determined. When the observed data length is finite, the solutions of both BLAST and TAST asymptotically converge in the mean square sense to the same optimum solution with convergence rates $O(\frac{1}{N})$, where N is the observed data length. Moreover, we also examine the finite sample output MSE and the finite sample output SINR of both BLAST and TAST. When the observed data length is finite, the finite sample output MSE of both BLAST and TAST asymptotically converge in the mean square sense to the same optimum MSE with convergence rates $O(\frac{1}{N})$. Similarly, when the observed data length is finite, the finite sample output SINR of both BLAST and TAST asymptotically converge in the mean square sense to the same optimum SINR respectively with convergence rates $O(\frac{1}{N})$. The output probability error of the BLAST and the TAST algorithms are analyzed for infinite sample case and finite sample case. Using the central limit theorem, approximate analytic expressions of the output probability error of BLAST and TAST are obtained. Numerical results are presented to examine these analytic results. Simulation results show that for the DOA difference between the desired signal and the interferences is zero, the BLAST algorithm performs well while the cyclic beamforming algorithms fail. Comparing the theoretical results with the simulation results, the theoretical results and simulation results match well. These results also show that the use of such blind adaptive technique to extract desired signals from spectrally or spatially overlapping interferences is promising.

7.2 Suggestions of Future Work

Although the two blind adaptive algorithms are developed and their performances are studied, there are some interesting issues worth of investigations. These future research work can be as following:

- In this thesis, we just exploit the second order cyclostationarity to develop the algorithms. How to exploit higher order cyclostationarity to improve the performances of the proposed algorithms is worth to be investigated.
- In the proposed algorithms, we just exploits the cyclostationarity of signals. If we exploit both cyclostationarity and other signal properties such as constant modulus of signals simultaneously, we maybe able to propose other new space-time processing algorithms.
- In practice, for uncertainty of the channel model and uncertainty of the cycle frequencies exploited, robust blind adaptive space-time filtering algorithm is worth to be developed.

Appendix A

Proofs of Eqs (3.2.20) and (5.3.8) and Proof of Property 5.1

A.1: Proofs of Eqs. of (3.2.20) and (5.3.8)

In this Appendix, we use the gradient method to obtain the optimum solution of the TA-FRESH filter in Chapter 3 and the optimum solution of the TAST filter in Chapter 5. Because the TA-FRESH filter can be viewed as a special case of the TAST filter, we just prove the optimum solution of the TAST filter.

Proof:

$$e_{TST}(n) = s(n)e^{j2\pi\alpha' n} - \boldsymbol{q}_{TST}^{\dagger}\tilde{\boldsymbol{x}}(n)$$

$$\nabla J_{TST} = \frac{\partial J_{TST}}{\partial \boldsymbol{q}_R} + j\frac{\partial J_{TST}}{\partial \boldsymbol{q}_I}, \qquad \boldsymbol{q}_{TST} = \boldsymbol{q}_R + j\boldsymbol{q}_I$$

where $\boldsymbol{q}_R$ and $\boldsymbol{q}_I$ are the real part and the imaginary part of $\boldsymbol{q}_{TST}$.

$$\begin{aligned} J_{TST} &= \langle e_{TST}(n)e_{TST}^{*}(n)\rangle = \langle s(n)s^{*}(n)\rangle - \boldsymbol{q}_{TST}{}^{\dagger}\left\langle s^{*}(n)e^{-j2\pi\alpha' n}\tilde{\boldsymbol{x}}(n)\right\rangle \\ &\quad -\boldsymbol{q}_{TST}^{T}\left\langle s(n)e^{j2\pi\alpha' n}\tilde{\boldsymbol{x}}^{*}(n)\right\rangle + \boldsymbol{q}_{TST}{}^{\dagger}\left\langle \tilde{\boldsymbol{x}}(n)\tilde{\boldsymbol{x}}^{\dagger}(n)\right\rangle \boldsymbol{q}_{TST} \end{aligned}$$

$$\frac{\partial J_{TST}}{\partial \boldsymbol{q}_R} = -\left\langle s^{*}(n)e^{-j2\pi\alpha' n}\tilde{\boldsymbol{x}}(n)\right\rangle - \left\langle s(n)e^{j2\pi\alpha' n}\tilde{\boldsymbol{x}}^{*}(n)\right\rangle + 2\left\langle \tilde{\boldsymbol{x}}(n)\tilde{\boldsymbol{x}}^{\dagger}(n)\right\rangle \boldsymbol{q}_R$$

$$\frac{\partial J_{TST}}{\partial \boldsymbol{q}_I} = -j\left\langle s(n)e^{j2\pi\alpha' n}\tilde{\boldsymbol{x}}^*(n)\right\rangle + j\left\langle s^*(n)e^{-j2\pi\alpha' n}\tilde{\boldsymbol{x}}(n)\right\rangle + 2\left\langle \tilde{\boldsymbol{x}}(n)\tilde{\boldsymbol{x}}^\dagger\right\rangle \boldsymbol{q}_I$$

$$\nabla J_{TST} = \frac{\partial J_{TST}}{\partial \boldsymbol{q}_R} + j\frac{\partial J_{TST}}{\partial \boldsymbol{q}_I} = -2\left\langle s^*(n)e^{-j2\pi\alpha' n}\tilde{\boldsymbol{x}}(n)\right\rangle + 2\left\langle \tilde{\boldsymbol{x}}(n)\tilde{\boldsymbol{x}}^\dagger(n)\right\rangle \boldsymbol{q}_{TST}$$

Let $\nabla J_{TST} = 0$, we obtain

$$\boldsymbol{q}_{TST} = \boldsymbol{R}_{\tilde{x}\tilde{x}}^{-1}\left\langle \tilde{\boldsymbol{x}}(n)s^*(n)e^{-j2\pi\alpha' n}\right\rangle = \boldsymbol{R}_{\tilde{x}\tilde{x}}^{-1}\boldsymbol{\rho}_{\tilde{x}s'} \quad \square$$

A.2: Proof of Property 5.1

Proof: The input $x(n)$ consists of the desired signal components, the interference components, and the noise components. Thus,

$$\tilde{\boldsymbol{x}}(n) = \tilde{\boldsymbol{s}}(n) + \tilde{\boldsymbol{u}}(n) + \tilde{\boldsymbol{\nu}}(n)$$

where $\tilde{\boldsymbol{s}}(n)$, $\tilde{\boldsymbol{u}}(n)$ and $\tilde{\boldsymbol{\nu}}(n)$ are defined in Eqs. (5.2.7), (5.2.12), and (5.2.17) respectively. The reference signal $r(n)$ is,

$$r(n) = (s(n) + u(n) + \nu(n))e^{j2\pi\alpha' n}$$

where $u(n) = \sum_{k=1}^{K_o} u_k(n)$. Because $s(n)$, $u(n)$, and $\nu(n)$ are independent, under the infinite sample time average realization, we have

$$\left\langle \tilde{\boldsymbol{s}}(n)u^*(n)e^{-j2\pi\alpha' n}\right\rangle = 0 \qquad \left\langle \tilde{\boldsymbol{s}}(n)\nu^*(n)e^{-j2\pi\alpha' n}\right\rangle = 0$$

$$\left\langle \tilde{\boldsymbol{u}}(n)s^*(n)e^{-j2\pi\alpha' n}\right\rangle = 0 \qquad \left\langle \tilde{\boldsymbol{u}}(n)\nu^*(n)e^{-j2\pi\alpha' n}\right\rangle = 0$$

$$\left\langle \tilde{\boldsymbol{\nu}}(n)s^*(n)e^{-j2\pi\alpha' n}\right\rangle = 0 \qquad \left\langle \tilde{\boldsymbol{\nu}}(n)u^*(n)e^{-j2\pi\alpha' n}\right\rangle = 0.$$

So we obtain:

$$\boldsymbol{q}_{BST} = \boldsymbol{R}_{\tilde{x}\tilde{x}}^{-1}\left(\left\langle \tilde{\boldsymbol{s}}(n)s^*(n)e^{-j2\pi\alpha' n}\right\rangle + \left\langle \tilde{\boldsymbol{u}}(n)u^*(n)e^{-j2\pi\alpha' n}\right\rangle + \left\langle \tilde{\boldsymbol{\nu}}(n)\nu^*(n)e^{-j2\pi\alpha' n}\right\rangle\right)$$

Because we choose the parameters α_m and α' satisfy Eq. (5.3.10), we obtain

$$\left\langle \tilde{\boldsymbol{u}}(n)u^*(n)e^{-j2\pi\alpha' n} \right\rangle = 0.$$

Similarly, we have

$$\left\langle \tilde{\boldsymbol{\nu}}(n)\nu^*(n)e^{-j2\pi\alpha' n} \right\rangle = 0.$$

So we obtain

$$\boldsymbol{q}_{BST} = \boldsymbol{R}_{\tilde{\boldsymbol{x}}\tilde{\boldsymbol{x}}}^{-1}\boldsymbol{\rho}_{\tilde{\boldsymbol{s}}\tilde{\boldsymbol{s}}'} = \boldsymbol{q}_{opt}.$$

Using Eq. (5.3.8) and noting $s(n)$, $u(n)$, and $\nu(n)$ are independent, similiarly we obtain

$$\boldsymbol{q}_{TST} = \boldsymbol{R}_{\tilde{\boldsymbol{x}}\tilde{\boldsymbol{x}}}^{-1}\boldsymbol{\rho}_{\tilde{\boldsymbol{s}}\tilde{\boldsymbol{s}}'} = \boldsymbol{q}_{opt}. \quad \square$$

Appendix B

Approximation of Uncorrelation Assumption

In this appendix, we examine the uncorrelation assumption in Chapter 3 and the uncorrelation assumption in Chapter 6. Because the uncorrelation assumption in Chapter 3 can be viewed as a special case in Chapter 6, we just discuss the uncorrelation assumption in Chapter 6. In order to simplify our analysis, we assume that the filter coefficient vector $\boldsymbol{q}_{BST}$ is uncorrelated with the input white noise $\nu(n)$, the input desired binary signal $d(n)$ and the input interfering binary signals $d_u(n)$. For the infinite sample time average realization, using the property 5.1, we note that the filter coefficients vector of the BLAST filter $\boldsymbol{q}_{BST}$ is a constant vectors $\boldsymbol{q}_{opt}$ which is defined in Eq. (5.3.11). Therefore, the uncorrelation assumption is valid in the infinite sample case. For the finite sample time average realization, the filter coefficient vectors $\hat{\boldsymbol{q}}_{BST}(N)$ are random vectors with an unknown probability density function. It is difficult to examine the uncorrelation assumption theoretically in the finite sample case. Here, we use an experimental method to examine the assumption. We do K times experiments. For the kth experiments, We generate kth random samples of the correlation

$$\boldsymbol{g}_k(N) = a_k(N)\boldsymbol{q}_k(N),$$

where $a_k(N)$ denotes input binary signal or the input white noise in the kth experiment, $q_k(N)$ denotes the finite sample time average realization of the filter coefficients $\hat{q}_{BST}(N)$ in the kth experiment, N is the number of data length. We calculate the normalized correlation value

$$\bar{g} = \frac{\left\| \frac{1}{K} \sum_k g_k(N) \right\|^2}{\frac{1}{K} \sum_k \|g_k(N)\|^2}.$$

In the following example, we choose $K = 20000$, where K is number of experiments. Given N, where N is the data length. Let $\bar{g}_d$ denote the normalized correlation between input desired signal and the finite sample time average realization of filter coefficients $\hat{q}_{BST}(N)$. $\bar{g}_u$ denote the normalized correlation between input interfering signal and the finite sample time average realization of filter coefficients $\hat{q}_{BST}(N)$. $\bar{g}_v$ denote the normalized correlation between input noise and the finite sample time average realization of filter coefficients $\hat{q}_{BST}(N)$. Given the input SIR=0dB, and SNR=0dB. We choose $N = 15$, $N = 25$, $N = 50$, and $N = 150$ respectively, where N is the data length. The desired and interfering signal are BPSK signals as given by Eqs. (6.7.1) and (6.7.2) respectively. The baud rates of the desired signal and the interference are equal which are 5kHz. The carrier frequency offset of the desired signal is fixed at $f_1 = 10$kHz and that of the interference is fixed at $f_2 = 17$kHz, so that the spectral overlapping between the two signals is 30%. The sampling rate $f = 100$kHz. For the parameters of the BLAST and TAST filters, the number of sensors is chosen at $L = 3$, the length of FIR filters in each FRESH filter is chosen at $N_o = 6$, the number of the branches of FRESH filter is chosen at $M = 2$. The frequency shift in the two branches are set at $\alpha_1 = 20$kHz, $\alpha_2 = -20$kHz respectively. The shift frequency used in the reference path of the BLAST filter is set at $\alpha' = 0$kHz. Both the input SIR and the input SNR are fixed at 0dB. The DOA difference between the desired signal and the interference is fixed at 0°. We obtain the following correlation values in Table B.1. From Table B.1, we can see that these correlation values are very small. When we fixed the number of data length N at 15 and the spectral overlapping is 30%, we change the DOA difference to be $0°, 2°, 5°$, and 10° respectively, we obtain the following correlation values in Table B.2. From Table B.2, we can see that these correlation values are very small. When we fixed the number of data length N at 15 and the DOA

	N=10	N=25	N=50	N=150
$\bar{g}_d$	0.4513×10^{-4}	0.5206×10^{-4}	0.1876×10^{-4}	0.1884×10^{-4}
$\bar{g}_u$	0.4362×10^{-4}	0.7884×10^{-4}	0.2322×10^{-4}	0.7760×10^{-4}
$\bar{g}_v$	0.7359×10^{-4}	0.4472×10^{-4}	0.2456×10^{-4}	0.0677×10^{-4}

Table B.1: The normalized correlation between the input signal and filter coefficients against data length N=10, 25, 50, and 150 for K=20000

	0°	2°	5°	10°
$\bar{g}_d$	0.4513×10^{-4}	0.4417×10^{-4}	0.4282×10^{-4}	0.4176×10^{-4}
$\bar{g}_u$	0.4362×10^{-4}	0.4338×10^{-4}	0.4298×10^{-4}	0.4248×10^{-4}
$\bar{g}_v$	0.7359×10^{-4}	0.7431×10^{-4}	0.7576×10^{-4}	0.7597×10^{-4}

Table B.2: The normalized correlation between the input signal and filter coefficients against the different DOA difference 0°, 2°, 5°, and 10° for K=20000.

difference at 10°, we change the spectral overlapping to be 40%, 30% 20%, and 10% respectively, we obtain the following correlation values in Table B.3. From Table B.3, we can see that these correlation values are very small. From Table B.1 to Table B.3, we can see that these correlation values are very small. Therefore, we say the uncorrelation assumption is valid in the finite symbol case.

	40%	30%	20%	10%
$\bar{g}_d$	0.5266×10^{-4}	0.4513×10^{-4}	0.4719×10^{-4}	0.5167×10^{-4}
$\bar{g}_u$	0.3873×10^{-4}	0.4362×10^{-4}	0.4975×10^{-4}	0.4480×10^{-4}
$\bar{g}_v$	0.1025×10^{-4}	0.0736×10^{-4}	0.0703×10^{-4}	0.0657×10^{-4}

Table B.3: The normalized correlation between the input signal and filter coefficients against the different spectral overlapping 40%, 30%, 20%,and 10% for K=20000.

Appendix C

Approximation of γ_o by a Gaussian Distribution

In this appendix, we discuss the approximation accuracy of γ_o by a Gaussian distribution in Chapter 4 and Chapter 6. Because the case in Chapter 4 can be viewed as a special case in Chapter 6, we just discuss the approximation accuracy of γ_o by a Gaussian distribution in Chapter 6. Re-write the definition of γ_o here for convenience

$$\begin{aligned}\gamma_o &= \sum_{\lambda=1}^{L}\sum_{k=1}^{N_o+L_2-1}\sum_{l=1}^{J}\sum_{m=0}^{L_2-1} g(-k) \\ &\quad \mathrm{Re}\left[h_{\lambda l}(k-m)e^{-j2\pi\alpha_l(k-m)}p(m)e^{-j2\pi\alpha_l m}e^{-j2\pi(\lambda-1)\theta_s}\right]\cos(2\pi\Delta f_c m)\cos(2\pi\Delta f_c k) \\ &\quad +\sum_{\lambda=1}^{L}\sum_{k=1}^{N_o+L_2-1}\sum_{l=J+1}^{M}\sum_{m=0}^{L_2-1} g(-k) \\ &\quad \mathrm{Re}\left[h_{\lambda l}(k-m)e^{-j2\pi\alpha_l(k-m)}p(m)e^{-j2\pi\alpha_l m}e^{j2\pi(\lambda-1)\theta_s}\right]\cos(2\pi\Delta f_c m)\cos(2\pi\Delta f_c k).\end{aligned}$$

Here, the filter coefficient $h_{\lambda,m}(n)$ $(\lambda = 1,2,\cdots L, m = 1,2,\cdots M)$ denotes the impulse response of the mth FIR filter in the lth FRESH filter, where M and L are the number of the branch of the FRESH filter and the number of sensors respectively. These filter coefficients consist of the filter coefficient vector of the BLAST filter $\boldsymbol{q}_{BST}$ which is defined in Eq. (5.3.3). For the infinite sample time average realization of $\boldsymbol{q}_{BST}$, $\boldsymbol{q}_{BST}$ is the constant

vector q_{opt} which is defined in Eq. (5.3.11). For the finite sample time average realization of q_{BST}, q_{BST} is the random vector $\hat{q}_{BST}(N)$ which is defined in Eq. (5.4.2). $\hat{q}_{BST}(N)$ is the function of N, where N is the data length. Because γ_o is linear combination of these filter coefficients, we see that γ_o is a constant for the infinite data length case. For the finite data length case, as the linear combination of a large number of random variables $h_{\lambda,m}(n)$, γ_o can be approximated by Gaussian distribution with the mean

$$\begin{aligned}\mu_{\gamma_o} &= \sum_{\lambda=1}^{L}\sum_{k=1}^{N_o+L_2-1}\sum_{l=1}^{J}\sum_{m=0}^{L_2-1} g(-k) \\ &\quad \mathrm{Re}\left[E[h_{\lambda l}(k-m)]e^{-j2\pi\alpha_l(k-m)}p(m)e^{-j2\pi\alpha_l m}e^{-j2\pi(\lambda-1)\theta_s}\right]\cos(2\pi\Delta f_c m)\cos(2\pi\Delta f_c k) \\ &\quad +\sum_{\lambda=1}^{L}\sum_{k=1}^{N_o+L_2-1}\sum_{l=J+1}^{M}\sum_{m=0}^{L_2-1} g(-k) \\ &\quad \mathrm{Re}\left[E[h_{\lambda l}(k-m)]e^{-j2\pi\alpha_l(k-m)}p(m)e^{-j2\pi\alpha_l m}e^{j2\pi(\lambda-1)\theta_s}\right]\cos(2\pi\Delta f_c m)\cos(2\pi\Delta f_c k)\end{aligned}$$

and the variance

$$\sigma^2_{\gamma_o} = E[\gamma_o^2] - \mu^2_{\gamma_o}.$$

The probability density function (pdf) of γ_o is therefore,

$$p_{\gamma_o}(z) = \frac{1}{\sqrt{2\pi\sigma^2_{\gamma_o}}}\exp\left(-\frac{(z-\mu_{\gamma_o})^2}{2\sigma^2_{\gamma_o}}\right).$$

Now we use experimental method to demonstrate the accuracy of the approximation. Given the data length N, SIR=0dB, and SNR=0dB, we do K times experiments to generate K samples of the filter coefficient $h_{\lambda,m}(n)$. We use the kth sample of the filter coefficients to compute the kth value of γ_o. When K is large enough, we obtain a long sequence of $\gamma_o(N)$. For the finite data length case, $\gamma_o(N)$ is a random sequence. For the experimentally generated γ_o, a histogram Hist(b_i, y_i) can be obtained, where b_i is the center of ith bin, the bin size b_s is given by $b_{i+1} - b_i$ and y_i is the accumulation number. We normalize a histogram by

$$\bar{y}_i = \frac{y_i}{b_s\sum_i y_i}$$

such that

$$\sum_i \bar{y}_i b_s = 1.$$

In the following examples, we choose $K = 100000$, where K is number of experiments. We choose $N = 15$, $N = 25$, $N = 50$, and $N = 150$ respectively, where N is the data length. The number of bins of the histograms is chosen to be 50. The desired and interfering signal are BPSK signals as given by Eqs. (6.7.1) and (6.7.2) respectively. The baud rates of the desired signal and the interference are equal which are 5kHz. The carrier frequency offset of the desired signal is fixed at $f_1 = 10$kHz and that of the interference is fixed at $f_2 = 17$kHz, so that the spectral overlapping between the two signals is 30%. The sampling rate $f = 100$kHz. For the parameters of the BLAST and TAST filters, the number of sensors is chosen at $L = 3$, the length of FIR filters in each FRESH filter is chosen at $N_o = 6$, the number of the branches of FRESH filter is chosen at $M = 2$. The frequency shift in the two branches are set at $\alpha_1 = 20$kHz, $\alpha_2 = -20$kHz respectively. The shift frequency used in the reference path of the BLAST filter is set at $\alpha' = 0$kHz. Both the input SIR and the input SNR are fixed at 0dB. The DOA difference between the desired signal and the interference is fixed at 0°. We plot these histograms of γ_o with the assumption of the pdf of γ_o against different data length 15, 25, 50, and 150 in Fig. C.1(a) to C.1(d) respectively. Comparing these histograms with the assumption of the pdf of γ_o, we can see heuristically how accurate the approximation is. Moreover we use the square error between the experimental histogram and the theoretical curve to be a measure of the approximation accuracy. The results are in the Table C.1.

$$d^2 = \sum (\bar{y}_i - p_{\gamma_o}(b_i))^2 b_s^2.$$

It can be observed from Figs. C.1(a) to C.1(d), and Tables C.1 that the approximation of γ_o as a Gaussian distribution with the mean μ_{γ_o} and the variance $\sigma^2_{\gamma_o}$ is accurate. Moreover, it also can be observed from Table C.1 that the mean of γ_o is increased and the variance of γ_o is decreased when the number of data length is increased. When we fixed the number of data length N at 15, we plot these histograms of γ_o with the assumption of the pdf of γ_o against different DOA difference $0°, 2°, 5°$, and $10°$ in Fig. C.2(a) to C.2(d) respectively. Comparing

these histograms with the assumption of the pdf of γ_o, we can see heuristically how accurate the approximation is. Moreover we use the square error between the experimental histogram and the theoretical curve to be a measure of the approximation accuracy. The results are in the Table C.2. It can be observed from Figs. C.2(a) to C.2(d), and Tables C.2 that the approximation of γ_o as a Gaussian distribution with the mean μ_{γ_o} and the variance $\sigma^2_{\gamma_o}$ is accurate. Moreover, it also can be observed from Table C.2 that the mean of γ_o is increased and the variance of γ_o is almost unchanged when the DOA difference is increased. When we fixed the number of data length N at 15 and the DOA difference at 10°, we plot these histograms of γ_o with the assumption of the pdf of γ_o against different spectral overlapping 40%, 30% 20%, and 10% in Fig. C.3(a) to C.3(d) respectively. Comparing these histograms with the assumption of the pdf of γ_o, we can see heuristically how accurate the approximation is. Moreover we use the square error between the experimental histogram and the theoretical curve to be a measure of the approximation accuracy. The results are in the Table C.3. It can be observed from Figs. C.3(a) to C.3(d), and Tables C.3 that the approximation of γ_o as a Gaussian distribution with the mean μ_{γ_o} and the variance $\sigma^2_{\gamma_o}$ is accurate. Moreover, it also can be observed from Table C.3 that the mean of γ_o is increased and the variance of γ_o is reduced when the spectral overlapping is reduced. Moreover, to investigate the Gaussinity of γ_o further, we use same scenarios above and change the input SNR to be 10 dB and 20 dB respectively. The mean and the variance of γ_o and the mean square error between the experimental histogram and the theoretical pdf of γ_o are tablized in Table C.4 to Table C.9. The related histogram comparisons are shown in Fig. C.4 to Fig. C.9. It can be observed from Figs. C.4 to C.9, and from Tables C.4 to C.9 that the approximation of γ_o as a Gaussian distribution with the mean μ_{γ_o} and the variance $\sigma^2_{\gamma_o}$ is accurate.

	N=15	N=25	N=50	N=150
$\hat{\mu}_{\gamma_o}$	0.3409	0.3472	0.3514	0.3539
$\hat{\sigma}^2_{\gamma_o}$	6.8×10^{-4}	3.5×10^{-4}	1.5×10^{-4}	4.9×10^{-5}
d^2	2.5×10^{-5}	9.7×10^{-6}	5.2×10^{-6}	6.4×10^{-5}

Table C.1: The mean and the variance of γ_o and the mean square error between the experimental histogram and the theoretical pdf curve of γ_o for N=15, 25, 50, and 150 when the input SNR is 0dB, the DOA difference is 0°, and the spectral overlapping is 30%

	0°	2°	5°	10°
$\hat{\mu}_{\gamma_o}$	0.3409	0.3425	0.3498	0.3684
$\hat{\sigma}^2_{\gamma_o}$	6.8×10^{-4}	6.8×10^{-4}	6.8×10^{-4}	6.8×10^{-4}
d^2	2.6×10^{-5}	2.6×10^{-5}	3.0×10^{-5}	2.9×10^{-5}

Table C.2: The mean and the variance of γ_o and the mean square error between the experimental histogram and the theoretical pdf curve of γ_o for 0°, 2°, 5°, and 10° when the input SNR is 0dB, the data length is 15, and the spectral overlapping is 30%

	40%	30%	20%	10%
$\hat{\mu}_{\gamma_o}$	0.3596	0.3684	0.3764	0.3844
$\hat{\sigma}^2_{\gamma_o}$	8.6×10^{-4}	6.8×10^{-4}	6.0×10^{-4}	5.7×10^{-4}
d^2	4.0×10^{-4}	2.9×10^{-5}	7.7×10^{-6}	1.4×10^{-5}

Table C.3: The mean and the variance of γ_o and the mean square error between the experimental histogram and the theoretical pdf curve of γ_o for 40%, 30%, 20%, and 10% when the input SNR is 0dB, the data length is 15, and the DOA difference is 10°

	N=15	N=25	N=50	N=150
$\hat{\mu}_{\gamma_o}$	0.4106	0.4123	0.4135	0.4142
$\hat{\sigma}^2_{\gamma_o}$	3.3×10^{-4}	1.6×10^{-4}	6.8×10^{-5}	2.0×10^{-5}
d^2	4.9×10^{-5}	2.3×10^{-5}	8.8×10^{-6}	9.8×10^{-6}

Table C.4: The mean and the variance of γ_o and the mean square error between the experimental histogram and the theoretical pdf curve of γ_o for N=15, 25, 50, and 150 when the input SNR is 10dB, the DOA difference is 0°, and the spectral overlapping is 30%

	0°	2°	5°	10°
$\hat{\mu}_{\gamma_o}$	0.4106	0.4154	0.4313	0.4506
$\hat{\sigma}^2_{\gamma_o}$	3.3×10^{-4}	3.2×10^{-4}	2.9×10^{-4}	2.8×10^{-4}
d^2	4.9×10^{-5}	4.7×10^{-5}	3.9×10^{-5}	3.2×10^{-5}

Table C.5: The mean and the variance of γ_o and the mean square error between the experimental histogram and the theoretical pdf curve of γ_o for 0°, 2°, 5°, and 10° when the input SNR is 10dB, the data length is 15, and the spectral overlapping is 30%

	40%	30%	20%	10%
$\hat{\mu}_{\gamma_o}$	0.4490	0.4506	0.4521	0.4541
$\hat{\sigma}^2_{\gamma_o}$	5.4×10^{-4}	2.8×10^{-4}	1.8×10^{-4}	1.5×10^{-4}
d^2	7.6×10^{-5}	3.2×10^{-5}	6.0×10^{-6}	1.2×10^{-5}

Table C.6: The mean and the variance of γ_o and the mean square error between the experimental histogram and the theoretical pdf curve of γ_o for 40%, 30%, 20%, and 10% when the input SNR is 10dB, the data length is 15, and the DOA difference is 10°

	N=15	N=25	N=50	N=150
$\hat{\mu}_{\gamma_o}$	0.4223	0.4226	0.4229	0.4231
$\hat{\sigma}^2_{\gamma_o}$	2.9×10^{-4}	1.4×10^{-4}	5.7×10^{-5}	1.7×10^{-5}
d^2	6.9×10^{-5}	2.8×10^{-5}	1.9×10^{-5}	1.0×10^{-5}

Table C.7: The mean and the variance of γ_o and the mean square error between the experimental histogram and the theoretical pdf curve of γ_o for N=15, 25, 50, and 150 when the input SNR is 20dB, the DOA difference is 0°, and the spectral overlapping is 30%

	0°	2°	5°	10°
$\hat{\mu}_{\gamma_o}$	0.4223	0.4435	0.4632	0.4696
$\hat{\sigma}^2_{\gamma_o}$	2.9×10^{-4}	2.4×10^{-4}	2.3×10^{-4}	2.2×10^{-4}
d^2	6.9×10^{-5}	5.7×10^{-5}	3.2×10^{-5}	3.0×10^{-5}

Table C.8: The mean and the variance of γ_o and the mean square error between the experimental histogram and the theoretical pdf curve of γ_o for 0°, 2°, 5°, and 10° when the input SNR is 20dB, the data length is 15, and the spectral overlapping is 30%

	40%	30%	20%	10%
$\hat{\mu}_{\gamma_o}$	0.4694	0.4696	0.4698	0.4705
$\hat{\sigma}^2_{\gamma_o}$	5.1×10^{-4}	2.2×10^{-4}	1.1×10^{-4}	8.8×10^{-5}
d^2	6.1×10^{-5}	3.0×10^{-5}	1.7×10^{-5}	1.1×10^{-5}

Table C.9: The mean and the variance of γ_o and the mean square error between the experimental histogram and the theoretical pdf curve of γ_o for 40%, 30%, 20%, and 10% when the input SNR is 20dB, the data length is 15, and the DOA difference is 10°

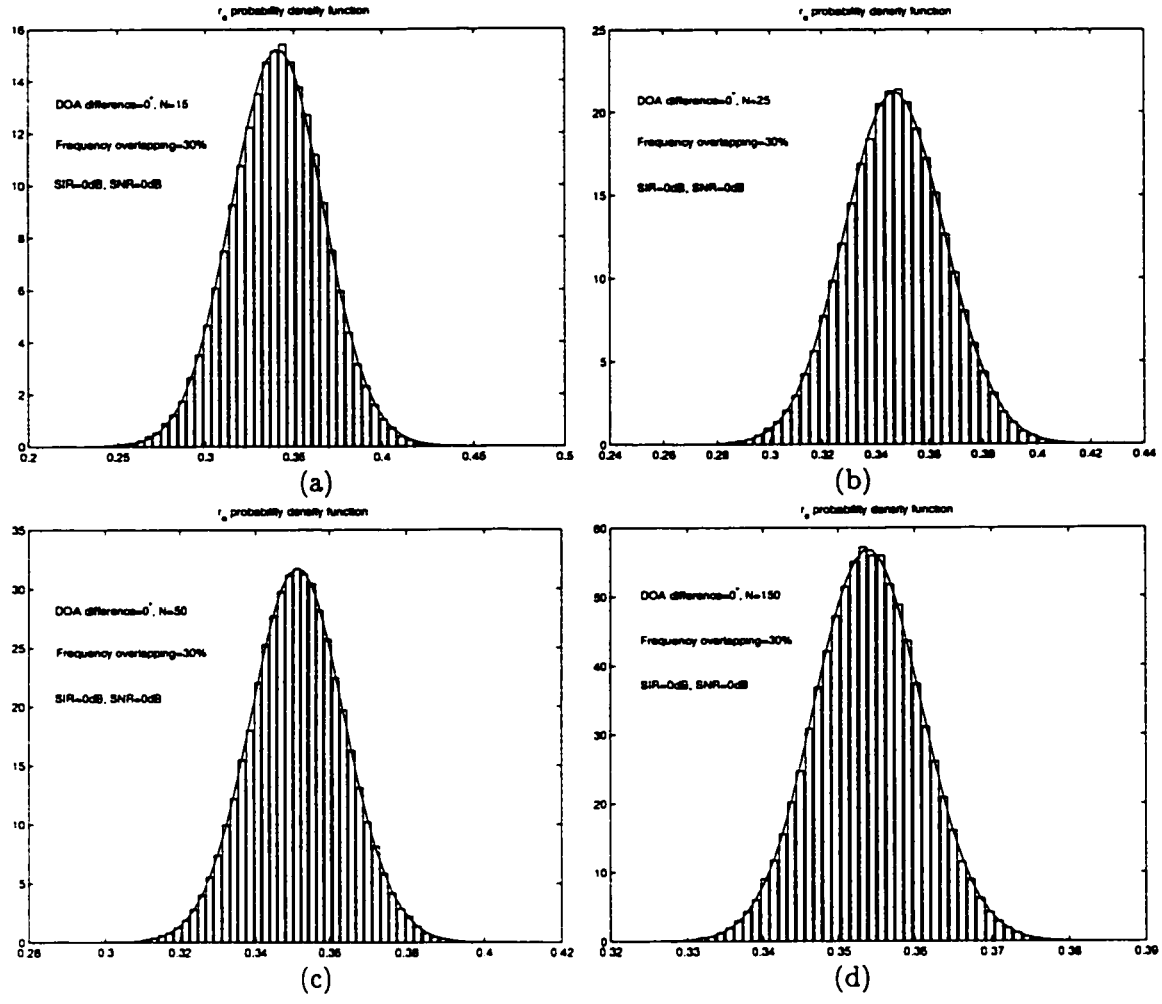

Figure C.1: Comparison between the experimental histogram and the theoretical pdf curve of γ_o for N=15, 25, 50, and 150 when the input SNR is 0dB

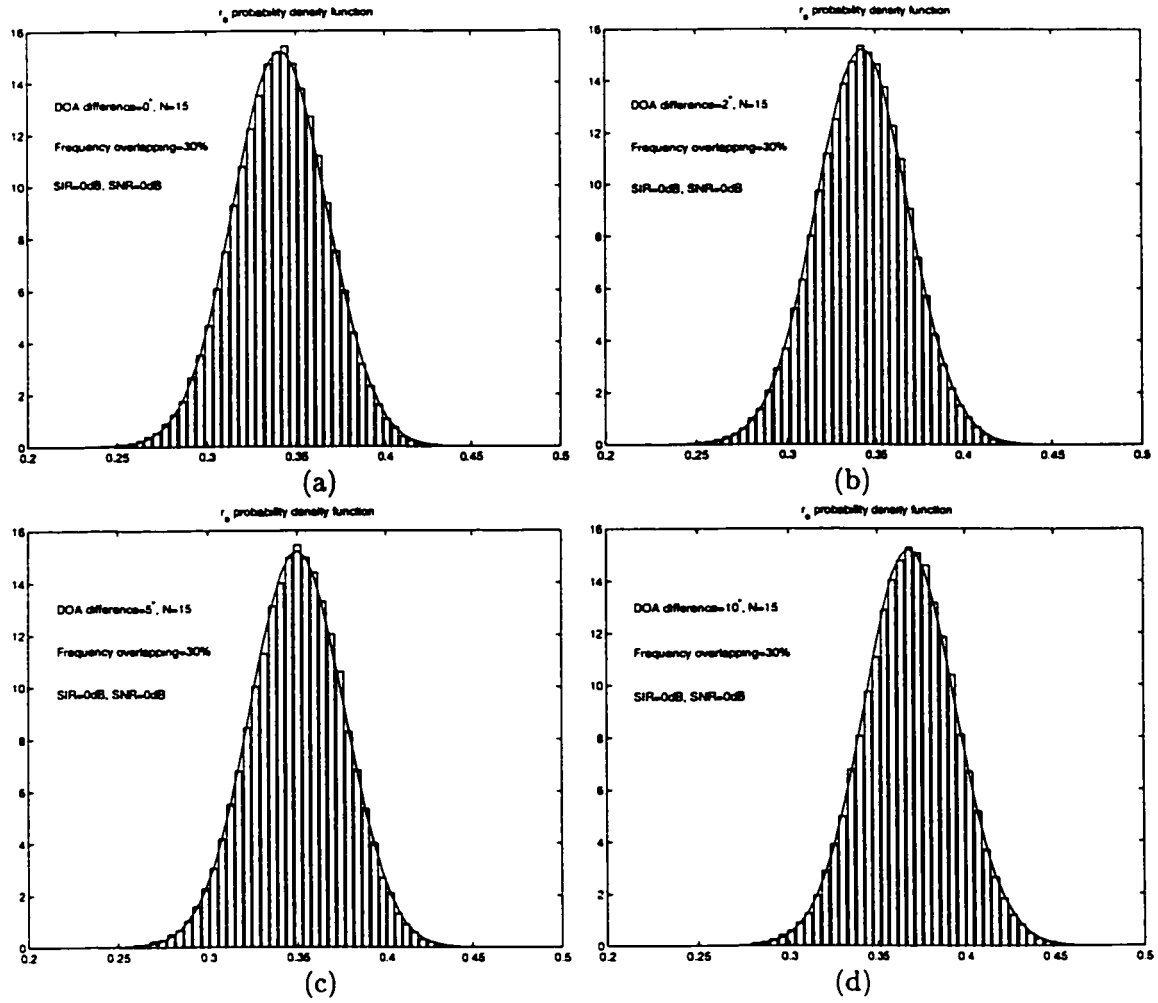

Figure C.2: Comparison between the experimental histogram and the theoretical pdf curve of γ_o for the DOA difference 0°, 2°, 5°, and 10° when the input SNR is 0dB

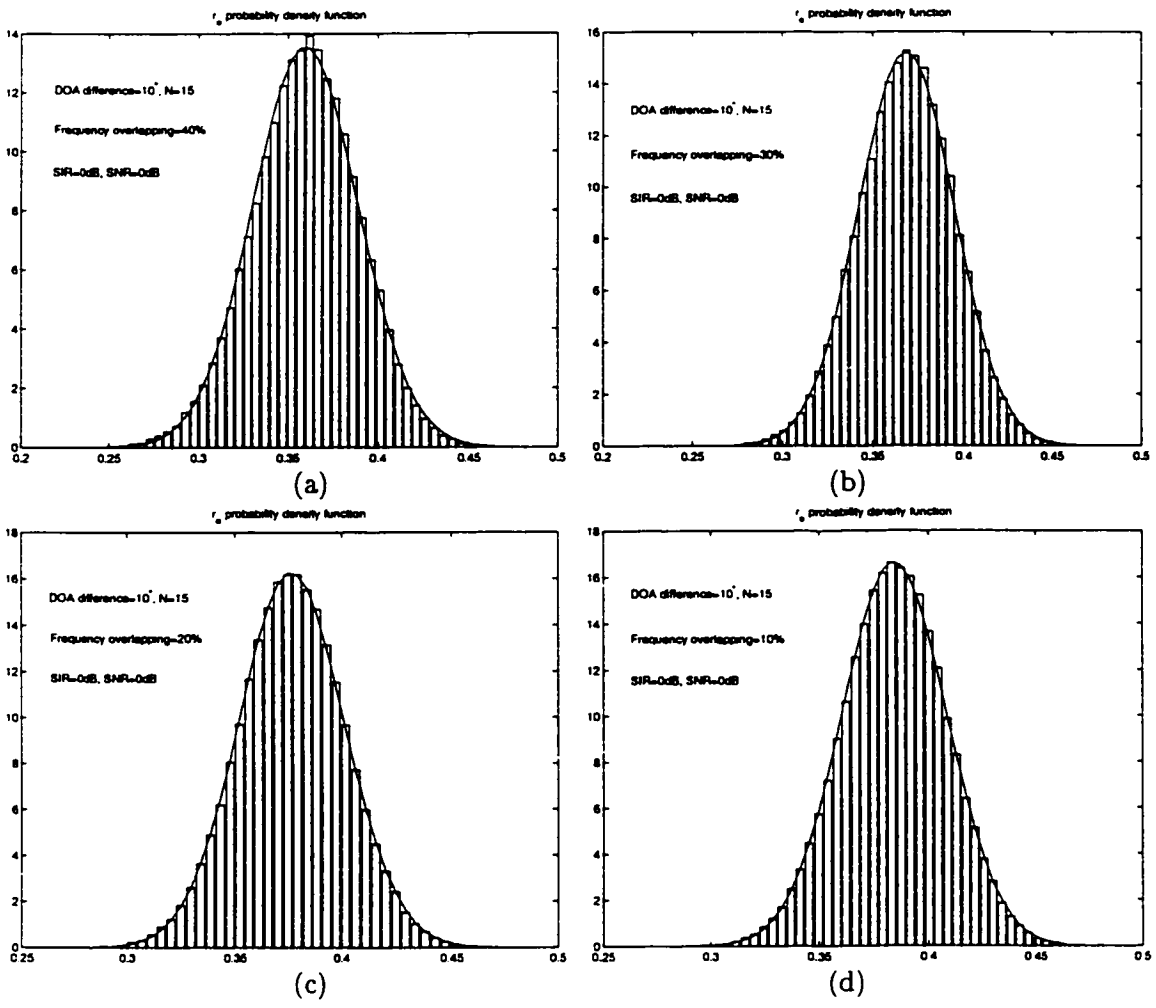

Figure C.3: Comparison between the experimental histogram and the theoretical pdf curve of γ_o for different spectral overlapping 40%, 30%, 20%, and 10% when input SNR is 0dB

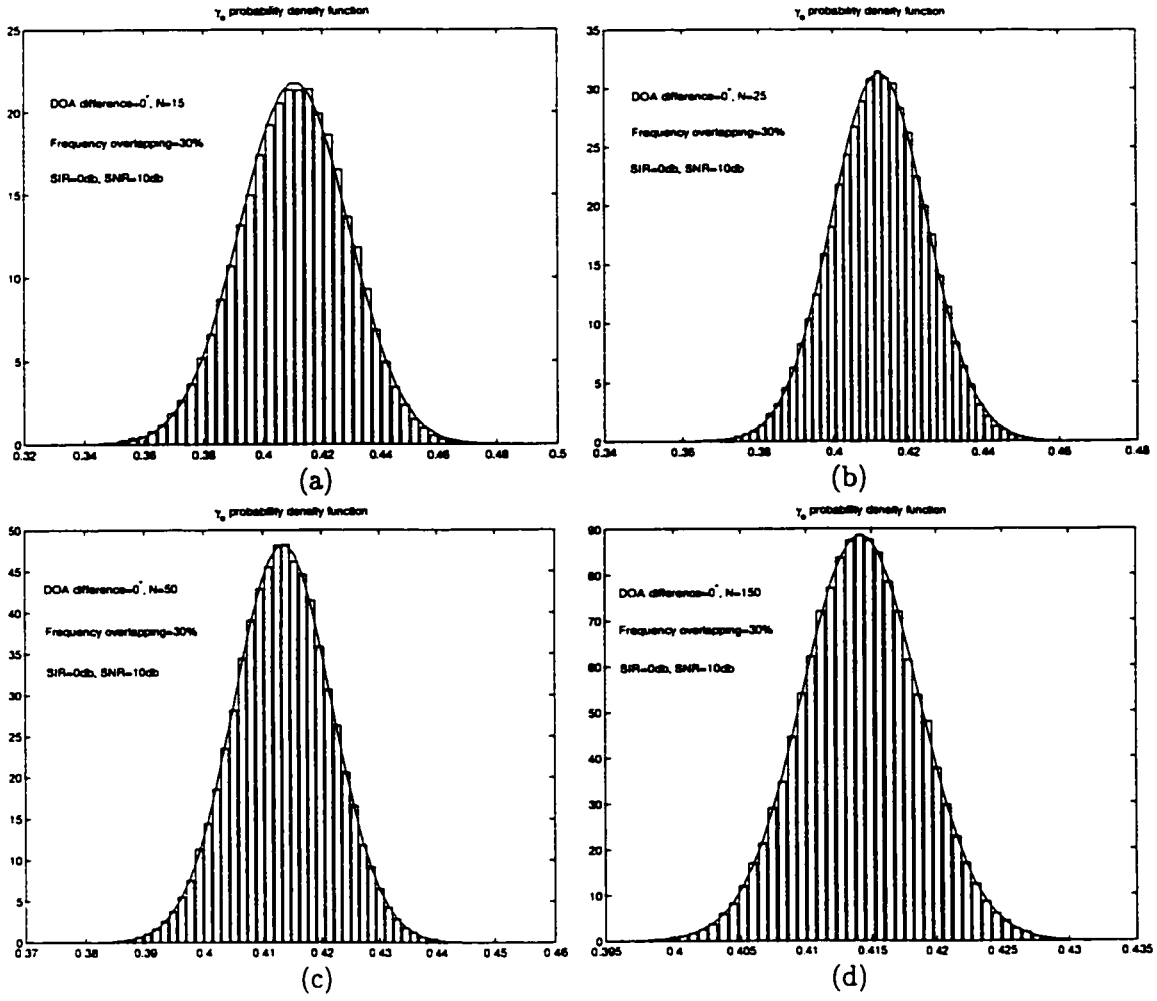

Figure C.4: Comparison between the experimental histogram and the theoretical pdf curve of γ_o for N=15, 25, 50, and 150 when the input SNR is 10dB

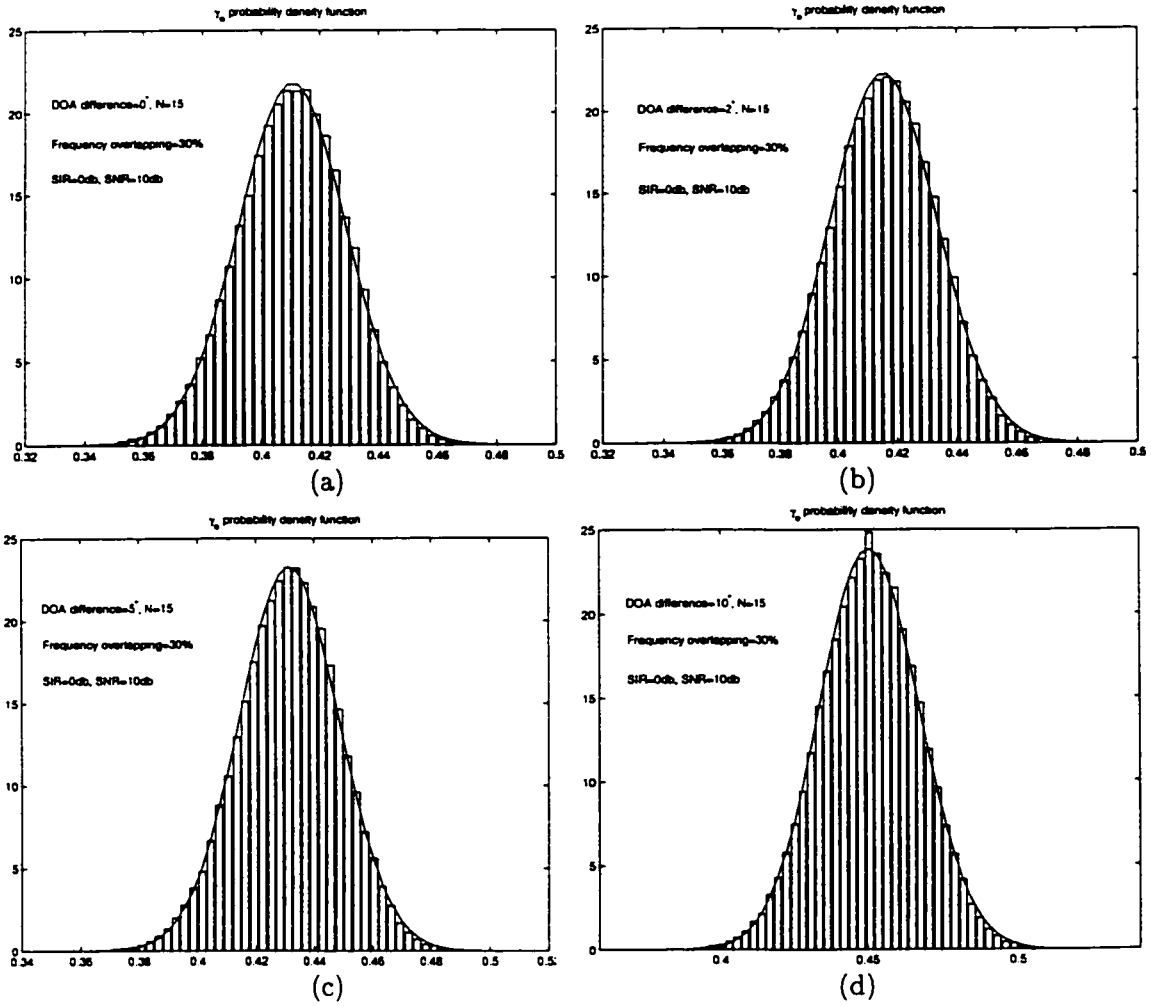

Figure C.5: Comparison between the experimental histogram and the theoretical pdf curve of γ_o for the DOA difference 0°, 2°, 5°, and 10° when the input SNR is 10dB

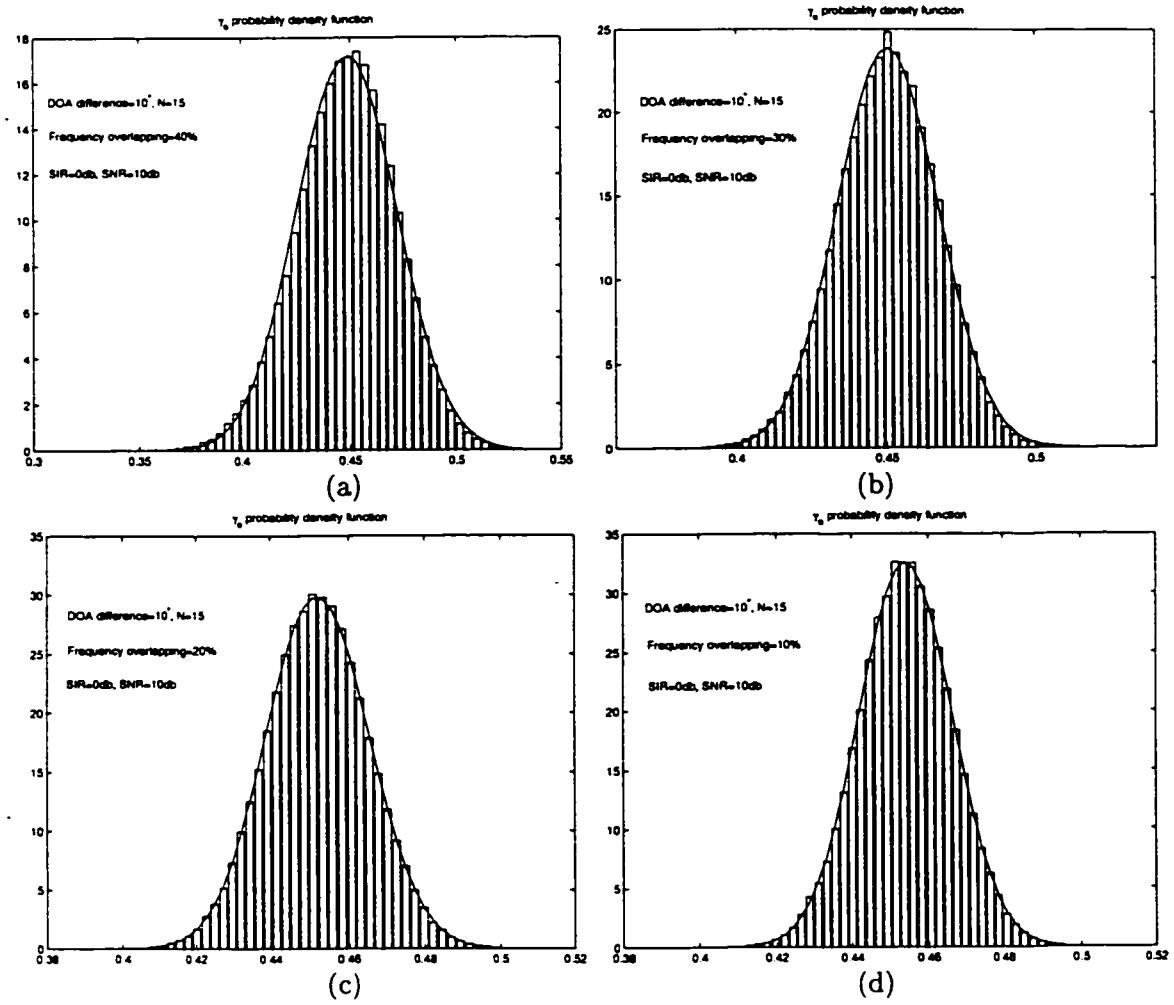

Figure C.6: Comparison between the experimental histogram and the theoretical pdf curve of γ_O for different spectral overlapping 40%, 30%, 20%, and 10% when input SNR is 10dB

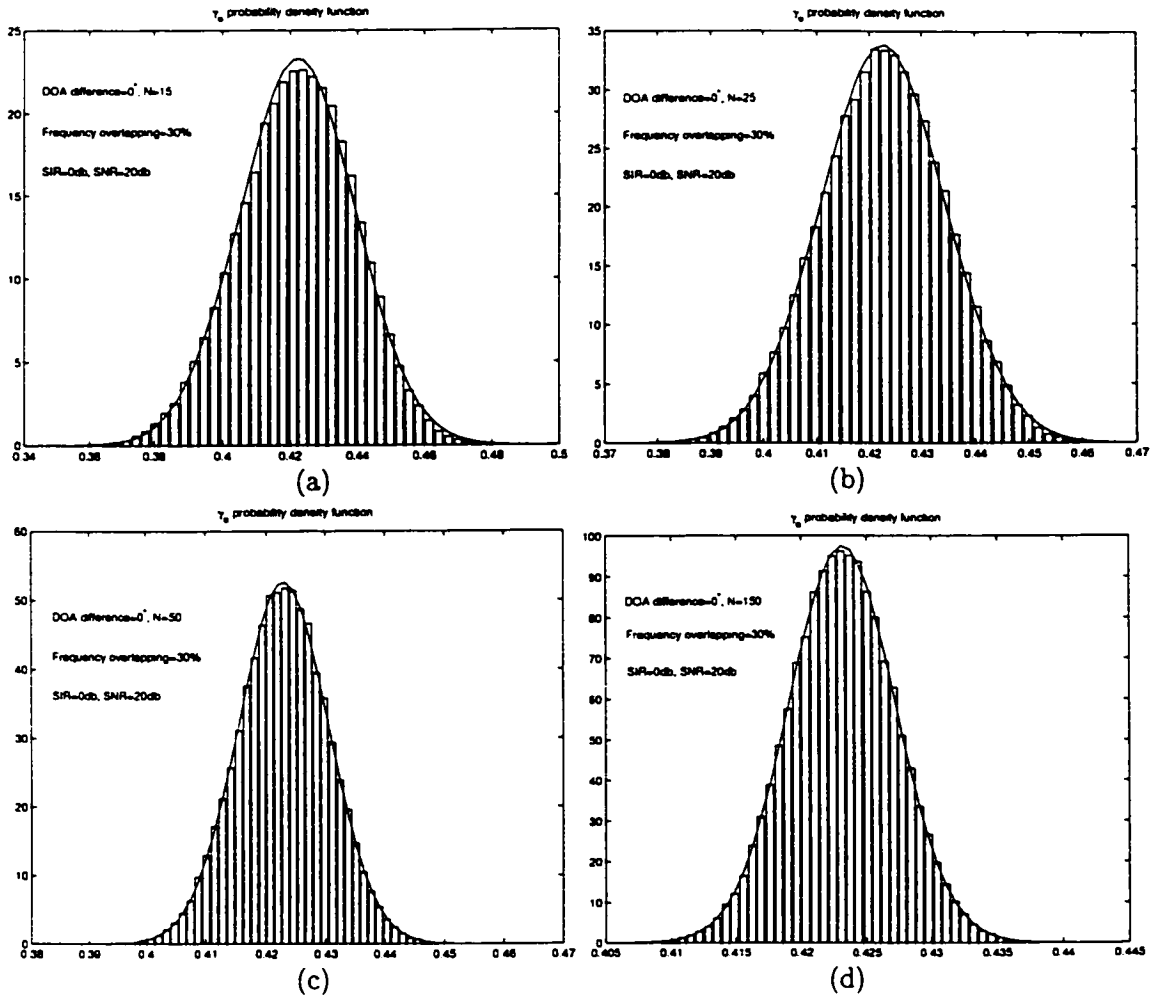

Figure C.7: Comparison between the experimental histogram and the theoretical pdf curve of γ_o for N=15, 25, 50, and 150 when the input SNR is 20dB

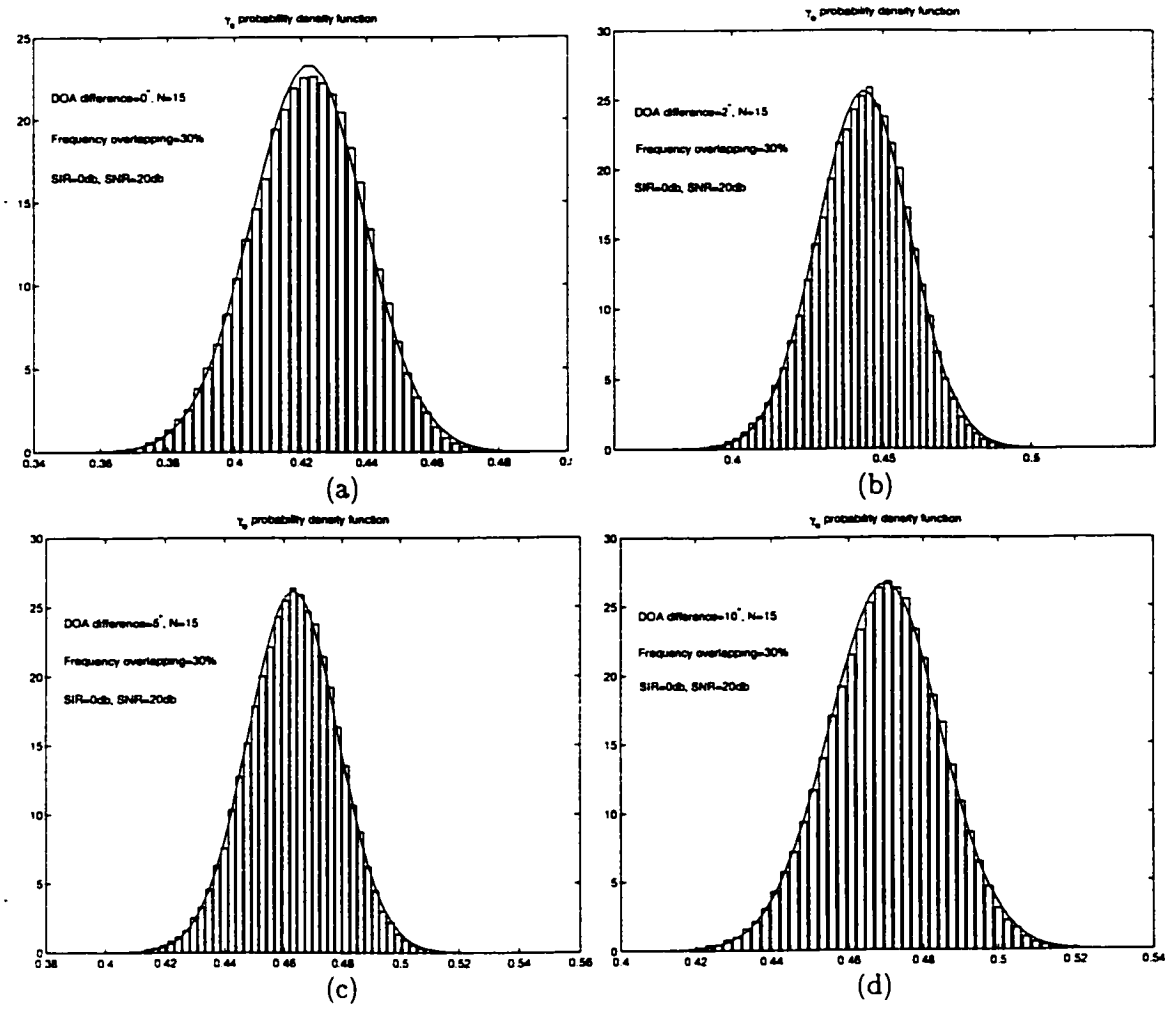

Figure C.8: Comparison between the experimental histogram and the theoretical pdf curve of γ_o for the DOA difference 0°, 2°, 5°, and 10° when the input SNR is 20dB

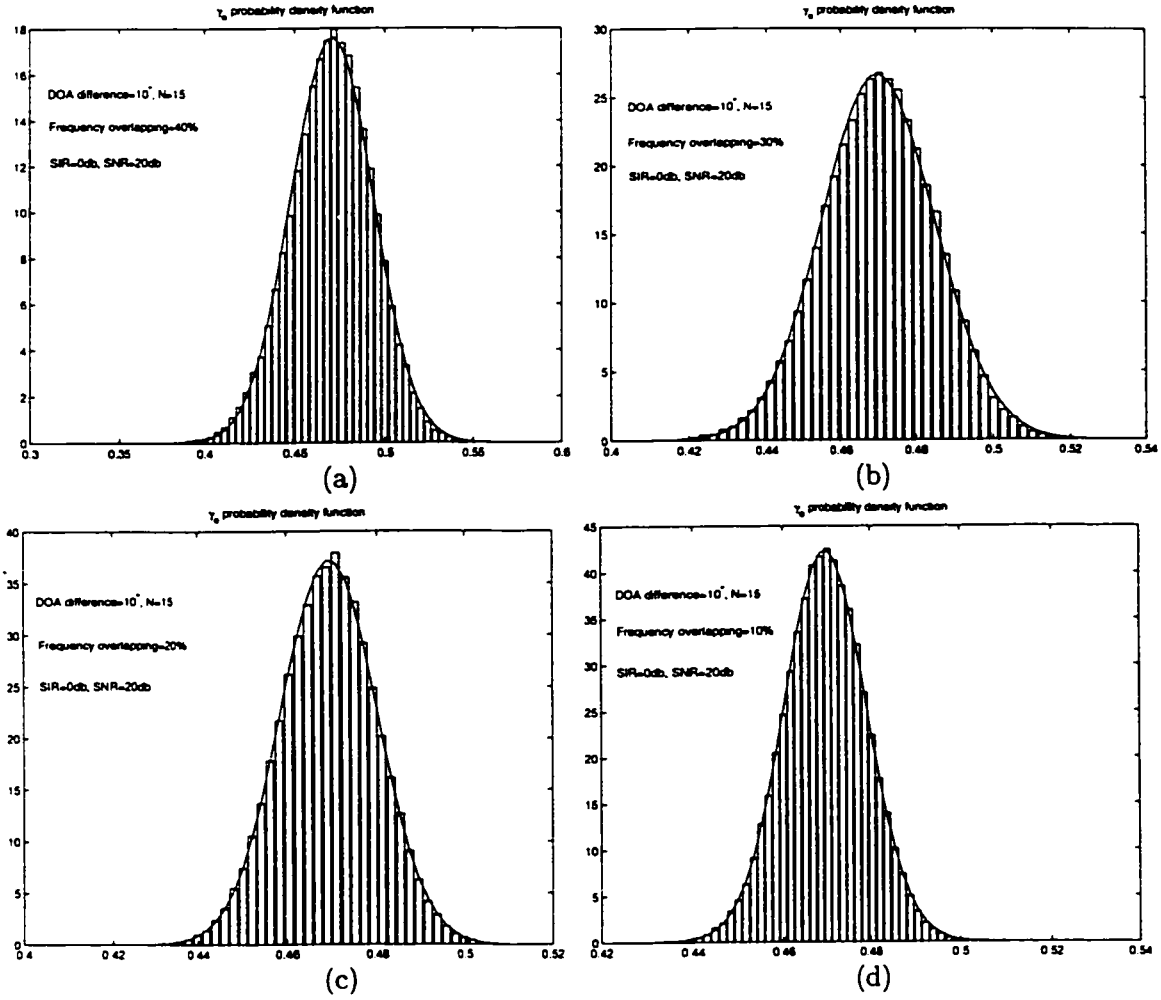

Figure C.9: Comparison between the experimental histogram and the theoretical pdf curve of γ_o for different spectral overlapping 40%, 30%, 20%, and 10% when input SNR is 20dB

Appendix D

Approximation of η_e by a Gaussian Distribution

In this appendix, we discuss the approximation accuracy of η_e by a Gaussian distribution in Chapter 4 and Chapter 6. Because the case in Chapter 4 can be viewed as a special case in Chapter 6, we just discuss the approximation accuracy of η_e by a Gaussian distribution in Chapter 6. Re-write the definition of η_e here for convenience

$$\eta_e(n) = \eta(n) + \xi_{ISI}(n) + \xi_{CTI}(n)$$

where $\eta(n)$, $\xi_{ISI}(n)$, and $\xi_{CTI}(n)$ are the output noise, output ISI, and output CTI respectively. $\eta(n)$, $\xi_{ISI}(n)$, and $\xi_{CTI}(n)$ are defined in Eqs. (6.3.1), (6.4.7), and (6.5.2) respectively.

As the result of large amounts of random variables acting together, η_e can be approximated by Gaussian distribution with zero mean

$$\mu_{\eta_e} = E[\eta_e] = E[\eta] + E[\xi_{ISI}] + E[\xi_{CTI}] = 0$$

and the variance

$$\sigma^2_{\eta_e} = \sigma^2_{\eta} + \zeta_{ISI} + \zeta_{CTIave}$$

σ_η^2, ζ_{ISI} and ζ_{CTIave} are the variance of η, ξ_{ISI} and ξ_{CTI} and they are defined in Eqs. (6.3.4), (6.4.12) and (6.5.11) respectively.

The pdf of η_e is therefore,

$$p_{\eta_e}(z) = \frac{1}{\sqrt{2\pi\sigma_{\eta_e}^2}} \exp\left(-\frac{z^2}{2\sigma_{\eta_e}^2}\right).$$

Now we use experimental method to demonstrate the accuracy of the approximation. Given the data length N, SIR=0dB, and SNR=0dB, we do K times experiments to generate K samples of the filter coefficient $h_{\lambda,m}(n)$. Using the kth sample of the filter coefficients and the input noise, input desired symbols, and input interfering symbols to compute the kth value of η_e, we obtain a long random sequence of $\eta_e(N)$. For the experimentally generated η_e, a histogram Hist(b_i, y_i) can be obtained, where b_i is the center of ith bin, the bin size b_s is given by $b_{i+1} - b_i$ and y_i is the accumulation number. We obtain normalized histogram.

In the following examples, we choose $K = 100000$, where K is number of experiments. We choose $N = 15$, $N = 25$, $N = 50$, and $N = 150$ respectively, where N is the data length. The number of bins of the histograms is chosen to be 50. The desired and interfering signals are BPSK signals as given by Eqs. (6.7.1) and (6.7.2) respectively. The baud rates of the desired signal and the interference are equal which are 5kHz. The carrier frequency offset of the desired signal is fixed at $f_1 = 10$kHz and that of the interference is fixed at $f_2 = 17$kHz, so that the two signals overlap on 30%. The sampling rate $f = 100$kHz. For the parameters of the BLAST and TAST filters, the number of sensors is chosen at $L = 3$, the length of FIR filters in each FRESH filter is chosen at $N_o = 6$, the number of the branches of FRESH filter is chosen at $M = 2$. The frequency shift in the two branches are set at $\alpha_1 = 20$kHz, $\alpha_2 = -20$kHz respectively. The shift frequency used in the reference path of the BLAST filter is set at $\alpha' = 0$kHz. The input SIR and the input SNR are fixed at 0dB respectively. The DOA difference between the desired signal and the interference is fixed at 0°. We plot these histograms of η_e with the assumption of the pdf of η_e against different data length 15, 25, 50, and 150 in Fig. D.1(a) to D.1(d) respectively. Comparing these histograms with the assumption of the pdf of η_e, we can see

heuristically how accurate the approximation is. Moreover we use the square error between the experimental histogram and the theoretical curve to be a measure of the approximation accuracy.

$$d^2 = \sum(\bar{y}_i - p_{\eta_e}(b_i))^2 b_s^2.$$

The results are in the Table D.1. It can be observed from Figs. D.1(a) to D.1(d), and Tables D.1 that the approximation of η_e as a Gaussian distribution with the zero mean and the variance σ_{η_e} is accurate. Moreover, it also can be observed from Table D.1 that the variance of η_e is decreased when the number of data length is increased. When we fixed the number of data length N at 15, we plot these histograms of η_e with the assumption of the pdf of η_e against different DOA difference $0°, 2°, 5°$, and $10°$ in Fig. D.2(a) to D.2(d) respectively. Comparing these histograms with the assumption of the pdf of η_e, we can see heuristically how accurate the approximation is. Moreover we use the square error between the experimental histogram and the theoretical curve to be a measure of the approximation accuracy. The results are in the Table D.2. It can be observed from Figs. D.2(a) to D.2(d), and Tables D.2 that the approximation of η_e as a Gaussian distribution with the zero mean and the variance $\sigma^2_{\eta_e}$ is accurate. Moreover, it also can be observed from Table D.2 that the variance of η_e is almost unchanged when the DOA difference is increased. When we fixed the number of data length N at 15 and the DOA difference at $10°$, we plot these histograms of η_e with the assumption of the pdf of η_e against different spectral overlapping 40%, 30%, 20%, and 10% in Fig. D.3(a) to D.3(d) respectively. Comparing these histograms with the assumption of the pdf of η_e, we can see heuristically how accurate the approximation is. Moreover we use the square error between the experimental histogram and the theoretical curve to be a measure of the approximation accuracy. The results are in the Table D.3. It can be observed from Figs. D.3(a) to D.3(d), and Tables D.3 that the approximation of η_e as a Gaussian distribution with the zero mean and the variance $\sigma^2_{\eta_e}$ is accurate. Moreover, it also can be observed from Table D.3 that the variance of η_e is reduced when the frequency overlapping is reduced.

	N=15	N=25	N=50	N=150
$\hat{\mu}_{\eta_e}$	5.9 $\times 10^{-5}$	8.0 $\times 10^{-5}$	-8.0 $\times 10^{-5}$	-5.8 $\times 10^{-5}$
$\hat{\sigma}^2_{\eta_e}$	0.0038	0.0031	0.0026	0.0022
d^2	9.9 $\times 10^{-6}$	3.4 $\times 10^{-6}$	9.3 $\times 10^{-6}$	1.2 $\times 10^{-5}$

Table D.1: The mean and the variance of η_e and the mean square error between the experimental histogram and the theoretical pdf curve of η_e for N=15, 25, 50, and 150 when the input SNR is 0dB, the DOA difference is 0°, and the spectral overlapping is 30%

	0°	2°	5°	10°
$\hat{\mu}_{\eta_e}$	5.9 $\times 10^{-5}$	3.0 $\times 10^{-5}$	-2.1 $\times 10^{-7}$	-1.7 $\times 10^{-5}$
$\hat{\sigma}^2_{\eta_e}$	0.0038	0.0038	0.0037	0.0036
d^2	9.9 $\times 10^{-6}$	1.0 $\times 10^{-5}$	6.3 $\times 10^{-6}$	8.0 $\times 10^{-6}$

Table D.2: The mean and the variance of η_e and the mean square error between the experimental histogram and the theoretical pdf curve of η_e for 0°, 2°, 5°, 10° when the input SNR is 0dB, the data length is 15, and the spectral overlapping 30%.

	40%	30%	20%	10%
$\hat{\mu}_{\eta_e}$	1.0 $\times 10^{-4}$	-1.7 $\times 10^{-5}$	1.5 $\times 10^{-4}$	1.9 $\times 10^{-5}$
$\hat{\sigma}^2_{\eta_e}$	0.0048	0.0036	0.0032	0.0030
d^2	8.8 $\times 10^{-6}$	8.0 $\times 10^{-6}$	9.0 $\times 10^{-6}$	9.6 $\times 10^{-6}$

Table D.3: The mean and the variance of η_e and the mean square error between the experimental histogram and the theoretical pdf curve of η_e for 40%, 30%, 20%, 10% when the input SNR is 0dB, the data length is 15, and the DOA difference is 10°

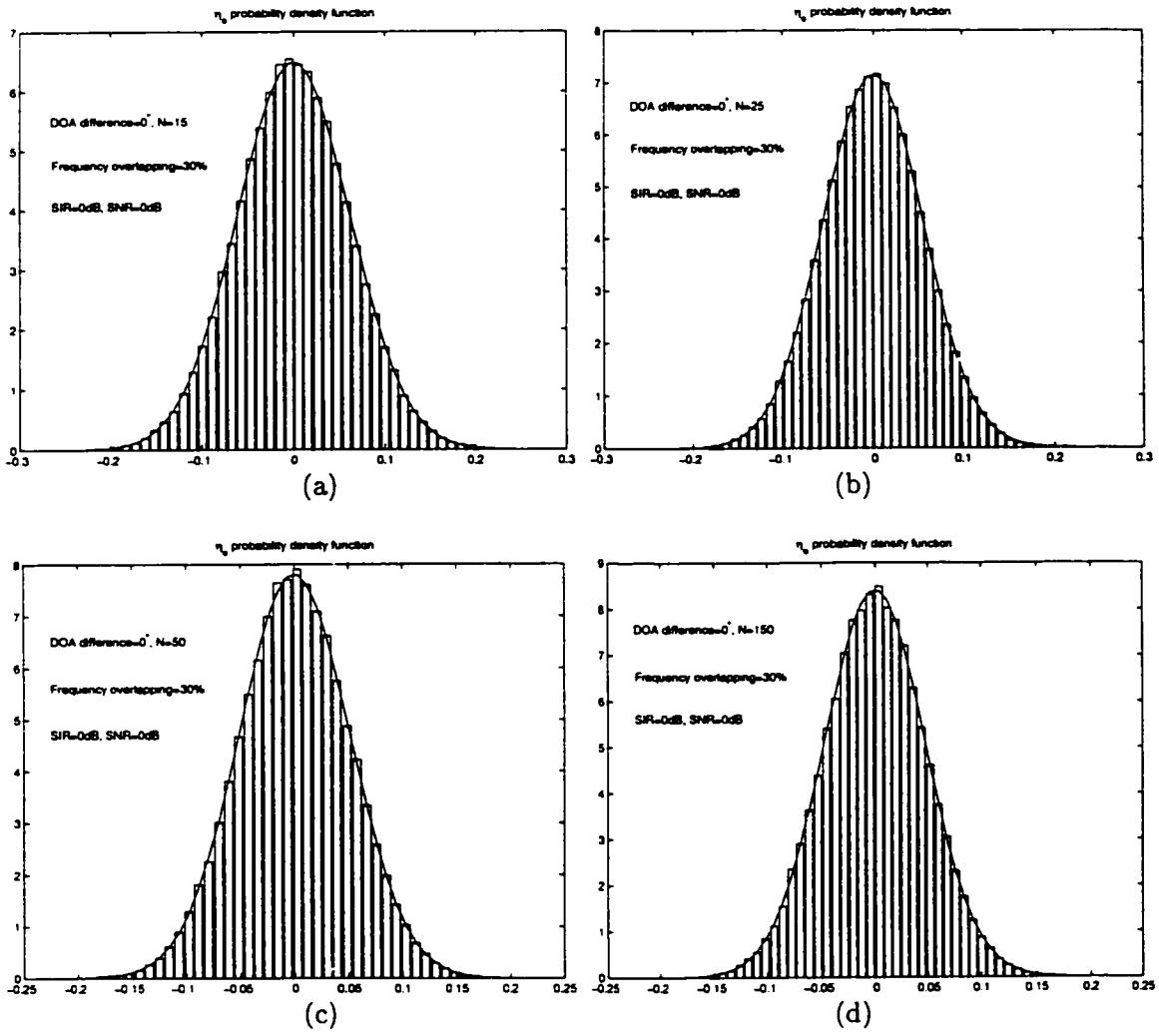

Figure D.1: Comparison between the experimental histogram and the theoretical pdf curve of η_e for N=15, 25, 50, 150 when the input SNR is 0dB

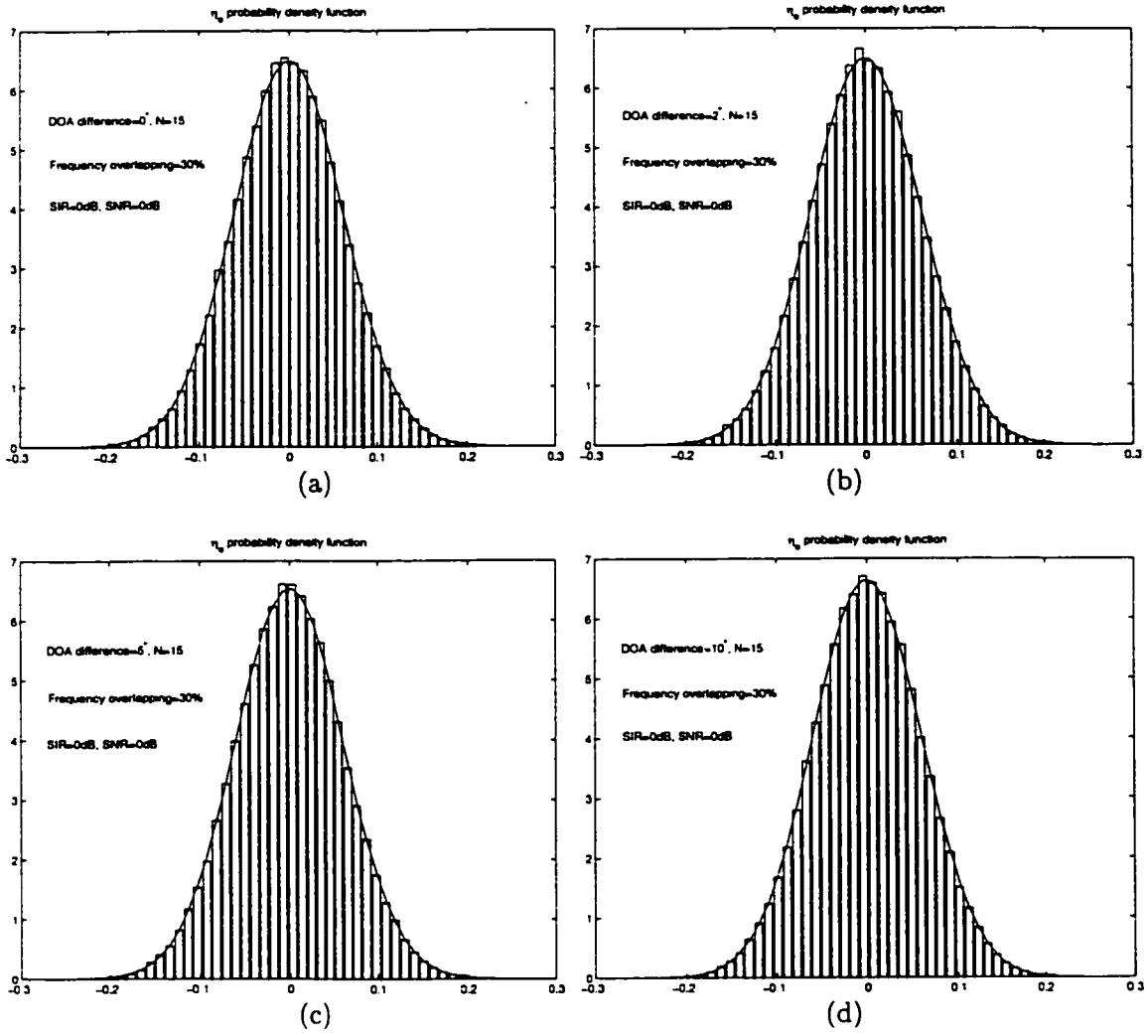

Figure D.2: Comparison between the experimental histogram and the theoretical pdf curve of η_e for the DOA difference 0°, 2°, 5°, 10° when the input SNR is 0dB

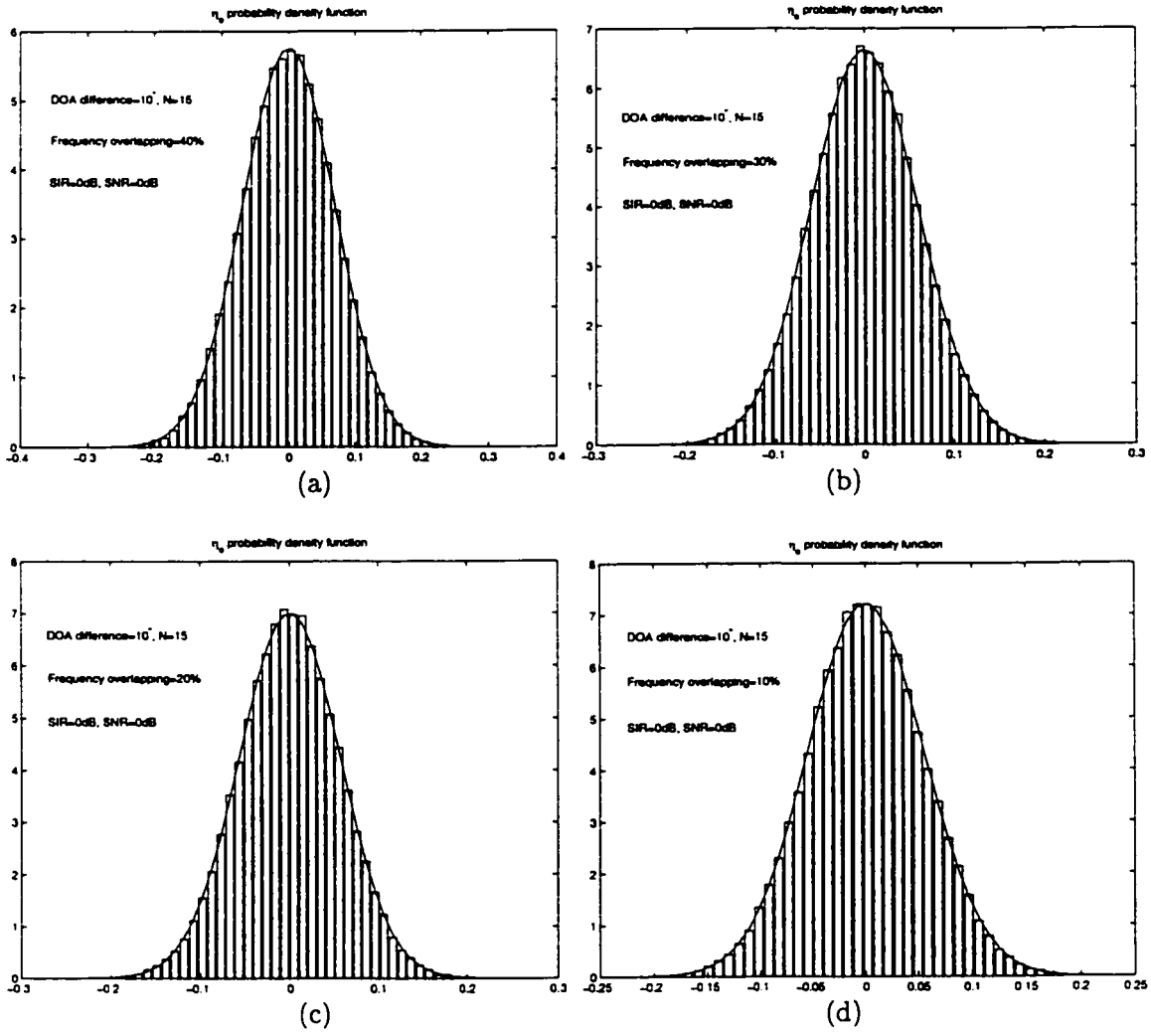

Figure D.3: Comparison between the experimental histogram and the theoretical pdf curve of η_e for different spectral overlapping 40%, 30%, 20%, 10% when the input SNR is 0dB

Appendix E

Proofs of Eqs. (4.6.13) and (6.6.14)

Show that

$$\frac{1}{2}\int_{-\infty}^{\infty}\frac{1}{\sqrt{2\pi\sigma_{\gamma_o}^2}}\exp^{\frac{-(\gamma_o-\mu_{\gamma_o})^2}{2\sigma_{\gamma_o}^2}}\operatorname{erfc}\left(\frac{\gamma_o}{\sqrt{2\sigma_{\eta_e}^2}}\right)d\gamma_o=\frac{1}{2}\operatorname{erfc}\left(\sqrt{\frac{(\mu_{\gamma_o})^2}{2\sigma_{\gamma_o}^2+2\sigma_{\eta_e}^2}}\right)$$

Proof: Let $\gamma=\gamma_o-\mu_{\gamma_o}$ and noting that $\operatorname{erfc}(x)=\frac{2}{\sqrt{\pi}}\int_x^{\infty}e^{-z^2}dz$, we have

$$\begin{aligned}\text{Left side} &= \frac{1}{2}\int_{-\infty}^{\infty}\frac{1}{\sqrt{2\pi\sigma_{\gamma_o}^2}}\exp^{\frac{-\gamma^2}{2\sigma_{\gamma_o}^2}}\operatorname{erfc}\left(\frac{\gamma+\mu_{\gamma_o}}{\sqrt{2\sigma_{\eta_e}^2}}\right)d\gamma \qquad \text{(E.0.1)}\\ &= \frac{1}{2}\int_{-\infty}^{\infty}\frac{1}{\sqrt{2\pi\sigma_{\gamma_o}^2}}\exp^{\frac{-\gamma^2}{2\sigma_{\gamma_o}^2}}\frac{2}{\sqrt{\pi}}\int_{\frac{\gamma+\mu_{\gamma_o}}{\sqrt{2\sigma_{\eta_e}^2}}}^{\infty}\exp^{-z^2}dzd\gamma\end{aligned}$$

Let $w=-\left(z-\frac{\gamma+\mu_{\gamma_o}}{\sqrt{2\sigma_{\eta_e}^2}}\right)$, that is, $z=-\left(w-\frac{\gamma+\mu_{\gamma_o}}{\sqrt{2\sigma_{\eta_e}^2}}\right)$,

$$\begin{aligned}\text{Left side} &= \frac{1}{2}\int_{-\infty}^{\infty}\frac{1}{\sqrt{2\pi\sigma_{\gamma_o}^2}}\exp^{\frac{-\gamma^2}{2\sigma_{\gamma_o}^2}}\frac{2}{\sqrt{\pi}}\int_{-\infty}^{0}\exp^{-\left(w-\frac{\gamma+\mu_{\gamma_o}}{\sqrt{2\sigma_{\eta_e}^2}}\right)^2}dwd\gamma\\ &= \frac{1}{\sqrt{2\pi^2\sigma_{\gamma_o}^2}}\int_{-\infty}^{\infty}\int_{-\infty}^{0}\exp^{-\left[\frac{\gamma^2}{2\sigma_{\gamma_o}^2}+\left(w-\frac{\gamma+\mu_{\gamma_o}}{\sqrt{2\sigma_{\eta_e}^2}}\right)^2\right]}dwd\gamma \qquad \text{(E.0.2)}\end{aligned}$$

We note that

$$\frac{\gamma^2}{2\sigma_{\gamma_o}^2}+\left(w-\frac{\gamma+\mu_{\gamma_o}}{\sqrt{2\sigma_{\eta_e}^2}}\right)^2 = \frac{\sigma_{\eta_e}^2}{\sigma_{\gamma_o}^2+\sigma_{\eta_e}^2}\left(w-\frac{\mu_{\gamma_o}}{\sqrt{2\sigma_{\eta_e}^2}}\right)^2 + \left(\frac{1}{2\sigma_{\gamma_o}^2}+\frac{1}{2\sigma_{\eta_e}^2}\right)\left(\gamma-\frac{\left(\frac{w}{\sqrt{2\sigma_{\eta_e}^2}}-\frac{\mu_{\gamma_o}}{2\sigma_{\eta_e}^2}\right)}{\left(\frac{1}{2\sigma_{\gamma_o}^2}+\frac{1}{2\sigma_{\eta_e}^2}\right)}\right)^2 \tag{E.0.3}$$

Substitutiing Eq. (E.03) into Eq. (E.02) and let $v=\sqrt{\left(\frac{1}{2\sigma_{\gamma_o}^2}+\frac{1}{2\sigma_{\eta_e}^2}\right)}\left(\gamma-\frac{\frac{w}{\sqrt{2\sigma_{\eta_e}^2}}-\frac{\mu_{\gamma_o}}{2\sigma_{\eta_e}^2}}{\left(\frac{1}{2\sigma_{\gamma_o}^2}+\frac{1}{2\sigma_{\eta_e}^2}\right)}\right)$ and noting that $\frac{1}{\sqrt{\pi}}\int_{-\infty}^{\infty}e^{-v^2}dv=1$, we obtain

$$\frac{1}{\sqrt{\pi}}\int_{-\infty}^{\infty}\exp^{-\left(\frac{1}{2\sigma_{\gamma_o}^2}+\frac{1}{2\sigma_{\eta_e}^2}\right)\left(\gamma-\frac{\frac{w}{\sqrt{2\sigma_{\eta_e}^2}}-\frac{\mu_{\gamma_o}}{2\sigma_{\eta_e}^2}}{\left(\frac{1}{2\sigma_{\gamma_o}^2}+\frac{1}{2\sigma_{\eta_e}^2}\right)}\right)^2}d\gamma=\frac{1}{\sqrt{\left(\frac{1}{2\sigma_{\gamma_o}^2}+\frac{1}{2\sigma_{\eta_e}^2}\right)}} \tag{E.0.4}$$

Therfore, we obtain

$$\text{Left side}=\frac{1}{\sqrt{2\pi\sigma_{\gamma_o}^2}}\frac{1}{\sqrt{\left(\frac{1}{2\sigma_{\gamma_o}^2}+\frac{1}{2\sigma_{\eta_e}^2}\right)}}\int_{-\infty}^{0}\exp^{-\frac{\sigma_{\eta_e}^2}{\sigma_{\gamma_o}^2+\sigma_{\eta_e}^2}\left(w-\frac{\mu_{\gamma_o}}{\sqrt{2\sigma_{\eta_e}^2}}\right)^2}dw \tag{E.0.5}$$

Let $x=-\sqrt{\frac{\sigma_{\eta_e}^2}{\sigma_{\gamma_o}^2+\sigma_{\eta_e}^2}}\left(w-\frac{\mu_{\gamma_o}}{\sqrt{2\sigma_{\eta_e}^2}}\right)$, we obtain

$$\text{Left side}=\frac{1}{\sqrt{\pi}}\int_{\frac{\mu_{\gamma_o}}{\sqrt{2\sigma_{\gamma_o}^2+2\sigma_{\eta_e}^2}}}^{\infty}e^{-x^2}dx=\frac{1}{2}\text{erfc}\left(\sqrt{\frac{(\mu_{\gamma_o})^2}{2\sigma_{\gamma_o}^2+2\sigma_{\eta_e}^2}}\right)=\text{right side.}\ \square \tag{E.0.6}$$

Bibliography

[1] W. C. Y. Lee, *Mobile Cellular Telecommunications Systems*, McGraw-Hill, New York, 1988.

[2] L. C. Godara, "Applications of Antenna Array to Mobile Communications, Part I: Performance Improvement, Feasibility, and System Considerations," *Proc. of the IEEE.*, vol. 85, no. 7, July 1997.

[3] L. C. Godara, "Applications of Antenna Array to Mobile Communications, Part II: Beam-Forming and Direction-of Arrival Considerations," *Proc. of the IEEE.*, vol. 85, no. 8, Aug. 1997.

[4] D. J. Goodman, "Trends in Cellular and Cordless Communications," *IEEE Communication Magazine,* vol. 75, no. 4, pp. 31-40, June 1991.

[5] T. Upadhyay and G. Dimos, "Test Results on Mitigation of SATCOM-Introduced Interference to GPS Operation," *Proc. of ION GPS'95,* pp. 1-8, CA, Sept. 1995.

[6] J. J. Spilker, "GPS Signal Structure and Performance Characteristics," *GPS Positioning System*, vol. 1, pp. 29-54, Washington, D. C., 1985.

[7] S. Haykin, *Adaptive Filter theory*, 2nd Edition, John Wiley & Sons, New York, 1991.

[8] A. Chevreuil and P. Loubaton, "On the use of conjugate cyclo-stationarity: A blind second-order multi-user equalization method," *Proc. ICASSP'96*, pp. 2439-2442, Atlanta, GA, USA, 1996.

[9] A. J. Paulraj and C. B. Papadias, "Space-Time Processing for Wireless Communications," *IEEE Signal Processing Magazine*, Nov. 1997.

[10] G. B. Giannakis, "Filter Banks for Blind Channel Identification and Equalization," *IEEE Signal Processing Letters*, vol. 4, no. 6, pp. 184-187, June 1997.

[11] A. Chevreuil and P. Loubaton, "Blind Second-Order Identification of FIR Channels: Forced CS and Structured Subspace Method," *IEEE Signal Processing Letters*, vol. 4, no. 7, pp. 204-206, July 1997.

[12] E. Serpeding and G. B. Giannakis, "Modulation Induced CS for Blind Channel Identification and Equalization," *Proc. Conf. on Information Sciences and Systems*, Baltimore, MD, 1997.

[13] W. A. Gardner, "Cyclic Wiener Filtering: Theory and Method," *IEEE Trans. Comm.*, vol. 41, no. 1, pp. 151-163, 1993.

[14] O. L. Frost, "An Algorithm for Linearly Constrained Adaptive Array Processing," *Proc. of IEEE*, vol. 60, no. 8, Aug. 1972.

[15] Q. Wu and K. M. Wong, "Blind Adaptive Beamforming for Cyclostationary Signals," *IEEE Trans. Signal Processing*, vol. 44, no. 11, Nov. 1996.

[16] J. Zhang, K. M. Wong and Z. Q. Luo, "Blind Adaptive FRESH Filtering for Signal Extraction," *IEEE Trans. on Signal and Processing*, vol. 47, no. 5, pp. 1394-1402, May, 1999.

[17] J. Zhang, K. M. Wong and Z. Q. Luo, "A Generalized Structure of Blind Adaptive FREquency-Shift Filter for Signal Extraction," *IEEE ISCAS'97*, vol. II, pp. 1197-1200, Hong Kong, June, 1997.

[18] J. Zhang and K. M. Wong, "A New Kind of Adaptive FREquency SHift Filter," *IEEE ICASSP'95*, vol. 2, pp. 913-916, Detroit, MI, 1995.

[19] K. M. Wong, Q. Wu, and P. Stoica, "Generalized Correlation Decomposition Applied to Array Processing in Unknown Noise Environment," in S. Haykin (Ed) *Advances in Spectrum Analysis and Array Processing*, Prentice Hall, 1995.

[20] W. A. Gardner, *Statistical Spectral Analysis: A Non-Probabilistic Theory*, Englewood Cliffs, NJ, Prentice-Hall, 1987.

[21] G. V. Moustakides, "Study of the Transient Phase of the Forgetting Factor RLS," *IEEE Trans. on Signal and Processing*, vol. 45, no. 10, pp. 2468-2476, Oct. 1997.

[22] W. A. Gardner and L. E. Franks, "Characterization of Cyclostationary Random Signal Processes," *IEEE Trans. Information Theory*, vol. 21, pp. 4-14, Jan. 1975.

[23] S. Haykin, *Communication Systems*, 2nd Edition, John Wiley & Sons, New York, 1983.

[24] W. A. Brown, *On the Theory of Cyclostationary Signals*, Ph.D dissertation, Dept. of EECS, Univ. of California, Davis, 1987.

[25] V. J. Mathews, S. H. Cho, "Improved Convergence Analysis of Stochastic Gradient Adaptive Filters Using the Sign Algorithm," *IEEE Trans. Acoustics, Speech, and Signal Processing,*, vol. ASSP-35, no. 4, April 1987.

[26] A. Leon-Garcia, *Probability and Random Processes for Electrical Engineering*, 2nd Edition, Addison-Wisley, 1994.

[27] K. M. Wong, "Wavelet Packet Division Multiplexing and Wavelet Packet Design Under Timing Error Efforts ", *IEEE Trans., Signal Processing*, vol. 45, no. 12, Dec. 1997.

[28] S. Anderson, M. Millnert and M. Viberg, "An Adaptive Array for Mobile Communication Systems," *IEEE Trans. Vehic. Tech.*, vol. 40, pp. 230-236, Feb. 1991.

[29] B. G. Agee, S. V. Schell, and W. A. Gardner, "Spectral Self-Coherence Restoral: A New Approach to Blind Adaptive Signal Extraction Using Antenna Arrays," *Proc. of IEEE*, vol. 78, no. 4, pp. 753-767, 1990.

[30] S. T. Alexander, *Adaptive Signal Processing: Theory and Applications*, Springer-Verlag, New York Inc., 1986.

[31] M. C. Jeruchim, *Simulation of Communication Systems*, Plenum Press, New York and London, 1996.

[32] V. H. MacDonald, "The Cellular Concept," *Bell Sys. Tech. J.*, vol. 58, no.1, pp. 15-41, Jan., 1979.

[33] J. H. Winters, "On the Capacity of Radio Communication Systems with Diversity in a Rayleigh Fading Environment," *IEEE J. Select. Areas in Comm.*, vol. SAC-5, pp. 871-877, June 1987.

[34] W. A. Gardner, "Exploitation of Spectral Redundancy in Cyclostationary Signals," *IEEE ASSP Magazine*, pp. 14-36, April 1997.

[35] H. Cox, R. M. Zeskind and M. M. Own, "Robust Adaptive Beamforming," *IEEE Trans. Acoustics, Speech, and Signal Processing*, vol. ASSP-35, no. 10, pp. 1365-1376, Oct. 1987.

[36] K. M. Buckley, "Spatial Filtering with Linearly Constrained Minimum Variance Beamformers," *IEEE Trans. Acoustics, Speech, and Signal Processing*, vol. ASSP-35, no. 3, March 1987.

[37] W. A. Gardner, "*Introduction to Random Processes with Applications Signals and Systems*," 2nd edition, New York, McGraw-Hill, 1989.

[38] W. M. Brown. "Conjugate Linear Filtering," *IEEE Trans. Information Theory*. vol. IT-15, pp. 462-465, 1969.

[39] E. R. Ferrara, "Frequency-Domain Implementations of Periodically Time-Varying Filters," *IEEE Trans Acoust., Speech, Signal Processing*, vol. ASSP-33, pp. 883-892, 1985.

[40] W. A. Gardner, "The Structure of Linear Least Mean Square Estimators for Synchronous M-ary Signals," *IEEE Trans. Information Theory*, vol. IT-19. pp. 240-243, 1973.

[41] M. Abdulrahman and D. D. Falconer, "Cyclostationary Crosstalk Suppression by Decision Feedback Equalization on Digital Subscriber Loops," *IEEE J. Select. Areas Comm.* vol. 10, pp. 640-649, 1992.

[42] S. M. Kay, *Modern Spectral Estimation, Theory & Application*, Prentice-Hall, New Jersey, 1987.

[43] L. W. Couch, *Digital and Analog Communication System*, 2nd Edition, Macmillan, New York, 1987.

[44] M. L. Skolnik, *Introduction to Radar Systems*, pp. 359-366, McGraw-Hill, New York, 1980.

[45] S. J. Campanella and J. V. Harrington, "Satellite Communications Networks," *IEEE Proceeding* , vol. 72, no. 11, pp. 1506-1519, Nov. 1984.

[46] W. C. Y. Lee, "Overview of Cellular CDMA", *IEEE Trans. Vehic. Tech.*, vol. 40, no. 2, pp. 291-302, May 1991.

[47] R. G. Vaughan, "On Optimum Combing at the Mobile", *IEEE Trans. Vehic. Tech.*, vol. COM-40, 1992.

[48] B. D. Van Veen and K. M. Buckley, "Beamforming: A Versatile Approach to Spatial Filtering," *IEEE ASAP Mag.*, pp. 4-24, April 1988.

[49] W. A. Gardner, S. V. Schell and P. Murphy, "Multiplication of Cellular Radio Capacity by Blind Adaptive Spatial Filtering," *International Conference on Selected Topic in Wireless Communications*, Vancouver, B.C., Canada, June 1992.

[50] K. Murota and K. Hirade, "GMSK Modulation for Digital Mobile Radio Telephony," *IEEE Trans. Comm.*, vol. COM-29, no. 7, pp. 1044-1050, July 1981.

[51] S. Shin and P. T. Mathiopoulos, "Differentially Detected GMSK Signals in CCI Channels for Mobile Cellular Telecommunication Systems," *IEEE Trans. Vehic. Tech.*, vol. VT-42, no. 3, pp. 289-293, Aug. 1993.

[52] K. Feher, "Modems for Emerging Digital Cellular-Mobile Radio System," *IEEE Trans. Vehic. Tech.*, vol. VT-40, no. 2, pp. 355-365, May 1991.

[53] S. V. Schell and W. A. Gardner, "Maximum Likelihood and Common Factor Analysis-Based Blind Adaptive Spatial Filtering for Cyclostationary Signals," *ICASSP'93*, vol. 4, pp. 292-295, Minneapolis, MN, USA, April 1993.

[54] K. Raith and J. Uddenfeldt, "Capacity of Digital Cellular TDMA Systems," *IEEE Trans. Vehic. Tech.*, vol. VT-40, no. 2, pp. 323-332, May 1991.

[55] S. C. Swales, M. A. Beach, D. J. Edwards, and J. P. McGeehan, "The Performance Enhancement of Multibeam Adaptive Base Station Antennas for Cellular Land Mobile Radio Systems," *IEEE Trans. Vehic. Tech.*, vol. VT-39, pp. 56-67, Feb. 1990.

[56] K. S. Gilhousen, A. Viterbi, and C. E. Wheatley, "On the Capacity of a Cellular CDMA System," *IEEE Trans. Vehic. Tech.*, vol. VT-40, no. 2, pp. 80-82, May 1991.

[57] J. Zhang and Ding Zuo, "A Design of Manpower Resource Intelligent Management System," *IEEE Proceedings of Intelligent Information Processing & System, ICIIPS-92* Beijing, China, 1992.

[58] J. Zhang, "Analysis and Improvement of Large Digital Control Machine Programming System," *Proceedings of the Eighth CMS National Conference*, China, 1992.

[59] J. Zhang, "Design and Realization of Oil Price Forecasting Expert System," *A Journal of Chinese Association of Automation*, vol. 20, pp. 7-13, ISSN 02-0411, 1991.

[60] J. Zhang, "A New Analysis Method for LSS Diagram Model," *ACTA Automatica Sinica*, vol. 15, pp. 68-72, no. 1, ISSN 0254-4156, 1989.

[61] T. I. Haweel and P. M. Clarkson, "Analysis and Generalization of a Median LMS Algorithm," *Proc. of the IEEE ICASSP*, pp. 1269-1272, 1990.

[62] J. R. Treichler, C. R. Johnson, and M. Larimore, *Theory and Design of Adaptive Filters*, New York, John Wily & Sons, 1987.

[63] B. Widrows, S. D. Stearns, *Adaptive Signal Processing*, Prentice Hall, 1985.

[64] O. Agazzi, D. G. Messerrschmitt, and D. A. Hodges, "Nonlinear Echo Cancellation of Data Signals," *IEEE Trans. Comm.*, vol. COM-30, pp. 2421-2433, Nov. 1982.

[65] A. Weiss and D. Mitra, "Digital Adaptive Filters: Conditions for Convergence, Rates of Convergence, Effects of Noise and Errors Arising from the Implementation," *IEEE Trans. Information Theory*, vol. 25, no. 6, pp. 637-652, Nov. 1979.

[66] D. F. Marshall, W. K. Jenkins, and J. J. Murphy, "The Use of Orthogonal Transforms for Improving Performance of Adaptive Filters," *IEEE Trans. Circuit and System*, vol. CS-36, pp. 474-483, April 1989.

[67] M. L. Honig and D. G. Messerschmitt, *Adaptive Filter: Structures, Algorithm and Applications*, Boston, MA, Kluwer Academic, 1984.

[68] O. Macchi and E. Eweda, "Second-Order Convergence Analysis of Stochastic Adaptive Linear Filtering," *IEEE Trans. Automatic Control*, vol. AC-28, pp. 76-85, Jan. 1983.

[69] C. B. Papadias, "Globally Convergent Blind Source Separation Based on a Multiuser Kurtosis Maximization Criterion," *IEEE Trans. Signal Processing*, vol. 48. No. 12, pp. 3508-3509, Dec. 2000.

[70] G. H. Golub and C. F. Van Loan, *Matrix Computations*, Johns Hopkins Univ. Press, 1996.

[71] Q. Wu, K. M. Wong and R. Ho, "A Fast Algorithm for Adaptive Beamforming of Cyclic Signals," *Proceeding of Wireless 93*, Calgary, Canada, July 1993.

[72] W. D. Rummler, "A New Selective Fading Model: Application to Propagation Data," *The Bell System Technical Journal*, pp. 1037-1071, May 1979.

[73] P. Hoeher, "A Statistical Discrete-Time Model for the WSSUS Multipath Channel," *IEEE Trans. Vehic. Technology*, vol. 41, Nov. 1992.

[74] P. A. Bello, "Characterization of Randomly Time-invariant Linear Channels," *IEEE Trans. Comm. Systems*, vol. CS-11, pp. 360-393, Dec. 1963.

[75] S. Ohmori, S. Taira and M. W. Austin, "Tracking Error of Phased Array Antenna," *IEEE Trans. Antenna and Propagation*, vol. 39, no. 1, pp. 80-82, Jan. 1991.

[76] D. R. Brillinger, *"Time Series Data Analysis and Theory,"* New York, Holt, Rinehart and Winston, 1981.

[77] M. Kaveh and A. J. Barabell, "The Statistical Performance of the MUSIC and the Minimum-Norm Algorithms in Resolving Plane Waves in Noise," *IEEE Trans. Acoust., Speech, Signal Processing*, vol. 34, pp. 331-341, Apr. 1986.

[78] S. U. Pillai and B. H. Kwon, "Performance Analysis of MUSIC-Type High Resolution Estimations for Direction Finding in Correlated and Coherent Scenes," *IEEE Trans. Acoust., Speech, Signal Processing*, vol. 37, pp. 1176-1189, Aug. 1989.

[79] J. H. Hudson, *"The Algebraic Eigenvalue Problem,"* New York, Oxford University Press, 1965.

[80] T. W. Anderson, *"Introduction to Multivariate Statistical Analysis,"* 2nd Edition, New York, 1984.

[81] J. E. Mazo, "On the Independence Theory of Equalizer Convergence," *Bell Sys. Tech. Journal*, vol. 58, pp 963-993.

[82] J. Litva, *"Digital Beamforming in Wireless Communications,"* Artech House, Inc., 1996.

[83] R. T. Compton, *"Adaptive Antennas-Concepts and Performance,"* Englewood Cliffs, New Jersey, New York, Oxford University Press, 1965.

[84] R. J. Muirhead, *"Aspects of Multivariate Statistical Theory,"* John Wiley & Sons, Inc., 1982.

[85] K. S. Shanmugan, *"Random Signals: Detection, Estimation and Data Analysis,"* John Wiley & Sons, Inc., 1988.

[86] A. N. Shiryaev, *"Probability,"* 2nd Edition, Springer-Verlag Inc., New York, 1996.